Improving downstream processing for viral vectors and viral vaccines

Piergiuseppe Nestola

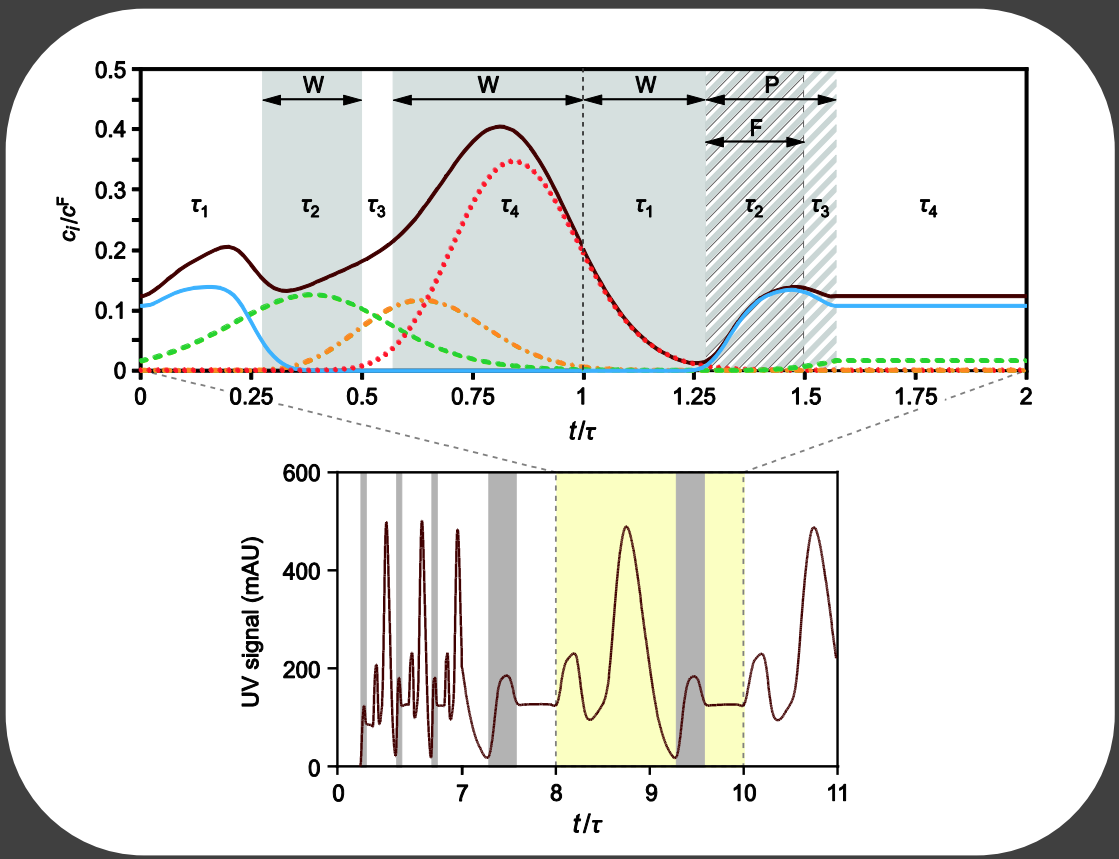

Dissertation presented to obtain the Ph.D degree in Chemical Engineering

Instituto de Tecnologia Química e Biológica António Xavier | Universidade Nova de Lisboa

Oeiras, March, 2015

INSTITUTO DE TECNOLOGIA QUÍMICA E BIOLÓGICA ANTÓNIO XAVIER /UNL

Knowledge Creation

Improving downstream processing for viral vectors and viral vaccines

Piergiuseppe Nestola

Dissertation presented to obtain the Ph.D degree in Chemical Engineering

Instituto de Tecnologia Química e Biológica António Xavier | Universidade Nova de Lisboa

Oeiras, March, 2015

INSTITUTO
DE TECNOLOGIA
QUÍMICA E BIOLÓGICA
ANTÓNIO XAVIER /UNL

Knowledge Creation

Improving downstream processing for viral vectors and viral vaccines

by Piergiuseppe Nestola

First Edition, December 2014

Cover:
Temporal concentration profiles in the outlet effluent of the two-column, size-exclusion simulated counter-current process. Top figure represents the simulated profiles for a full cycle under cycling steady state conditions. Bottom figure displays the experimental UV signal (239 nm) measured for the first five cycles of operation.

ITQB-UNL/IBET, Animal Cell Technology Unit
Instituto de Tecnologia Química e Biológica
Universidade Nova de Lisboa
Apartado 12, 2781-901 Oeiras, Portugal
Phone:+351 214469458 Fax: +351 214421161
http://www.itqb.unl.pt
http://www.ibet.pt
http://tca.itqb.unl.pt

Copyright© 2014 by Piergiuseppe Nestola
All rights reserved Printed in Portugal

A Irina e alla mia famiglia

Contents

Foreword

This thesis dissertation represents four years of research conducted at the Animal Cell Technology Unit of *Instituto de Technologia Química e Biológica/Universidade Nova de Lisboa* and at *Instituto de Biologia Experimental e Technológia* (iBET) under supervision of Professor Manuel Carrondo and Professor José Paulo Mota.

The work presented here is the result of a fruitful collaboration between Sartorius Stedim Biotech and iBET. The project aims to create new processes and materials for improving downstream processing for viral vectors and viral vaccines. Adenovirus, which constitutes a relevant system for both gene therapy and vaccination, was used as a model. The use of state-of-the-art technology combined with innovative continuous processes contributed to build robust and cost-effective strategies for purification of complex biopharmaceuticals. The project was funded by The Portuguese Science Foundation (FCT-MCTES) (SFRH/BD/82032/2011) and Sartorius Stedim Biotech.

Piergiuseppe Nestola
Oeiras, Portugal

Acknowledgements

This thesis would not have been possible without the support of a number of people. I would like to thank each and all of you for your contribution to this work.

First of all, I would like to thank my supervisor, Prof. Manuel Carrondo for his support, scientific rigour and for pushing me to the very best. You contributed a great deal to my professional and scientific growth.

I also want to thank my co-supervisor Prof. Paulo Mota, for the bright and simple way of teaching and explaining the fundamentals of adsorption processes. I have learned so much from your experience and scientific knowledge; I am very grateful for having had the opportunity to work together.

I also want to thank Prof. Paula Alves for having given me the opportunity to work at the Animal Cell Technology Unit, for providing the infrastructure to develop an excellent work, and for the confidence from the very first day. Thank you so much!

I am very grateful to the whole downstream team, in particular to Dr. Cristina Peixoto for being such a great mentor, for providing the support and for sharing the ups and downs of the scientific research life – I will never forget these four years in your lab; to Dr. Ricardo Silva – for the great help in the modelling part, for the patience in explaining the simulating moving bed concept (SMB), and above all it was a pleasure to be your colleague the last year of my research; I would also like to thank the former members of the downstream lab, Duarte and Patricia, and new members Barbara and Sofia –it was a pleasure to work with you. I wish you all the best in your future professional careers.

I would like to thank Sartorius Stedim Biotech for the opportunity to undertake this PhD project, especially Dr. Louis Villain for the guidance, enlightening discussions and constructive criticism. I have learned a lot about surface chemistry and all the issues, challenges and future trends of membrane chromatography. It was a pleasure working with you and your team at Sartorius in Goettingen.

I thank all the ACTU members for the great time I have spent with you in these four years. In particular I would like to thank Marcous Sousa and Manuel

Garrido for the nice nights out talking about science, bioreactors and bioprocesses over a couple of beers; Sofia Almeida and Claudia Queiroga– for the relaxing cinema nights and for all the laughs.

Special thanks to Marco Patrone. I guess one entire page of acknowledgements would not be enough to express how grateful I am for having had the opportunity to discuss with you all my ideas, doubts and scientific issues. We arrived almost at the same time here at iBET, and you were a great companion during my PhD journey. Thank you for revealing all the "mysteries" about molecular biology and for showing me a different perspective.

Many thanks to my former Crucell colleagues, in particular Sarah and Jeremy. Overall I decided to undertake a project on adenovirus was also because I truly enjoyed my time at Crucell.

Un grazie ai miei genitori e alla mia famiglia per il grosso incondizionato supporto. Un grazie ai miei amici del mitico collegio Madama di Torino, vi prometto che verro a visitarvi piu spesso; ai miei amici di infanzia Danilo e Alessandro sempre presenti anche se le nostre strade hanno preso cammini diversi durante tutti questi anni. Grazie a tutti.

And last but not least – a big big big thank to Irina for being such a great partner and for always being there for me. Thank you for your patience, support and understanding during these four years. I look forward to our new adventures together in Switzerland.

Jury

Dr. Uwe Gottschalk, Chief Technology Officer, Lonza.

Prof. Dr. Bernt Nilsson, Department of Chemical Engineering, Lund University.

Dr. Isabelle Knott, Director, Head of GQC Biology and Raw Materials, GSK.

Dr. Miguel Prazeres, Senior researcher at Instituto Superior Técnico–BioEngineering Research Group Centre for Biological and Chemical Engineering Department of Bioengineering.

Supervisors
Prof. Dr. Manuel Carrondo, Chemical and Biochemical Engineering, FCT-UNL, and Director, iBET.

Prof. Dr. José Paulo Mota, Chemical and Biochemical Engineering, Requimte/CQFB, Chemistry Department FCT-UNL.

Thesis publications

Nestola P, Peixoto C, Silva RJS, Alves PM, Mota JPB, Carrondo MJT. Improved virus purification processes for vaccines and gene therapy. *Biotechnology and Bioengineering*, Accepted.

Nestola P, Martins DL, Peixoto C, Roederstein S, Schleuss T, Alves PM, Mota JPB, Carrondo MJT. Evaluation of novel large cut-off ultrafiltration membranes for adenovirus serotype 5 (Ad5) concentration *PlosOne*, doi:10.1371/journal.pone.0115802.

Nestola P, Villain L, Peixoto C, Martins DL, Alves PM, Carrondo MJT, Mota JPB. Impact of grafting on the design of new membrane adsorbers for adenovirus purification. *Journal of Biotechnology* 2014; 181:1-11.

Nestola P, Silva RJS, Peixoto C, Alves PM, Mota JPB, Carrondo MJT. Adenovirus purification by two-column, size-exclusion, simulated countercurrent chromatography. *Journal of Chromatography A* 2014; 1347:111-121.

Nestola P, Silva RJS, Peixoto C, Alves PM, Carrondo MJT, Mota JPB. Robust design of adenovirus purification by two-column, simulated countercurrent, size-exclusion chromatography. *Journal of Biotechnology*, Accepted.

Nestola P, Peixoto C, Villain L, Alves PM, Carrondo MJT, Mota JPB. Rational development of flowthrough purification strategies for viruses and VLP. *In final preparation.*

Nomenclature

c_{B}	Solute concentration in bulk solution
ΔR	Biacore signal
δ	Standard deviation
ϵ_{o}	Column porosity (-)
η_0	Refractive index buffer solution with salt concentration c_0
$\tilde{\eta}_{\mathrm{B}}$	Refractive index of the dry solute
η_{B}	Refractive index of a salt solution with a dissolved biological solute
γ_{w}	Shear rate (s^{-1})
μ	Viscosity (Pa s)
Q_{E}	Elution flow rate (mL/min)
Q_{F}	Feed flow rate (mL/min)
τ_k	Duration of each steps (min)
v_{B}	Specific volume of the biological solute
A_f	Peak asymmetry factor (-)
c^{in}	Concentration in the feed mixture (μg/mL)
d	Inner diameter of the fibers (m)
h	Flow channel height in cassette modules (m)
J	Flux (LMH=L m^{-2} h^{-1})
K	Hydraulic permeability (m)
L	Column length (cm)

N Number of theoretical plates

n Number of fibers in hollow fiber modules (m)

N/L Number of theoretical plates of meter of column length(m^{-1})

Pe Peclet Number (-)

Q Volumetric flow rate (mL min^{-1})

q_i^* Concentration in the adsorbed phase (mg/mL)

v Linear velocity (m s^{-1})

V_c Column volume (cm^3)

V_o Void column (cm^3)

w Flow channel width in cassette modules (m)

3C-PCC Three Column Periodic Counter Current Chromatography

AC Affinity Chromatography

Ad5 Adenovirus serotype 5

ATF Alternative Tangential Flow

ATPS Aqueous Two-Phase Separation

AVV Adeno-associated virus

BFF Body Feed Filtration

$BTP_{10\%}$ Breakthrough point at 10%

CIM Convective Interaction Media

CQAs Critical Quality Attributes

$DBC_{10\%}$ Dynamic Binding Capacity at 10%

DE Diatomaceous Earth

DEAE Diethylaminoethanol

DGC Density Gradient Centrifugation

DoE Design of Experiment

EBA Expanded Bed Adsorption

EMA European Medicines Agency

FDA Food and Drug Administration

FSCs Flat Sheet Cassettes

FT Flow-through

GNP Gold Nanoparticles

GSSR Gradient with Steady-State Recycling

HF Hollow Fiber

HIC Hydrophobic Interaction Chromatography

IEX Ion-exchange

IP Infectious Particle

MCSGP Multicolumn Countercurrent Solvent Gradient Purification

MF Microfiltration

MMC Mix-Mode Chromatography

MVs Membrane Volumes

$NWP_{20°C}$ Normalized water permeability corrected for 20°C (LMH bar^{-1})

PAA Polyallyalime

PEG Polyethylene Glycol

PEI Polyethyleneimine

PES Polyethersulfone

PS Polysulfone

PSD Particle size distribution (-)

PVDF Polyvinylidene Fluoride

QbD Quality by Design

RC Regenerated Cellulose

S4FF Sepharose 4 Fast Flow]

SCCC Simulated Counter Current Chromatography

SEC Size Exclusion Chromatography

SMA Steric Mass Action

SMB Simulating Moving Bed

SXC Steric Exclusion Chromatography

TFF Tangential Flow Filtration

UF Ultrafiltration

VLP Virus Like Particle

xRC Cross-linked Regenerated Cellulose

Summary

Viral vectors are playing an increasingly important role in the vaccine and gene therapy fields. The broad spectrum of potential applications, together with expanding medical markets, drives the efforts to improve the production processes for viral vaccines and viral vectors. Developing countries, in particular, are becoming the main vaccine market. It is thus critical to decrease the cost per dose, which is only achievable by improving the production process. In particular advances in the upstream processing have substantially increased bioreactor yields, shifting the bioprocess bottlenecks towards the downstream processing. The work presented in this thesis aimed to develop new processes for adenoviruses purification. The use of state-of-the-art technology combined with innovative continuous processes contributed to build robust and cost-effective strategies for purification of complex biopharmaceuticals.

An introduction in chapter 1 reviews the current advances in the purification development for viral vectors and viral vaccines. Emphasis is given to novel strategies for process intensification, such as continuous or semi-continuous systems based on multicolumn technology, opening up process efficiency. Part II of the thesis focuses on the understanding and improving the performance of unit operation, such as ultrafiltration and anion exchange chromatography. Chapter 2 describes the development of a novel class of ultrafiltration (UF) cassettes for virus concentration/diafiltration. A detailed study was conducted to evaluate the effects of (i) membrane materials, namely polyethersulfone (PES), regenerated cellulose (RC), and highly cross-linked RC (xRC), (ii) nominal cut-off, and (iii) UF device geometry at different production scales. The results indicate that the xRC cassettes with a cut-off of approximately 500 kDa are able to achieve a 10-fold concentration factor with 100% recovery of particles with a process time twice as fast as that of a commercially available hollow fiber.

Chapter 3 reports the impacts of quaternary amine ligand density and matrix structure, namely hydrogel-grafted and directly-grafted, on state-of-the-art chromatographic membranes operated in bind-and-elute mode for the purification of adenovirus serotype 5. The results show that the hydrogel-grafted membranes are

more suitable for virus purification than the directly grafted ones. By reducing the number of grafted ligands to low (1.7 μmol/cm^2) or medium (2.4 μmol/cm^2) density, it is possible to increase the recovery of purified virus by 60% compared to a highly charged membrane (3.3 μmol/cm^2) that yielded a recovery rate lower than 30%. Overall, this work gives an outstanding contribution to the understanding and development of new membrane adsorbers specifically designed for virus purification.

In part III we step into the design of a new processes. Chapter 4 reports the design and experimental validation of a simple quasi-continuous, open-loop, two-column countercurrent chromatographic process for size-exclusion purification of adenovirus serotype 5 (Ad5). The pilot-scale run yielded a virus recovery of 86%, and a clearance of 90% and 89% for DNA and HCP, respectively, without any fine tunning of the predetermined operating parameters. These figures compare very favorably against single-column batch chromatography for the same volume of size-exclusion resin. However, and most importantly, the virus yield was increased from 57% for the batch system to 86% for the two-column SEC process because of internal recycling of the mixed fractions of contaminated Ad5, even though the two-column process was operated strictly in an open-loop configuration. And last, but not least, the productivity was increased by 6-fold with the two-column process. Chapter 5 validates the robustness of the 2-column process described in chapter 4. A general procedure for robust design evaluation under parameter uncertainty is described. The robust design is exemplified on the case where the column volume and interparticle porosity are subject to uncertainty. As expected, to increase the robustness of the 2CSMB-SEC process it is necessary to reduce its productivity and increase its solvent consumption. Nevertheless, the design solution given by the proposed robust approach is the least detrimental of all possible feasible candidate solutions.

Finally in chapter 6 a rational design of a flowthrough process was implemented by using Surface plasmon resonance (SPR) as scale down tools. The design space predicted by SPR experiments was employed to design a flowthourgh process using a salt tolerant membrane adsorber (STIC) from Sartorius Stedim Biotech and Capto Core 700 resin from Ge Healthercare connected in series. The full process development showed that the DNA clearance achieved is roughly 4 logs reduction. Also, virus recovery is boosted, especially in the first chromatographic unit operation (STIC membranes) where summing up the virus in FT and the virus eluted the recovery is close to 100%. As for HCP reduction is 5 logs, however while most of the DNA clearance is achieved in the STIC membrane, the

HCP reduction is mainly achieved by using the Capto Core 700. This thesis has contributed to fields of gene therapy, vaccination and bioengineering of complex pharmaceuticals by developing innovative downstream processes. This was possible by combining state-of-the-art materials and matrices, with computer aided process and simulation. We firmly believe that strategies developed herein pave the way for creating improved cost-effective processes yielding higher productivity.

Resumo

Os vectores virais têm uma importância crescente na área das vacinas e da terapia génica.Um vasto conjunto de aplicações assim como novos mercados resultam num interesse crescente na optimizao dos respectivos processos de produo. Os pases em vias de desenvolvimento so um dos principais alvos, sendo por isso crtico a diminuição do custo por dose. Nas últimas décadas foram efectuados grandes avanos na rea de produção tendo o passo limitante sido desviado para a purificação dos respectivos biofármacos. O trabalho desenvolvido e apresentado nesta tese teve como objectivo o desenvolvimento de novos processos de purificação para adenovirus através de novas tecnologias e combinando processos continuos, integrados e economicamente sustentáveis para a purificação de biofármacos complexos. No captulo I são descritos os principais avanços e desafios tecnológicos com que se depara a purificao de vacinas e vectores virais. O ênfase é colocado em novas estratégias para intensificação de processo como o uso de sistemas continuos ou de várias colunas de forma a aumentar a eficiência. Na segunda parte da tese o objectivo é compreendere melhorar cada uma das operações unitárias tais como a ultrafiltração ou a cromatografia de troca aniónica. No capítulo 2 descreve-se o desenvolvimento de uma nova classe de cassetes de ultrafiltração para concentração e diafiltração de virus. Um estudo detalhado foi conduzido por forma a avaliar o efeito dos materiais, nomeadamente polietersulfona, celulose regenerada e diferentes tamanhos e geometrias de poro. No capítulo 3 descreve-se o impacto da densidade de um ligando com amina quaternária e da densidade da matriz, nomeadamente com implantes de hidrogel ou implantes directos. Os resultados mostram que as menbranas com implantes de hidrogel são mais apropriadas para purificação de vrus. Por redução do número de ligando implantado é possível aumentar o rendimento de vírus purificados para 60% comparando com as que têm alta densidade de ligando em que o rendimento é menor do que 30%. Globalmente este trabalho contribui para o aprofundar do conhecimento e desenvolvimento the novas membranas de cromatografia desenhadas especificamente para vírus. Na parte III inicia-se o desenho de novos processos. No capítulo 4 reporta-se o desenho e a validação experimental de um sistema de quase continuo de duas

colunas em contra corrente para a purificação por exclusão molecular de adenovrus. O processo piloto teve um rendimento de 86% e uma remoção de DNA de 90% e de proteína de 89%. O resultado mais significativo foi o aumento do rendimento de 57% para 86% quando se passou do tradicional leito fixo para para o sistema de duas colunas de exclusão molecular. Por fim um aumento de 6 vezes da produtividade do sistema foi conseguido. No capítulo 5 validou-se a robustez do sistema descrito no capítulo anterior. É também descrito um procedimento geral para o desenho robusto através da inclusão de incerteza em parâmetros como o volume de coluna e a porosidade intraparticular.

Como seria expectvel, o incremento da robustez do processo 2CSMB-SEC feito custa da reduo da produtividade e do aumento do consumo de eluente. No entanto, a soluo obtida atravs desta metodologia a menos penalizante do conjunto de solues possveis.

Por fim, no capítulo 6 o desenho racional de um processo em que não há ligação do produto à matriz foi implementado usando SPR em escala reduzida. Foram usadas membranas tolerantes ao sal (STIC) da Sartorius Stedim e a resina Capto Core 700 da GE ligadas em série. O desenvolvimento completo do processo mostra que se consegue reduzir 4 logs de DNA assim como um aumento na recolha de vírus. Tal como a redução de proteínas das células hospedeiras é 5 logs. A maior parte do DNA é removido na primeira membrana e as proteínas na resina. Globalmente esta tese contribui para a área da terapia génica, vacinas e bioengenharia de fármacos complexos através do desenvolvimento de inovadores processos de purificação. Isto só foi possvel através da combinação de materiais e matrizes inovadoras, com o suporte de modelação matemática e simulação. Acreditamos que as estratégias desenvolvidas neste trabalho contribuem significativamente para melhorar processos economicamente viáveis e mais produtivos.

Part I

State-of-the-art

CHAPTER 1

Introduction

Adapted from:

Nestola P, Peixoto C, Silva RJS, Alves PM, Mota JPB, Carrondo MJT. Improved virus purification processes for vaccines and gene therapy. *Biotechnology and Bioengineering*; Accepted.

Abstract

Downstream processing of virus particles for vaccination or gene therapy is becoming critical as upstream titers keep improving. Moreover, the growing pressure to develop cost-efficient processes has brought forward new downstream trains. This review aims at analyzing the state-of-the-art in viral downstream purification processes, encompassing the classical unit operations and their recent developments. Emphasis is given to novel strategies for process intensification, such as continuous or semi-continuous systems based on multicolumn technology, opening up process efficiency. Process understanding in the light of the pharmaceutical quality by design (QbD) initiative is also discussed. Finally, an outlook of the upcoming breakthrough technologies is presented.

Keywords: Downstream bioprocessing, vaccines, gene therapy, process intensification, continuous purification

1.1 Introduction

Viral vectors are playing an increasingly important role in the vaccine and gene therapy fields (Morenweiser, 2005). Vaccines are entering a renaissance period after thirty years where few changes were introduced. They continue to be an attractive health care tool as well as sustainable business for several reasons: (i) vaccine demand has grown rapidly over the past decade in particular due to emerging markets, (ii) many important medical needs are unmet where vaccines may play a decisive role; (iii) previously intractable targets may now be within reach for vaccination because of advances in immunology and microbiology and a better understanding of pathogenesis (Smith et al., 2011). Moreover, the vaccine sector is not so prone to sharp revenue declines from expiration of patents unlike the rest of the pharmaceutical industry. Finally, high complexity of the vaccine products is a barrier to the entry of new competitors, which new technologies can overcome (Josefsberg and Buckland, 2012).

The first vaccines consisted mainly in live attenuated viruses (e.g., smallpox, rabies) or inactivated bacteria (e.g., pertussis). Nowadays new technologies are employed, such as the development of purified and inactivated viruses (e.g., hepatitis A), virus-like particles (e.g, hepatitis B,human papilloma virus and influenza) (Margine et al., 2012; Pushko et al., 2011; Kang et al., 2012a; Chackerian, 2007), and polysaccharides (e.g., pneumococcal vaccines) (Miller et al., 2011). Amongst these new trends, viral vectors are becoming important, as they allow the simultaneous expression of multiple antigens while avoiding the safety risks associated with the use of the whole pathogenic virus (Liniger et al., 2007).

Viral vectors that have been used in the past include poxvirus, herpesvirus, and adenovirus (Geels and Ye, 2010). In particular, adenoviruses are considered one of the most suitable platforms for vaccine development because they are efficient at delivering DNA to the target cells (McConnell, 2009). Different human serotypes are under evaluation for developing effective vaccines: Ad26, Ad35, and Ad5, for HIV and Malaria (Zak et al., 2012; Baden et al., 2013; Ouédraogo et al., 2013; Majhen et al., 2014) and, more recently, chimpanzee adenovirus (Ewer et al., 2013; Nébié et al., 2014).

In the gene therapy field, although nonviral delivery approaches are becoming common, viral vectors remain by far the most used tools, employed in over two-thirds of the clinical trials performed to date (Ginn et al., 2013). Adenovirus has been the most used vector (23.3% of the clinical trials carried out worldwide), followed by retrovirus (19.9%) and then other less widely adopted viruses, such as

poxvirus (5.0%), adeno-associated virus (4.9%), and herpes simplex virus (3.1%) (Ginn et al., 2013). Nevertheless, so far the first approved gene therapy product is Glybera®, based on adeno-associated virus, which is indicated for the treatment of familial lipoprotein lipase deficiency, an ultra-rare disease that leads to potentially fatal pancreatisis (Salmon et al., 2014).

The broad spectrum of potential applications, together with expanding medical markets, drives the efforts to improve the production processes for viral vaccines and gene therapy vectors (Wolff and Reichl, 2008). Developing countries, in particular, are becoming the main vaccine market (Makinen et al., 2012; Oyston and Robinson, 2012). It is thus critical to decrease the cost per dose, which is only achievable by improving the production process.

Advances in upstream processing have substantially increased the bioreactor yields. For example, cell densities of 10^8 cells/ml have been recently obtained using PER.C6 in a perfusion bioreactor (Vellinga et al., 2014). With such cell density, a 1000-liter perfusion bioreactor could theoretically yield up to 10^{19} adenovirus particles (10^5 VP/cell $\times$ 10^{11} cells/liter $\times$ 1000 liters). Such reported yields are shifting the process bottlenecks towards the downstream processing (DSP) part. Moreover, because DSP accounts for up to 70% of the overall production cost, its improvement will establish more cost effective processes (Morenweiser, 2005).

The main aim of downstream processing is to eliminate contaminants, either process related (e.g., bovine serum albumin, Benzonase, extractables, and leachables) or product related (e.g., host cell proteins, DNA, proteoglycans, and glycosaminoglycans); other product-related impurities include free proteins, aggregates, and empty capsids. The ultimate goal is to obtain a product with high purity, potency, and quality, which can meet the stringent guidelines of the regulatory authorities, such as the FDA and EMA (Table 1.1).

Table 1.1: *General specifications for biotechnological products (EMEA, 1999; ICH, 1999, 2007)*

Attribute	Specification
Appearance and description	Color Physical state Clarity/turbidity (Qualitative statement)
Identity	Several tests may be required: Physicochemical Biological Immunochemical (Highly specific but may be qualitative)
Purity	
Product-related impurities	Degraded product Truncated forms Molecular variants Aggregates
Process-related impurities	Host cell protein (HCP) Host cell DNA Media components/ancillaries Enzymes/chemicals Leachables
Potency	Cell- or Animal-based tests
Quantity	Protein mass or Potency (if applicable)
Safety	Sterility Adventitious viruses Endotoxins/Pyrogens Mycoplasma
General	pH Osmolarity

Virus and viral vectors are complex biopharmaceutical products, which vary in size, shape, and surface structures. The isoelectric point (pI), the surface hydrophobicity, presence or absence of an envelope, and the particle lability, can

play important roles in the design of the downstream train (Wolff and Reichl, 2011). Given this complexity, an effective purification of the bioproduct can only be achieved by a combination of several unit operations (Fig. 1.1).

This review focuses on the available downstream processing strategies for viral vaccines and gene therapy vectors, including technological advances and emerging industrial trends. To be more precise, the classical unit operations, namely precipitation, flocculation, centrifugation, micro and ultrafiltration, bead-based chromatography, and convective chromatographic matrices are reviewed. Emphasis is given to (semi-)continuous purification trains employing simulated moving bed (SMB) or SMB-type technologies, negative mode chromatography with novel matrices, and the discussion of relevant case studies. Process characterization and understanding in light of the pharmaceutical Quality by Design (QbD) initiative is also addressed.

1.2 Harvest

The first steps of the purification train are heavily influenced by the characteristics of the bioreactor bulk, namely cell density and viability or by the nature of the product release, either secreted by budding or cell lysis.

In cases of a lytic virus production, such as adenovirus (Ad) or adeno-associated (AVV) virus, the viruses are recovered by collecting both the intra- and extra-cellular fractions, and thus, an additional step is taken to release the virus (Altaras et al., 2005; Silva et al., 2010a). The cell lysis can be performed using different methods, such as freeze-thaw, detergents, homogenizer, or sonication. Among the non-ionic detergents, Triton^{TM} X-100 has often been the preferred choice (Altaras et al., 2005; Peixoto et al., 2008; Fernandes et al., 2012). Incubating the bulk with detergent is efficient, fast, robust, easily scalable, cost-effective, and does not require any investment in equipment; however, removal of such additives has to be confirmed.

Although cell lysis enables the recovery of intra-celullar virus it also releases the host cell DNA and proteins, which need to be removed from the final product. Host cell DNA is of special concern because it not only substantially increases the viscosity of the bioreaction bulk, but, more importantly, the regulatory requirements set the DNA acceptable levels between 10 ng and 10 pg per dose, depending on the type of product, medical indication, production host, and administration route. Therefore, the majority of published research work and disclosed patents refer to an incubation step with nuclease (e.g., Benzonase®),

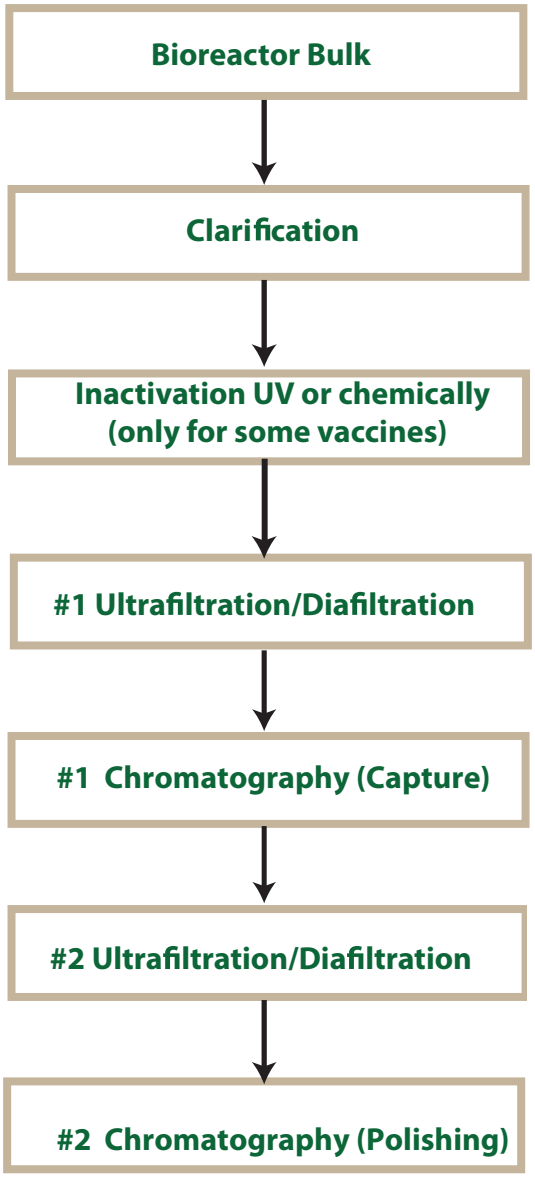

Figure 1.1: *Standard flow chart of unit operations required for viral purification trains. Ultrafiltration/Diafiltration and chromatographic unit operations are usually intermittently repeated.*

either simultaneously with cell lysis or after clarification (Altaras et al., 2005; Peixoto et al., 2008; Fernandes et al., 2012; Segura et al., 2011). For enveloped virus, such as retrovirus, baculovirus, lentivirus, influenza, or enveloped VLP, cell lysis is not required since the virus is secreted by the producer cell through a budding process.

Selective precipitation has been suggested as an alternative to nuclease treatment for the removal of host cell DNA (Goerke et al., 2005; Konz et al., 2005). Cationic detergents, such as domiphen bromide, are able to precipitate DNA as well as adenoviral particles (both negatively charged and mildly hydrophobic). For example it was demonstrated that fine adjustment of the precipitant concentration enables up to 90 % DNA removal with more than 90 % adenovirus recovery (Goerke et al., 2005).

Kröber et al. (2010) implemented a DNA precipitation method for influenza vaccine: polyethyleneimine (PEI) was used, and the optimal conditions were obtained through a DoE approach achieving DNA removal of 85%. Selective DNA precipitation has the advantage of being inexpensive, easily scalable (precipitated DNA can be removed by depth filter), and suitable for high cell density processes. Indeed, it has been shown that replacing Benzonase endonuclease with precipitation results in savings of 0.5 million USD for 100 liters of high cell density culture (Vellinga et al., 2014). Nevertheless, for the sake of completeness, it should be mentioned that Benzonase is witnessing a patent cliff, and several competitors are now appearing: Denerase (Sartorius Stedim Biotech), Cyanase (RiboSolution), Pierce Universal Nuclease (Thermo Scientific), just to name a few. This will likely cause a substantial decrease in nuclease price and, thus, be beneficial for process cost improvement.

1.3 Clarification

A suitable clarification step should efficiently remove cell debris and large aggregates (product or process-related), while maintaining and protecting the quality of the product in the flowthrough stream (Vicente et al., 2011b). The ultimate goal is to prepare the bioreactor bulk for further downstream processing, such as chromatography and ultrafiltration. Centrifugation and membrane filtration are the two most common unit operations utilized in this initial step.

Centrifugation is a unit operation widely used at laboratory scale to clarify bioreactor bulks. At industrial scale, continuous flow centrifugation is the process of choice. The most commonly utilized centrifuge configurations are tube cen-

trifuge, chamber centrifuge, and disc centrifuge. Only disc-stack centrifugation can operate in a semi-continuous way; these centrifuges are continuously fed with suspensions, clarified liquid is continuously removed, and solids are intermittently ejected (Jungbauer, 2013). The scalability of these centrifuges, particularly scaling down, is important for optimizing continuous processes. The smallest, commercially-available, continuous disc-stack centrifuge with intermittent solid removal must be fed at a minimum rate of 1 L/min. This rate is far too high for laboratory-scale optimization experiments, particularly when a continuous operation must be tested for several hours or days. A laboratory scaled-down continuous operation should mimic the shear stress conditions experienced by the fluid in regular conventional centrifuge. Thus, attempts are justified to develop scale-down tools for small-scale, continuous centrifuges (Boychyn et al., 2001; Westoby et al., 2011; Chatel et al., 2014).

On the other hand, microfiltration (MF) has been gaining favour as an alternative to centrifugation, and can be easily scaled up and implemented in a cGMP setting. MF membranes have pore sizes in the 0.1–10 μm range and can be classified as depth filters or "regular" filters depending on whether the solids are retained across the filter depth or only at its surface. Additionally, depth filters may include the use of filter aids, e.g., diatomaceous earth (DE), to modify their structure and charge (Ostreicher et al., 2008). Depth filters have been used for a wide variety of VLPs and viruses (enveloped and non-enveloped) with recovery yields reaching 90 % (Peixoto et al., 2008; Fernandes et al., 2012; Vicente et al., 2009; Kalbfuss et al., 2007; Peixoto et al., 2007). Depth filters are usually preferred for feed streams with high biomass content, sometimes lysed bulk, due to their ability to remove solids and impurities by different mechanisms (size exclusion and hydrophobic and/or electrostatic interactions) (Yigzaw et al., 2006).

Careful selection of the filter (pore size, filter material, and number and sequence of filter units) and operational parameters (inlet flow rate, pressure drop, conductivity, and pH) must be assessed in order to avoid virus loss and to retain solids and soluble impurities along the whole depth of the filter and not only at its surface. Essentially, the trade-off between feed flow rate/throughput and filter capacity/impurity removal should be evaluated (Singh et al., 2013; Roush and Lu, 2008).

Membrane microfiltration has also been performed either in normal (dead-end) or tangential flow (TFF) mode (Rodrigues et al., 2007b; Kalbfuss et al., 2007). Microfiltration is usually performed under low pressure, especially TFF (less than 0.7 bar), and is better suited for low-cell density bulks fermentation bulks (Liu

et al., 2010). However, membrane fouling or shear stress-induced cell lysis can become an issue for virus filtration (van Reis and Zydney, 2007).

The latest advances in upstream processing in terms of high cell density and increased protein titers are challenging the above-mentioned unit operations. As noted above, it has been recently reported that PER.C6 cell line is able to reach up to 10^8 cell/mL for HIV vaccine candidate productions , (Vellinga et al., 2014), and MDCK were infected with influenza virus (A/PR/8/34 (H1N1)) at 50×10^6 viable cell density (Genzel et al., 2014). Both results were obtained by employing a novel alternating tangential flow (ATF) perfusion system.

To cope with such high cell densities, novel microfilter configurations based on old established filter aids has been proposed in several patents. First, a thin protective layer of filter aid, called the precoat, is built up on the filter septum by recirculating a filter aid slurry. After precoating, small amounts of filter aid (body feed) are regularly added to the bioreaction bulk to be filtered. As filtering progresses, the filter aid, mixed with the suspended solids from the unfiltered bioreaction bulk, is deposited on the precoat. Thus, a new filtering surface is continuously formed. Such configuration reportedly permits an enhanced adsorption during mixing and the formation of a highly porous and permeable cake (body feed) supported by the filter aid, similarly to what is done in the brewing industry where diatomaceous earth (DE) is used to clarify beer (Freeman and McKechnie, 2003). Several patent applications claim that the body feed filtration (BFF) avoids membrane fouling and enables lower pressure operation over longer times at higher flow rates without compromising impurity removal. Recently published work (Thomassen et al., 2013) refers to the use of diatomaceous earth for clarification of poliovirus. In particular, Celite (577) filter aid deposited on stainless steel mesh filter with 75 μm pore size, followed by 0.45 and 0.22 μm, was used. However, the performance of this method was not disclosed and its potential remains unexplored.

As an alternative to centrifuges, small-scale decanters, with throughputs up to 30 ml/min, are commercially available, but the separation efficiency may be too low for many separation problems in the downstream processing of complex biopharmaceuticals (Jungbauer, 2013). Overall, the availability of small-scale equipment may be a driver for changing and improving operational modalities.

1.4 Concentration

Ultrafiltration (UF) is a key operation since large-scale processes produce high volumes of bulk (up to 2 kL for vaccines and 20 kL for mAbs), (Farid, 2007a) which should be concentrated 10–100 times prior to being further purified by chromatography. The volumetric concentration and exchange buffer of the virus bulk is critical not only to obtain high titer vector stocks in the proper formulation buffer, but also to reduce the handled volume; the latter accelerates the downstream processing and keeps the scalability of the purification train under manageable levels (Tatsis and Ertl, 2004).

Ultrafiltration is a pressure-driven separation process that employs anisotropic membranes with molecular weight cut-offs (MWCO) ranging from 0.5 to 1000 kDa (van Reis and Zydney, 2007). The MWCO is defined as the minimum molecular weight at which 90% of the solute is retained by the membrane. Ultrafiltration membranes are generally composed by two main layers: a thick macroporous support that provides mechanical strength, and a thin skin layer that is responsible for membrane selectivity and permeability (Liu et al., 2010). UF membranes can be manufactured using different polymers, such as regenerated cellulose (RC), polysulfone (PS), polyethersulfone (PES), and polyvinylidene fluoride (PVDF); RC and modified RC have often shown the best trade-off between low (unspecific) protein binding, mechanical strength, and resistance to cleaning procedures (chemical agents and temperature) (Liu et al., 2010; Zydney, 2009; van Reis and Zydney, 2006).

Ultrafiltration is frequently used to concentrate the bioproduct of interest. Consequently, the ultrafiltered concentrated feed suspension is obtained in the retentate stream and not in the permeate stream. UF membranes are selected in order to ensure rejection of the product of interest while impurities pass through the membrane to the permeate side. The medium, in which the product is suspended, may be exchanged by adding a buffer to the feed reservoir as the ultrafiltration progresses in a process called diafiltration, which is a technique that uses ultrafiltration membranes to completely remove, replace, or lower the concentration of salts or solvents from the original solution.

If the buffer is added at the same rate at which the permeate is removed, in the absence of membrane rejection, the concentration of a given component in the medium will decrease exponentially (Castino and Wickramasinghe, 1996).

UF is usually performed in tangential flow mode, wherein the cross flow at the membrane surface creates a “sweeping action” that avoids or lessens concentration

polarization and gel layer formation. UF processes are usually operated at a constant transmembrane pressure; however, operation at constant permeate flux or constant permeate pressure are also implemented in engineering practice (Liu et al., 2010). These are normally preferred when unfavorable effects, such as enhanced fouling or product quality deterioration, are associated with high concentration of the retained species at the membrane surface (Paulen et al., 2012). For most downstream processes of viral vectors UF is usually operated at constant transmembrane pressure.

The transmembrane pressure generally used in the downstream processing of viruses is between 0.5 and 1.4 bar, while the optimum cross flow rate can vary greatly due to particular structural stability of the virus: enveloped viruses are more labile than non-enveloped viruses and, thus, more prone to shear-induced damage (Rodrigues et al., 2007b; Subramanian et al., 2008). The membrane modules can be stacked in different geometries, such as, for example, flat-sheet cassette or hollow fibers (HF).

Although UF cassettes result in greater shear rates, these modules provide shorter processing times as the hydrodynamics of the flow channel is more effective than in HF at avoiding concentration polarization and gel layer formation (van Reis and Zydney, 2007; Wolff and Reichl, 2011). However, the majority of the published reports refers to the use of hollow fiber (HF) modules for virus processing (Wolff and Reichl, 2011; Rodrigues et al., 2007a) due to the fact that HF modules provide wider flow paths resulting in lower shear rates (van Reis and Zydney, 2007; Wolff and Reichl, 2011).

Ultrafiltration has been widely used for concentration as well as for buffer exchange (diafiltration, DF), and is present in almost every virus DSP described in the literature (Segura et al., 2013; Bandeira et al., 2012; Kamen and Henry, 2004; Rodrigues et al., 2007b; Segura et al., 2012; Wickramasinghe et al., 2005; Kalbfuss et al., 2007; Subramanian et al., 2008). The membranes used in virus UF have MWCOs in the range of 100–750 kDa allowing for reasonably high virus recovery (70–85 %). Despite increasing efforts in developing robust downstream processing, most of the research in the field of virus purification has focused on the chromatographic steps. Nevertheless a few papers have provided an in-depth study of the concentration/UF step: Negrete et al. (2014) optimized the use of hollow fibers for VLP concentration, Wickramasinghe et al. (2005) evaluated several PES membranes (micro and ultrafiltration) for the concentration of influenza virus, and Grzenia et al. (2008) evaluated four different small cut-off PES membranes for the purification of parvovirus particles. The rest of the available literature

is focused on virus removal by ultrafiltration membranes for biopharmaceuticals purification (Antony et al., 2014; Wickramasinghe et al., 2010; Peinador et al., 2011).

The ideal UF membrane should yield a very high separation factor, thus high product retention, but also a very high permeability. As correctly pointed out by Mehta and Zydney (2005), such membranes are not yet available in the market.

1.5 Density gradient centrifugation

Density gradient centrifugation (DGC), either with sucrose, caesium chloride, or iododixanol gradients, is a well-known and established, classic purification technique, generally used to purify limited amounts of bulk for preclinical studies. Briefly, the principle of the method is the separation of particles according to differences in density and, thereby, when applied to viruses to separate them from lighter and heavier cellular material. The main advantage of this technique is the ability to combine the concentration and purification steps in a single unit operation. Also, the technique offers a good resolution for separating full virions from empty capsids, which is very difficult to achieve by chromatography.

Although it is theoretically possible to band approximately 10^{15} virus particles in a single run with large-scale continuous ultracentrifugation, from an operational point of view the technique ends up being very laborious and very expensive to scale up. At large scale, DGC requires high capital and facility investments (Altaras et al., 2005). We are not aware of any reported attempts in the open literature to use DGC for large-scale manufacturing. The only notable exceptions are the continuous ultracentrifugation processes developed in the early 70's for influenza virus (Reimer et al., 1967)., Another issue in gradient ultracentrifugation is the citotoxicity of CsCl, extensively used for adeno- and adeno-associated viruses, which requires extensive dialysis to eliminate the residual CsCl from the final product. Given the drawbacks presented above, it is understandable that scalable chromatographic separation techniques have been the preferred techniques for large-scale DSP.

1.6 Chromatography

Chromatography has been widely used in the downstream processing of virus particles for capture, concentration, and purification of the feedstock. The chromatographic separation is driven by the selective physico-chemical interactions

between the viruses and closest impurities and the stationary phase; the separation can also be based on molecular sieving. Viruses have been purified using three different arrangements of the stationary phases: bead-based packed beds, membrane adsorbers, and monoliths. Beads are widely used in all the biopharmaceutical industry; nevertheless, for the vaccine purification they suffer from two main disadvantages: (i) limited flow rate imposed the compromise between pressure drop and mass transfer resistances, (ii) and, in most cases, low dynamic binding capacity, because the surface available for adsorption is limited to the external bead area. Viruses have sizes that range from 30 nm to 300 nm or larger and, as such, they cannot diffuse into the pores of most commercial adsorbent beads. However, bead-based chromatography is still used for purification of poliovirus and adeno-associated virus since the size of these viral particles, at around 30 nm, does not pose limited diffusion issues (Thomassen et al., 2013; Chahal et al., 2007).

Convective chromatography media, such as membranes and monoliths, offer substantial improvements in capacity, recovery, and reduction of process time. To date monoliths have generally offered large capacity and high resolution; they consist of a single block of a material with highly interconnected macropores through which the; biomolecules are transported by essentially convective flux (D'Souza et al., 2013); they are thus also known as convective interaction media (CIM). Monolithic columns are based on polymethacrylate and are manufactured with a radial geometrical design. Their use for viral purification has been extensively evaluated in the last years, both for enveloped and non-enveloped viruses. Recent examples include lentivirus , (Bandeira et al., 2012), baculovirus, (Gerster et al., 2013), rubella (Forcic et al., 2011), enterovirus 71 (Venkatachalam et al., 2014), and canine adenovirus purification (Fernandes et al., 2012). However, monoliths have shown to be prone to clogging, especially when high host cell DNA is present in the bioreactor bulk, although increasing the monolith pore size up to 6 μm is expected to solve this issue (Benčina et al., 2007).

Membrane adsorbers have emerged as a cost-effective strategy for processing large volumes of feed streams; they have been used in the biopharmaceutical industry almost exclusively in flowthrough mode for mAb purification (Weaver et al., 2013). They consistently yield low pressure drop and little compression or channelling, which simplifies the operating conditions. Furthermore, they are often used as a disposable unit, eliminating the need for lengthy cleaning and validation procedures. It should be pointed out that monoliths are following the same trend.

Despite the aforementioned advantages, membranes still have some drawbacks, such as low capacity and poor resolution. More recently, membrane adsorption chromatography has been applied to the purification of viral vectors in bind-and-elute mode, yielding recoveries of 60–80% (McNally et al., 2014; Nestola et al., 2014b; Peixoto et al., 2008).

Besides the three main adsorbent configurations used in virus purification, several surface chemistries are employed for the separation of the virus particles. The most common chromatographic modes are ion-exchange (IEX), affinity chromatography (AC), hydrophobic interaction (IC), mix-mode chromatography (MMC), and size exclusion chromatography (SEC).

Size exclusion chromatography can only be achieved with bead-based porous media and not with membrane adsorbers or monoliths. The separation is based on the difference in molecular size between the virus particles and the impurities; the former are excluded from the porous matrix and, hence, elute in the interparticle volume, whereas the latter elute through the porous matrix at different rates. The operation conditions of SEC are gentle, allowing to maintain infectivity and immunogenicity, especially critical for labile viruses. SEC is often used at the later stage of the downstream train and often employed as a polishing step. However, purification schemes where SEC is followed by IEX have also been reported in the literature; two prominent examples are the works of Kalbfuss et al. (2007) and Eglon et al. (2009) for influenza and adenovirus, respectively. The main drawbacks of SEC are low capacity, product dilution, and poor pressure resistance of the matrix. Despite these disadvantages this technique has been used in several viral purification trains reported in the literature.

Currently, the purification of viruses by using IEX is typically operated in the positive (bind-elute) mode: most of the impurities are collected in the flow-through pool, while the virus particles and some of the impurities are retained in the matrix. Due to the differences in charge of the different biomolecules it is possible to use this process with high resolution elution gradients, separating the solutes into fractionated cuts, even though they are closely related. Based on the isoeletric point of the viruses, anionic or cationic exchangers are used. Among the anionic-exchange chemistries, diethylaminoethanol (DEAE) and quaternary ammonium (Q) ligands are the most utilized. However, due to the multipoint adsorption nature of the viruses to the matrix, ligand densities and chemistry need to be carefully selected. Nestola et al. (2014b) and Vicente et al. (2011a) have shown that optimal ligand densities are below 2.2 μmol/cm^2 for adenovirus and baculovirus purification and enveloped and non-enveloped virus, respectively.

Moreover, not only the ligand density, but also the membrane structure with the presence of the hydrogel layer, appear to play an important role in the adsorption process (Nestola et al., 2014b).

One drawback of the Q ligand is that the binding is compromised at high salt concentration. Therefore, new ligands based on primary amine have been investigated. STIC® chromatography membranes (Sartorius Stedim Biotech) and ChromaSorb (Merck Millipore) are two examples of commercially available products based on primary amine ligands. Nevertheless, there is still a limited number of published work on the performance analysis of these novel chromatographic ligands (Woo et al., 2011) (Kang et al., 2012b). Moreover, no attempts to use membrane chromatography in flow-through mode for virus purification have been reported in the open literature. As for the cation exchangers they are mainly used for viruses with isoelectric points above 6; some influenza strains have been purified by using sulfonic acid chemistry as reported by Banjac et al. (2014).

Affinity chromatography is based on the specific and reversible adsorption of a ligand with a component of the virus capsid. This technique has been extensively used at laboratory scale. Some examples are zinc affinity for adenovirus (Lee et al., 2009), influenza (Opitz et al., 2009), heparin (Wolff et al., 2010; de las Mercedes Segura et al., 2007) and specific antibody or antibody fragments (Cameron-Smith and Harbour, 2001). However, affinity chromatography at a larger scale requires strong and specific interaction; ideally, the ligand should have a high binding kinetic constant and mild dissociation conditions. Currently, in the biopharmaceutical industry the most used affinity chemistry used at a large scale is Protein A for mAb purification. Recently a recombinant version of F25 monoclonal antibody was used for the purification of a new recombinant factor VIII. The F25 monoclonal antibody was found to recognize an epitope within the C-terminal part of the heavy chain from amino acid residue 725 to 740 (Thim et al., 2010). The current large cost for the purification and immobilization of the ligand makes affinity chromatography very costly to scale-up for virus purification; also representing a drive for the search of new cheaper ligands.

HIC chromatography has been rarely used, except for some specific applications in Vaccinia virus (Wolff et al., 2010). This is mainly due to the fact that high salt concentration, and sometimes also kosmotropic salts, are needed, which can affect the integrity of the virus capsid. This is especially critical when viral vectors are used in gene therapy, where maintaining the infective titers throughout the purification train is critical.

Multimodal or mixed-mode (MM) chromatography simultaneously employs

various multimodal binding mechanisms, such as ionic interaction, hydrogen bonding, and hydrophobic interaction. A typical example of MM media is hydroxyapatite (HAp). HAp is a very complex crystalline compound that adsorbs a wide variety of substances; the mechanisms underlying virus adsorption to HAp are, however, still obscure. Recently, the purification of dengue virus with 64% recovery was reported (Yae et al., 2012). The same research group investigated the fundamental mechanism of adsorption and desorption of dengue virus onto HAp media by scanning electron microscopy (SEM) (Saito et al., 2013). In this study, dengue viruses were bound to the HAp surface by electronic interactions, and, subsequently, virus envelope fusion was thought to occur with temperature dependence. These results suggested that virus-HAp interactions were substantially similar to virus-cell interactions.

Notwithstanding the use of the well established technologies for virus separation discussed above, some new concepts have been recently proposed, such as steric exclusion chromatography (SXC). The principle is based on the capture of the target biomolecule at a non-reactive hydrophilic surface by its mutual steric exclusion of polyethylene glycol (PEG) (Lee et al., 2012). No direct chemical interaction between the target and the solid phase is required. Elution is achieved by reducing the PEG concentration. The selectivity is generally dominated by the size of the target biomolecule and the size and concentration of the PEG. The above mentioned study focused on the purification of IgM and bacteriophage M13K07, but the authors claim that the principle can be applied to other viruses or large biopharmaceuticals as a replacement of size-exclusion chromatography (SEC). There are, however, some fundamental differences between the two size-exclusion techniques. Whereas in SXC the selectivity correlates with molecular size, with larger species retained more strongly than smaller species, the reverse applies in SEC. Also, Lee et al. (2012) successfully implemented SXC in hydroxyl-substituted polymethacrylate monoliths, which provide a hydrophilic surface and support convective mass transport that is unaffected by the viscosity of the PEG; SEC is still limited to the packed-bed configuration.

Most of the applications described in the literature for virus purification are based on positive mode, where the target product binds to the matrix. Nevertheless, negative modes are being developed and an interesting review by Lee et al. (2014) details several applications. In particular, new bead-based resins have been developed for intermediate virus purification and polishing in flow-through mode. Iyer et al. (2011) proposed the increase of the mean bead diameter to maximize the binding capacity for the impurities and reduce the overall column

surface available for virus binding. GE Healthcare recently launched Capto Core 700, a resin composed of an active core, functionalized with octylamine ligand, and an inactive porous shell that excludes larger molecules from entering the core, thus allowing them to be collected in the flow-through. The core has multimodal binding ligands that allow operation at various ranges of pH and NaCl concentrations. Recent work showed that the amount of ovalbumin was greatly reduced in a influenza A purification process (Blom et al., 2014); and the same resin was successfully used for the polishing step of canine adenovirus (Fernandes et al., 2012).

One apparent limitation of negative mode is due to the difficulty to efficiently remove the impurities as compared to positive-mode chromatography; thus so far, negative mode has been implemented only as a polishing step. Although much work is still required to promote negative-mode chromatography as a purification platform, its potential should not be underestimated, especially for viral vaccines where different serotypes or strains may influence the binding and elution behavior, leading to routine optimization for every new viral vaccine candidate in the pipeline.

1.7 Disposable technologies

Disposable technologies are very appealing for bioprocessing and can definitely play an important role in many process intensification strategies. Disposable equipment became popular for upstream production in the 1990s, with the advent of single-use media bags and bioreactors and the use of disposable capsules for sterile filtration. Over the next few years, disposable concepts also began to appear in downstream processing. Initially, there were only buffer bags and devices for normal flow filtration, including virus filtration and guard filters for chromatographic columns, but gradually more complex concepts were introduced, including disposable devices for tangential flow filtration and chromatography (Gottschalk, 2010).

Most of the DSP unit operations described in the previous section are ready to be fully disposable, from the clarification and concentration to the chromatography for both capture and polishing. Furthermore, GE Akta devices have also the possibility for disposable flow-path.

A disadvantage of current single-use systems is the limitation in the scale of operation. While disposable bioreactors for cell culture are available up to 2000 L, the current single-use DSP technologies are struggling to keep up with these

capacities. For very large-scale DSP applications, it is difficult to find pumps, piping, and probes that are actually single-use. However, at development and pilot scales, or for small commercial production, some fully single-use systems (such as the Sius TFF Skid) already represent good solutions for single-use implementation. This scale-related limitation can also be partially solved when systems are used in continuous mode.

1.8 Process intensification

Process intensification is an approach to process development originally pioneered in the chemical industry by ICI (Imperial Chemical Industries, London, UK) in the early 90's. The aim was to reduce plant size while maintaining productivity, thus decreasing cost of goods by lessening capital investments and overhead costs. Process intensification requires new concepts to manage plant throughput when existing technologies are approaching their physical limit, as is the case of DSP in the biopharmaceutical industry. Indeed, the increasing interest in vaccines and gene therapy, together with the need to decrease the cost per dose, has led to the development of new chromatographic tools or their conversion from other application areas (Barut et al., 2005; Riordan et al., 2009; Vicente et al., 2011a).

A classic viral downstream process consists of discrete sequential unit operations, such as the ones described in the previous sections. The number of unit operations can vary greatly depending on the final product specification, therapeutic dose, and administration route (i.e., oral, blood, intranasal, etc.). However, by connecting previously separate unit operations or combining individual steps into one unit operation, product losses and process economics can be minimized. Integrated processes are required to reduce the number of processing steps to simplify handling, and to shorten the time that a sensitive labile product such as an enveloped virus, has to be in contact with harsh conditions, with the overall aim to reduce the total processing cost and increasing product quality.

One solution that could streamline the downstream train is the implementation of technologies such as aqueous two-phase partition (ATPS) and expanded-bed adsorption (EBA), which could potentially combine two or more unit operations in a single step (D'Souza et al., 2013) (Table 1.2).

Table 1.2: *Process intensification approaches recently employed in viral downstream processing. SXC, EBA, and ATPS stand for, respectively, steric-exclusion chromatography, expanded-bed adsorption, and aqueous two–phase separation; Rec is a shorthand for recovery.*

Purification tool	Virus	Rec (%)	Ref.
Capto Core 700	Influenza,	69	(Fernandes et al., 2012)
	Canine Adenovirus	86	(Blom et al., 2014)
SXC	Bacteriophage M13K07	90	(Lee et al., 2012)
EBA	Adenovirus (Ad5)	65	(Peixoto et al., 2006)
ATPS	Adenovirus	90	(Negrete et al., 2007)
	Adeno associate (AVV8)	97	(Guo et al., 2012)
	VLP Rotavirus	85	(Benavides et al., 2006)
	VLP B19	92	(Luechau et al., 2011)

Aqueous two-phase systems are spontaneously formed by mixing two solutions of different polymers (PEGs, dextran, polyacrilates) or a polymer and a kosmotropic salt (phosphate, citrate, sulphate). The partitioning of the biomolecule can then occur into one of the two phases. ATPS has been employed for a variety of protein separations, including mAbs (Oelmeier et al., 2010). Recent work has demonstrated that high product yield and large HCP reduction can be achieved (Cramer and Holstein, 2011). So far, ATPS has barely been explored for virus recovery. A few examples include adenovirus recovery from a crude lysate of HEK293 by using PEG 300-phosphate system yielding 90% of infectious particles (Negrete et al., 2007), and recovery of adeno-associated serotype 8 virus (AVV8) (Guo et al., 2012). The latter employed 10%PEG8000-13.2 $(NH_4)_2SO_4$ at pH 8.0 in HEPES buffer, yielding a purity even higher than conventional CsCl gradient density centrifugation methods. Lately, ATPS was also investigated for the purification of VLPs, namely rotavirus (Benavides et al., 2006) and B19 (Luechau et al., 2011) with recoveries of 85% and 92%, respectively. The main advantage of ATPS is its feasibility to operate in a continuous mode. However, the incorporation of this technology into an industrial setting is still lagging. This can be attributed to the fact that the mechanisms governing the partition of complex biopharmaceuticals are still not well understood, and the development of the method is rather empirical and laborious. Nevertheless, new advances in high throughput screening (HTPS) can eliminate these bottlenecks. Indeed promising preliminary results have been shown by using monoclonal antibody by Oelmeier et al. (2012). The same research group investigated the partition of avidin protein in aqueous two phase separation by HTPS (Diederich et al., 2013).

Expanded bed chromatography (EBA) is based on the utilization of a fluidized

bed whose expansion is controlled by the upward flow of the mobile phase. EBA can process crude feedstock and can potentially replace the clarification and capture steps. The first generation of EBA adsorbents (Streamline, GE Healthcare), which consisted of slightly heavier agarose beads, was successfully applied to the purification of Adenovirus serotype 5 (Ad5) (Peixoto et al., 2006; Lusky, 2005). Nevertheless, some of the EBA drawbacks are mainly related to an unfavorable biomass-adsorbent interaction,and led to the failure of several proposed industrial processes (D'Souza et al., 2013). However, the development of second-generation EBA adsorbents (Rhobust, DSM) has led to a significant improvement; these new EBA beads are high density tungsten carbide-cored beads coated with cross-linked agarose, and are available with several types of functionalities. Although the new EBA media presents clear advantages over the first generation of materials, such as high operational flow rates up to 300–600 cm/h, they have not yet been applied for processing viral vaccines and vectors.

One process-based way to reduce the overall cost of the downstream chromatographic steps is by changing to continuous processing mode; this, in principle, yields higher throughput, lower buffer consumption, higher capacity utilization and reduced column volumes, hence increased productivity. In particular, simulating moving bed (SMB) chromatography, which is the best practical implementation of continuous countercurrent solid-fluid chromatography (Seidel-Morgenstern et al., 2008; Silva et al., 2012), is now widely applied for the binary separation of small molecules, in particular chiral compounds under isocratic elution conditions (Francotte and Richert, 1997; Rajendran et al., 2009).

Studies concerning continuous downstream bioprocessing have targeted mostly proteins and monoclonal antibodies (mAb) (Aumann and Morbidelli, 2007; Silva et al., 2010b; Bochenek et al., 2013); this is primarily because the biopharmaceutical industry is currently dominated by these bioproducts. The systems currently employed in biopharmaceutical industry are as: MCSGP, GSSR, 3C-PCC, Bio-SC, and Capture SMB. All of them have proven their ability to purify complex multicomponent biological mixtures at laboratory scale with typically two to three (maximum of four) columns (Nicoud, 2014). Recently, Genzyme and Genentech's scientists have developed a continuous process for purification of mAbs and recombinant therapeutic enzymes using HIC and affinity chromatography (Warikoo et al., 2012; Godawat et al., 2012; Mahajan et al., 2012).

In the conventional batch operation the chromatographic matrix is loaded until product breakthrough is detected at the outlet (i.e., 5–10% of feed concentration). This means that only a fraction (between 30 and 70%) of the chromatographic

resin capacity is used, because breakthrough happens before the matrix gets fully loaded. In 3C-PCC, Bio-SC, and Capture SMB the breakthrough effluent is loaded onto the next column enabling the loading of the first column until exhaustion (up to static binding capacity). A similar approach is concurrently employed to the other steps of the cycle (such as elution, washing, and equilibration). This strategy enables reduced buffer consumption, shorter processing times and better matrix usage (with concurrent investment and facility footprint savings) (Godawat et al., 2012; Warikoo et al., 2012).

To date, the continuous purification of large biomolecules, such as viruses, has rarely been explored. Kröber et al. (2013) recently implemented a classical three-zone, open-loop SMB for influenza virus purification. Elution was performed isocratically by employing a size-exclusion medium. These authors have successfully increased the productivity by switching to simulated countercurrent operation. The only drawback of the proposed process was the co-elution of DNA with the virus since the bulk was not pretreated with benzonase. Nevertheless, this was the first attempt of using SMB in virus purification.

More recently Nestola et al. (2014a) proposed more compact, efficient, simulated countercurrent chromatographic (SCCC) process that was used for adenovirus purification. As used for the earlier cited work on influenza, a SEC medium was employed but the number of columns used was reduced from three to two. The performance of the process yielded a 6-fold productivity increase, and boosted recovery yield to 86% coupled with clearances of 90% and 89% for DNA and HCP, respectively. These two works are, so far, the state-of-the-art for continuous or quasi-continuous chromatography for viral vaccine or vectors (Table 1.3).

Table 1.3: *(Semi-)continuous chromatography applications in viral processing based on simulating moving bed (SMB) technology. SFF4 stands for Sepharose 4 Fast Flow (GE Healthcare).*

	3-column SMB	2-column SCC
Media	Size exclusion (SFF4)	Size exclusion (SFF4)
Elution type	Isocratic	Isocratic
Virus	Influenza (H1N1)	Adenovirus (Ad5)
Recovery (%)	70	86.3
Productivity	3.8-fold increase	6.1-fold increase
Feed	Continuous	Quasi-continuous
Cycle design	Triangle theory	Non-linear optimization
Reference	(Kröber et al., 2013)	(Nestola et al., 2014)

A classic approach for the design of an SMB process is depicted in Fig. 1.2:

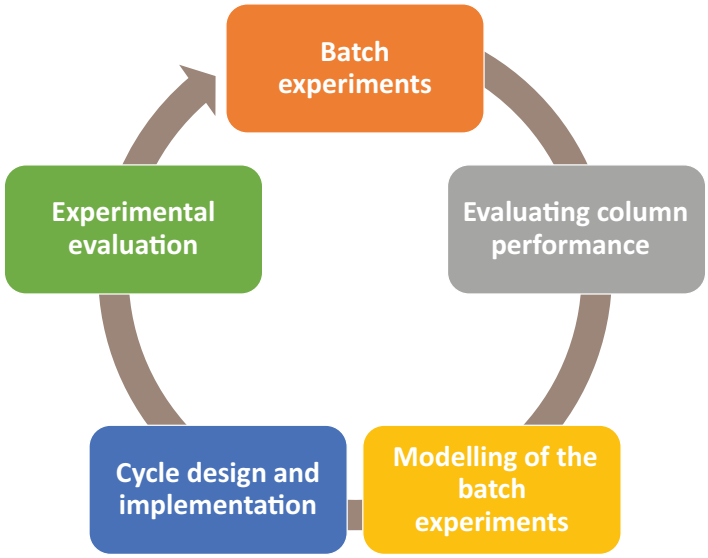

Figure 1.2: *Classic design steps to undergo for the implementation of an SMB technology.*

(i) the chromatograms from batch experiments provide the basic information about the retention factors and broadening of the peaks of interest, (ii) the packing reproducibility and efficiency of the SMB columns are assessed; (iii) the batch experiments are frequently modeled to a finer extent to better predict the propagation of the concentration fronts under conditions of finite column efficiency and overloaded conditions; (iv) the SMB cycle is designed based on the previously determined chromatographic data; (v) finally, the cycle is validated experimentally and the operating parameters are fine-tuned if deemed necessary.

Despite the clear advantages of continuous chromatography, as demonstrated by the works cited above, the biopharmaceutical industry is still hesitating to switch to continuous or quasi-continuous, multi-column chromatography. This is, in part, due to the fact that innovation in this industry has traditionally been more product- than process-oriented, but also due to the increased complexity in terms of process design and validation. However, companies like Tarpon are mitigating these issues by commercializing a fully disposable system called BioSMB. It is also often argued that the volume processed for viral vector or vaccines is rather modest, and therefore continuous processing would not have a large added value. Although this argument can be accepted to some extent, the pressure for a significant decrease of the cost per dose, thus the cost of goods,

is a strong driver for switching from batch to continuous chromatography in line with the trend followed by other industries in the past (Nicoud, 2014). The current tendency in the biopharmaceutical industry is a decrease of the number of chromatographic columns used in the downstream train, which makes the implementation of continuous operation somewhat less relevant. This is not a strong drawback, provided that the plant is well designed and the simulated counter-current contact between the fluid phase and the adsorbent media is maintained.

Overall, chromatography is only a part of the global process including upstream and downstream, and real improvements are really beneficial when a large part of the process is switched to continuous. In this respect there is still work to be done, although some of the examples cited above constitute a promising start.

1.9 Process understanding

Proper understanding and characterization of the process is needed to move towards a full process intensification. Also, in many ways the Quality by Design (QbD) initiative requires a thorough understanding of the product and its manufacturing process (McCurdy et al., 2011). For QbD, the product- and process-knowledge base must include an understanding of the variability in raw materials, the relationship between the process's and product's critical quality attributes (CQAs), and the association between CQAs and the product's clinical properties.

Downstream optimization still relies mainly on empirical-based strategies because most of the biophysico-chemical properties of complex biomolecules are not fully understood. Nevertheless, new tools, mainly related to high throughput screening, are easing the problem. It is appropriate to distinguish two main tools that are used for process understanding, namely Design of Experiments (DoE) and mechanistic or semi-empirical model-based knowledge (Fig.1.3).

In this section both methods are briefly explored, although their application in vaccine process development has been scarcely reported in the literature.

DoE relies on the fitting of multivariate data to an empirical function, usually linear or quadratic with interaction terms, which can be used to provide information about the system (maxima and minima, trends as parameters are changed, etc.). Statistical theory is used to select values of each factor to generate the data, and to maximize the information about the function parameters. Randomization of the order of experiments minimizes, as far as possible, the effects of

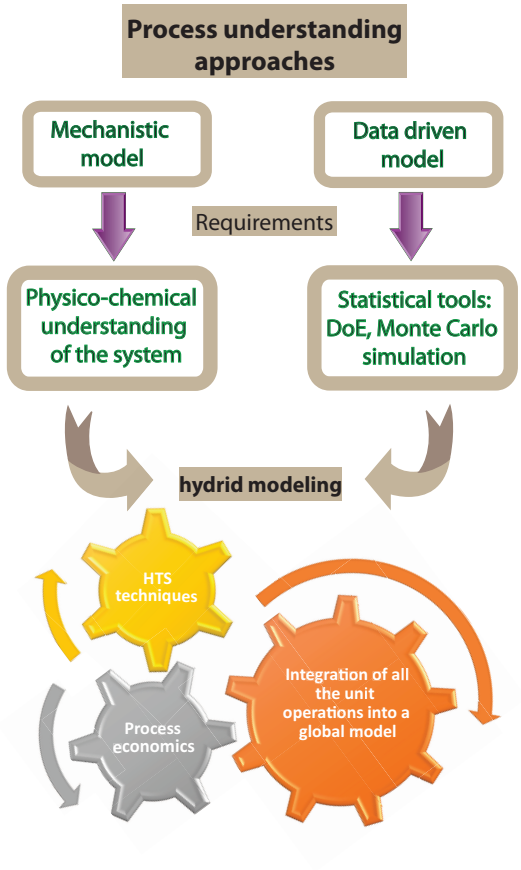

Figure 1.3: *Different approaches to increase process knowledge in downstream processing. Mechanistic modeling requires a deep understanding of the physico-chemical property of the system, whereas a data-driven model requires the use of statistical tools such as DoE or Monte Carlo simulations. However, the two approaches can complement each other and provide more robust process knowledge, together with the use of high throughput screening techniques, the integration of all the unit operations and the process economics parameters.*

any uncontrolled variables (e.g., laboratory temperature), which contribute to the repeatability variance but do not affect the results in a systematic way (Hibbert, 2012).

Although often considered as an industrial optimization tool, the number of scientific publications employing DoE has increased in the last years (Hibbert, 2012). Nestola et al. (2014b) implemented a DoE evaluation on a 96-well platform for assessing the effect of the stationary phase's ligand density and salt concentration on adenovirus adsorption/desorption. A similar approach was used for optimization of baculovirus purification (Vicente et al., 2011a). Although the DoE approach is able to deliver helpful information, mainly for assessing the critical parameters of the design space, its use is considered as a black box approach, since it does not provide fundamental information regarding the mechanistic model that governs the biomolecule–resin interaction.

Mechanistic knowledge had been used, to some extent, in the design and optimization of virus downstream processing trains. For IEX chromatography of biomolecules, the most utilized adsorption model is the steric mass action (SMA) model (Brooks and Cramer, 1992), which can predict the binding and elution behaviour if good estimations of the characteristic charge, equilibrium constants, and steric factors are available. Some efforts have been initiated to describe a VLP elution chromatogram using the SMA model (Vicente et al., 2008). However, in this preliminary study the contribution of the impurities (many of them with unknown properties) was not included in the multicomponent model. When the SMA model is applied to describe the IEX mechanism of large biopharmaceuticals, it is somewhat difficult to determine the characteristic charge, as shown by Yamamoto et al. (2007) who studied the retention behavior of oligo-DNA onto an anionic exchange monolith. Indeed, for a characteristic charge larger than ca. 50 it can be quite challenging to determine this parameter experimentally. However, even more trickier is to use the SMA model in model-based process design and optimization due to the difficulties of numerically solving the differential material balance of an IEX adsorber for large values of the characteristic charge.

Nonlinear mathematical programming was used in another study (Nestola et al., 2014b) in an attempt to determine adsorption isotherms by an inverse method based on the fitting of the breakthrough curves of adenovirus particles and its related impurities (HCP and DNA). Partition coefficients and column efficiency measurements have also been used for the optimal design of a two-column SMB cycle for adenovirus purification with excellent agreement between the experimental concentration profiles and the theoretical ones (Nestola et al.,

2014a).

Despite the recent advances in process understanding by using more or less complex mathematical modelling tools, most of the works described in the literature are focused on the design or optimization of a single unit operation, mainly chromatography, although ultrafiltration has also been the subject of modeling efforts; e.g., Kanani and Ghosh (2007) described a novel approach for predicting permeate flux decline in constant pressure mode, while Paulen et al. (2012) reported an optimum feeding strategy for diafiltration. Nonetheless, model-based global optimization of the whole process by integrating several unit operations has not been attempted so far.

A common approach in the biopharmaceutical industry is the use of simulation software for cost of goods estimation intended to model all the aspects of the process. Well known examples are Intelligen SuperPro Designer, Aspen Batch Plus, and, more recently, BioSolve. This type of software is best suited to provide a format for process management, using material and energy balances to answer scheduling questions, explore equipment change-outs, and calculate cost data. However, the ability of simulation software to accurately predict unit operation scale-up and perform bioprocess optimization is limited (Shanklin et al., 2001). Still, several papers are available describing process economics for different mAbs (Stonier et al., 2012; Farid, 2007b), but for viral vaccines no data are available in the literature with the exception of a very recent study of VLP process economics (Chuan et al., 2014). In this study, Monte Carlo simulation was employed to identify the variance in the unit production cost (UPC) and, through bioprocess simulation data, it was shown that a vaccine could be manufactured at 1 cent (USD) per dose using bioreactor sizes of 500 and 300 L.

Finally, for an ideal process understanding, the combination of a response model (DoE) with a mechanistic model should be considered. The combination of the two modeling approaches is often referred to as hydrid modeling. Published studies in which this modeling strategy was implemented require the use of high throughput screening (HTS) methods for the determination of physicochemical and thermodynamic properties (Nfor et al., 2009). By using HTS, Nfor et al. (2012) estimated the linear IEX isotherm parameters of a crude protein mixture (effective charge and equilibrium constant) from multiple linear NaCl-gradient experiments according to the approach of Cramer and co-workers, (Gadam et al., 1993; Ladiwala et al., 2005), while the steric factor was estimated by inverse fitting (Osberghaus et al., 2012) using experimental salt-gradient chromatograms obtained under overloaded conditions. For this purpose, the major protein peaks

were defined as pseudo components, that is, groups of proteins showing comparable retention/elution behaviour. To our knowledge, the application of this kind of approach for viral vaccines and vectors has not been reported to date.

Acknowledgments

Support for PhD scholarship from Sartorius Stedim Biotech and from the Portuguese Science Foundation FCT-MCTES (SFRH/BD/82032/2011, PTDC/EBB-BIO/119501/2010, and EXPL/BBB-EBB/0790/2012) is gratefully acknowledged. The authors do not have any conflicts of interest.

References

Altaras, N. E., Aunins, J. G., Evans, R. K., Kamen, A., Konz, J. O., and Wolf, J. J. (2005). Production and formulation of adenovirus vectors. *Adv Biochem Eng Biotechnol*, *99*, 193–260.

Antony, A., Blackbeard, J., Angles, M., and Leslie, G. (2014). Non-microbial indicators for monitoring virus removal by ultrafiltration membranes. *J Membr Sci*, *454*, 193–199.

Aumann, L., and Morbidelli, M. (2007). A continuous multicolumn countercurrent solvent gradient purification (MCSGP) process. *Biotechnol Bioeng*, *98*, 1043–1055.

Baden, L. R., Walsh, S. R., Seaman, M. S., Tucker, R. P., Krause, K. H., Patel, A., Johnson, J. A., Kleinjan, J., Yanosick, K. E., Perry, J. et al. (2013). First-in-human evaluation of the safety and immunogenicity of a recombinant adenovirus serotype 26 hiv-1 env vaccine (ipcavd 001). *J Infect Dis*, *207*, 240–247.

Bandeira, V. S., Peixoto, C., Rodrigues, A. F., Cruz, P., Alves, P., Coroadinha, A. S., and Carrondo, M. (2012). Downstream Processing of Lentiviral Vectors: releasing bottlenecks. *Hum Gene Ther Methods*, *23*, 255–263.

Banjac, M., Roethl, E., Gelhart, F., Kramberger, P., Jarc, B. L., Jarc, M., Štrancar, A., Muster, T., and Peterka, M. (2014). Purification of vero cell derived live replication deficient influenza a and b virus by ion exchange monolith chromatography. *Vaccine*, *32*, 2487–2492.

Barut, M., Podgornik, A., Brne, P., and Štrancar, A. (2005). Convective interaction media short monolithic columns: enabling chromatographic supports for the separation and purification of large biomolecules. *J Sep Sci*, *28*, 1876–1892.

Benavides, J., Mena, J. A., Cisneros-Ruiz, M., Ramírez, O. T., Palomares, L. A., and Rito-Palomares, M. (2006). Rotavirus-like particles primary recovery from insect cells in aqueous two-phase systems. *J Chromatogr B*, *842*, 48–57.

Benčina, K., Benčina, M., Podgornik, A., and Štrancar, A. (2007). Influence of the methacrylate monolith structure on genomic dna mechanical degradation, enzymes activity and clogging. *J Chromatogr A*, *1160*, 176–183.

Blom, H., Åkerblom, A., Kon, T., Shaker, S., van der Pol, L., and Lundgren, M. (2014). Efficient chromatographic reduction of ovalbumin for egg-based influenza virus purification. *Vaccine*, *http://dx.doi.org/10.1016/j.vaccine.2014.04.033*.

Bochenek, R., Marek, W., Piatkowski, W., and Antos, D. (2013). Evaluating the performance of different multicolumn setups for chromatographic separation of proteins on hydrophobic interaction chromatography media by a numerical study. *J Chromatogr A*, *1301*, 60–72.

Boychyn, M., Yim, S., Ayazi Shamlou, P., Bulmer, M., More, J., and Hoare, M. (2001). Characterization of flow intensity in continuous centrifuges for the development of laboratory mimics. *Chem Eng Sci*, *56*, 4759–4770.

Brooks, C. A., and Cramer, S. M. (1992). Steric mass action ion exchange: displacement profiles and induced salt gradients. *AIChE J.*, *38*, 1969–1978.

Cameron-Smith, R., and Harbour, C. (2001). Removal of poliovirus type 1 from a protein mixture using an immunoaffinity chromatography column. *Biomed Chromatogr*, *15*, 471–483.

Castino, F., and Wickramasinghe, S. (1996). Washing frozen red blood cell concentrates using hollow fibres. *J Membr Sci*, *110*, 169–180.

Chackerian, B. (2007). Virus-like particles: flexible platforms for vaccine development. *Expert Rev Vaccines*, *6*, 381–390.

Chahal, P. S., Aucoin, M. G., and Kamen, A. (2007). Primary recovery and chromatographic purification of adeno-associated virus type 2 produced by baculovirus/insect cell system. *J Virol Methods*, *139*, 61–70.

Chatel, A., Kumpalume, P., and Hoare, M. (2014). Ultra scale-down characterization of the impact of conditioning methods for harvested cell broths on clarification by continuous centrifugationrecovery of domain antibodies from rec e. coli. *Biotechnol Bioeng*, *111*, 913–924.

Chuan, Y. P., Wibowo, N., Lua, L. H., and Middelberg, A. P. (2014). The economics of virus-like particle and capsomere vaccines. *Biochem Eng J*, *http://dx.doi.org/doi:10.1016/j.bej.2014.06.005*.

Cramer, S. M., and Holstein, M. A. (2011). Downstream bioprocessing: recent advances and future promise. *Curr Opin Chem Eng*, *1*, 27–37.

Diederich, P., Amrhein, S., Hämmerling, F., and Hubbuch, J. (2013). Evaluation of peg/phosphate aqueous two-phase systems for the purification of the chicken egg white protein avidin by using high-throughput techniques. *Chem Eng Sci*, *104*, 945–956.

D'Souza, R. N., Azevedo, A. M., Aires-Barros, M. R., Krajnc, N. L., Kramberger, P., Carbajal, M. L., Grasselli, M., Meyer, R., and Fernández-Lahore, M. (2013). Emerging technologies for the integration and intensification of downstream bioprocesses. *Pharm Bioprocess*, *1*, 423–440.

Eglon, M. N., Duffy, A. M., O'Brien, T., and Strappe, P. M. (2009). Purification of adenoviral vectors by combined anion exchange and gel filtration chromatography. *J Gene Med*, *11*, 978–989.

EMEA (1999). Specifications: test procedures and acceptance criteria for biotechnological/biological products. *ICH Q6B*, .

Ewer, K. J., OHara, G. A., Duncan, C. J., Collins, K. A., Sheehy, S. H., Reyes-Sandoval, A., Goodman, A. L., Edwards, N. J., Elias, S. C., Halstead, F. D. et al. (2013). Protective cd8+ t-cell immunity to human malaria induced by chimpanzee adenovirus-mva immunisation. *Nat Commun*, *4*, 2836.

Farid, S. S. (2007a). Process economics of industrial monoclonal antibody manufacture. *J Chromatogr B*, *848*, 8–18.

Farid, S. S. (2007b). Process economics of industrial monoclonal antibody manufacture. *J Chromatogr B*, *848*, 8–18.

Fernandes, P., Peixoto, C., Santiago, V. M., Kremer, E. J., Coroadinha, A. S., and Alves, P. M. (2012). Bioprocess development for canine adenovirus type 2 vectors. *Gene Ther*, *20*, 353–360.

Forcic, D., Brgles, M., Ivancic-Jelecki, J., Šantak, M., Halassy, B., Barut, M., Jug, R., Markušić, M., and Štrancar, A. (2011). Concentration and purification of rubella virus using monolithic chromatographic support. *J Chromatogr B*, *879*, 981–986.

Francotte, E. R., and Richert, P. (1997). Applications of simulated moving-bed chromatography to the separation of the enantiomers of chiral drugs. *J Chromatogr A*, *769*, 101–107.

Freeman, G. J., and McKechnie, M. T. (2003). Filtration and Stabilization of Beers. In A. G. H. Lea, and J. R. Piggott (Eds.), *Fermented Beverage Production* (pp. 365–392). Springer.

Gadam, S. D., Jayaraman, G., and Cramer, S. M. (1993). Characterization of non-linear adsorption properties of dextran-based polyelectrolyte displacers in ion-exchange systems. *J Chromatogr A*, *630*, 37–52.

Geels, M., and Ye, K. (2010). Developments in high-yield system expressed vaccines and immunotherapy. *Recent Pat Biotechnol*, *4*, 189.

Genzel, Y., Vogel, T., Buck, J., Behrendt, I., Ramirez, D. V., Schiedner, G., Jordan, I., and Reichl, U. (2014). High cell density cultivations by alternating tangential flow (atf) perfusion for influenza a virus production using suspension cells. *Vaccine*, *32*, 2770–2781.

Gerster, P., Kopecky, E.-M., Hammerschmidt, N., Klausberger, M., Krammer, F., Grabherr, R., Mersich, C., Urbas, L., Kramberger, P., Paril, T., Schreiner, M., Nöbauer, K., Razzazi-Fazeli, E., and Jungbauer, A. (2013). Purification of infective baculoviruses by monoliths. *J Chromatogr A*, *1290*, 36–45.

Ginn, S. L., Alexander, I. E., Edelstein, M. L., Abedi, M. R., and Wixon, J. (2013). Gene therapy clinical trials worldwide to 2012–an update. *J Gene Med*, *15*, 65–77.

Godawat, R., Brower, K., Jain, S., Konstantinov, K., Riske, F., and Warikoo, V. (2012). Periodic counter-current chromatography - design and operational considerations for integrated and continuous purification of proteins. *Biotechnol J*, *7*, 1496–1508.

Goerke, A. R., To, B. C. S., Lee, A. L., Sagar, S. L., and Konz, J. O. (2005). Development of a novel adenovirus purification process utilizing selective precipitation of cellular DNA. *Biotechnol Bioeng*, *91*, 12–21.

Gottschalk, U. (2010). Disposables in downstream processing. *Adv. Biochem. Eng. Biotechnol.*, *115*, 171–183.

Grzenia, D. L., Carlson, J. O., and Wickramasinghe, S. R. (2008). Tangential flow filtration for virus purification. *J Membr Sci*, *321*, 373–380.

Guo, P., El-Gohary, Y., Prasadan, K., Shiota, C., Xiao, X., Wiersch, J., Paredes, J., Tulachan, S., and Gittes, G. K. (2012). Rapid and simplified purification of recombinant adeno-associated virus. *J Virol Methods*, *183*, 139–146.

Hibbert, D. B. (2012). Experimental design in chromatography: A tutorial review. *J Chromatogr B*, *910*, 2–13.

ICH (1999). Viral safety evaluation of biotechnology products derived from cell lines of human or animal origin. *ICH Q5A(R1)*, .

ICH (2007). Evaluation and recommendation of pharmacopoeial texts for use in the ICH regions. *ICH Q4B*, .

Iyer, G., Ramaswamy, S., Asher, D., Mehta, U., Leahy, A., Chung, F., and Cheng, K.-S. (2011). Reduced surface area chromatography for flow-through purification of viruses and virus like particles. *J Chromatogr A*, *1218*, 3973–3981.

Josefsberg, J. O., and Buckland, B. (2012). Vaccine process technology. *Biotechnol Bioeng*, *109*, 1443–1460.

Jungbauer, A. (2013). Continuous downstream processing of biopharmaceuticals. *Trends Biotechnol*, *31*, 479–492.

Kalbfuss, B., Genzel, Y., Wolff, M., Zimmermann, A., Morenweiser, R., and Reichl, U. (2007). Harvesting and concentration of human influenza A virus produced in serum-free mammalian cell culture for the production of vaccines. *Biotechnol Bioeng*, *97*, 73–85.

Kamen, A., and Henry, O. (2004). Development and optimization of an adenovirus production process. *J Gene Med*, *6*, S184–S192.

Kanani, D. M., and Ghosh, R. (2007). A constant flux based mathematical model for predicting permeate flux decline in constant pressure protein ultrafiltration. *J Membr Sci*, *290*, 207–215.

Kang, S. M., Kim, M. C., and Compans, R. W. (2012a). Virus-like particles as universal influenza vaccines. *Expert Rev Vaccines*, *11*, 995–1007.

Kang, Y. K., Ng, S., Lee, J., Adaelu, J., Qi, B., Persaud, K., Ludwig, D., and Balderes, P. (2012b). Development of an alternative monoclonal antibody polishing step. *BioPharm International*, *25*, 34–46.

Konz, J. O., Lee, A. L., Lewis, J. A., and Sagar, S. L. (2005). Development of a purification process for adenovirus: controlling virus aggregation to improve the clearance of host cell DNA. *Biotechnol Prog*, *21*, 466–472.

Kröber, T., Knöchlein, A., Eisold, K., Kalbfuß-Zimmermann, B., and Reichl, U. (2010). Dna depletion by precipitation in the purification of cell culture-derived influenza vaccines. *Chem Eng Technol*, *33*, 941–959.

Kröber, T., Wolff, M., Hundt, B., Seidel-Morgenstern, A., and Reichl, U. (2013). Continuous purification of influenza virus using simulated moving bed chromatography. *J Chromatogr A*, *1307*, 99–110.

Ladiwala, A., Rege, K., Breneman, C. M., and Cramer, S. M. (2005). A priori prediction of adsorption isotherm parameters and chromatographic behavior in ion-exchange systems. *Proc Natl Acad Sci U. S. A.*, *102*, 11710–11715.

Lee, D.-S., Kim, B.-M., and Seol, D.-W. (2009). Improved purification of recombinant adenoviral vector by metal affinity membrane chromatography. *Biochem Biophys Res Commun*, *378*, 640–644.

Lee, J., Gan, H. T., Latiff, S. M. A., Chuah, C., Lee, W. Y., Yang, Y.-S., Loo, B., Ng, S. K., and Gagnon, P. (2012). Principles and applications of steric exclusion chromatography. *J Chromatogr A*, *1270*, 162–170.

Lee, M. F. X., Chan, E. S., and Tey, B. T. (2014). Negative chromatography: Progress, applications and future perspectives. *Process Biochem*, *49*, 1005–1011.

Liniger, M., Zuniga, A., and Naim, H. Y. (2007). Use of viral vectors for the development of vaccines. *Expert Rev Vaccines*, *6*, 255–266.

Liu, H. F., Ma, J., Winter, C., and Bayer, R. (2010). Recovery and purification process development for monoclonal antibody production. *MAbs*, *2*, 480–499.

Luechau, F., Ling, T. C., and Lyddiatt, A. (2011). Recovery of b19 virus-like particles by aqueous two-phase systems. *Food Bioprod Process*, *89*, 322–327.

Lusky, M. (2005). Good Manufacturing Practice Production of Adenoviral Vectors for Clinical Trials. *Hum Gene Ther*, *16*, 281–291.

Mahajan, E., George, A., and Wolk, B. (2012). Improving affinity chromatography resin efficiency using semi-continuous chromatography. *J Chromatogr A*, *1227*, 154–162.

Majhen, D., Calderon, H., Chandra, N., Fajardo, C. A., Rajan, A., Alemany, R., and Custers, J. (2014). Adenovirus-based vaccines for fighting infectious diseases and cancer: Progress in the field. *Hum Gene Ther*, *25*, 301–317.

Makinen, M., Kaddar, M., Molldrem, V., and Wilson, L. (2012). New vaccine adoption in lower-middle-income countries. *Health Policy Plan.*, *27*, 39–49.

Margine, I., Martinez-Gil, L., Chou, Y. Y., and Krammer, F. (2012). Residual baculovirus in insect cell-derived influenza virus-like particle preparations enhances immunogenicity. *PloS one*, *7*, e51559.

McConnell, M. J. (2009). *Adenovirus as a Vaccine Platform*. ProQuest.

McCurdy, V., Migliaccio, G., Nosal, R., and Spavins, J. (2011). A pharma manufacturer's view of quality by design. *Pharm Technol*, *35*, s34–s39.

McNally, D., Darling, D., Farzaneh, F., Levison, P., and Slater, N. (2014). Optimised concentration and purification of retroviruses using membrane chromatography. *J Chromatogr A*, *1340*, 24–32.

Mehta, A., and Zydney, A. L. (2005). Permeability and selectivity analysis for ultrafiltration membranes. *J Memb Sci*, *249*, 245–249.

de las Mercedes Segura, M., Kamen, A., Lavoie, M.-C., and Garnier, A. (2007). Exploiting heparin-binding properties of MoMLV-based retroviral vectors for affinity chromatography. *J Chromatogr B*, *846*, 124–131.

Miller, E., Andrews, N. J., Waight, P. A., Slack, M. P., and George, R. C. (2011). Effectiveness of the new serotypes in the 13-valent pneumococcal conjugate vaccine. *Vaccine*, *29*, 9127–9131.

Morenweiser, R. (2005). Downstream processing of viral vectors and vaccines. *Gene Ther*, *12*, 103–10.

Nébié, I., Edwards, N. J., Tiono, A. B., Ewer, K. J., Sanou, G. S., Soulama, I., Sanon, S., Diarra, A., Yaro, J. B., Kangoye, D. et al. (2014). Assessing chimpanzee adenovirus serotype 63 (chad63) neutralizing antibodies prior to the evaluation of a candidate malaria vaccine regimen based on viral vectors. *Clin Vaccine Immunol*, *21*, 901–903.

Negrete, A., Ling, T. C., and Lyddiatt, A. (2007). Production of adenoviral vectors and its recovery. *Process Biochem*, *42*, 1107–1113.

Negrete, A., Pai, A., and Shiloach, J. (2014). Use of hollow fiber tangential flow filtration for the recovery and concentration of hiv virus-like particles produced in insect cells. *J Virol Methods*, *195*, 240–246.

Nestola, P., Silva, R. J., Peixoto, C., Alves, P. M., Carrondo, M. J., and Mota, J. P. (2014a). Adenovirus purification by two-column, size-exclusion, simulated countercurrent chromatography. *J Chromatogr A*, *1347*, 111–121.

Nestola, P., Villain, L., Peixoto, C., Martins, D. L., Alves, P. M., Carrondo, M. J., and Mota, J. P. (2014b). Impact of grafting on the design of new membrane adsorbers for adenovirus purification. *J Biotechnol*, *181*, 1–11.

Nfor, B. K., Ahamed, T., Pinkse, M. W., van der Wielen, L. A., Verhaert, P. D., van Dedem, G. W., Eppink, M. H., van de Sandt, E. J., and Ottens, M. (2012). Multidimensional fractionation and characterization of crude protein mixtures: Toward establishment of a database of protein purification process development parameters. *Biotechnol Bioeng*, *109*, 3070–3083.

Nfor, B. K., Verhaert, P. D., van der Wielen, L. A., Hubbuch, J., and Ottens, M. (2009). Rational and systematic protein purification process development: the next generation. *Trends Biotechnol*, *27*, 673–679.

Nicoud, R.-M. (2014). The amazing ability of continuous chromatography to adapt to a moving environment. *Ind Eng Chem Res*, *53*, 3755–3765.

Oelmeier, S. A., Dismer, F., and Hubbuch, J. (2010). Application of an aqueous two-phase systems high-throughput screening method to evaluate mAb HCP separation. *Biotechnol Bioeng*, *108*, 69–81.

Oelmeier, S. A., Ladd Effio, C., and Hubbuch, J. (2012). High throughput screening based selection of phases for aqueous two-phase system-centrifugal partitioning chromatography of monoclonal antibodies. *J Chromatogr A*, *1252*, 104–114.

Opitz, L., Hohlweg, J., Reichl, U., and Wolff, M. W. (2009). Purification of cell culture-derived influenza virus a/puerto rico/8/34 by membrane-based immobilized metal affinity chromatography. *J Virol Methods*, *161*, 312–316.

Osberghaus, A., Hepbildikler, S., Nath, S., Haindl, M., von Lieres, E., and Hubbuch, J. (2012). Determination of parameters for the steric mass action model. a comparison between two approaches. *J Chromatogr A*, *1233*, 54–65.

Ostreicher, E. A., Arnold, T. E., and Conway, R. S. (2008). Charge Modified Filter Media. In M. W. Jornitz, and T. H. Meltzer (Eds.), *Filtration and Purification in the Biopharmaceutical Industry* (pp. 23–46). Informa Healthcare.

Ouédraogo, A., Tiono, A. B., Kargougou, D., Yaro, J. B., Ouédraogo, E., Kaboré, Y., Kangoye, D., Bougouma, E. C., Gansane, A., Henri, N. et al. (2013). A phase 1b randomized, controlled, double-blinded dosage-escalation trial to evaluate the safety, reactogenicity and immunogenicity of an adenovirus type 35 based circumsporozoite malaria vaccine in burkinabe healthy adults 18 to 45 years of age. *PloS one*, *8*, e78679.

Oyston, P., and Robinson, K. (2012). The current challenges for vaccine development. *J Med Microbiol*, *61*, 889–894.

Paulen, R., Fikar, M., Foley, G., Kovács, Z., and Czermak, P. (2012). Optimal feeding strategy of diafiltration buffer in batch membrane processes. *J Membr Sci*, *411*, 160–172.

Peinador, R. I., Calvo, J. I., ToVinh, K., Thom, V., Prádanos, P., and Hernández, A. (2011). Liquid–liquid displacement porosimetry for the characterization of virus retentive membranes. *J Membr Sci*, *372*, 366–372.

Peixoto, C., Ferreira, T., Carrondo, M., Cruz, P., and Alves, P. (2006). Purification of adenoviral vectors using expanded bed chromatography. *J Virol Methods*, *132*, 121–126.

Peixoto, C., Ferreira, T. B., Sousa, M. F. Q., Carrondo, M. J. T., and Alves, P. M. (2008). Towards purification of adenoviral vectors based on membrane technology. *Biotechnol Prog*, *24*, 1290–1296.

Peixoto, C., Sousa, M. F. Q., Silva, A. C., Carrondo, M. J. T., and Alves, P. M. (2007). Downstream processing of triple layered rotavirus like particles. *J Biotechnol*, *127*, 452–461.

Pushko, P., Pearce, M. B., Ahmad, A., Tretyakova, I., Smith, G., Belser, J. A., and Tumpey, T. M. (2011). Influenza virus-like particle can accommodate multiple subtypes of hemagglutinin and protect from multiple influenza types and subtypes. *Vaccine*, *29*, 5911–5918.

Rajendran, A., Paredes, G., and Mazzotti, M. (2009). Simulated moving bed chromatography for the separation of enantiomers. *J Chromatogr A*, *1216*, 709–738.

Reimer, C., Baker, R., Newlin, T., Cline, G., Anderson, N. et al. (1967). Purification of large quantities of influenza virus by density gradient centrifugation. *J Virol*, *1*, 1207–1216.

van Reis, R., and Zydney, A. (2006). Membrane processes in biotechnology: An overview. *Biotechnol Adv*, *24*, 482–492.

van Reis, R., and Zydney, A. (2007). Bioprocess membrane technology. *J Memb Sci*, *297*, 16–50.

Riordan, W., Heilmann, S., Brorson, K., Seshadri, K., He, Y., and Etzel, M. (2009). Design of salt-tolerant membrane adsorbers for viral clearance. *Biotechnol Bioeng*, *103*, 920–929.

Rodrigues, T., Carrondo, M. J. T., Alves, P. M., and Cruz, P. E. (2007a). Purification of retroviral vectors for clinical application: Biological implications and technological challenges. *J Biotechnol*, *127*, 520–541.

Rodrigues, T., Carvalho, A., Carmo, M., Carrondo, M. J. T., Alves, P. M., and Cruz, P. E. (2007b). Scaleable purification process for gene therapy retroviral vectors. *J Gene Med*, *9*, 233–243.

Roush, D. J., and Lu, Y. (2008). Advances in Primary Recovery: Centrifugation and Membrane Technology. *Biotechnol Prog*, *24*, 488–495.

Saito, M., Kurosawa, Y., and Okuyama, T. (2013). Scanning electron microscopy-based approach to understand the mechanism underlying the adhesion of dengue viruses on ceramic hydroxyapatite columns. *PloS one*, *8*, e53893.

Salmon, F., Grosios, K., and Petry, H. (2014). Safety profile of recombinant adeno-associated viral vectors: focus on alipogene tiparvovec (glybera®). *Expert Rev Clin Pharmacol*, *7*, 53–65.

Segura, M. M., Kamen, A. A., and Garnier, A. (2011). Overview of Current Scalable Methods for Purification of Viral Vectors. In O.-W. Merten, and M. Al-Rubeai (Eds.), *Viral Vectors for Gene Therapy: Methods and Protocols* (pp. 89–116). Totowa, NJ: Humana Press.

Segura, M. M., Mangion, M., Gaillet, B., and Garnier, A. (2013). New developments in lentiviral vector design, production and purification. *Expert Opin Biol Ther*, *13*, 987–1011.

Segura, M. M., Puig, M., Monfar, M., and Chillón, M. (2012). Chromatography Purification of Canine Adenoviral Vectors. *Hum Gene Ther Methods*, *23*, 182–197.

Seidel-Morgenstern, A., Keßler, L. C., and Kaspereit, M. (2008). New Developments in Simulated Moving Bed Chromatography. *Chem Eng Technol*, *31*, 826–837.

Shanklin, T., Roper, K., Yegneswaran, P., and Marten, M. R. (2001). Selection of bioprocess simulation software for industrial applications. *Biotechnol Bioeng*, *72*, 483–489.

Silva, A. C., Peixoto, C., Lucas, T., Küppers, C., Cruz, P. E., Alves, P. M., and Kochanek, S. (2010a). Adenovirus vector production and purification. *Curr Gene Ther*, *10*, 437–455.

Silva, R. J., Rodrigues, R. C., Osuna-Sanchez, H., Bailly, M., Valéry, E., and Mota, J. P. (2010b). A new multicolumn, open-loop process for center-cut separation by solvent-gradient chromatography. *J Chromatogr A*, *1217*, 8257–8269.

Silva, R. J. S., Rodrigues, R. C. R., and Mota, J. P. B. (2012). Relay simulated moving bed chromatography: Concept and design criteria. *J Chromatogr A*, *1260*, 132–142.

Singh, N., Pizzelli, K., Romero, J. K., Chrostowski, J., Evangelist, G., Hamzik, J., Soice, N., and Cheng, K. S. (2013). Clarification of recombinant proteins from high cell density mammalian cell culture systems using new improved depth filters. *Biotechnol Bioeng*, *110*, 1964–1972.

Smith, J., Lipsitch, M., and Almond, J. W. (2011). Vaccine production, distribution, access, and uptake. *Lancet*, *378*, 428–438.

Stonier, A., Simaria, A. S., Smith, M., and Farid, S. S. (2012). Decisional tool to assess current and future process robustness in an antibody purification facility. *Biotechnol Prog*, *28*, 1019–1028.

Subramanian, S., Altaras, G. M., Chen, J., Hughes, B. S., Zhou, W., and Altaras, N. E. (2008). Pilot-Scale Adenovirus Seed Production through Concurrent Virus Release and Concentration by Hollow Fiber Filtration. *Biotechnol Prog*, *21*, 851–859.

Tatsis, N., and Ertl, H. C. J. (2004). Adenoviruses as vaccine vectors. *Mol Ther*, *10*, 616–629.

Thim, L., Vandahl, B., Karlsson, J., Klausen, N., Pedersen, J., Krogh, T., Kjalke, M., Petersen, J., Johnsen, L., Bolt, G. et al. (2010). Purification and characterization of a new recombinant factor viii (n8). *Haemophilia*, *16*, 349–359.

Thomassen, Y. E., van 't Oever, A. G., Vinke, M., Spiekstra, A., Wijffels, R. H., van der Pol, L. A., and Bakker, W. A. M. (2013). Scale-down of the inactivated polio vaccine production process. *Biotechnol Bioeng*, *110*, 1354–1365.

Vellinga, J., Smith, J. P., Lipiec, A., Majhen, D., Lemckert, A., van Ooij, M., Ives, P., Yallop, C., Custers, J., and Havenga, M. (2014). Challenges in manufacturing adenoviral vectors for global vaccine product deployment. *Hum Gene Ther*, *25*, 318–327.

Venkatachalam, A. R. K., Szyporta, M., Kiener, T. K., Balraj, P., and Kwang, J. (2014). Concentration and purification of enterovirus 71 using a weak anion-exchange monolithic column. *Virol J*, *11*, 99.

Vicente, T., Faber, R., Alves, P. M., Carrondo, M. J. T., and Mota, J. P. B. (2011a). Impact of ligand density on the optimization of ion-exchange membrane chromatography for viral vector purification. *Biotechnol Bioeng*, *108*, 1347–1359.

Vicente, T., Mota, J. P. B., Peixoto, C., Alves, P. M., and Carrondo, M. J. T. (2011b). Rational design and optimization of downstream processes of virus particles for biopharmaceutical applications: Current advances. *Biotechnol Adv*, *29*, 869–878.

Vicente, T., Peixoto, C., Carrondo, M. J. T., and Alves, P. M. (2009). Purification of recombinant baculoviruses for gene therapy using membrane processes. *Gene Ther*, *16*, 766–775.

Vicente, T., Sousa, M. F., Peixoto, C., Mota, J. P., Alves, P. M., and Carrondo, M. J. (2008). Anion-exchange membrane chromatography for purification of rotavirus-like particles. *J Membr Sci*, *311*, 270–283.

Warikoo, V., Godawat, R., Brower, K., Jain, S., Cummings, D., Simons, E., Johnson, T., Walther, J., Yu, M., Wright, B., McLarty, J., Karey, K. P., Hwang, C., Zhou, W., Riske, F., and Konstantinov, K. (2012). Integrated continuous production of recombinant therapeutic proteins. *Biotechnol Bioeng*, *109*, 3018–3029.

Weaver, J., Husson, S. M., Murphy, L., and Wickramasinghe, S. R. (2013). Anion exchange membrane adsorbers for flow-through polishing steps: Part II. Virus, host cell protein, DNA clearance, and antibody recovery. *Biotechnol Bioeng*, *110*, 500–510.

Westoby, M., Rogers, J. K., Haverstock, R., Romero, J., and Pieracci, J. (2011). Modeling industrial centrifugation of mammalian cell culture using a capillary based scale-down system. *Biotechnol Bioeng*, *108*, 989–998.

Wickramasinghe, S. R., Kalbfuß, B., Zimmermann, A., Thom, V., and Reichl, U. (2005). Tangential flow microfiltration and ultrafiltration for human influenza A virus concentration and purification. *Biotechnol Bioeng*, *92*, 199–208.

Wickramasinghe, S. R., Stump, E. D., Grzenia, D. L., Husson, S. M., and Pellegrino, J. (2010). Understanding virus filtration membrane performance. *J Membr Sci*, *365*, 160–169.

Wolff, M. W., and Reichl, U. (2008). Downstream Processing: From Egg to Cell Culture-Derived Influenza Virus Particles. *Chem Eng Technol*, *31*, 846–857.

Wolff, M. W., and Reichl, U. (2011). Downstream processing of cell culture-derived virus particles. *Expert Rev Vaccines*, *10*, 1451–1475.

Wolff, M. W., Siewert, C., Hansen, S. P., Faber, R., and Reichl, U. (2010). Purification of cell culture-derived modified vaccinia ankara virus by pseudo-affinity membrane adsorbers and hydrophobic interaction chromatography. *Biotechnol Bioeng*, *107*, 312–320.

Woo, M., Khan, N. Z., Royce, J., Mehta, U., Gagnon, B., Ramaswamy, S., Soice, N., Morelli, M., and Cheng, K. S. (2011). A novel primary amine-based anion exchange membrane adsorber. *J Chromatogr A*, *1218*, 5386–92.

Yae, K., Maiko, S., Shintaro, K., and Tsuneo, O. (2012). Purification of dengue virus particles by one-step ceramic hydroxyapatite chromatography. *WJV*, *2012*, 155–160.

Yamamoto, S., Nakamura, M., Tarmann, C., and Jungbauer, A. (2007). Retention studies of dna on anion-exchange monolith chromatography binding site and elution behavior. *J Chromatogr A*, *1144*, 155–60.

Yigzaw, Y., Piper, R., Tran, M., and Shukla, A. A. (2006). Exploitation of the adsorptive properties of depth filters for host cell protein removal during monoclonal antibody purification. *Biotechnol Prog*, *22*, 288–296.

Zak, D. E., Andersen-Nissen, E., Peterson, E. R., Sato, A., Hamilton, M. K., Borgerding, J., Krishnamurty, A. T., Chang, J. T., Adams, D. J., Hensley, T. R. et al. (2012). Merck ad5/hiv induces broad innate immune activation that predicts cd8+ t-cell responses but is attenuated by preexisting ad5 immunity. *PNAS*, *109*, E3503–E3512.

Zydney, A. L. (2009). Membrane technology for purification of therapeutic proteins. *Biotechnol Bioeng*, *103*, 227–230.

Part II

Development of novel materials and matrices

CHAPTER 2

Evaluation of novel large cut-off ultrafiltration membranes for adenovirus serotype 5 (Ad5) concentration

---

Adapted from:

Nestola P, Martins DL, Peixoto C, Roederstein S, Schleuss T, Alves PM, Mota JPB, Carrondo MJT. Evaluation of novel large cut-off ultrafiltration membranes for adenovirus serotype 5 (Ad5) concentration. *PlosOne*; doi:10.1371/journal.pone.0115802

Abstract

The purification of virus particles and viral vectors for vaccine and gene therapy applications is gaining increasing importance in order to deliver a fast, efficient, and reliable production process. Ultrafiltration (UF) is a widely employed unit operation in bioprocessing and its use is present in several steps of the downstream purification train of biopharmaceuticals. However, to date few studies have thoroughly investigated the performance of several membrane materials and cut-offs for virus concentration/diafiltration. The present study aimed at developing a novel class of UF cassettes for virus concentration/diafiltration. A detailed study was conducted to evaluate the effects of (i) membrane materials, namely polyethersulfone (PES), regenerated cellulose (RC), and highly cross-linked RC (xRC), (ii) nominal cut-off, and (iii) UF device geometry at different production scales. The results indicate that the xRC cassettes with a cut-off of approximately 500 kDa are able to achieve a 10-fold concentration factor with 100% recovery of particles with a process time twice as fast as that of a commercially available hollow fiber. DNA and host cell protein clearances, as well as hydraulic permeability and fouling behavior, were also assessed.

Keywords: ultrafiltration, virus concentration, vaccine, cassettes, hydraulic permeability.

2.1 Introduction

Viruses and virus like particles (VLP) are playing an increasingly important role in the vaccine gene and cell therapy fields. Adenoviruses (Ads), in particular, are considered one of the most suitable platforms for production of viral vaccines and gene therapy vectors; they are medium-sized (90–100 nm), nonenveloped, icosahedral viruses composed of a nucleocapsid and linear, non-segmented double stranded (ds) DNA genome that is about 36 kb long. The use of recombinant Ads for vaccination and gene therapy requires fast and highly efficient purification protocols that yield high recovery of infectious particles, maintain viral infectivity, and effectively remove contaminating DNA and host cell proteins, while also concentrating the viral samples for final delivery.

The downstream purification train of biopharmaceuticals has been extensively developed in the past years by combining different chromatographic steps, namely ion-exchange (Nestola et al., 2014) and size-exclusion chromatography (and, less frequently, affinity chromatography), intermingled with concentration and ultra/diafiltration steps (Eglon et al., 2009; Konz et al., 2005a,b; Burova and Ioffe, 2005; Peixoto et al., 2008; Goerke et al., 2005).

Ultrafiltration (UF) is a key operation, as large-scale processes produce high volumes of bulk (up to 2 kL for vaccines or 20 kL for mAbs (Farid, 2007)) that must be concentrated 10–100 times to be further purified by chromatography. The volumetric concentration and buffer exchange of virus bulks are critical not only to obtain high titer vector stocks in the proper formulation buffer, but also to reduce the handled volume; the latter accelerates the downstream processing and keeps the scalability of the purification train at a manageable level (Tatsis and Ertl, 2004).

UF membranes can be synthesized from different polymers, such as regenerated cellulose (RC), polysulfone (PS), polyethersulfone (PES), or polyvinylidene fluoride (PVF), although RC and highly cross-linked RC display better trade-off between low (unspecific) protein binding, mechanical strength, and resistance to cleaning procedures (chemical agents and temperature).

UF is usually operated in tangential flow mode, where the cross flow at the membrane surface creates a “sweeping action” that avoids or lessens concentration polarization and gel layer formation, thus inhibiting membrane clogging. UF processes are usually operated at constant transmembrane pressure,

$$\Delta P_{\mathrm{T}} = \frac{P_{\mathrm{F}} + P_{\mathrm{R}}}{2} - P_{\mathrm{P}}, \tag{2.1}$$

where P_F is the feed pressure, P_R is the retentate pressure, and P_P is the permeate pressure. However, constant permeate flux or constant permeate pressure operations are also implemented in practice (Liu et al., 2010). These are normally preferred when unfavorable effects, such as enhanced fouling or product quality deterioration, are associated with high concentration of retained species at the membrane wall (Paulen et al., 2012). The work presented here is, however, focused on constant-ΔP_T operation.

In viral downstream processes, ΔP_T is usually between 0.5 and 1.4 bar, while the optimal cross flow rates can vary greatly due to the different structural stabilities of the various types of viruses; enveloped viruses are more labile than non-enveloped viruses and, thus, more prone to shear-induced damage (Rodrigues et al., 2007b; Subramanian et al., 2008).

The membrane modules can also be assembled under different arrangements, for example flat sheet cassettes (FSCs) or hollow fibers (HFs). The majority of the published work refers to the use of HF modules for virus processing (Wolff and Reichl, 2011; Rodrigues et al., 2007a) due to the fact that HF modules provide wider flow paths with lower shear rates (van Reis and Zydney, 2007; Wolff and Reichl, 2011).

UF has been widely used both for concentration and for buffer exchange (diafiltration, DF), and is present in almost every virus DSP described in the literature (Segura et al., 2013; Bandeira et al., 2012; Kamen and Henry, 2004; Rodrigues et al., 2007b; Segura et al., 2012; Wickramasinghe et al., 2005; Kalbfuss et al., 2007; Subramanian et al., 2008) and disclosed patents (Luitjens and van Herk, 2012; Konz et al., 2008; Weggeman and van Corven, 2005). The membranes used in virus UF have MWCOs in the range of 100–750 kDa allowing for high virus recovery (70–85%).

Despite the effort in developing robust downstream processes and platforms, most of the research in the field of virus purification has been focused on the chromatographic steps. Indeed, only a few works have investigated thoroughly the concentration/UF steps: Negrete et al. (2014) optimized the use of a hollow fiber for concentration of virus like particles (VLP), while Wickramasinghe et al. (2005) evaluated several PES membranes (micro and ultrafiltration) for the concentration of influenza virus; also, Grzenia et al. (2008) evaluated four different small cut-off PES membranes for the purification of parvovirus particles. The rest of the literature is essentially focused on virus removal by UF membranes (Antony et al., 2014; Wickramasinghe et al., 2010; Peinador et al., 2011). It should be pointed out that in the present work the viruses are not a contaminant but the product;

therefore, the aim here is to concentrate and purify adenoviruses for viral vaccine or gene therapy applications.

The ideal UF membrane should have a very high separation factor, thus high product retention, and very high permeability. As correctly pointed out by Mehta and Zydney (2005) and Cramer and Holstein (2011) such membranes are currently not available in the market.

The present study aimed to develop a novel class of UF cassettes for adenovirus type 5 (Ad5) concentration/diafiltration. Typical membranes with cut-offs in the range of 300 to 1000 kDa were compared, since most of the HF membranes for viral processes have these cut-off sizes. While PES membranes with pore sizes in this range are known to have quite open structures, RC membranes are typically much tighter even when their pore size is not narrowed by adsorptive phenomena during process operation; thus, current commercially available RC membranes are not suited for typical viral vaccine processes (virus diameters around 100 nm).

A detailed study was conducted to evaluate the effect of membrane material, namely PES, RC, and highly cross-linked RC (xRC), nominal cut-off, and ultrafiltration device geometry. In the first part of the work, the hydraulic permeabilities of a set of membranes, which include eight R&D prototypes were evaluated. Hydraulic permeabilities were assessed for the clean membranes, after usage, and after cleaning-in-place (CIP). In the second part of the work, a 10-fold concentration step followed by 5 diafiltrations was performed under constant-ΔP_{T} conditions. The separation factor (total Ad5 recovery and infectivity) and selectivity towards the major impurities, such as host cell proteins (HCPs) and DNA, were determined and the throughput of each device was appraised. The outperforming membranes were then scaled up and produced in standard manufacturing equipment. Ultimately, the present study identified a new large cut-off membrane able to achieve a ten-fold concentration factor with higher throughput and 100% infective Ad5 recovery.

2.2 Materials and Methods

2.2.1 Adenovirus production

The Ad5 production based on HEK 293 cells cultured in Ex-cell 293 serum-free media was performed in a 5 L working volume bioreactor (Sartorius Stedim Biotech, Germany). The dissolved oxygen was controlled at 50% air saturation by a N_2/O_2/air mixture delivered by a sparger. The aeration rate was 0.01 vvm

(vessel volumes per minute). The pH-value was controlled at 7.2 ± 0.05 by aeration with CO_2 in the gas mixture and by base addition (1 M $NaHCO_3$). The temperature was controlled at 37°C using an external water-filled jacket. Mixing was provided by two 6-segment Ruston impellers with the agitation rate controlled between 60 and 210 rpm. The bioreactor inoculum was 0.5×10^6 cells/mL, the cell concentration at infection (CCI) was 10^6 cells/mL, and a MOI of 5 was used. The bioreactor was harvested 48 hours post infection (hpi).

2.2.2 Harvest and clarification

After the Ad5 bioreactor harvest, the cells were lysed by adding Triton X-100 (X100, SIGMA-ALDRICH , Switzerland) to a final concentration of 0.1% (w/w). Simultaneously, Benzonase (Merck Millipore, Germany) was added to a final concentration of 50 U/mL. The virus-containing bioreactor bulk was incubated at 37°C for 2 h.

Clarification of the Ad5 bulk was performed using a Sartopore® 2 filter with $0.8 + 0.45$ μm pore size (Sartorius Stedim Biotech, Germany). Before filtration, the module was primed with 3 capsule volumes of TRIS buffered saline, pH 8.0 (Sigma-Aldrich, Switzerland). The virus-containing bulk was loaded to the filter at a constant flow rate equivalent to 150 L/m^2/h (LMH) using a Tandem 1082 Pump (Sartorius Stedim Biotech, Germany). The 5 L clarified bulk was transferred into 450 ml Nalgene bottles and frozen at −80°C until further use. The performances of the UF membranes were all assessed with material from this batch with the same concentration of Triton and Benzonase in order to avoid any batch-to-batch variability.

2.2.3 Ultrafiltration setup

The ultrafiltration cassettes were kindly provided by Sartorius Stedim Biotech, Germany, while the 750 kDa hollow fiber module was purchased (GE Healthcare Life Sciences, Sweden). The membrane modules were set up according to the manufactures' instructions. Briefly, a Tandem 1082 Pump (Sartorius Stedim Biotech, Germany) was used to pump the clarified bulk into the membrane device, the retentate was recycled to the feed container, and the permeate was collected separately (Fig. 2.1). The transmembrane pressure, ΔP_{T}, was controlled by adjusting the retentate flow rate using a flow restriction valve.

Before the experiments, the membranes were thoroughly rinsed with ultrapure water (Grade 1, as defined in ISO 3696). The membrane permeability was

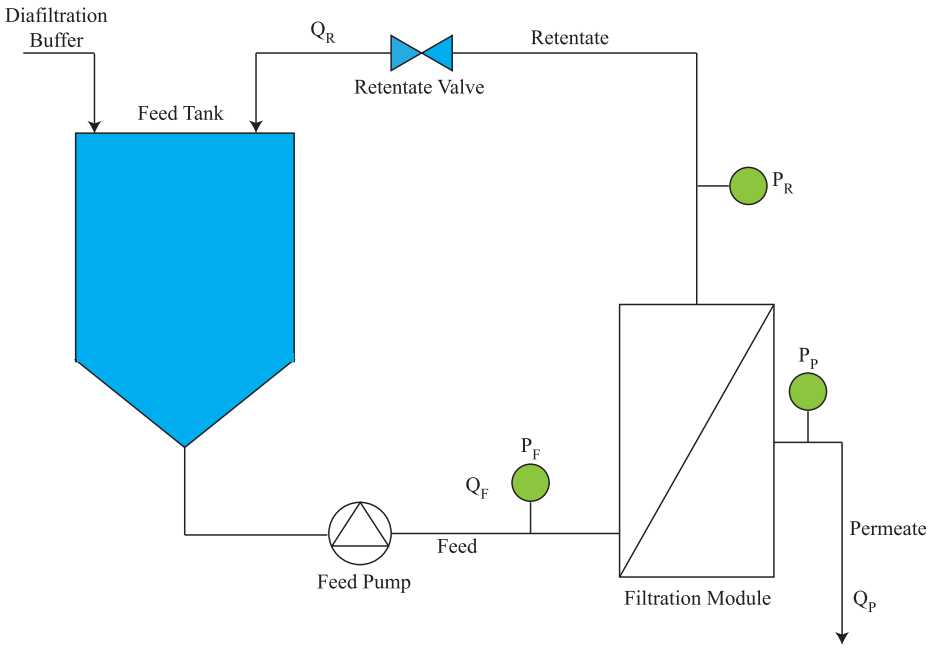

Figure 2.1: *Set-up of the filtration unit employed in the experiments. The bulk was fed using a Tandem 1082 Pump and the retentate recirculated to the feed tank. the pressure was monitored by in-line transducers at the inlet, retentate outlet, and permeate outlet.* ΔP_T *was kept constant at 1–1.2 bar by a flow restriction valve. TRIS saline buffer at pH 8 was used as diafiltration buffer.*

determined by the normalized water permeability at 20°C, $\mathrm{NWP}_{20^\circ\mathrm{C}}$, expressed in units of L m^{-2} h^{-1} bar^{-1} (LMH/bar) .

The $\mathrm{NWP}_{20^\circ\mathrm{C}}$ was calculated based on pure water permeate fluxes (J_w) measured at five different values of ΔP_T between 0.4 and 2.0 bar, according to

$$\mathrm{NWP}_{20^\circ\mathrm{C}} = \frac{K}{\mu} = \left(\frac{J_\mathrm{w}}{\Delta P_\mathrm{T}}\right)\left(\frac{\mu}{\mu_{20^\circ\mathrm{C}}}\right), \tag{2.2}$$

where the viscosity ratio $\mu/\mu_{20^\circ\mathrm{C}}$ is a temperature correction factor that adjusts the value of NWP from the experimental temperature to 20°C (Kestin et al., 1978). The $\mathrm{NWP}_{20^\circ\mathrm{C}}$ value was measured before and after each experiment, and after the CIP.

After conditioning the UF system with diafiltration buffer (20 mM TRIS, pH 8.0, 25 mM NaCl), 450 mL of clarified feedstock containing Ad5 were concentrated 10-fold and then diafiltered five times. The UF/DF test was performed at a constant ΔP_T of 1.2 bar and at a constant feed flow rate (cross-flow) equivalent to a linear velocity $u = 0.202$ m/s (cf.Table 2.1).

The linear velocity was the same in all experiments to ensure the same tangential flow/force in the various prototypes in order to properly assess their performance with respect to MWCO and type of membrane material. As shown in previous work by our group and others (Segura et al., 2012; Vicente et al., 2009; Negrete et al., 2014), a ΔP_T of 1.2 bar is a suitable pressure value for virus concentration.

The membrane load was kept constant at 22.5 L/m^2 for the membranes with areas of 200 cm^2 and 225 cm^2, whereas for the devices with 155 cm^2 the membrane load was 29.0 L/m^2. This difference was due to the minimum working volume of 45 mL allowed by our experimental set-up. Throughout the filtration process, samples of the retentate (1 mL) were collected and stored at −80°C for further analysis.

The shear rate at the wall, $\gamma_\mathrm{w} = \tau_\mathrm{w}/\mu$, where τ_w is the shear stress and μ is the fluid viscosity, was calculated as follows for the two membrane configurations (Cheryan, 1998):

$$\gamma_\mathrm{w} = \frac{8u}{d} = \frac{32Q}{n\pi d^3} \quad \text{(hollow fiber)}, \tag{2.3}$$

$$\gamma_\mathrm{w} = \frac{6u}{h} = \frac{6Q}{wh^2} \quad \text{(cassette, } w \gg h\text{)}. \tag{2.4}$$

Here, u and Q are the cross-flow mean fluid velocity and volumetric flow rate, respectively; n is the number of fibers of the hollow fiber, and d is inner diameter

Table 2.1: *Membrane characteristics and feed flow rates used.*

[h]

Membrane	Development stage	Filter material	Filter area (cm^2)	Configuration	Dimension $w \times h$ (10^{-3} m)	Cross section (10^{-5} m^2)	Q_F (mL/min)
Type B[b]	R&D prototype	RC	200	Cassette	30×0.38	1.14	138
Type C[a]	R&D prototype	RC	200	Cassette	30×0.38	1.14	138
Type D[a]	R&D prototype	xRC	200	Cassette	30×0.38	1.14	138
Type E[b]	R&D prototype	xRC	200	Cassette	30×0.38	1.14	138
Type # 2[c]	R&D prototype	PES	200	Cassette	30×0.30	0.90	109
Type # 4[c]	R&D prototype	PES	200	Cassette	30×0.30	0.90	109
HF 3[a]	R&D prototype	PES	155	Hollow fiber	18×0.50 $(n \times r)$	1.41	171
HF 5[b]	R&D prototype	PES	155	Hollow fiber	18×0.50 $(n \times r)$	1.41	171
Type F[d]	Pilot production	xRC	200	Cassette	30×0.38	1.14	138
Type H[e]	Pilot production	xRC	200	Cassette	30×0.38	1.14	138
HF 7[e]	Commercial	PES	225	Hollow fiber	13×0.50 $(n \times r)$	1.02	124

RC: regenerated cellulose.
xRC: regenerated cellulose modified with a highly hydrophilic cross-linking.
PES: polyethersulfone.
a, *b*, and *c* are, respectively, the low, medium, and high MWCO prototypes within the 300–1000 kDa range.
d and *e* are, respectively, the low and high MWCO prototypes within the 500–750 kDa range;
w and h are the width and height of the cassette flow channel.
n is the number of fibers in the hollow fiber module and r is the internal radius of the fibers.

of the fibers; w and h are the width and height of the cassette channel.

The CIP procedure consisted of washing the UF system with 1 M NaOH at a flow rate of 500 mL/min and then a 60-min incubation. After this treatment the system was rinsed with ultrapure water until the outlet stream reached pH 7. For the Ad5 runs, all procedures were performed at 20–22°C.

2.2.4 Scanning Electron Microscopy (SEM)

SEM images of membrane cross sections were prepared by rinsing the membrane samples in Arium^{TM} pure water and soaking them with Sakura Tissue Tek O.C.T.^{TM}compound resin prior cutting the membranes with a Leica CM3050 S cryo microtome. The samples were sputtered with a 5 nm layer of gold under vacuum in an Emitech K550 Sputter Coater and subsequently transferred to the FEI Quanta 200F SEM featuring a FEG (Schottky field emission gun) and ETD (Everhart Thomley Detector) under high vacuum ($10\times^{-10}$ mbar) for imaging. Version 2.4 of xT Microscope Control software was used for image collection and instrument control.

2.2.5 Sieving curve

A mixture of technical dextrans (purchased from SERVA Electrophoresis) was prepared in pure water added with 0,05% sodium azide (NaN_3). A sample of this feed solution was prepared for SEC analysis. Filtration was performed for flat sheet membranes in Amicon stirred cells (type 8200) under quasi non convective flow (TMP ¡ 20 mbar) or for hollow fiber modules using a peristaltic pump under similar conditions. Samples were collected at the permeate outlet after equilibrating the membrane and discarding twice the dead volume on the permeate side. Retentate samples were taken after filtration. A subsequent SEC analysis was performed on an Agilent 1100 integrated SEC system using a PSS Suprema Linear XL column. Pure water with a content of 0.05% sodium azide (NaN_3) was used as an eluent at a flow rate of 1 mL/min. Detection of the polymer was performed via RI detection. A dextran standard calibration based on narrowly distributed PSS polymer standards was used to determine the proper molecular weight. Molecular weight distribution of feed, permeate and retentate samples as well as sieve curves and cut-offs were calculated using PSS Unichrom software.

2.2.6 Gold nanoparticles rejection protocol

Gold nanoparticle solutions with particle sizes of 50 nm and 100 nm were purchased from BBI, sodiumdoceylsulfate (SDS) was purchased from Sigma-Aldrich, and pure water was produced using an Arium pro VF Ultrapure Water System. An amount of 1 g of SDS was dissolved in 1000 g of pure water under vigorous stirring. Afterwards, 10 mL of each solution of gold nanoparticles (50 nm and 100 nm) were diluted with 90 mL of SDS solution (1 g/L). The diluted solutions were stored in the fridge at 3°C and equilibrated under room temperature prior to filtration.

Filtration was performed in an Amicon 8010 stirred cell. First, 10 mL of SDS buffer were filtrated by applying a pressure of 1 bar. Subsequently, 10 mL of the diluted solution were transferred into the Amicon stirred cell and 8 mL were filtered by applying a pressure of 1 bar while stirring at 1100 rpm. Extinction of feed solution permeate was determined by UV-/vis-spectroscopy using a PerkinElmer Spectrophotometer Lambda 16 at a wavelength of 524 nm (50 nm nanoparticles) and 570 nm (100 nm nanoparticles).

2.2.7 Total virus particle quantification

Total virus particle concentration and size distribution were measured using a NanoSIGHT NS500 (NanoSIGHT Ltd, UK). The samples were diluted in D-PBS (Gibco®, UK) to get a virus concentration in the instrument's linear range (10^8–10^9 particles/mL). For each sample, three 60-second videos were acquired and particles between 70 and 130 nm were considered.

2.2.8 Infectious virus particles titration

For Ad5 titration, 293 cells were seeded at 0.25×10^6 cells per well in 24-well flat bottom plates (Nunc, Denmark). After 24 h, the cells from three wells were trypsinized and the cell concentration was determined. The cell culture medium was removed from the remaining wells and replaced with 1 mL of viral suspensions (10^{-1}–10^{-6}) diluted in fresh medium. After 17 to 20 hours, the cells were collected in Dulbecco's phosphate-buffered saline (D-PBS, Gibco®, UK) with 5% FBS and immediately analyzed by flow cytometry (CyFlow®space, Partec GmbH, Germany). Both the initial feedstock and the samples collected during the 10-fold concentration steps were analyzed in the same assay, thus using the same cell culture, to eliminate assay-to-assay variability. The infectious particle (IP) recovery, IP_{rec}, was calculated as follows:

$$IP_{\mathrm{rec}}\ (\%) = 100\,\frac{IP_{\mathrm{f}} \times V_{\mathrm{f}}}{IP_{\mathrm{i}} \times V_{\mathrm{i}}}, \tag{2.5}$$

where IP_{i} is the initial infectious particle concentration and IP_{f} is the value at the end of the 10-fold concentration step; V_{i} represents the initial volume and V_{f} the final volume obtained after the 10-fold concentration step.

2.2.9 DNA quantification

Total DNA was quantified using the fluorescence-based Quant-iT$^{\mathrm{TM}}$ PicoGreen® assay kit (Invitrogen$^{\mathrm{TM}}$, UK) according to the manufacturer's protocol. In order to avoid matrix interference, the samples were diluted between 2–256-fold with the reaction buffer provided.

2.2.10 Protein analysis

Total protein was quantified using the BCA Protein Assay Kit (Thermo Fisher Scientific, USA) according to the manufacturer's protocol. Bovine serum albumin (BSA) was used for the calibration curve. In order to avoid matrix interference, the samples were diluted between 2 and 256-fold.

Host cell protein was quantified using the HEK 293 HCP ELISA Kit (Cygnus Technologies, USA) following the manufacturer's protocol. The standard curve was done using the provided 293 HCP standards. Dilutions of $1/10^3$, $1/5\times10^3$, and $1/10^4$ were performed in order to avoid dose hook effects and to allow interpolation. All analytical assays were performed in triplicate.

2.3 Results and discussion

The selection of an appropriate membrane to improve the concentration/diafiltration step is critical to ease the entire downstream train. With this objective in mind, three membrane materials—RC (regenerated cellulose), xRC (highly cross-linked RC), and PES (polyethersulfone)—were evaluated. First, the evaluation of the R&D prototype is presented; then, the selected best performing membrane is manufactured and scaled-up in a standard manufacturing casting line. The cut-offs of the R&D pilot and production prototypes ranked between 300 and 1000 kDa. Table 2.1 summarizes the membrane characteristics, which are discussed in detail below.

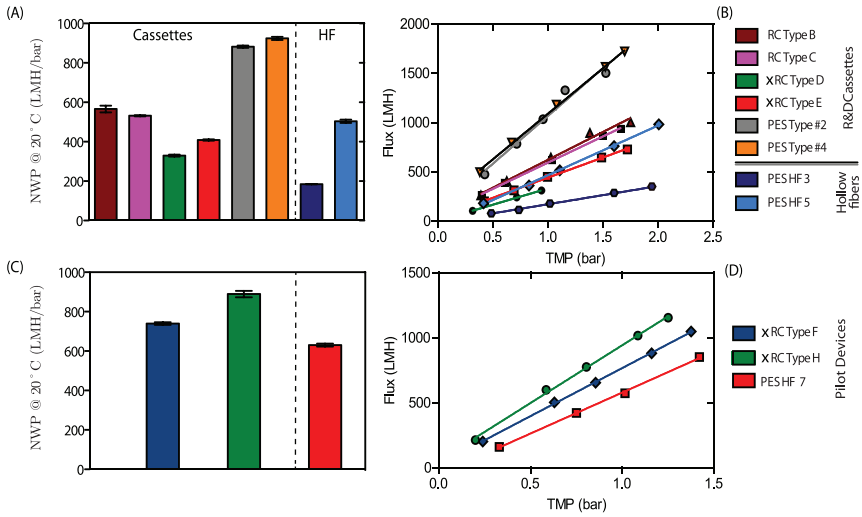

Figure 2.2: $NWP_{20°C}$ *(average ± SEM) for the different UF membranes. (A) R&D prototype devices with different materials, namely RC, xRC, and PES. (C) The pilot production devices were only made of xRC and compared against commercially available GE HF 750 kDa (PES UF 7). (B, D) water flux (LMH) at various values of* ΔP_T *ranging between 0.5 and 2 bar.*

2.3.1 Evaluation of R&D membrane prototype

Hydraulic permeability

All eight UF prototypes were characterized by their normalized water permeability, $NWP_{20°C}$; these values are plotted in Figs. 2.2A and 2.2B. As expected, the results show that increasing the pore size leads to an increase in permeate flux for the same transmembrane pressure (ΔP_T). This is in agreement with the findings of Wickramasinghe et al. (2005) and other authors.

The two PES cassettes (type #2 and type #4) registered the highest $NWP_{20°C}$, ca. 880–925 LMH/bar, and MWCO around 1000 kDa. Although both PES cassettes are within the same MWCO range, the PES type #4 cassette was designed to be slightly more open; this is confirmed by its enhanced $NWP_{20°C}$. Both RC cassettes exhibited $NWP_{20°C}$ values close to 560 LMH/bar, whereas that of xRC only reached 400 LMH/bar. The HF modules showed lower permeabilities than the PES and RC-based cassettes. As expected, the lower MWCO of PES HF 3 (roughly 300 kDa) resulted in lower permeability than PES HF 5 (roughly 500 kDa).

The water flux permeability was measured after membrane usage and after

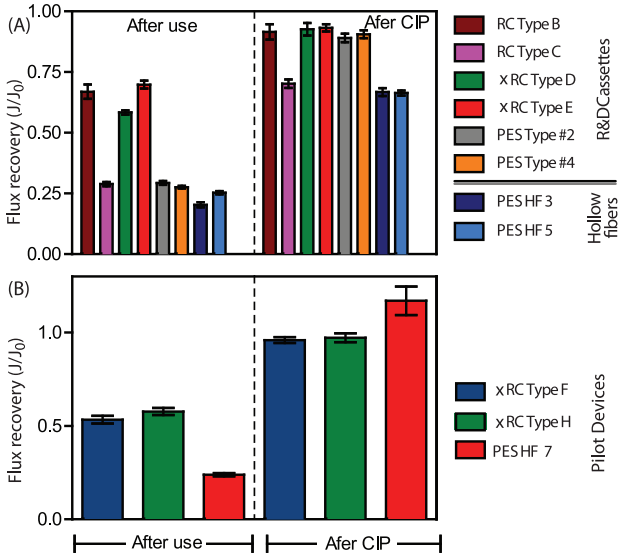

Figure 2.3: *Flux recoveries (average±SEM) after use and after CIP with 1M NaOH for different R&D prototypes (Fig.A) and for the pilot production devices (Fig.B). In both cases the highly cross-linked regenerate cellulose (xRC) was able to achieve higher flux recovery after use compared to the PES based membranes. After CIP all the membranes recovered their initial flux with the exception of PES HF 3 and 5 and RC type C.*

cleaning in place. This measurement assesses the degree of irreversible/strongly associated foulants accumulated on the membrane during filtration. On the other hand, the after-CIP flux recovery gives the loss of permeability after a complete cycle. This metric is an industrially relevant indicator as it serves as benchmark of membrane performance, and is used to assess performance decay as well as the effectiveness of CIP protocols.

The flux recoveries, J/J_0, where J and J_0 are the fluxes after and before membrane usage, are given in Fig. 2.3A.

The water flux recovery after use was nearly 3-fold greater for the RC and xRC than for the PES-based material. A significant water flux permeability decay indicates the presence of fouling or nonspecific, irreversible adsorption. Since PES is hydrophobic, this leads to increased fouling compared to the regenerated cellulose.

However, except for the PES-based HF prototype and RC Type C, after CIP with NaOH 1M the flux was restored in all cassettes. The type B membrane and the two xRC cassettes regained their permeability, since their flux loss ranged between 7% and 11%, indicating that these UF modules withstood a complete

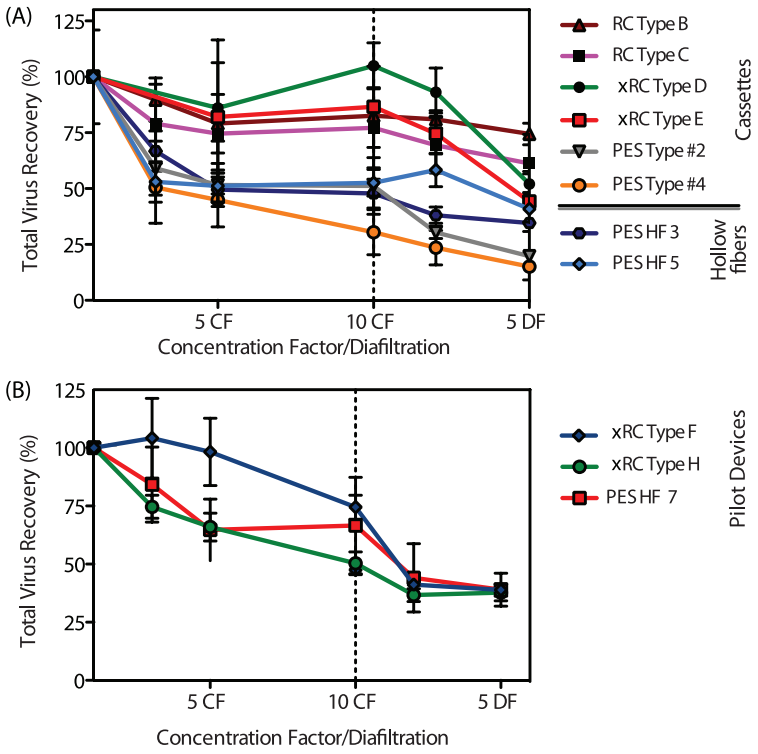

Figure 2.4: *Total virus particle recovery as function (average ±SEM) of the concentration/diafiltration volume for different R&D prototypes (Fig.A) and for the pilot production devices (Fig.B). The plots display the same process first operating in concentration mode and then diafiltration. In both cases the highly cross-linked regenerate cellulose xRC showed the highest recovery yield when compared to PES menbranes.*

cycle and might be used as a repeated-use device; the effect of the number of cycles on the long-term behavior of these membranes was not assessed. The remaining modules (RC type C and the two PES hollow fibers) showed a decreased of water permeability after one cycle; these devices are not suited for repeated use.

Virus Recovery

Ultrafiltrated samples were collected at the retentate side upon achieving 3, 5, and 10 concentration factors (CF) and also after 2 and 5 diafiltrations (DF). The samples were further analyzed to determine the filtration performance of each UF device. Fig. 2.4A and Table 2.2 show the total particle and infectious particle recoveries, respectively.

All RC-based cassettes achieved total particle recoveries ranging from 69% to 93% after 2 DFs. Contrarily, the PES-based membranes permeated virus particles, as indicated by the low total particle recoveries (23–58 %). This was partially anticipated, since the PES cassettes presented the highest MWCO (ca. 1000 kDa).

The infectious particle (IP) data given in Table 2.2 are consistent with the total particle recoveries except for the PES Type #2 cassette. In particular, all the RC-based cassettes were able to recover between 79% and 100% of IPs at the end of the concentration step. Interestingly, of these four modules, the ones with larger MWCO (RC type B and xRC type E) were those yielding higher IP recoveries, close to 100%. This result points out the importance of optimizing the choice of cassette and MWCO for the lowest processing time to avoid loss of infectivity.

Following the trend observed for total particle recovery, the type #2 PES cassette recovered more infectious particles than the PES #4 module. Noteworthy, is the higher recovery of infectious particles than that of total particles; this is more pronounced for the PES type #2 prototype. The reason for this can be attributed to the presence of incomplete viral particles or empty capsids that are removed during the ultrafiltration process by several mechanisms, such as adsorption and sieving and/or entrapment in the larger pores. Vellekamp et al. (2001) showed that empty capsids have a slightly different shape than infectious particles, and their surface appears rounder when observed by electron microscopy. Their stability might also be compromised and, therefore, they may be are more prone to shear stress damage. These features, combined with the higher permeability of the PES Type #2 cassette, may explain the enhanced infectious viral recovery and reduced total particle recovery. Also, the PES Type #2 cassette performed poorly in the flux recovery test after usage, suggesting the occurrence of virus entrapment leading to membrane fouling. The PES cassettes have the same type of membrane material and the same MWCO; however, it is known that slight differences, such as a broader (or narrower) pore size distribution, can impact the virus recovery achieved by the membrane (van Reis and Zydney, 2007). Indeed, the PES#4 prototype was manufactured with a slightly broader pore size distribution; this is also evident by looking at the superior clean water flux that this membrane displays.

The HF prototypes yielded low IP recoveries. In particular, the HF 3 module took seven times longer than the type B or type E prototypes to complete the same 10-fold concentration step. Still, the HF 3 module showed a moderate IP recovery ($60 \pm 4\%$). This can be explained by the longer processing time, which

Table 2.2: *Recovery of infectious particles (IP) and processing time for 10-fold concentration for the different pilot production and R&D UF devices.*

Device	Material	Water flux ($L/m^2/h/bar$)	Processing time (min)	IP recovery (%±SEM)	DNA clearance (%±SEM)	HCP clearance (%±SEM)	Shear rate (s^{-1})
Type B	RC	590	14	94 ± 14	57 ± 0.76	68 ±3.91	3186
Type C	RC	566	30	85 ± 11	55 ± 0.63	73 ± 6.54	3186
Type D	xRC	390	24	72± 11	63 ± 1.71	79 ± 4.72	3186
Type E	xRC	400	14	100± 13	57± 3.91	71 ± 9.78	3186
Type #2	PES	900	19	89 ± 16	70 ± 2.71	86 ± 8.67	4037
Type #4	PES	924	17	54 ± 11	73 ± 4.27	90 ±2.8	4037
HF 3	PES	185	105	60± 4	64 ± 2.59	77 ± 12	1613
HF 5	PES	504	48	8 ± 2	51 ± 2.41	70 ± 0.72	1613
Type F	xRC	739	17	100 ± 12	48 ± 0.90	57 ± 20.1	3186
Type H	xRC	889	17	93.6 ± 16	46 ± 0.61	58 ± 9.64	3186
HF 7	PES	630	26	100± 13	66 ± 1.78	86 ± 22.9	1619

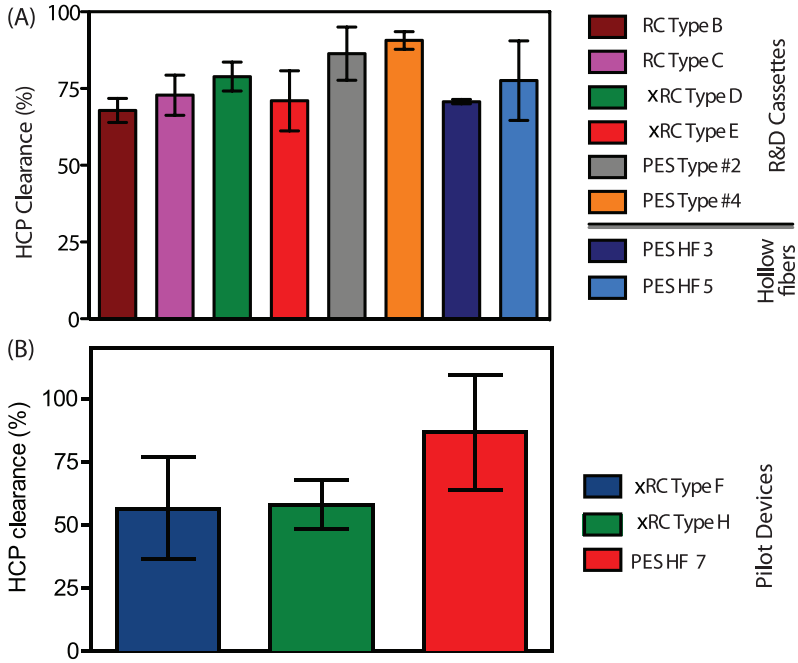

Figure 2.5: *HCP clearance (average ±SEM) as a function of the concentration/diafiltration volume for different R&D prototypes (Fig.A) and for the pilot production devices (Fig.B).Both figure display the HCP clearance value after 10 fold concentration. The HCP clearance does not show important differences among the different cassettes and or HF. A slight increase in clearance is observed for the PES based cassettes and for the GE HF 750 kDa (PES HF 7).*

may give rise to enhanced adsorptive interactions between the hydrophobic PES material and the virus particles. The lower flux recovery after usage and after cleaning in place supports the hypothesis of strong hydrophobic-driven adsorption.

Impurity clearance

The HCP analysis given in Fig. 2.5A shows that the two PES cassettes were able to remove 86–91 % of the HCP present; this was expected given their high MWCO and hydrophobic properties. The only exceptions are the HF 3 and HF 5 prototypes as these were in the 300 kDa and 500 kDa ranges, respectively. It is likely that high molecular weight HCPs can easily pass through the 1000 kDa pores of the PES membrane cassette.

One of the challenges of Ad purification is host cell DNA removal, not only because the bioprocess comprises a cell lysis step (Silva et al., 2012) but also

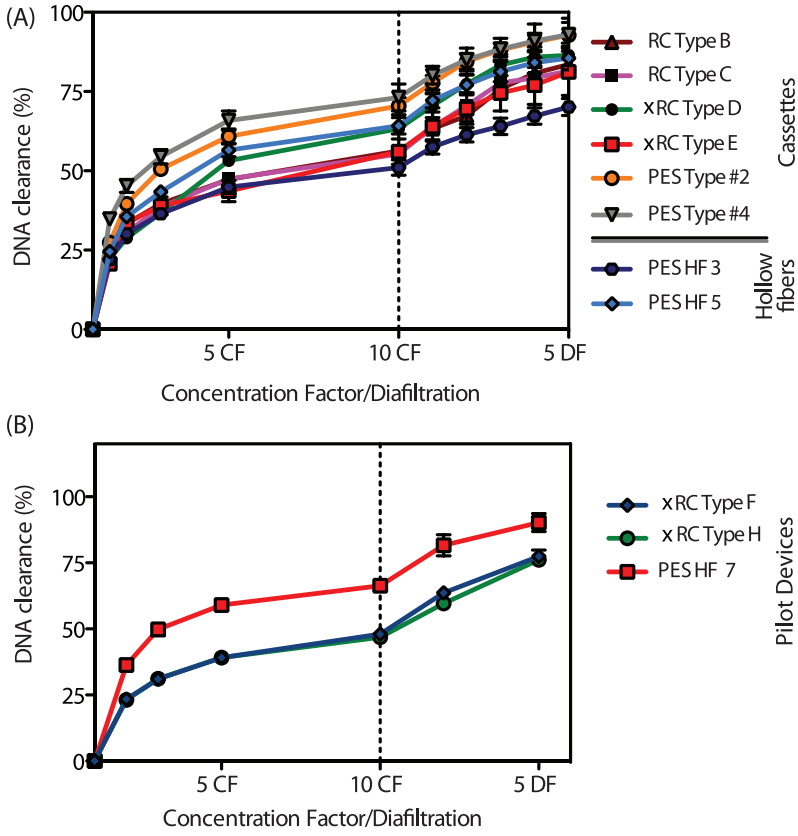

Figure 2.6: *DNA clearance as a function (average ±SEM) of the concentration/diafiltration volume for different R&D prototypes (Fig.A) and for the pilot production devices (Fig.B). The plots display the same process first operating in concentration mode and then diafiltration.*
Both for the R&D and pilot production devices the PES-based membranes lead to an increased DNA removal comparing to their RC and xRC counterparts.

because it has been shown that DNA can associate with the virus particles resulting in co-purification of both species (Konz et al., 2005a). Both PES-based cassettes enabled higher DNA clearance, ca. 85%, than the remaining prototypes (Fig. 2.6).

The types B, C, D, E, and HF 5 prototypes showed intermediate DNA clearances (67–70%) and the HF 3 showed the worst DNA clearance (61 %) (Fig. 2.6 A). Both the HCP and DNA clearance data are in agreement and point out both PES cassettes as the best modules with respect to impurity removal. However, when the TP and IP data are also taken into account, these modules were not as

efficient as the RC-based membranes.

Productivity

The permeate flux over time and membrane throughput (feed processed per membrane area per unit time, L m^{-2} h^{-1}, or LMH) were evaluated for all UF prototypes studied. The membranes with higher cut-off, namely type B and PES type #4, showed an initial marked flux decrease before a steady state was achieved. The higher the clean water flux, the lower is the resistance to the permeate side of the membrane. Low membrane resistance results in initially high permeate flow for the clean membrane. This will cause rapid convection of particles and small contaminants towards the membrane surface leading to rapid flux decline (Wickramasinghe et al., 2005; Belfort et al., 1994).

Fig. 2.7 A shows that all R&D membranes were able to maintain a stable flux due to the constant-ΔP_{T} operation, except for type D which showed a marked flux decrease between 300 to 405 mL of permeate volume (between 3 to 10 CF). This indicates the starting point of fouling, which may be due to the low MWCO. Indeed, this membrane yielded the lowest clean water flux (Fig. 2.2).

2.3.2 Identification of a suitable membrane

Among the R&D prototypes, the PES hollow fiber modules showed the worst performance under the conditions evaluated. This is supported by the lower IP recoveries and longer processing times. While the HF 5 module lost nearly all viruses, the HF 3 prototype was still able to recover 60% of infective particles but the long processing time is a considerable disadvantage. The results obtained with the PES R&D prototypes, namely the values of total particle recovery, are below what has been reported in the literature for this MWCO range. For instance, 300 kDa HFs from GE are able to concentrate 10-fold an Ad5 bulk with 90 % IP yield (Peixoto et al., 2008). The only exception is the PES Type#,2 which yielded an IP recovery of 89%. However, the lower flux recovery after use and after CIP makes this membrane less attractive for processing large volumes of feedstock.

The RC-based R&D prototypes showed better performances, especially with respect to the IP recovery. In particular, type B and type E membranes registered superior IP recoveries than what has been reported for Ad5 ultrafiltration (Peixoto et al., 2008; Segura et al., 2012; Subramanian et al., 2008), indicating that the shear rates used did not damage the adenovirus virions. These membranes displayed similar HCP clearance (68% and 71%) and DNA clearance (67% and

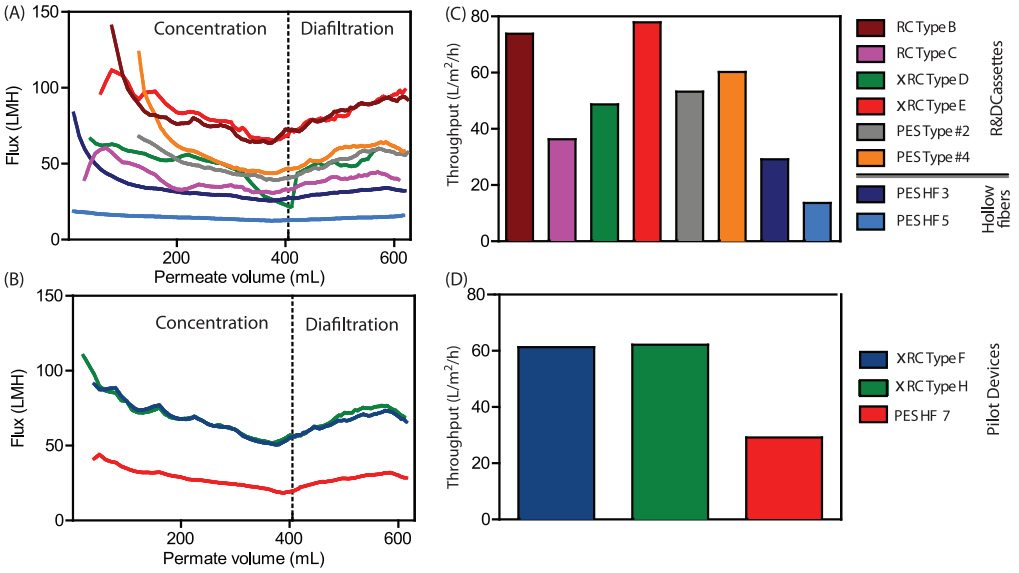

Figure 2.7: *Flux decay curves as a function of the filtration time Fig.(A and (B). Throughput (liter of feed processed in the unit of time (h), given a defined membrane area (m^2)) Fig. C and D. The value reported in Fig. C and D are after to 10-fold concentration and 2 diafiltration volume.*
For the large cut off R&D membranes a strong flux decay is observed at the beginning of the filtration(Fig A). Pilot production devices and GE HF 750 (PES HF 7) show the same decay profile (Fig.B). Cassettes with RC Type B and xRC Type E show the highest throughput (Fig. C). , the throughput for the GE HF 750 is 2 fold less compared to the pilot production cassette membranes (Fig.D).

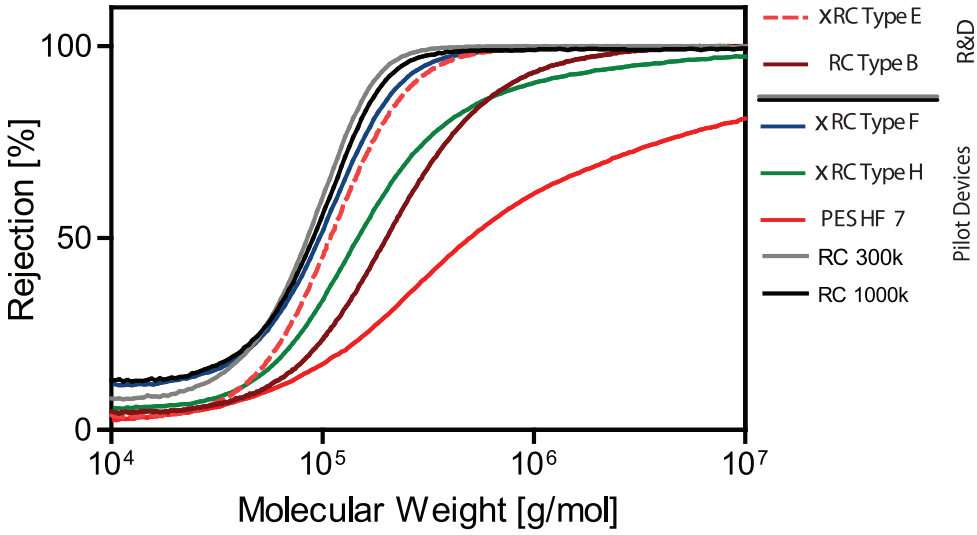

Figure 2.8: *Sieving curve for visualization of different pore size by using different molecular weight dextrans, ranking between 10^5 and 10^8 g/mol. RC and xRC exhibit a narrower rejection range than the other membranes and, therefore, a more homogeneous pore size distribution. Two commercially available RC cassette are compared against showing tighter pore sizes even for the membrane rated as 1000 kDa. GE HF 750 kDa (PES HF 7) exhibits the largest cut-off and wider pore size distribution.*

70%, respectively). The throughput capacities of these two modules are rather high, being able to process up to 77 L of feed in 1 hour using a 1 m^2 ultrafiltration module. It should be pointed out that the throughput analysis was done by taking into account a 10-fold concentration step and 2 buffer exchanges. Considering that UF is often employed at an early stage in the downstream processing train, high recovery yields and high throughput capacities are preferred over enhanced impurity removal rates, although here there are still remarkable.

Taking into account these features, the type B and type E membranes served as base for the design and scale-up to the manufacturing casting line. Sieving curves showed that rejection profile of the selected R%D prototype is comparable to the profile of the pilot devices, namely type F and type H (Fig. 2.8).

It is also important to point out that the two UF modules that displayed superior throughputs (Fig. 2.7 B), RC Type B and xRC Type E, were also the ones that gave the highest virus recoveries (Fig. 2.9). A commercial PES hollow fiber with 750 kDA MWCO from GE healthcare, hereafter referred to as PES HF 7, was chosen as benchmark reference. These new pilot production devices were evaluated by performing the same type of experiments for the R&D prototypes.

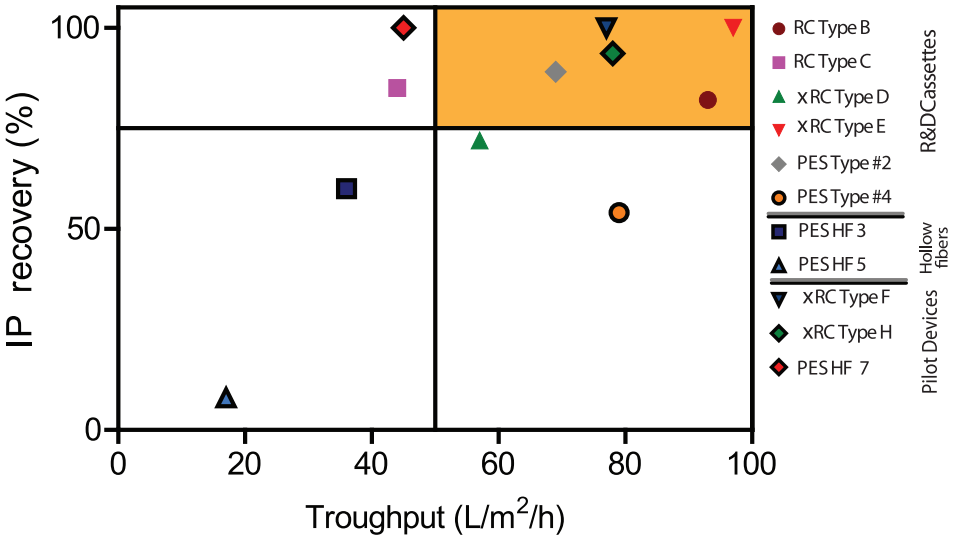

Figure 2.9: *Trade-off between throughput, indicated as liter of feed processed in the unit of time (h), given a defined membrane area (m^2), and infective particle recovery yield. The values referrer at 10 times concentration factor.*
The orange area on the right top corner depicts the best membranes. RC and xRC membranes showed the highest throughput coupled with high recovery yield.

2.3.3 Evaluation of the pilot production devices

The pilot-production cassettes were optimized to increase their water flux permeability. The membranes and cassettes were manufactured on standard production-scale manufacturing equipment and were designed to be scalable to large-area devices. xRC was the material chosen for the pilot production due to the goods values obtained for the various performance metrics discussed in this work. Relevant process performance, such as recovery of infectious particle (IP) and total particle (TP) recoveries, were the main drivers for this choice.

The xRC type H cassette (ca. 750 kDa) exhibited the highest $NWP_{20°C}$ of the pilot devices, 889 LMH/bar, as seen in Fig. 2.2C and D. This is in accordance with its high MWCO as observed by the sieving curves plotted in Fig. 2.8. The type F cassette showed a smaller $NWP_{20°C}$ of 739 LMH/bar, but still larger than that of HF 7, which was determined to be 630 LMH/bar. The lower permeability of the GE 750 kDa HF (PES HF 7) is somewhat puzzling. The sieving curve in Fig.2.8 shows a higher MWCO for HF 7 than for the cassettes, therefore a higher water flux would be expected. On the other hand, HF 7 has a much broader sieving curve than the cassettes, which indicates that the HF 7's permeability is

controlled by the fraction of smallest pores in its pore size distribution.

Regarding the water flux after cleaning in place, the two xRC cassettes fully recovered their permeability (96% and 97% flux recovery). This provides a good indication being reusable. Indeed these membranes were also optimized to sustain several CIP cycles, as this is an important feature for process robustness. In particular, when comparing the Type B and E membranes water flux after CIP with the pilot production devices have an increased flux recovery of 3-4% (Fig. 2.3 A and B).

Contrarily, the HF 7 showed a performance decay after CIP, since its hydraulic permeability increased by 17 %. This can cause a change in the product and/or impurities retention rate when the membrane is reused.

Concerning total particle recoveries ranged from 50 % (type H) up to 75 % (type F) after 10-fold concentration (Fig. 2.4 B); however, after two diafiltration (DF) volumes the recovery yield decreased to 40 % for all tested membranes. This effect is essentially membrane independent and most likely due to the formulation of the diafiltration buffer; in particular increasing ionic strenght and/or adding polysorbate 80 might overcome this issues, as shown by Konz et al. (2005a)

As for the impurities clearance, xRC type F and type H cassettes removed 67 and 68 % of HCP, respectively, while the PS-based HF 7 was able to achieve 86% HCP clearance (Fig. 2.5 B). The higher HCP protein clearance registered by the HF might be due to the different filter material, which is more hydrophobic than RC, and thus more prone to adsorption.

For the Type F and Type H pilot device cassettes, the DNA clearance after two DFs was 64 and 60%, respectively, while the HF 7 was able to remove 82% of DNA present in the Ad5 feed (Fig 2.6 B).

The superior performance in DNA clearance of the GE HF can be attribute to the higher MWCO as shown in Fig.2.8 allowing DNA to go trough the permeate side. However, DNA can also adsorb onto the membrane surface due to the hydrophobic nature of the PES material.

Regarding the removal of impurities, the PES HF gave rise to a slightly improved DNA and HCP clearance comparing with xRC cassettes. This increased impurity removal might be due to adsorption phenomenon rather than a size exclusion mechanism as the filter material's proprieties are more hydrophobic (Liu et al., 2010; Zydney, 2009).

Infectivity for the type F and HF 7 membranes was maintained yielding 100% of IPs, while Type H membrane achieved 94 % IP recovery. Despite being rated with the same MWCO as the type H cassette, the HF 7 was able to recover

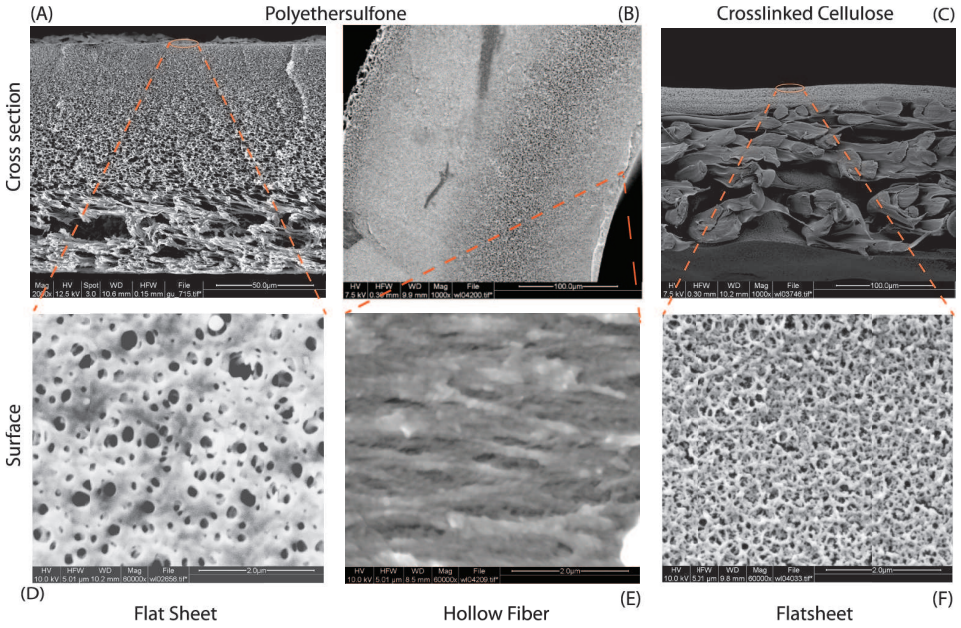

Figure 2.10: *Figure 10. SEM pictures of PES membrane, xRC Type F membrane and HF 7. Figures A, B and C indicate the cross section structure for the flat sheet membrane and hollow fiber, while figures D, E and F illustrate the surface structure.*

a slightly more infective Ad5. The membranes were also evaluated based on their rejection of gold nanoparticles (GNP) of 100 nm (approximately the size of adenovirus) and 50 nm. Almost all the membranes showed a 50% rejection of the 50 nm GNPs and almost completely held back the 100 nm GNPs (Tab.2.3).

The membrane materials, xRC and PES, were also investigated by SEM analysis (Figs. 2.10). The main morphological difference appears to be related to the support layer, which shows a more neat and smooth pattern in the xRC. While one membrane is supported by a non-woven fabric, both filters feature an asymmetric sponge like structure, which is relevant for membrane stability but has low to none effect in the filtration process. All retention is performed at the very top layer of the filters (skin layer). Surface images confirm the asymmetry structures. (Fig.2.10 D, E and F).

Nevertheless within that structure adsorption of contaminants can occur due to steric or hydrophobic interaction, the latter of which is more present for PES based membranes.

The Type F cassette presented the best overall results among the assayed membranes. This is supported by the complete recovery of infective Ad5, with a

Table 2.3: *Characterization of xRC, RC and PES ultrafiltration devices. Permeability of a protein solution of gamma-globuline (Glb) and rejection of gold nanoparticles (GNP) is shown*

Module	Material	Prototype	Permeability protein solution (LMH)	Rejection Glb (160 kDa) (%)	Rejection GNP (50nm) (%)	Rejection GNP (100nm) (%)
Cassette	RC	Type B	919	11	47	95
Cassette	xRC	Type E	179	47	52	96
Cassette	xRC	Type F	489	N/A	49	97
Cassette	xRC	Type H	1915	3	57	97
Cassette	PES	Type #2	83	81	43	96
Hollow fiber	PES	HF 7	130	32	63	95

remarkable improvement compared with the data described in the literature for 500 kDa HF (Peixoto et al., 2008).

Another important feature of the Type F (and H) cassette(s) is their higher throughput compared with the HF 7. For instance, the Type F module is capable of processing up to 61 L of Ad5 clarified bulk within 1 h using a 1 m^2-membrane while the GE HF can process only 29 L with the same time and membrane area (considering a 10-fold concentration and 2 DF).

Although the Type F throughput is 20 % lower compared to those obtained for the best R&D prototypes previously evaluated, careful comparison of such values is required since the previous membranes' MWCO might be slightly different and the manufacturing process was different.

2.4 Conclusions

This work presented an in-depth characterization of several ultrafiltration membranes. We have identified UF membrane modules alternative to the currently available HF devices traditionally used for virus purification. A cassette based on highly cross-linked regenerated Cellulose (xRC, close to 500 kDa and herein referred to as type E), which showed the best performance among the R&D prototypes, was successfully scaled up to a pilot production casting line. The resulting type F module showed better performance than a commercially available hollow fiber (750 kDa). The key advantage of this UF module is the substantially shorter processing time coupled with complete infectious particle recovery (100%) and is, therefore, suggested for Ad5 concentration.

Acknowledgments

Financial support from Sartorius Stedim Biotech and from the Portuguese Science Foundation (FCT-MCTES) (SFRH/BD/82032/2011 PTDC/EBB-BIO/101992/2008 and PTDC/EBB- BIO/119501/2010) is gratefully acknowledged.

References

Antony, A., Blackbeard, J., Angles, M., and Leslie, G. (2014). Non-microbial indicators for monitoring virus removal by ultrafiltration membranes. *J. Membr. Sci.*, *454*, 193–199.

Bandeira, V. S., Peixoto, C., Rodrigues, A. F., Cruz, P., Alves, P., Coroadinha, A. S., and Carrondo, M. (2012). Downstream processing of lentiviral vectors: releasing bottlenecks. *Hum Gene Ther Methods*, *23*, 255–263.

Belfort, G., Davis, R. H., and Zydney, A. L. (1994). The behavior of suspensions and macromolecular solutions in crossflow microfiltration. *J. Membr. Sci.*, *96*, 1 – 58.

Burova, E., and Ioffe, E. (2005). Chromatographic purification of recombinant adenoviral and adeno-associated viral vectors: methods and implications. *Nat Rev Genet*, *12*, S5–S17.

Cheryan, M. (1998). Performance and engineering models. In M. Cheryan (Ed.), *Ultrafiltration and Microfiltration Handbook* (pp. 113–170). Lancaster: Taylor & Francis.

Cramer, S. M., and Holstein, M. A. (2011). Downstream bioprocessing: recent advances and future promise. *Curr. Opin. Chem. Eng.*, *1*, 27–37.

Eglon, M. N., Duffy, A. M., O'Brien, T., and Strappe, P. M. (2009). Purification of adenoviral vectors by combined anion exchange and gel filtration chromatography. *J Gene Med*, *11*, 978–989.

Farid, S. S. (2007). Process economics of industrial monoclonal antibody manufacture. *J Chromatogr B*, *848*, 8–18.

Goerke, A. R., To, B. C. S., Lee, A. L., Sagar, S. L., and Konz, J. O. (2005). Development of a novel adenovirus purification process utilizing selective precipitation of cellular DNA. *Biotechnol. Bioeng.*, *91*, 12–21.

Grzenia, D. L., Carlson, J. O., and Wickramasinghe, S. R. (2008). Tangential flow filtration for virus purification. *J. Membr. Sci.*, *321*, 373–380.

Kalbfuss, B., Genzel, Y., Wolff, M., Zimmermann, A., Morenweiser, R., and Reichl, U. (2007). Harvesting and concentration of human influenza A virus produced in serum-free mammalian cell culture for the production of vaccines. *Biotechnol. Bioeng.*, *97*, 73–85.

Kamen, A., and Henry, O. (2004). Development and optimization of an adenovirus production process. *J. Gene Med.*, *6*, S184–S192.

Kestin, J., Sokolov, M., and Wakeham, W. A. (1978). Viscosity of liquid water in the range -8C to 150C. *J Phys Chem Ref Data*, *7*, 941–948.

Konz, J. O., Lee, A. L., Lewis, J. A., and Sagar, S. L. (2005a). Development of a purification process for adenovirus: controlling virus aggregation to improve the clearance of host cell DNA. *Biotechnol Prog*, *21*, 466–472.

Konz, J. O., Lee, A. L., To, B. C. S., and Goerke, A. R. (2008). Methods of adenovirus purification. *US Patent 0118970 A1*, .

Konz, J. O., Livingood, R. C., Bett, A. J., Goerke, A. R., Laska, M. E., and Sagar, S. L. (2005b). Serotype specificity of adenovirus purification using anion-exchange chromatography. *Hum Gene Ther*, *16*, 1346–1353.

Liu, H. F., Ma, J., Winter, C., and Bayer, R. (2010). Recovery and purification process development for monoclonal antibody production. *MAbs*, *2*, 480–499.

Luitjens, A., and van Herk, H. (2012). Method for the production of Ad26 adenoviral vectors. *US Patent 0315696 A1*, .

Mehta, A., and Zydney, A. L. (2005). Permeability and selectivity analysis for ultrafiltration membranes. *J Memb Sci*, *249*, 245–249.

Negrete, A., Pai, A., and Shiloach, J. (2014). Use of hollow fiber tangential flow filtration for the recovery and concentration of hiv virus-like particles produced in insect cells. *J. Virol. Methods*, *195*, 240–246.

Nestola, P., Villain, L., Peixoto, C., Martins, D. L., Alves, P. M., Carrondo, M. J., and Mota, J. P. (2014). Impact of grafting on the design of new membrane adsorbers for adenovirus purification. *J Biotechnol*, *181*, 1–11.

Paulen, R., Fikar, M., Foley, G., Kovács, Z., and Czermak, P. (2012). Optimal feeding strategy of diafiltration buffer in batch membrane processes. *J. Membr. Sci.*, *411*, 160–172.

Peinador, R. I., Calvo, J. I., ToVinh, K., Thom, V., Prádanos, P., and Hernández, A. (2011). Liquid–liquid displacement porosimetry for the characterization of virus retentive membranes. *J. Membr. Sci.*, *372*, 366–372.

Peixoto, C., Ferreira, T. B., Sousa, M. F. Q., Carrondo, M. J. T., and Alves, P. M. (2008). Towards purification of adenoviral vectors based on membrane technology. *Biotechnol Prog*, *24*, 1290–1296.

van Reis, R., and Zydney, A. (2007). Bioprocess membrane technology. *J Memb Sci*, *297*, 16–50.

Rodrigues, T., Carrondo, M. J. T., Alves, P. M., and Cruz, P. E. (2007a). Purification of retroviral vectors for clinical application: Biological implications and technological challenges. *J Biotechnol*, *127*, 520–541.

Rodrigues, T., Carvalho, A., Carmo, M., Carrondo, M. J. T., Alves, P. M., and Cruz, P. E. (2007b). Scaleable purification process for gene therapy retroviral vectors. *J. Gene Med.*, *9*, 233–243.

Segura, M. M., Mangion, M., Gaillet, B., and Garnier, A. (2013). New developments in lentiviral vector design, production and purification. *Expert Opin Biol Ther*, *13*, 987–1011.

Segura, M. M., Puig, M., Monfar, M., and Chillón, M. (2012). Chromatography purification of canine adenoviral vectors. *Hum Gene Ther Methods*, *23*, 182–197.

Silva, A. C., Simão, D., Sousa, M. F. Q., Peixoto, C., Cruz, P., Carrondo, M. J. T., and Alves, P. M. (2012). Production and purification of Ad vectors: current status and future needs for Adenovirus vector production. In O. Cohen-Haguenauer (Ed.), *The CliniBook: Clinical gene transfer state of the art* (pp. 245–250). Paris: EDK.

Subramanian, S., Altaras, G. M., Chen, J., Hughes, B. S., Zhou, W., and Altaras, N. E. (2008). Pilot-scale adenovirus seed production through concurrent virus release and concentration by hollow fiber filtration. *Biotechnol Prog*, *21*, 851–859.

Tatsis, N., and Ertl, H. C. J. (2004). Adenoviruses as vaccine vectors. *Mol Ther*, *10*, 616–629.

Vellekamp, G., Porter, F. W., Sutjipto, S., Cutler, C., Bondoc, L., Liu, Y.-H., Wylie, D., Cannon-Carlson, S., Tang, J. T., Frei, A. et al. (2001). Empty capsids in column-purified recombinant adenovirus preparations. *Hum. Gene Ther.*, *12*, 1923–1936.

Vicente, T., Peixoto, C., Carrondo, M. J. T., and Alves, P. M. (2009). Purification of recombinant baculoviruses for gene therapy using membrane processes. *Gene Ther*, *16*, 766–775.

Weggeman, M., and van Corven, E. J. J. M. (2005). Virus purification methods. *European Patent 1780269 B1*, .

Wickramasinghe, S. R., Kalbfuß, B., Zimmermann, A., Thom, V., and Reichl, U. (2005). Tangential flow microfiltration and ultrafiltration for human influenza A virus concentration and purification. *Biotechnol. Bioeng.*, *92*, 199–208.

Wickramasinghe, S. R., Stump, E. D., Grzenia, D. L., Husson, S. M., and Pellegrino, J. (2010). Understanding virus filtration membrane performance. *J. Membr. Sci.*, *365*, 160–169.

Wolff, M. W., and Reichl, U. (2011). Downstream processing of cellculture-derived virus particles. *Expert Rev Vaccines*, *10*, 1451–1475.

Zydney, A. L. (2009). Membrane technology for purification of therapeutic proteins. *Biotechnol. Bioeng.*, *103*, 227–230.

CHAPTER 3

Impact of grafting on the design of new membrane adsorbers for adenovirus purification

---

Adapted from:

Nestola P, Villain L, Peixoto C, Martins DL, Alves PM, Carrondo MJT, Mota JPB. Impact of grafting on the design of new membrane adsorbers for adenovirus purification. *Journal of Biotechnology* 2014; 181:1-11

Abstract

The impacts of quaternary amine ligand density and matrix structure, namely hydrogel grafted and directly grafted, on state-of-the-art chromatographic membranes operated in bind-and-elute mode were evaluated for the purification of adenovirus serotype 5. The experiments were performed on a 96-well plate membrane holder, which is a convenient high-throughput screening tool for obtaining the best operating conditions for a process yield optimization. The results show that the hydrogel-grafted membranes are more suitable for virus purification than the directly grafted ones. By reducing the number of grafted ligands to low (1.7 μmol/cm^2) or medium (μmol/cm^2) density, it is possible to increase the recovery of purified virus by 60% compared to a highly charged membrane (3.3 μmol/cm^2) that yielded a recovery rate lower than 30%. In the reported experiments, Sartobind®Q, chosen as benchmark comparison, provides a better compromise between high recovery and large dynamic binding capacity. Overall, this work contributes to the understanding and development of new membrane adsorbers specifically designed for virus purification.

Keywords: membrane chromatography; ligand density; hydrogel grafting; adenovirus adsorption; virus purification

3.1 Introduction

Adenoviruses are considered to be one of the most suitable platforms for producing viral vaccines and gene therapy vectors. These viruses can be produced using complementary cell lines in both adherent and suspension culture systems, such as HEK–293 or PER-C6 cells, or A549 for oncolytic adenovirus (Segura et al., 2008). Despite the recognized interest in these viral vectors, the development of an integrated downstream purification platform for adenoviruses is not yet mature. The complexity of this biopharmaceutical product is partly related to the large batch-to-batch variability of the bio-reaction bulk, which is a challenge for the development of reliable and robust purification processes (Morenweiser, 2005). Moreover, it is still a hurdle to achieve a high-purity grade while keeping host cell protein (HCP) and deoxyribonucleic acid (DNA) within the limits set by regulatory authorities.

Chromatography is a well-established purification tool of recombinant adenovirus used for vaccine and gene therapy. Indeed, ion exchange (IEX) chromatography is the most used technique for the purification of complex biopharmaceuticals. However, packed-bed chromatography suffers from a number of disadvantages: the pressure drop across the bed is usually high and may increase during operation due to media deformation or blockage, and pore diffusion is slow and often leads to degradation of the protein product. In addition, packed beds display a relatively small dynamic binding capacity for virus particles at common process-scale linear velocities of 150-450 cm/h, because binding is restricted to the surface of conventional resin particles (Weaver et al., 2013).

Convective chromatography media, such as membranes and monoliths, offer substantial improvements in capacity, recovery, and reduction of process time (Hahn et al., 2007). To date, monoliths have generally offered larger capacity and higher resolution than membranes (Gerster et al., 2013; Whitfield et al., 2009), but the latter have proven to be less prone to clogging, and their relatively low cost has made it practical to discard them after a single use rather than to invest additional resources on developing and validating regeneration and sanitization procedures.

Membrane adsorbers are used in the biopharmaceutical industry almost exclusively in flowthrough mode for mAb purification (Boi, 2007; Knudsen et al., 2001; Zhou and Tressel, 2006). More recently, membrane adsorption chromatography has been applied to the purification of viral vectors using a bind-and-elute mode, yielding good overall recovery rates (Lee et al., 2009; Peixoto et al., 2006, 2008).

However, two major challenges still remain: on one hand, the adequate removal of contaminants (DNA and HCP) that are closely related with the viral product, and on the other hand, the low binding capacity for highly concentrated feeds. There is, therefore, a need for developing membrane chromatography specifically designed for virus purification (Riordan et al., 2009; Vicente et al., 2011).

The best virus recovery yields reported to date have been obtained with ligands containing quaternary ammonium ions grafted onto the surface of a macroporous membrane to produce a strong anion-exchange adsorber; examples of such membrane adsorbers include Sartobind®Q (Sartorius Stedim Biotech, Germany) and Mustang Q®(PALL, Life Sciences, USA) (Wang et al., 2009; Weaver et al., 2013). The design of new matrices with appropriate ligand density and degree of grafting is key for further improving the performance of the bind-and-elute purification mode for viruses.

This paper studies the effects of ligand density and membrane structure on the binding and elution of adenovirus serotype 5 (Ad5) feed stock. Ad5 was chosen as a model virus given its wide utilization and robustness. Two different membrane platforms manufactured by Sartorius Stedim Biotech (SSB), respectively hydrogel grafted and directly grafted, were evaluated using a 96-well plate membrane holder. In the hydrogel-grafted membrane the ligand is immobilized via a hydrogel support (Zhong et al., 2011), creating a tentacle-like structure; this structure is currently used in Sartobind®Q. In the directly grafted membrane the ligand is directly coupled to the cellulose membrane backbone (Fig.3.1). In the first part of this study the membrane binding and virus recovery are assessed under various operating conditions, namely, pH, buffer type, and ionic strength. In the second part of this work, the dynamic binding capacities of the hydrogel-grafted membranes for the target product (Ad5) and its related impurities (DNA and HCP) are determined using a 96-well plate holder with a very small membrane volume. An attempt is made to elucidate the shapes of the breakthrough curves by matching the frontal analysis experiments to a simple equilibrium-dispersive adsorption breakthrough model.

3.2 Materials and methods

3.2.1 Cell line and medium

The 293 cells purchased from ATCC (ATCC-CRL-1573) were adapted to suspension and grown in a commercial serum-free medium, Ex-Cell 293 (SAFC

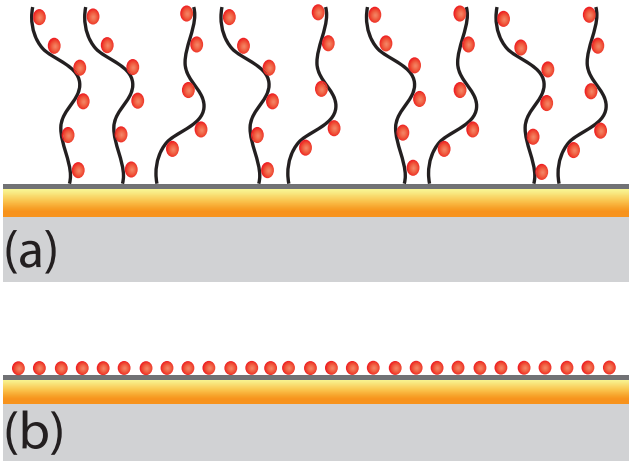

Figure 3.1: *Schematic representation of the two membrane structures: (A) hydrogel-grafted membrane in which the Q ligand is immobilized onto the tentacle-like structure, and (B) directly-grafted membrane in which the ligand is directly immobilized onto the membrane surface. The red dots represent the Q ligands.*

Biosciences, USA), supplemented with 4 mM of glutamine (Invitrogen, UK), and cultured in a humidified atmosphere of 8% CO2 in air at 37 C using shake flasks (Corning, USA).

3.2.2 Virus production

A replication-defective adenovirus, derived from adenovirus serotype 5 (Ad5) expressing GFP protein, was used. The virus particles were produced in a 2 L bioreactor with 1 L working volume (Sartorius Stedim Biotech, Germany). The agitation rate started at 70 rpm and the dissolved oxygen was controlled at 50% air saturation by gas mixture and stirred cascade control with an airflow of 0.01 L/min; pH was controlled at 7.2 by aeration with a CO^2 gas mixture and 1 M $NaHCO_3$; all infections were done at a cell concentration (CCI) of 106 cells/mL using a multiplicity of infection (MOI) of 5; the adenoviruses were harvested at 46 hpi.

3.2.3 Virus clarification and concentration

The bioreactor was harvested and treated with 0.1% Triton X100 (Sigma Aldrich, MO, USA) and incubated for 2 h at 37°C with 50 U/mL of Benzonase (Merck Millipore, Germany). Subsequently, the bulk was microfiltrated using 0.8 μm + 0.45 μm

Sartopore 2 (Sartorius Stedim Biotech, Germany) and concentrated/diafiltered with Vivaflow 100 (Sartorius Stedim Biotech, Germany) with a cut-off of 100 kDa. The concentration/diafiltration step was performed with both HEPES 50 mM and Tris 20 mM to produce two clarified bulks conditioned into two different buffer types. The bulk was stored in aliquots at 80°C until further use.

3.2.4 Quantification of total particles

The protocol for the quantification of total particles was a two-step procedure: DNA extraction according to the instructions on the High Pure Viral Nucleic Acid Kit (Roche) manual and real-time PCR. The determination of the number of viral DNA copies was performed by real-time PCR and LightCycler system (Roche Diagnostic) using Fast Start DNA master SYBR Green I kit to track a specific adenovirus 5 sequence (Roche Diagnostics). Internal plasmid of 2.07×10^9copies/μL was used as reference standard. The total particle concentration was also measured using Nanosight NS500 (NanoSight Ltd., UK), which also quantifies the particle size distribution.

3.2.5 Protein analysis

The protein profile analysis was done in 4-12% NuPage gradient pre-cast gels (Invitrogen). The gels were stained by Coomassie Instant Blue (Expedeon Ltd., UK) and the protein concentration was determined using BCA kits (Pierce, Rockford, USA) taking bovine serum albumin (BSA) as the standard protein.

3.2.6 DNA quantification

The DNA was quantified by QuanT-iT Picogreen kit (Invitrogen). After 5 min of incubation, the fluorescence was measured by Luminometery (Turner BioSystems). Purified DNA was used as standard.

3.2.7 Virus titration

The viruses were encoded for a GFP gene, thus infected cells were positive to GFP, and quantified by flow cytometry analysis with GFP fluorescence signal monitoring. The flow cytometric data were acquired using a CyFlow Space. The green fluorescent signal was measured in a photomultiplier tube after passing through a 525 nm band pass filter. GFP fluorescence of 2×10^4 single viable

cells per sample selected on FS versus SS scatter basis was analyzed and high fluorescent cells were gated.

3.2.8 Chromatography

The devices used for the DBC determination, with a bed volume of 23 μL, were connected to an kta Explorer 100 Air system or kta Explorer 10 (GE Healthcare) equipped with UV, conductivity, and pH detectors, and a fraction collector FRAC-950 (GE Healthcare). Before each experiment, the membranes were sanitized with 10 membrane volumes (MVs) of 1 M NaOH and then equilibrated with loading buffer until the pH and conductivity of the outflow reached the values of the load. After each experimental run all collected fractions were stored at 80°C for further analysis. High-throughput experiments were performed in a 96-well membrane holder device provided by Sartorius. The small-scale membrane adsorbers were assembled by mounting a stack of three membrane sheets into each cell of the 96-well holder to give a differential bed volume of 23 μL. Each cell was loaded with 500 μL of bioreaction bulk, corresponding to approximately 22 MVs; subsequently a vacuum of 0.35 bar was applied to force the whole liquid to flow through the membrane bed into the low-pressure side of the cell. The first elution step consisted of flowing 500 μL of 1 M NaCl through the membrane as running buffer; this step was then followed by a second elution step with 500 μL of 2 M NaCl. All the experiments were duplicated to ensure statistical significance.

3.3 Result and discussion

3.3.1 Hydrogel-grafted membranes

Protein binding

The results obtained with the hydrogel-grafted membranes are presented first. These membranes were functionalized by Sartorius Stedim Biotech with quaternary amine at three different ligand densities, namely 1.7, 2.4, and 3.3 μmol/cm^2; these ligand densities are hereafter referred to as low, medium, and high ligand densities, respectively (Table 3.1). The ligand densities were determined by acid/base titration by monitoring the corresponding conductivity curve. Besides the ligand density, the impacts of buffer type, namely 20 mM Tris and 50 mM HEPES, and pH (Table 3.2) were also evaluated.

Table 3.1: *Characteristics of the prototype hydrogel-grafted and directly-grafted membranes manufactured by Sartorius Stedim Biotech.*

Hydrogel-grafted membrane		Directly-grafted membrane	
Ligand density (μmol/cm^2)	Static BSA binding capacity (mg/cm^2)	Ligand density (μmol/cm^2)	Static BSA binding capacity (mg/cm^2)
1.7	0.51	0.5	N/A
2.4*	1.05	2.5	N/A
3.3	1.51	4.5	N/A

*Sartobind Q®membrane used as benchmark reference.

Table 3.2: *Experimental conditions for the runs with the hydrogel-grafted membranes: buffer type, ionic strength, and pH.*

Buffer		NaCl concentration (mM)	Load volume per well (μL)
20mM Tris	pH 8	0; 50; 100; 150; 200	500
20mM Tris	pH 7.5	0; 50; 100; 150; 200	500
50mm HEPES	pH 8	0; 50; 100; 150; 200	500
50mm HEPES	pH 7.5	0; 50; 100; 150; 200	500

In a first instance, protein binding was assessed by analyzing the flow-through with BCA kits (see Section 3.2.5). The total protein concentration obtained in the flow-through, c_p^{out} i.e., the concentration of total unbound protein in the 500 μL of bioreaction bulk flown through the membrane, showed an approximately linear correlation with increasing ionic strength. No significant differences were observed between the medium- and high-ligand densities. Given that all experiments used the same amount of bioreaction bulk, the amount of bound protein bound per unit membrane volume unit is $q_p = (V_{bulk}/V_m)(C_p^{in} - C_p^{out})$, where $V_{bulk}/V_m = 21.7$ is the number of membrane volumes of injected bulk and $c_p^{in} = 600$ μg/mL is the initial protein concentration in the bioreaction bulk. Hence, the dependence of q_p on the ionic strength is that the opposite of c_p^{out}.

On the other hand, the membrane with the lowest ligand density (1.7 μmol/cm^2) behaved differently, since it bound larger amounts of total protein (cf. two topmost plots of Fig. 3.2). This might seem contradictory, since a lower degree of grafting is expected to result in lower protein binding; however, previous studies (Wang et al., 2009; Wei et al., 2013; Wickramasinghe et al., 2006) suggest that this can be due to a decrease of the effective pore size with increasing grafting density for

grafting levels above a given threshold. Under these conditions, proteins with low binding charge might be excluded from the larger pores at high ligand densities. Indeed, the SDS–PAGE gel analyses shown in the bottom picture of Fig. 3.2 show increased bands of low and medium molecular weights for the hydrogel–grafted membrane, confirming that small proteins are excluded or displaced by other species of the bioreactor bulk. The SDS–PAGE was performed for the samples in HEPES buffer since they exhibited a pattern similar to those in Tris buffer.

The results obtained at a pH of 8.0 were very close to those reported above and are not described here for the sake of brevity.

DNA clearance

To assess the effect of ligand density on DNA removal, the membranes loaded with the same amount of adenovirus bulk were eluted with 500 μL of 1 M NaCl. No significant differences were observed for the medium- and high-charge densities, in contrast to the low-ligand density for which the amount of DNA eluted from the membrane showed a 2–fold decrease (top plots in Fig. 3.3). Noteworthy was the significant decrease of the eluted DNA with the increasing ionic strength of the load; the total desorbed protein as a function of the ionic strength of the load followed the same trend (data not shown). This is a well–know effect in IEX adsorption: at the solid–liquid interface the charged surface attracts counter–ions from the solution to form a "double layer" whose thickness is reduced with increasing ionic strength. When a protein or other biological components adsorb on an ion-exchange support, only a small fraction of their total surface area contacts the double layer (Wei et al., 2013). A thin double layer therefore limits the molecular contact area and thereby weakens the electrostatic interactions between the ion exchanger and the biological adsorbateprotein or DNA in the present caseresulting in a reduced adsorption capacity (Hunter and Carta, 2001a). In other words, increasing the ionic strength of the load reduces the available contact surface area, and thus the binding of a biological molecule, such as DNA.

After elution with 1 M NaCl, each well was eluted with 500 μL of 2 M NaCl solution to completely desorb the remaining DNA. In contrast to the elution with 1 M NaCl, the amount of DNA desorbed by subsequently eluting the membrane with 2 M NaCl increased only slightly with salt concentration for the loaded bulk in HEPES buffer; moreover, the corresponding results obtained for the Tris buffer were mostly independent of the ionic strength (bottom plots in Fig. 3.3). This is an expected result, given that the DNA desorbed in the second elution at 2 M NaCl is the residual amount that was more strongly bound to the membrane through

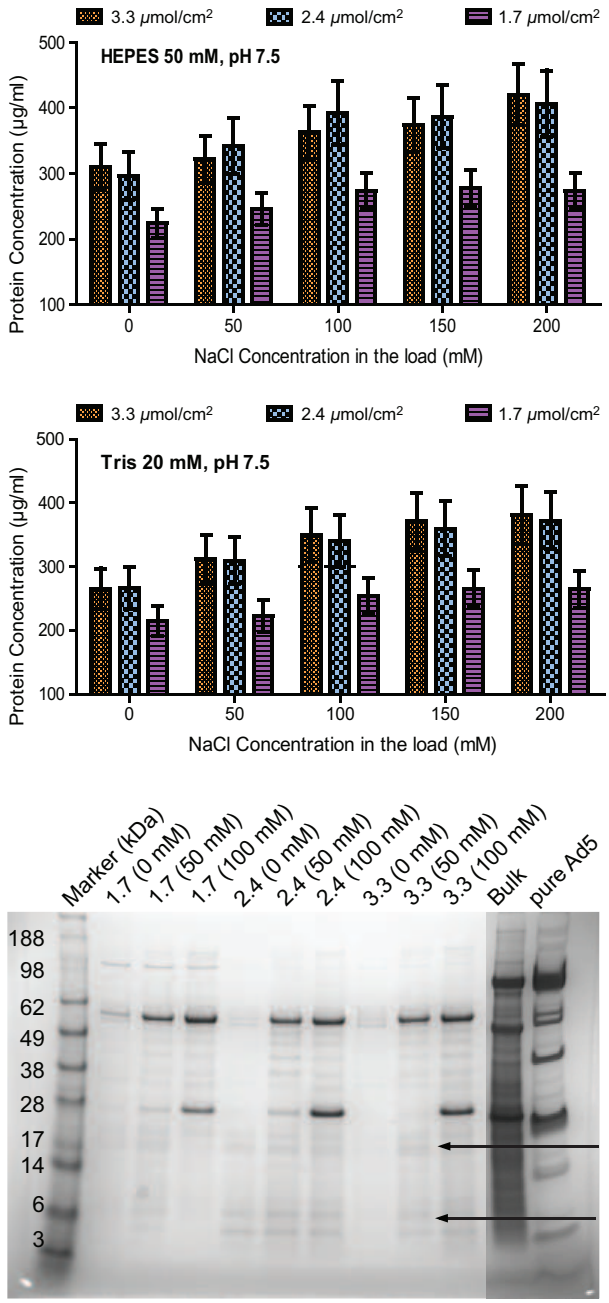

Figure 3.2: *(Top) Total protein concentration in the flow–through for the experiments with the hydrogel–grafted membranes at different ionic strengths in the loaded bulk (experiments performed in duplicated). (Bottom) SDS–PAGE analysis of the flow–through experiments. The ligand density is indicated at the top of each lane (1.7, 2.4, and 3.3 $\mu mol/cm^2$); the NaCl concentration in the loaded bulk is given in parentheses. The arrows point to the lower molecular weight limit of unbound protein due to the increased ligand density.*

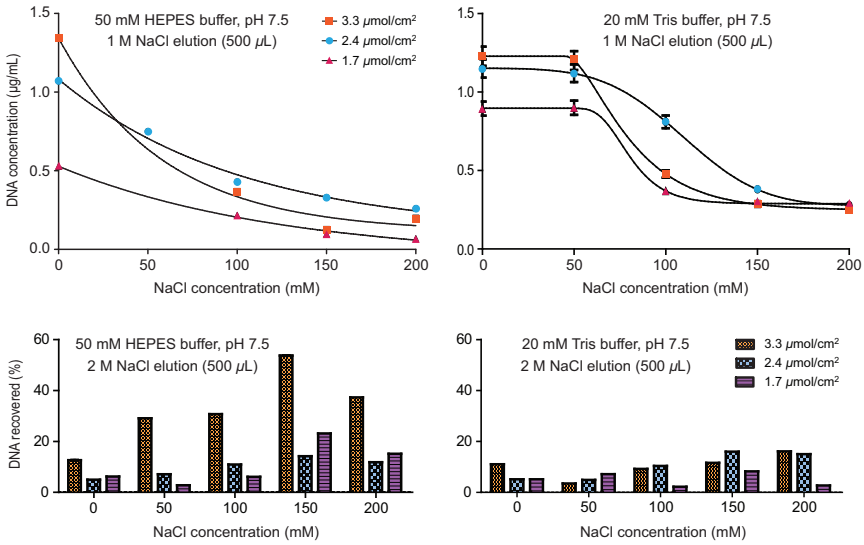

Figure 3.3: *DNA concentration in the 1 M NaCl eluted volume (top) and DNA recovery in the subsequent 2 M NaCl eluted volume for different ionic strengths in the loaded bulk. The buffer types in the loaded bulks were HEPES 50 mM and Tris 20 mM both at pH 7.5. Experiments were performed in duplicate and analyzed by PicoGreen kit. The lines in the top plots are a guide to the eye.*

unspecific mechanisms that are essentially independent of the ionic strength of the loading conditions.

Also, for an initial DNA concentration of 1.74 μg/mL in the loaded bioreaction bulk, no clear differences were observed between the 1 M NaCl elutions for the three ligand densities; on the other hand, when the membranes were eluted with 2 M NaCl, it is clear that the membrane with highest ligand density has a larger residual amount of bound DNA (25-40%) that is only desorbed at a strong ionic strength than the other two membranes (3-10%).

Given that the elution step with 2 M NaCl removed practically all the DNA still bound to the membranes, the amount of DNA bound in the loading step should then be equal to the cumulative amount of DNA recovered in the two elution steps. The bound DNA concentrations calculated this way were found to be proportional to the DNA concentrations recovered in the first elution step (1 M NaCl). The data plotted in the top-left graph of Fig. 3.3 can be converted to bound DNA concentration, expressed as g per mL of membrane volume, using a scale factor of 25 for the low- and medium-density membranes and a scale factor of 35 for the high-density membrane. Likewise, the conversion factors for the data obtained with Tris buffer (top-right plot of Fig. 3.3) are 22-25 for all ligand

Table 3.3: *Percentage of virus particles detected in the flow-through (FT) for ionic strengths of the load in the 0-200 mM NaCl range.*

Ligand density (μmol/cm^2)	Virus in FT (%)
1.7	3.6–13
2.4	1.8–6.1
3.3	1.0–2.7

densities. These results are in line with the data shown in the bottom plots of Fig. 3.3.

The results given above suggest that with increasing ligand density the DNA interacts with a higher number of charge sites in the surface of the tentacle-like hydrogel layer and, hence, that its displacement requires higher ionic strength. The results obtained at a pH of 8.0 were very close to those reported above and are not described here for the sake of brevity.

Virus recovery yield

The percentage of virus in the flow-through and the virus recovered in the 1 M NaCl elution step were determined for the conditions described above (cf. Table 3.2). It was not possible to measure the amount of virus recovered in the 2 M NaCl elution due to the damage of the particles that occurs at this ionic strength. As expected, the low-ligand density membrane gives the highest amount of virus in the flow-through, attaining levels of ca. 1.5×10^9 vp/mL for a salt concentration in the loaded bulk of 200 mM NaCl. The virus concentration in the flow-through for the high and medium ligand density is less influenced by the ionic strength over the range of measured concentrations (0-200 mM NaCl) (Table 3.3). This may be due to the increase of the electrostatic double layer and multipoint attachment resulting from the tentacle structure, which induces a more salt tolerant profile. The use of 50 mM HEPES, at either pH 7.5 or pH 8, gives virus recoveries between 50% and 90% on the membrane with medium ligand density (2.4 μmol/cm^2) (Fig. 3.4). The use of Tris buffer, on the other hand, does not give recovery yields higher than 20% under the best conditions; such low recovery yields were not expected, and there is no clear explanation for this. However, pragmatic evidence from the literature confirms that the 50 mM HEPES buffer is widely used for adenovirus purification, achieving fairly good recovery yields (Konz et al., 2005). It is worth noting that for the highest ligand density of 3.3 μmol/cm^2, not only did the total particle titer decrease but

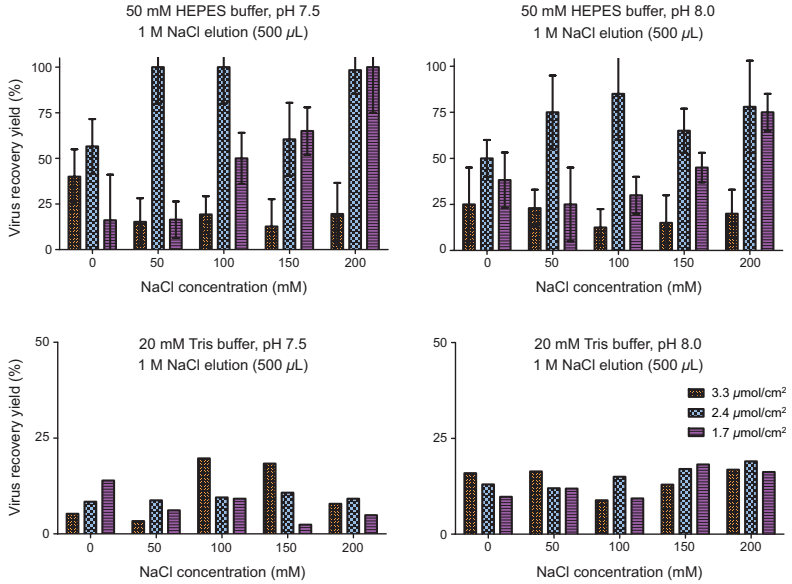

Figure 3.4: *Impact of ligand density of hydrogel-grafted membranes and buffer type of the bioreaction bulk on the virus recovery yield at 1 M NaCl elution. HEPES and Tris buffer were evaluated at two different pH values: 7.5 and 8. The virus concentration was assessed by RT-PCR and Nanosight.*

Table 3.4: *Concentration of infectious virus particles obtained at the best recovery conditions for each hydrogel-grafted membrane. Salt concentration refers to NaCl (mM) in 50 mM HEPES buffer at pH 7.0.*

Ligand density (μmol/cm^2)	Infectious virus particle (10^7 IP/mL)	Salt Concentration (mM)
1.7	62.5	200
2.4	58.7	150
3.3	5.37	0

also the infectivity was dramatically compromised (Table 3.4). This can be due to a damage of the virus's capside or fibers during the binding or, most likely, during the desorption step. Vicente et al. (2011) observed the occurrence of a similar behavior while purifying baculoviruses. Also, the virus entrapment into the hydrogel structure is likely to be enhanced at high ligand density (Tatárová et al., 2009), which explains the low recovery yield.

3.3.2 Directly-grafted membranes

Protein binding

The directly grafted membrane prototypes produced by Sartorius Stedim Biotech had the following three different ligand densities: 0.5, 2.5, and 4.5 μmol/cm^2 (Table 3.1); these values are comparable to those of the hydrogel-grafted membranes, especially those of the medium and high ligand densities. The structure of the directly-grafted membrane is different from that of the hydrogel-grafted one because the quaternary amine is directly immobilized onto the membrane's surface. The buffer used in the experiments was 50 mM HEPES at pH 7.5 because of its good performance with the hydrogel-grafted membranes. The NaCl concentrations evaluated were kept below 100 mM, since the binding to these membranes is seriously compromised at higher ionic strengths.

The analysis of the total protein concentration in the flow-through did not show any major differences between the 0.5 and 2.5 μmol/cm^2 ligand densities (Fig. 3.5, top graphic). However, as opposed to what was previously observed for the hydrogel-grafted membranes, the directly grafted membrane with the highest ligand density yielded a marked reduction on the protein content down to 250 μg/mL. This is corroborated by the SDS-PAGE analysis shown in the bottom picture of Fig. 3.5. This result supports our previous claim whereby increasing the grafting degree excludes some proteins from binding, as certain ligand sites will be shielded from the proteins.

Virus recovery yield

Fig. 3.6 presents the virus recovery yields obtained with the directly-grafted membranes. Although the ligand densities of these membranes are comparable to those of the hydrogel-grafted ones, the virus binding is compromised. The percentage of viruses in the flow-through for the membranes with 2.5 and 0.5 μmol/cm^2 ligand densities is ca. 60-70%, and even larger values are obtained if the ionic strength is increased. Only the membrane with 4.5 μmol/cm^2 ligand density yielded 25% of viruses in the flow-through. It is also worth mentioning that it was not possible to close the virus material balance for the hydrogel-grafted membranes, most likely due to irreversible binding or entrapment. On the other hand, in the experiments with the directly grafted membranes there was a fairly good agreement between the viruses in the flow-through and in the subsequently elution volume. This can be due to the inexistence of the tentacle structure and its

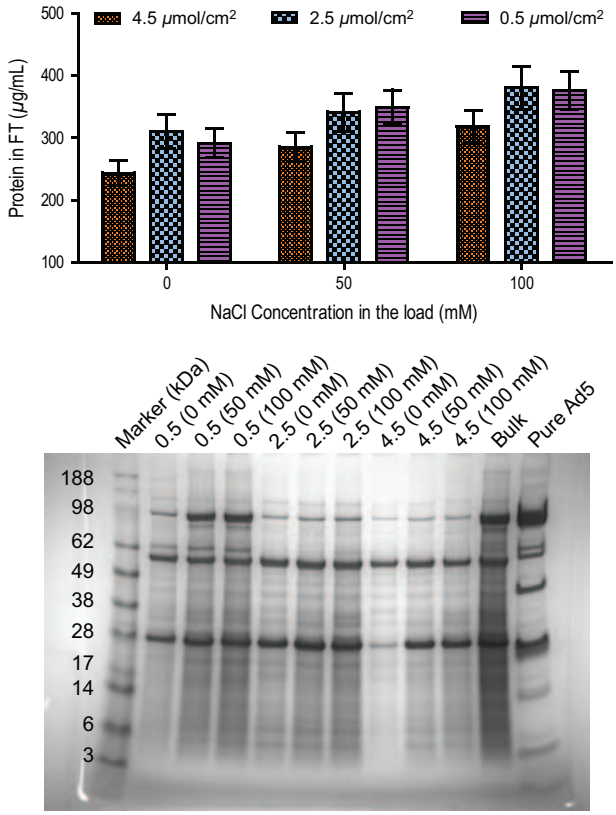

Figure 3.5: *(Top) Protein concentration in the flow-through for the experiments with the directly grafted membranes at different ionic strengths in the loaded bulk ranging from 0 to 100 mM NaCl (experiments performed in duplicated). All experiments were performed with 50 mM HEPES buffer at pH 7.5. (Bottom) SDS-PAGE analysis of the flow-through experiments. The ligand density is indicated at the top of each lane (0.5, 2.5, and 4.5 μmol/cm²); the NaCl concentration in the loaded bulk is given in parentheses.*

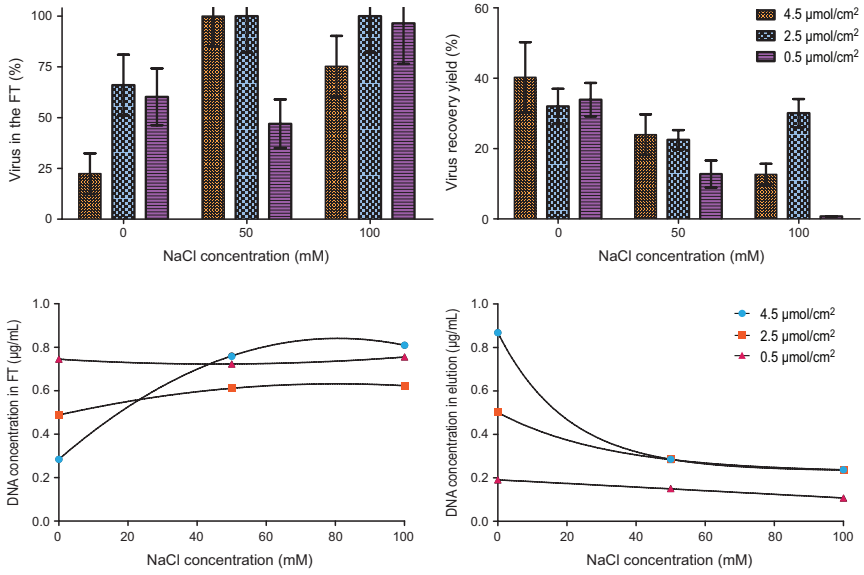

Figure 3.6: *The top panel gives the virus recovery yield and percentage of viruses in the flow through (FT) for the direct grafted membrane. The bottom panel shows the DNA both in FT and at 1 M NaCl elution. The fittings illustrate, respectively, the DNA increase in the FT at higher ionic strengths and the consequently exponential decay at 1 M elution.*

associated multipoint attachment. Furthermore, entrapment and steric hindrance are reduced because of the absence of the hydrogel support.

DNA clearance

The DNA clearance in bind-and-elute mode was evaluated and compared with the results obtained for the hydrogel-grafted membranes. In line with the results of proteins content, the amount of DNA captured with the highest ligand density is close to 60% of the initial DNA concentration presented in the load. The elution with 1 M NaCl has a substantially reduced amount of DNA when compared to a similar elution of the hydrogel-grafted membrane. Only the 4.5 μmol/cm^2 membrane shows a binding capacity comparable to the grafted membrane. Again, if the ionic strength is increased even slightly, the binding is reduced (Fig. 3.6). The amount of DNA detected upon further elution with 2 M NaCl is under the sensitivity limit of the assay, showing that DNA is already almost completely desorbed with 1 M NaCl.

3.3.3 Dynamic binding capacity of the hydrogel-grafted membranes

The results discussed above indicate that the hydrogel-grafted membrane is more suitable than the directly grafted membrane for a bind-and-elute purification, although there is still some room for improving the results obtained with the directly grafted membranes. Therefore, the dynamic binding capacities (DBCs) of the three hydrogel-grafted membranes for the virus and for the two contaminants were measured for a 50 mM HEPES buffer at pH 7.5.

The breakthrough curves shown in the left-hand-side plots of Fig. 3.7 were obtained by collecting and analyzing samples every 0.25 mL. The breakthrough curves illustrate the different shapes and quasi-horizontal plateaus obtained with the low-, medium- and high-ligand density, hydrogel-grafted membranes. In particular, it is interesting to observe that although the breakthrough curves exhibit the characteristic sigmoidal shape expected for a favorable isotherm, the titers in the flow-through do not reach the values in the feed bulk, but instead nearly stabilize at lower values, which is indicative of a pronounced tailing behavior; the only noteworthy exception is the breakthrough curve for DNA on the low-density membrane, which exhibits the expected Langmuir-type behavior with the correct horizontal plateau. In general, the experimental breakthrough curves are quite sharp, except those obtained with the high ligand density membrane. The sharpness of the breakthrough curve (i.e., smaller mass transfer zone) is one of the advantages of membrane chromatography over packed-bed chromatography (unless the binding kinetics is the limiting rate step): membrane adsorbers are usually not limited by pore diffusion because they operate under nearly convective flow conditions.

The apparent stabilization of the exit titer at a value below the value in the feed bulk over the duration of the experiment indicates that the membrane is retaining increasingly larger amounts of biological when the concentration in the liquid phase surpasses the concentration defined by the plateauthis follows from an overall material balance to the membrane adsorber by noting that the position in the adsorber that exhibits the most retarded dynamics during the binding step is precisely the one at the downstream end of the adsorber.

It is worth noting that the membranes under study are convective-flow media with pore sizes of around 3 μm, which are significantly larger than those of conventional resin beads used in packed-bed chromatography. For this reason, the porous structure of the membrane matrix is expected to significantly reduce

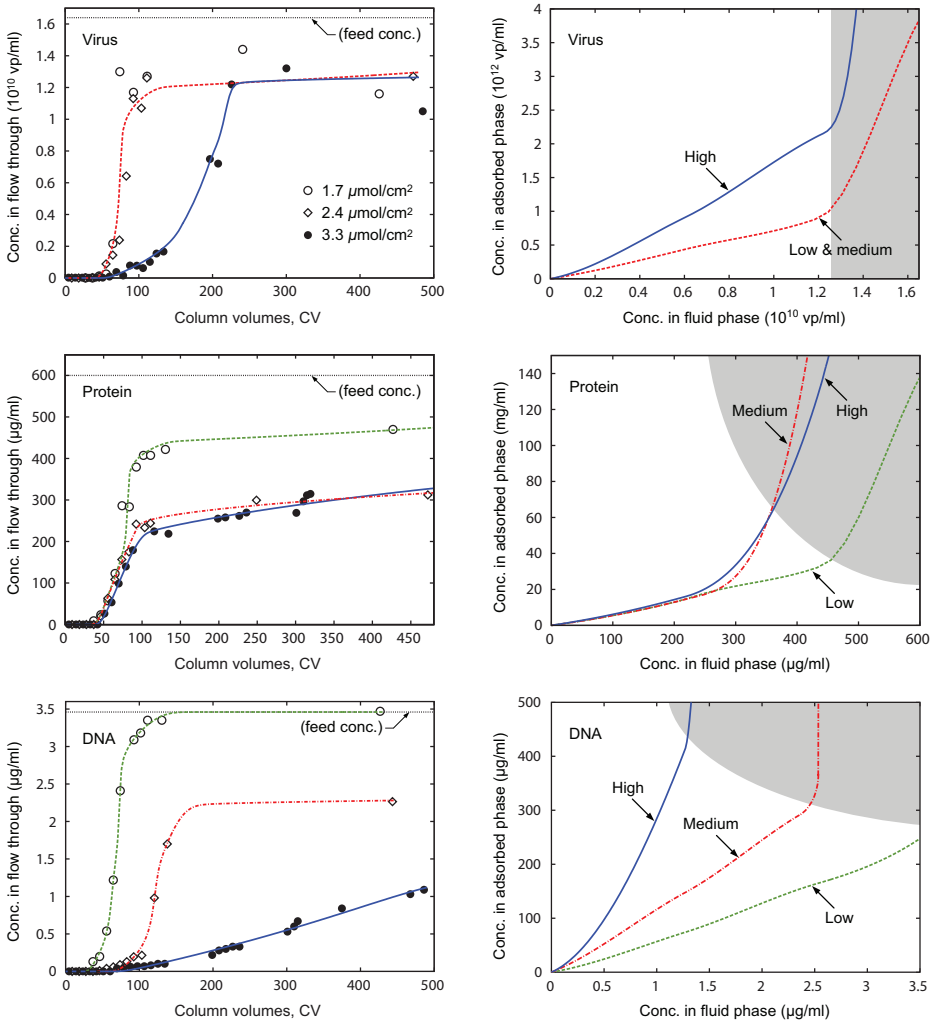

Figure 3.7: *Breakthrough curves (left) of the main components of the adenovirus bioreactor bulk for the low-, medium-, and high-ligand densities, hydrogel-grafted membranes with 50 mM HEPES buffer at pH 7.5; total protein, DNA, and virus contents were analyzed for each collected fraction. The right-hand-side plots show the apparent adsorption isotherms obtained by fitting the equilibrium-dispersed model given by Eqs. (3.1)–(3.6) to the experimental breakthrough data; the gray areas depict the regions where the fitting uncertainty is highest.*

the diffusional mass transfer resistances. Thus, the dynamics of the membrane adsorber should be essentially governed by the thermodynamics of adsorption rather than by mass transfer or kinetic resistances. Assuming that the adsorption process is equilibrium-controlled, the influence of the adsorption isotherm on the different shapes of the breakthrough curves can be put into evidence using a simple equilibrium-based, dispersed plug flow adsorption model. The model can be expressed as

$$\varepsilon\frac{\partial c_i}{\partial \theta} + \frac{\partial q_i}{\partial \theta} = \frac{1}{Pe}\frac{\partial^2 q_i}{\partial x^2} - \frac{\partial c_i}{\partial x}, \tag{3.1}$$

with boundary conditions

$$\left(c_i - \frac{1}{Pe}\frac{\partial c_i}{\partial x}\right)_{x=0} = \begin{cases} 0 & t < 0 \\ c_t^{in} & t > 0 \end{cases} \tag{3.2}$$

$$\left(\frac{\partial c_i}{\partial x}\right)_{x=1} = 0 \tag{3.3}$$

where i is the solute index, c is the solute concentration in the fluid phase (amount per unit volume), q is the solute concentration in the adsorbed phase (amount per unit adsorber volume), $x = z/L$ is a dimensionless coordinate along the axial length L of the membrane adsorber, and $\theta = Qt/V$ is a dimensionless time coordinate that gives the number of eluted column volumes (t is the dimensional time coordinate, Q is the volumetric flow rate, and V is the volume of the membrane adsorber); c^{in} is the concentration in the feed mixture.

The Pclet number, Pe, which is a simple measure of finite membrane efficiency, is used here to account for the combined effect of axial dispersion due to the convective transport through the membrane and the presumably small contribution from diffusional resistances; it also helps to stabilize the numerical solution. In the numerical fitting procedure Pe was fixed at 500. It is worth noting that the obtained breakthrough curves are not very sensitive to the selected value of Pe, unless it is set to a very small value or to a very high value. For example, doubling the value of Pe to 1000 or reducing it to 250 does not significantly change the simulated breakthrough profiles.

The equilibrium-dispersed model assumes that the adsorbed phase is in local equilibrium with the contacting bulk fluid, i.e., $q_i = q_i^*(c_i, ..., c_n)$, where q_i^* represents the adsorption isotherm for component i in the presence of the other n-1 solutes (i.e., under multicomponent conditions). Given that the experiments were performed for a single overall feed concentration of the bioreaction bulk

mixture, it is not possible to determine q_i^*. Instead, we shall concentrate on the apparent single-component adsorption isotherm, $q_i = q_i^*(c_i)$, which is the adsorption isotherm that gives the same breakthrough curve for component i under multicomponent conditions if the component was injected isolated at the same concentration as in the bioreaction bulk. Obviously, $q_i^*(c_i)$ can only be estimated up to the value of the feed concentration, c_i^{in}.

To determine the function $q_i^* = (c_i)$, we discretize it over the concentration range $c_i \, \epsilon \, [0, c_i^{in}]$ using third-order orthogonal collocation on finite elements (we have used three equal-sized elements)the left-most collocation point of the first element is set to 0 and the right-most collocation point of the last element is set to c_i^{in}. By definition $q_i^*(0) = 0$, so this value is fixed. To ensure continuity of the function value and its first derivative across elements, each boundary collocation point shared by two consecutive elements, say point $c_i^{(m)}$, must satisfy the C1 condition

$$\left(\frac{dq_i^*}{dc_i}\right)_{c_i^{(m)-}} = \left(\frac{dq_i^*}{dc_i}\right)_{c_i^{(m)+}} \tag{3.4}$$

The remaining unknown values of $q_i^*(c_i^{(k)})$ at the interior collocation points $c_i^{(k)}$ (and also at the right-most collocation point c_i^{in}) are determined by minimizing the sum of the squares of the deviations between the N_i experimental measurements of the breakthrough curve, $c_{i,exp}^{out}(t_j), j = 1, ..., N_i$, and the simulated values, $c_{i,exp}^{out}(t_j)$, i.e.,

$$f_{obj} = min_{q_i^*(c_i^{(k)})} \frac{1}{N_i} \sum_{j}^{N_i} [c_{i,exp}^{out}(t_j) - c_i^{out}(t_j)]^2 \tag{3.5}$$

To guarantee that the estimated shape of $q_i^*(c_i)$ is physically meaningful, the values of $q_i^*(c_i^{(k)})$ are further constrained by the following conditions that yield a monotonically increasing function of c_i:

$$q_i^*(c_i^{k+1}) > q_i^*(c_i^k) \quad \text{and} \quad \left(\frac{dq_i^*}{dc_i}\right)_{c_i^{(k)}} \geq 0 \tag{3.6}$$

The equilibrium-dispersed adsorption is discretized in both space and time (Araújo et al., 2008; Mota et al., 2007) ; to generate a sparse system of nonlinear algebraic that forms the set of equality constraints of the objective function given by Eq. (1). This nonlinear optimization problem was formulated in AMPL (R. Fourer, 2003)and solved with the interior-point solver Ipopt 3.10 (Wächter and Biegler, 2006) For each of the analyzed componentsvirus, total protein,

and DNAthe initial estimate of $q_i^*(c_i)$ was the linear adsorption isotherm that reproduces the experimental breakthrough time at half height ($c/2$)

The numerical results are summarized in Fig. 3.7, which on the left-hand-side plots compares the experimental breakthrough measurements against the simulation curves and on the right-hand-side plots shows the apparent single-component adsorption isotherms that best reproduce the experimental breakthrough curves. The first conclusion that can be drawn from Fig. 3.7 is that the observed breakthrough curves can be perfectly fit by adsorption-equilibrium relations satisfying the monotonic constraint. Note, however, that despite the excellent description of the breakthrough experiments, we are quite aware of the limitations of our modeling effort, namely the somewhat fuzzy physical meaning of $q_i^*(c_i)$ curves.

Below a given threshold concentration value each adsorption isotherm is approximately linear. We note that under these conditions the effects of axial dispersion, external mass transfer resistance, and diffusion are approximately additive (see, e.g., (Haynes and Sarma, 1973)). This means that in the modeling of chromatographic columns under linear equilibrium conditions it is seldom worth modeling the band broadening using a more complex descriptor than an overall Pclet number (or, alternatively, and overall effective rate coefficient) incorporating both effects of axial dispersion and the various mass transfer resistances (Ruthven, 1984).

Above a threshold concentration value, the amount adsorbed increases drastically with the solute concentrationsimilar to the behavior observed for a type III isotherm according to the IUPAC classification for vapor-solid equilibria (Rouquerol et al., 1994)-as if consequence of an "apparent stronger binding mechanism." One could argue that a plausible explanation is the entrapment or molecular sieving of the large biological particles due to the reduction of the unobstructed channel width created by the already bound particles at the outer edges of the tentacle structure of the membrane. Moreover, the thickness of the double layer has been shown to be direct proportional to the charge density (Kopaciewicz et al., 1983; Ståhlberg, 1999). Thus, the increase in charge density leads to an extended electrostatic double layer and consequently, also increases the interaction forces with the biological particles. Our membranes have pore size around 3 m, the virus particlesthe largest component in the bulkare approximately 100 nm (0.1 μm). Assuming cylindrical pore geometry, one monolayer of virus particles would reduce the unobstructed cross section of the pore by only 13%. Thus, it seems unlikely that the dense adsorbed phase can effectively block the passage of the large biological particles, even at the highest ligand density.

It is likely that aggregation effects may have taken place in our experiments: (i) virus aggregation at high concentrations, such as that of our breakthrough experimentsfor example, several studies (Altaras et al., 2005; Croyle MA, 2003; Konz et al., 2005) have demonstrated that Ad5 has an aggregation concentration dependent behavior; (ii) DNA can form complexes with the virus particles, since it may bind to positive local patches on the capside (Goerke et al., 2005; Konz et al., 2005); (iii) proteins can precipitate or aggregate due to the local high concentration on the membrane at the concentration conditions of the plateau phase (Whitley et al., 1991). It is worth noting that various explanations and theories have been advanced in the literature for the pronounced tailing behavior, including extra-column contributions, hindered diffusion, and steric hindrance (Weinbrenner and Etzel, 1994; Jin et al., 1994; Talbot et al., 2000). However, as Hunter and Carta (2001b) correctly point out, it is not trivial to elucidate the mechanisms of adsorption equilibrium and kinetics by matching breakthrough curves to theoretical models unless highly pure single-component feeds are employed. Nevertheless, although the modeling procedure employed above is embodied of some empiricism, it is still a useful tool for process design.

Despite the effects mentioned above, the shapes of the breakthrough curves suggest that if the membrane adsorber were operated with a more diluted feed, the gap between the breakthrough plateau and the initial feed stock concentration would be reduced. In the following discussion the breakthrough point at 10% height was taken as a reference measurement for comparison.

Table 3.5 summarizes the DBC at 10% and breakthrough points (BT) at 10% height for the virus, proteins, and DNA. Whereas for DNA the $DBC_{10\%}$ increases 5-fold when the ligand density is increased from 1.7 to 3.3 μmol/cm^2 (low to high level), such a substantial increase is less visible for the virus and not observed at all for the proteins. For the low-ligand density membrane the 10%-DBCs follow the sequence: virus $\approx$ proteins $>$ DNA, whereas for the medium ligand density membrane the sequence is DNA $>$ virus $\approx$ proteins, and for the high ligand density the sequence changes to DNA $>$ virus $>$ proteins. The 10%-DBCs obtained with the low ligand density membrane are nearly similar, yielding poor selectivity, but get progressively separated with increasing ligand density. However, the spreading of the breakthrough curve also increases with increasing ligand density, which is undesirable. Thus, although a highly decorated tentacle structure is desirable from a thermodynamic perspective it hinders the fast access of large particles to the whole tentacle structure.

Table 3.5: *Dynamic binding capacity of total protein, DNA, and virus for the three hydrogel-grafted membranes. Breakthrough point at 10% height $BTP_{10\%}$ is expressed in column volumes (CV).*

	Low ligand density		Medium ligand density		High ligand density	
	$BTP_{10\%}$ CV	$DBC^{a}_{10\%}$ (mg/cm^2)	$BTP_{10\%}$ CV	$DBC^{a}_{10\%}$ (mg/cm^2)	$BTP_{10\%}$ CV	$DBC^{a}_{10\%}$ (mg/cm^2)
Protein	57	0.98	57	0.98	63	1.90
DNA	50	0.023	103	0.0055	227	0.10
Virus	58	3.02	58	3.02	106	4.70

[a] $DBC_{10\%}$ for viruses is expressed in 10^{10} virus particle per squared centimeter (10^{10} vp/cm^2).

3.4 Conclusions

In this study the effect of membrane ligand density on the binding and elution of adenovirus (Ad5) and its associated impurities, such as DNA and total protein content, was evaluated. A complex bioreactor feed stock was used to obtain a more realistic approach compared to other studies where model proteins or pure product were used (Lu et al., 2013; Wang et al., 2006; Wrzosek and Polakovič, 2011; Wrzosek et al., 2009). The use a novel 96-well plate system coupled with the small-scale device significantly decreased the time needed for assessing the performance of the two membrane platforms.

The following conclusions can be drawn: (i) the hydrogel-grafted membranes yield higher virus recoveries than the directly grafted membranes; (ii) moving toward hydrogel-grafted membranes with ligand densities lower than 2.4 μmol/cm^2 led to virus recovery higher than 70%; (iii) the directly grafted membranes showed low binding for the virus and give rise to significant percentages of viruses in the flow-through, up to 60-70%.

The estimation of the design space for the two types of membranes points to the optimal conditions with respect to recovery, and clearly illustrates the different characteristics of the two membrane structures evaluated in this study (Fig. 8). A decreased ligand density and increased ionic strength to a value of 150-200 mM NaCl are suitable conditions for hydrogel-grafted membranes; on the other hand, increasing the ligand density and lowering the ionic strength to a maximum of 25 mM NaCl is more suitable for directly grafted membranes.

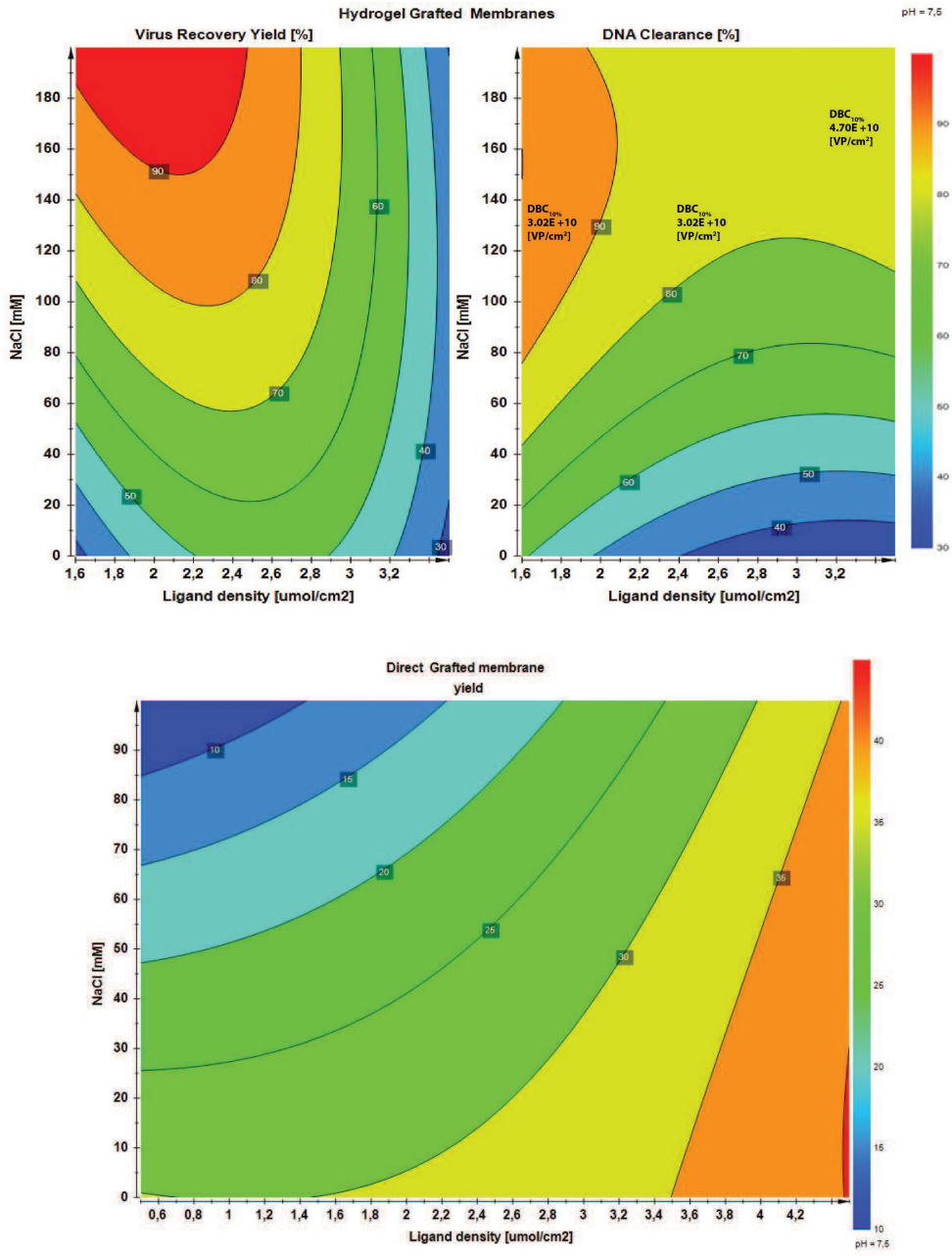

Figure 3.8: *Space design for the hydrogel and the directly grafted membranes. The top-right panel shows the best recovery yield conditions. The top-left panel shows the selectivity, where the red area gives the DNA clearance in the elution at 1 M NaCl. The bottom panel shows the predicted performance of the directly grafted membranes where increasing the ligand density and lowering the ionic strength yields higher recoveries.*

Acknowledgements

The authors thank Ana Carina Silva for the purified Ad5 material. Financial support from Sartorius Stedim Biotech and from the Portuguese Science Foundation (FCT-MCTES) (SFRH/BD/82032/2011and EXPL/BBB-EBB/0790/2012) is gratefully acknowledged.

References

Altaras, N. E., Aunins, J. G., Evans, R. K., Kamen, A., Konz, J. O., and Wolf, J. J. (2005). Production and formulation of adenovirus vectors. *Adv Biochem Eng Biotechnol*, *99*, 193–260.

Araújo, J. M., Rodrigues, R. C., and Mota, J. P. (2008). Determination of competitive isotherms of enantiomers by a hybrid inverse method using overloaded band profiles and the periodic state of the simulated moving-bed process. *J Chromatogr A*, *1189*, 302–313.

Boi, C. (2007). Membrane adsorbers as purification tools for monoclonal antibody purification. *J Chromatogr B*, *848*, 19–27.

Croyle MA, Q. K., Gerding K (2003). Role of the container/closure system and formulation on agitation-induced aggregation phenomena in recombinant adenoviral products. bioprocess j, 2003; 2(5): 35-41. *BioProcess J*, *2(5)*, 35–41.

Gerster, P., Kopecky, E.-M., Hammerschmidt, N., Klausberger, M., Krammer, F., Grabherr, R., Mersich, C., Urbas, L., Kramberger, P., Paril, T., Schreiner, M., Nöbauer, K., Razzazi-Fazeli, E., and Jungbauer, A. (2013). Purification of infective baculoviruses by monoliths. *J Chromatogr A*, *1290*, 36–45.

Goerke, A. R., To, B. C. S., Lee, A. L., Sagar, S. L., and Konz, J. O. (2005). Development of a novel adenovirus purification process utilizing selective precipitation of cellular DNA. *Biotechnol Bioeng*, *91*, 12–21.

Hahn, R., Tscheliessnig, A., Bauerhansl, P., and Jungbauer, A. (2007). Dispersion effects in preparative polymethacrylate monoliths operated in radial-flow columns. *J Biochem Biophys Methods*, *70*, 87–94.

Haynes, H. W., and Sarma, P. N. (1973). A model for the application of gas chromatography to measurements of diffusion in bidisperse structured catalysts. *AIChE J*, *19*, 1043–1046.

Hunter, A., and Carta, G. (2001a). Protein adsorption on novel acrylamido-based polymeric ion-exchangers: Iii. salt concentration effects and elution behavior. *J Chromatogr A*, *930*, 79–93.

Hunter, A. K., and Carta, G. (2001b). Effects of bovine serum albumin heterogeneity on frontal analysis with anion-exchange media. *J Chromatogr A*, *937*, 13–19.

Jin, X., Tarjus, G., and Talbot, J. (1994). An adsorption-desorption process on a line: kinetics of the approach to closest packing. *J Phys A*, *27*, L195.

Knudsen, H. L., Fahrner, R. L., Xu, Y., Norling, L. A., and Blank, G. S. (2001). Membrane ion-exchange chromatography for process-scale antibody purification. *J Chromatogr A*, *907*, 145–154.

Konz, J. O., Lee, A. L., Lewis, J. A., and Sagar, S. L. (2005). Development of a purification process for adenovirus: controlling virus aggregation to improve the clearance of host cell DNA. *Biotechnol Prog*, *21*, 466–472.

Kopaciewicz, W., Rounds, M., Fausnaugh, J., and Regnier, F. (1983). Retention model for high-performance ion-exchange chromatography. *J Chromatogr A*, *266*, 3–21.

Lee, D.-S., Kim, B.-M., and Seol, D.-W. (2009). Improved purification of recombinant adenoviral vector by metal affinity membrane chromatography. *Biochem Biophys Res Commun*, *378*, 640–644.

Lu, H.-L., Lin, D.-Q., Gao, D., and Yao, S.-J. (2013). Evaluation of immunoglobulin adsorption on the hydrophobic charge-induction resins with different ligand densities and pore sizes. *J Chromatogr A*, *1278*, 61–68.

Morenweiser, R. (2005). Downstream processing of viral vectors and vaccines. *Gene Ther*, *12*, 103–10.

Mota, J. P., Araújo, J. M., Rodrigues, R. et al. (2007). Optimal design of simulated moving-bed processes under flow rate uncertainty. *AIChE J*, *53*, 2630–2642.

Peixoto, C., Ferreira, T., Carrondo, M., Cruz, P., and Alves, P. (2006). Purification of adenoviral vectors using expanded bed chromatography. *J Virol Methods*, *132*, 121–126.

Peixoto, C., Ferreira, T. B., Sousa, M. F. Q., Carrondo, M. J. T., and Alves, P. M. (2008). Towards purification of adenoviral vectors based on membrane technology. *Biotechnol Prog*, *24*, 1290–1296.

R. Fourer, B. K., D.M. Gay (2003). *AMPL: A Modeling Language for Mathematical Programming*. Brooks/Cole Publishing Co.

Riordan, W., Heilmann, S., Brorson, K., Seshadri, K., He, Y., and Etzel, M. (2009). Design of salt-tolerant membrane adsorbers for viral clearance. *Biotechnol Bioeng*, *103*, 920–929.

Rouquerol, J., Avnir, D., Fairbridge, C., Everett, D., Haynes, J., Pernicone, N., Ramsay, J., Sing, K., and Unger, K. (1994). Recommendations for the characterization of porous solids (technical report). *Pure Appl Chem*, *66*, 1739–1758.

Ruthven, D. (1984). *Principles of Adsorption and Adsorption Processes*. John Wiley & Sons.

Segura, M. M., Alba, R., Bosch, A., and Chillón, M. (2008). Advances in helper-dependent adenoviral vector research. *Curr Gene Ther*, *8*, 222–235.

Ståhlberg, J. (1999). Retention models for ions in chromatography. *J Chromatogr A*, *855*, 3–55.

Talbot, J., Tarjus, G., Van Tassel, P., and Viot, P. (2000). From car parking to protein adsorption: an overview of sequential adsorption processes. *Colloids Surf A*, *165*, 287–324.

Tatárová, I., Faber, R., Denoyel, R., and Polakovič, M. (2009). Characterization of pore structure of a strong anion-exchange membrane adsorbent under different buffer and salt concentration conditions. *J Chromatogr A*, *1216*, 941–947.

Vicente, T., Faber, R., Alves, P. M., Carrondo, M. J. T., and Mota, J. P. B. (2011). Impact of ligand density on the optimization of ion-exchange membrane chromatography for viral vector purification. *Biotechnol Bioeng*, *108*, 1347–1359.

Wächter, A., and Biegler, L. T. (2006). On the implementation of an interior-point filter line-search algorithm for large-scale nonlinear programming. *Math Program*, *106*, 25–57.

Wang, J., Faber, R., and Ulbricht, M. (2009). Influence of pore structure and architecture of photo-grafted functional layers on separation performance of cellulose-based macroporous membrane adsorbers. *J Chromatogr A*, *1216*, 6490–6501.

Wang, L., Zhang, R., Eisenthal, R., and Hubble, J. (2006). An intrinsically shielded hydrogel for the adsorptive recovery of lysozyme. *Biotechnol Appl Biochem*, *45*, 37–42.

Weaver, J., Husson, S. M., Murphy, L., and Wickramasinghe, S. R. (2013). Anion exchange membrane adsorbers for flow-through polishing steps: Part II. Virus, host cell protein, DNA clearance, and antibody recovery. *Biotechnol Bioeng*, *110*, 500–510.

Wei, Y., Ma, J., and Wang, C. (2013). Preparation of high-capacity strong cation exchange membrane for protein adsorption via surface-initiated atom transfer radical polymerization. *J Membr Sci*, *427*, 197–206.

Weinbrenner, W. F., and Etzel, M. R. (1994). Competitive adsorption of α-lactalbumin and bovine serum albumin to a sulfopropyl ion-exchange membrane. *J Chromatogr A*, *662*, 414–419.

Whitfield, R. J., Battom, S. E., Barut, M., Gilham, D. E., and Ball, P. D. (2009). Rapid high-performance liquid chromatographic analysis of adenovirus type 5 particles with a prototype anion-exchange analytical monolith column. *J Chromatogr A*, *1216*, 2725–2729.

Whitley, R. D., Van Cott, K. E., Berninger, J. A., and Wang, N.-H. L. (1991). Effects of protein aggregation in isocratic nonlinear chromatography. *AIChE J*, *37*, 555–568.

Wickramasinghe, S., Carlson, J., Teske, C., Hubbuch, J., and Ulbricht, M. (2006). Characterizing solute binding to macroporous ion exchange membrane adsorbers using confocal laser scanning microscopy. *J Membr Sci*, *281*, 609–618.

Wrzosek, K., Gramblička, M., and Polakovič, M. (2009). Influence of ligand density on antibody binding capacity of cation-exchange adsorbents. *J Chromatogr A*, *1216*, 5039–5044.

Wrzosek, K., and Polakovič, M. (2011). Effect of ph on protein adsorption capacity of strong cation exchangers with grafted layer. *J Chromatogr A*, *1218*, 6987–6994.

Zhong, L., Scharer, J., Moo-Young, M., Fenner, D., Crossley, L., Honeyman, C. H., Suen, S.-Y., and Chou, C. P. (2011). Potential application of hydrogel-based strong anion-exchange membrane for plasmid dna purification. *J Chromatogr B*, *879*, 564–572.

Zhou, J. X., and Tressel, T. (2006). Basic concepts in q membrane chromatography for large-scale antibody production. *Biotechnol Prog*, *22*, 341–349.

Part III

Development and implementation of improved downstream processes

CHAPTER 4

Adenovirus purification by two-column, size-exclusion, simulated countercurrent chromatography

---

Adapted from:

Nestola P, Silva RJS, Peixoto C, Alves PM, Mota JPB, Carrondo MJT. Adenovirus purification by two-column, size-exclusion, simulated countercurrent chromatography. *Journal of Chromatography A* 2014; 1347:111-121.

Abstract

Adenovirus serotype 5 (Ad5) was successfully separated by size-exclusion chromatography (SEC) using a simple, yet efficient, two-column, quasi-continuous, simulated moving-bed process operated in an open-loop configuration. The operating cycle is divided into two identical half-cycles, each of them consisting of the following sequence of sub-steps: (i) elution of the upstream column and direction of the effluent of the downstream column to waste; (ii) elution of the upstream column and redirection of its effluent to waste while the downstream column is fed with the clarified bioreaction bulk and its effluent collected as purified product; (iii) operation of the system as in step (i) but collecting the effluent of the downstream column as product; (iv) elution of the upstream column and direction of its effluent to waste while the flow through the downstream column is temporarily halted. Clearance of impurities, namely DNA and host cell protein (HCP), were experimentally assessed. The pilot-scale run yielded a virus recovery of 86%, and a clearance of 90% and 89% for DNA and HCP, respectively, without any fine tunning of the predetermined operating parameters. These figures compare very favorably against single-column batch chromatography for the same volume of size-exclusion resin. However, and most importantly, the virus yield was increased from 57% for the batch system to 86% for the two-column SEC process because of internal recycling of the mixed fractions of contaminated Ad5, even though the two-column process was operated strictly in an open-loop configuration. And last, but not least, the productivity was increased by 6-fold with the two-column process. In conclusion, the main drawbacks of size-exclusion chromatography, namely low productivity and low product titer, were overcome to a considerable extent by an innovative two-column configuration that keeps the mixed fractions inside the system at all times.

Keywords: simulating moving bed; two-column chromatography; virus purification; size exclusion chromatography; downstream processing; adenovirus.

4.1 Introduction

Viral vectors are playing an increasingly important role in the vaccine and gene therapy fields. Adenoviruses (Ads), in particular, are considered one of the most suitable platforms for production of viral vaccines and gene therapy vectors. They are medium-sized (90–100 nm), nonenveloped, icosahedral viruses composed of a nucleocapsid and linear, non-segmented double stranded DNA genome that is about 36 kb long. Their broad tissue tropism and large transgene packing capacity make them attractive candidates for innovative virotherapies (Eglon et al., 2009). Adenoviruses can be produced in a complementary cell line in both adherent and suspension culture systems, such as HEK-293 or PER-C6 cells, or A549 for oncolytic therapies (Segura et al., 2008; Kamen and Henry, 2004).

The use of recombinant adenoviruses for vaccination and gene therapy requires fast and highly efficient purification protocols that yield high recoveries of infectious particles, maintain viral infectivity, and effectively remove contaminating DNA and host cell proteins (HCPs), while also concentrating the viral samples for final delivery. The concentration of adenoviruses is critical not only to obtain high titer vector stocks, but also to reduce the handled volume; the latter accelerates the downstream processing and keeps the scalability of the purification train at a manageable level (Tatsis and Ertl, 2004).

The downstream biopurification train has been extensively developed in the past years by combining different chromatography steps, namely ion-exchange (IEX)) and size-exclusion chromatography (SEC), and, less frequently, affinity chromatography, intermingled with concentration and ultra/diafiltration steps (Eglon et al., 2009; Konz et al., 2005a,b; Burova and Ioffe, 2005; Peixoto et al., 2006; Goerke et al., 2005).

To be more specific, the classical approach for adenovirus purification consists of three major steps—clarification, concentration/purification, and polishing—applied sequentially: (i) clarification of the harvested bioreaction bulk to remove cell and cell debris; (ii) ultra/diafiltration; (iii) anion exchange; (iv) ultra/diafiltration to concentrate the product; and (v) SEC as a final polishing step. The SEC step is usually carried out last, mainly because of its low productivity and low product titer. Usually in this final step the amount processed is reduced by 50 to 100 fold.

The purpose of the clarification step is to efficiently remove cell debris and large product- or process-related aggregates, while maintaining and protecting the product quality in the flow-through stream. The concentration step reduces

the volume of clarified bulk by effectively removing low molecular weight HCP, fragmented HC DNA, and possibly fragmented, product-related impurities, e.g., viral proteins. This step is a key factor for decreasing the upfront investment in downstream equipment and materials. If detergent was used to disrupt the cells, the diafiltration removes the detergent and associated lipids from the cells (Peixoto et al., 2007).

As with many bioactive therapies, there is a clear trend towards liquid chromatography as the core technique for vector purification, and its use is often integrated vertically within the DSP strategy, as it easily fits into the early capture stage as well as into the final purification phase. The use of high-performance liquid chromatography (HPLC) for large-scale adenoviral purification was first described by Huyghe et al. (1995) and several approaches have been applied since then, including IEX, SEC, hydrophobic interaction, and immobilized metal affinity chromatography (Blanche et al., 2000; Kalbfuss et al., 2008; Lee et al., 2009). Unlike traditional processes based on CsCl-gradient purification, HPLC offers a straightforward linear scale-up path, and procedures for purifying up to around 10^{14} input particles have been reported.

IEX chromatography of virus particles is typically operated in positive (bind-and-elute) mode: most of the impurities are collected in the flow-through pool, while the virus particles and some of the impurities are retained in the resin. Due to the differences in charge of the different components, it is possible to use this process with high-resolution elution gradients, separating the adsorbed materials into fractionated cuts, even though they are closely related.

SEC and ultra/diafiltration (usually by tangential flow filtration) are two other widely used processes at the very latest stage for formulating the product (Dormond et al., 2010; Peixoto et al., 2007; Rodrigues et al., 2007). However, purification schemes where SEC is followed by IEX have also been reported in the literature; two prominent examples are the works of Kalbfuss et al. (2007) and Eglon et al. (2009) for influenza and adenovirus, respectively. These schemes, when operated in batch mode, do not appear to be very cost efficient because they apply a low-productivity unit operation (SEC) at an early stage of the downstream train.

The increasing interest in vaccines and gene therapy, together with the need to decrease the cost per dose, has led to the development of new chromatographic tools or their conversion from other application areas (Barut et al., 2005; Lee et al., 2009; Riordan et al., 2009; Vicente et al., 2011). One process-based way to reduce the overall cost of the downstream chromatographic steps is by

changing to a continuous processing mode, which, in principle, yields higher throughput, lower buffer consumption, higher capacity utilization and reduced column volume, hence increased productivity. In particular, simulating moving bed (SMB) chromatography, which is the best practical implementation of continuous countercurrent solid-fluid chromatography (Seidel-Morgenstern et al., 2008; Silva et al., 2012), is now widely applied for the binary separation of small molecules, in particular chiral compounds under isocratic elution conditions (Francotte and Richert, 1997; Gomes et al., 2006; Rajendran et al., 2009).

Studies concerning continuous downstream bioprocessing have targeted mostly proteins and monoclonal antibodies (mAb) (Aumann and Morbidelli, 2007; Silva et al., 2010; Godawat et al., 2012; Warikoo et al., 2012; Krättli et al., 2013); this is primarily because the biopharmaceutical industry is currently dominated by these bioproducts. To date, the continuous purification of large biomolecules, such as viruses, has rarely been explored. Kröber et al. (2013) have recently implemented a classical three-zone, open-loop SMB for influenza virus purification. These authors have successfully increased the productivity by switching to simulated countercurrent operation, although the DNA and HCP clearances were not properly evaluated. In particular, since the bulk was not pretreated with benzonase, DNA co-eluted with the virus; also, HCP contaminants were not properly assessed due to the lack of an adequate ELISA kit for the utilized cell line (MDCK).

Despite the clear advantages of continuous chromatography, as demonstrated by the works cited above and others, the biopharmaceutical industry is somewhat skeptical about switching to continuous or quasi-continuous, multi-column chromatography. This is, in part, due to the fact that innovation in this industry has traditionally been more product- than process-oriented (Godawat et al., 2012), but also due to the increased complexity in terms of process design and validation. However, the implementation of single-use and ready-to-process technologies are mitigating these issues. Therefore, there seems to be room for exploring compact and efficient, simulated countercurrent, multi-column chromatographic processes for biopurification.

The present work reports on the design and experimental validation of a simple quasi-continuous, open-loop, two-column countercurrent chromatographic process for size-exclusion purification of adenovirus serotype 5 (Ad5). As mentioned above, SEC has been used in the past for both polishing and intermediate purification of adenoviruses (Eglon et al., 2009; Burova and Ioffe, 2005; Kalbfuss et al., 2008; Slepushkin et al., 2003). However, it is often claimed that the main drawbacks

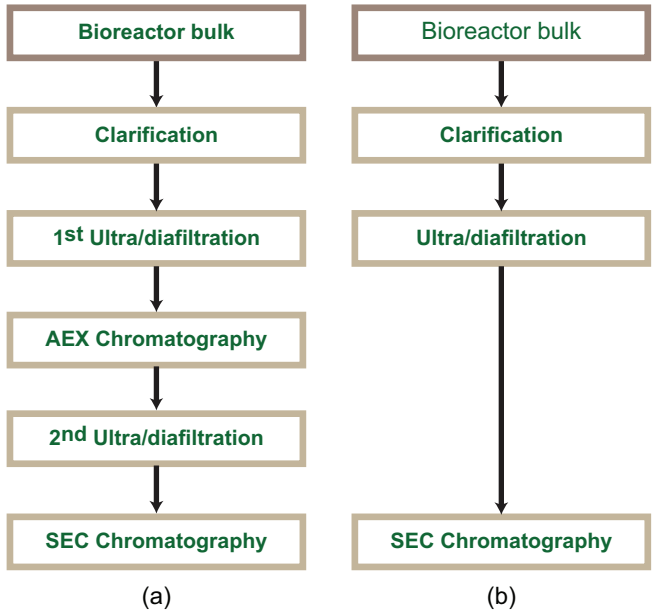

Figure 4.1: *(a) Standard downstream processing train for adenovirus purification and (b) the adopted streamlined Ad5 purification train for assessing the effectiveness of the two-column SMB-SEC step; in the streamlined train, the SMB-SEC step replaces the last three steps of the standard purification train.*

of SEC, namely low productivity and high product dilution, make it a costly purification step. Here, it is shown that these drawbacks can be eliminated to a large extent by switching from single-column batch operation to two-column SMB-type operation.

Because of the anticipated boost in performance obtained by switching to multi-column (quasi-)continuous operation, the Ad5 purification train employed for assessing the effectiveness of the enhanced SEC step was streamlined. Figure 4.1 shows schematics of the standard and streamlined purification trains; in the latter case, the SMB-SEC step is applied after the first ultra/diafiltration step and replaces the last three steps of the standard purification train.

The main reason for working with the streamlined purification train was to challenge the SMB-SEC step with a less purified bulk in order to prove that, once the classical limitations of SEC are alleviated, the standard purification train can be changed to meet specific needs in terms of cost reduction or purity requirements. Moreover, running the process with a less clean bulk gives more confidence on the performance assessment of the SMB-SEC step.

The paper is organized as follows. The materials and methods, including the

physical realization of the two-column SMB, are first described. Then, the design of the SEC step and the numerical tools employed to predict and optimize its operation are discussed. We then proceed with the experimental validation of the two-column process, demonstrating the stability of its cyclic steady behavior and operating robustness. Impurity clearance, namely DNA and HCP, were experimentally assessed on a cycle-to-cycle basis. Finally, the performance of the streamlined purification train, evaluated with respect to impurity clearance, productivity, and yield, is compared to that of a similar train but operated with a standard single-column batch SEC step to highlight the gains obtained by switching to the SMB-SEC design.

4.2 Materials and Methods

4.2.1 Cell line and medium

Two hundred and ninety-three cells of Human Embryonic kidney (HEK-293) purchased from ATCC (ATCC-CRL-1573) were adapted to suspension and grown in a commercial serum-free medium, Ex-Cell 293 (SAFC Biosciences, USA), supplemented with 4 mM of glutamine (Invitrogen, UK), in a humidified atmosphere of 8% CO_2 in air at 37°C using shake flasks (Corning, USA). The cells were routinely propagated twice a week using an inoculum of 0.5×10^6 cells/mL. Cell concentration and viability were determined by counting cells on a Fuchs-Rosenthal haemocytometer (Brand, Germany) using the trypan blue (Invitrogen, UK) dye exclusion method.

4.2.2 Virus production

We used a replication-defective adenovirus derived from serotype 5 adenovirus (Ad5) encoding for GFP protein. The viruses were produced in a 2 L bioreactor with 1 L working volume (Sartorius-Stedim Biotech, Germany). The agitation rate was set at 70 rpm and the dissolved oxygen was controlled at 50% air saturation by gas mixing and stirred cascade control with an airflow of 0.01 L/min; the pH was controlled at 7.2 by aeration with a gaseous CO_2 mixture and 1 M $NaHCO_3$; all infections were done at a cell concentration of 10^6 cells/mL using a multiplicity of infection of 5; the adenoviruses were harvested at 48 hours post-infection. The amount of infective particles (IP) in the bulk (before purification) was in the range 10^9–10^{10} IP/mL.

4.2.3 Clarification and concentration

Upon harvesting, the bioreaction bulk was supplemented with 0.1% Triton X100 (Sigma Aldrich, MO, USA) and incubated for 2 hours at 37°C with 50 U/mL of Benzonase (Merck Millipore, Germany) to digest the DNA and to release the adenoviral vectors from the intracellular material by cell lysis.

Subsequently, the bulk was microfiltrated using a Sartopore 2 membrane capsule (Sartorius Stedim Biotech, Germany) comprising a 0.8 μm prefilter and a 0.45 μm filter, and concentrated up to 10 times and diafiltered up to 5 times with 20 mM Tris & 150 mM NaCl at pH 8 on a Sartorius Stedim Biotech cassette prototype with an average cut-off of 750 kDa. Before use, the capsules were washed with one capsule volume of Milli Q water and two capsule volumes of buffer. The bulk was stored in aliquots at -80°C until further use.

4.2.4 Analytics

The protocol for the quantification of total viral particles was a two-step procedure: DNA extraction according to the instructions on the "High Pure Viral Nucleic Acid Kit" (Roche) manual and real-time PCR. The number of viral DNA copies was determined by real-time PCR and LightCycler system (Roche Diagnostics) using a Fast Start DNA master SYBR Green I kit to track a specific Ad5 sequence (Roche Diagnostics). Internal plasmid of 2.07×10^9 copies/μL was chosen as reference standard. The total particle concentrations were confirmed using Nanosight NS500 (NanoSight Ltd, UK), and the size distribution was determined. The average of the two measures was the value chosen for assessing the virus recovery yield. Protein profile analysis was performed in 4–12% NuPage gradient pre-cast gels (Invitrogen). The gels were stained by Coomassie Instant Blue (Expedeon Ltd, UK) and the protein concentration was determined using BCA kits (Pierce, Rockford, USA) and bovine serum albumin (BSA) as the standard protein. The protein were precipitated using 99% ethanol and incubated overnight at -20°C.

The amount of HCP was determined using a commercially available ELISA kit for HEK293 cell line (Cygnus Technologies, Inc.). The sample was diluted in PBS and the assay was performed according to the manufacture protocol, the 96 well plate was read by an absorbance microplate reader at 450/650 nm (SpectraMax 340). DNA was quantified by Quant-iT Picogreen DNA assay kit (Invitrogen). After 5 minutes of incubation, the fluorescence was measured by Luminometery (Turner BioSystems). Purified DNA was used as standard.

4.2.5 SEC medium and columns

The selected size-exclusion medium was Sepharose 4 Fast Flow (S4FF, GE Healthcare), which was supplied by the manufacturer with an average particle size of 90 μm (range of 45–165 μm). S4FF is based on a highly cross-linked 4% agarose matrix, which gives good physical stability and chromatographic qualities; its exclusion limit for globular proteins is ca. 3×10^7. This size-exclusion medium is suitable for use in our application, since, as shown next, it completely excludes the Ad5 particles from its porous matrix and, hence, they elute in the interparticle volume, whereas the impurities present in the clarified bioreaction bulk elute through the porous matrix at different rates.

The first preliminary data employed to design the process was the chromatogram for a small injection of the clarified bioreaction bulk in a XK 26/40 column (GE Healthcare; 2.6 cm i.d., maximum bed height of 40 cm) at a flow rate of 3 mL/min (data not shown because they are qualitatively similar to those discussed in § 4.3).

Before carrying out this experiment the fractionation properties of the column were assessed using a high molecular weight (HMW) gel filtration calibration kit (GE Healthcare, Buckinghamshire, UK) containing 5 globular proteins with molecular weights in the range 44,000 to 669,000 and Blue Dextran (BD) 2000. This kit was complemented with a small amount of CsCl-purified Ad5. The obtained results are summarized in Fig. 4.2.

BD 2000 is expected to be completely excluded from the S4FF's intraparticle porosity and, thus, its elution volume should be equal to the interparticle column volume, $V_o = \epsilon_o V_c$, where V_c is the geometric column volume and ϵ_o is the interparticle porosity of the S4FF medium. As expected, the elution volume for a short pulse of CsCl-purified Ad5 gave a value of V_o similiar to that obtained for BD (Fig. 4.2), which proves that the Ad5 particles are excluded from the S4FF matrix. The total porosity, $\epsilon = \epsilon_o + (1 - \epsilon_o)\epsilon_p$, where ϵ_p is the intraparticle porosity, was estimated from the elution peak for a small injection of 2% acetone as tracer.

By noting that the resolution in SEC varies with the square root of bed height (E.G. Malawer, 2004) it was estimated that the total bed height could be reduced to around 20–25 cm while keeping a reasonable separation between the virus peak and its closest impurity. We thus aimed at packing two columns with a bed height of ca. 10–12 cm.

Two XK 26/20 chromatographic columns (2.6 cm i.d., maximum bed height of

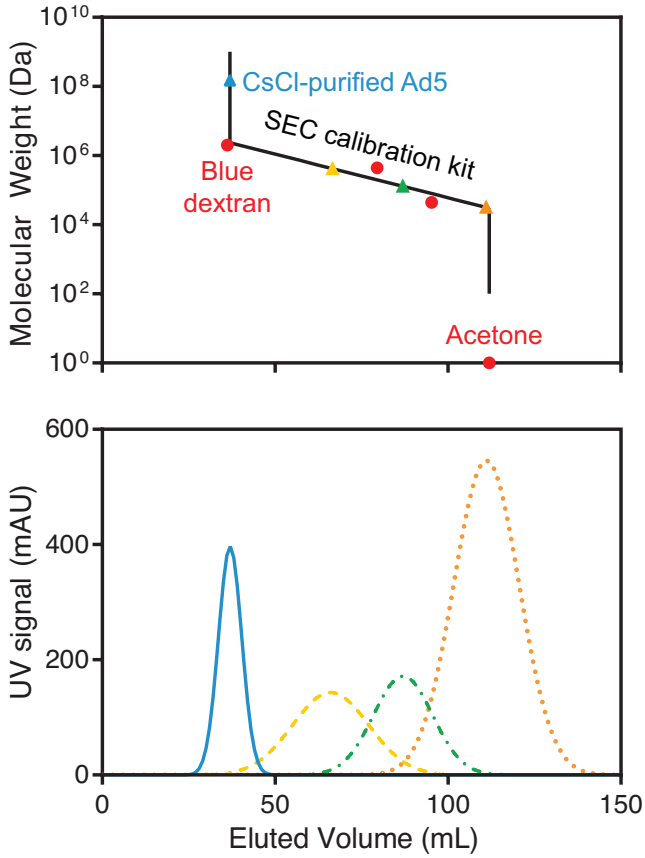

Figure 4.2: *Analysis of the pore size distribution of S4FF medium using a high molecular weight (HMW) gel filtration calibration kit (GE Healthcare, Buckinghamshire, UK) containing several protein standards complemented with the CsCl-purified Ad5. The Ad5 particles, like BD 2000, are excluded from the S4FF's porous matrix and elute in the void volume of the column.*

Table 4.1: *Characterization of the two XK 26/20 columns packed with S4FF. V_c and L are the volume and length of the column, N is the number of theoretical plates, A_f is the peak asymmetry factor, and N/L is the number of theoretical plates of meter of column length.*

		Column 1	Column 2
V_c	(cm^3)	55.2	57.3
L	(cm)	10.4	10.8
V_o	(cm^3)	16.8	15.2
N	(–)	281	220
A_f	(–)	1.25	1.0
N/L	(m^{-1})	2702	2037

20 cm) were slurry packed with S4FF according to the manufacturer's specifications. The excess ethanol supplied with SF44 was decanted and replaced with working buffer (20 mM Tris, 150 mM NaCl, pH 8) before packing into the columns. The columns were initially filled with 70% slurry of S4FF and allowed to settle by gravity overnight. The flow rate was then increased in stepwise fashion up to 4 mL/min (ca. 45 cm/h). The final, stabilized column lengths were 10.4 cm and 10.8 cm. No measures were taken to improve the balancing of the bed heights. Before each experiment the columns were sanitized with 1 M NaOH, washed with Milli Q water, and equilibrated with 5 bed volumes of running buffer (20 mM Tris, 150 mM NaCl, pH 8).

After packing the two columns, their efficiency was tested, as described above, to check the quality of the packing. The total porosity, ϵ, was estimated from the acetone elution peak; for completeness, the number of theoretical plates (N) measured with this tracer was also calculated (Table 4.1).

For a well-packed column of gel-filtration media the void volume V_o should be equivalent to approximately 30% of the total column volume V_c (GE-Healthcare). Table 4.1 shows that this is indeed the case of our two columns.

4.2.6 Experimental two-column SEC setup

Fig. 4.3 shows a schematic of the set of feasible flow diagrams for designing the operating cycle for the class of two-column, open-loop SEC processes considered in the present work; they represent the alternative configurations that can be considered for the implementation of any given step of the cycle.

The set includes the following configurations: (a) directing the flow to the next

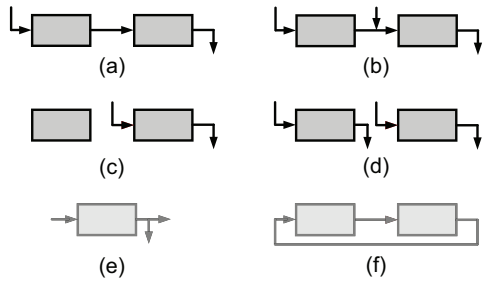

Figure 4.3: *Set of admissible flow-line configurations for designing a two-column, open-loop SEC purification step without outlet split flow: (a) complete direction of flow to the next column, (b) flow addition to the circulating stream, (c) frozen bed, and (d) complete withdrawal and flow injection at the same node. Each schematic represents a valid configuration for a given step of the two-column SEC cycle. For simplicity of design and robustness of operation, schematic* e *(outlet split flow) and schematic* f *(closed-loop recirculation) are excluded from the design, since configuration* e *cannot be implemented with simple two-way valves and configuration* f *requires an extra pump.*

column; (b) adding an external stream to the circulating flow; (c) freezing one column (temporarily stopping the flow through the column); and (d) withdrawing the effluent from one column while injecting an external stream into the other column. In this class of two-column, open-loop SEC processes the flow through a column is always in one of three states: (i) frozen, (ii) completely directed to the next column, or (iii) entirely diverted to either the product line or the waste line.

We have purposively excluded from the set of feasible configurations those in which the flow exiting one column is split into two or more streams — schematic *e* illustrates what is meant by split flow — or in which the flow is recirculated in closed loop (schematic *f*). The reason for discarding these configurations is to avoid the use of flow controllers or an extra pump; the objective is to design a SEC process that is physically realizable with simple two- or three-way valves to control the flow paths in the system and requires a minimum number of pumps — one for injecting the feed and another for injecting the mobile phase.

Figure 4.4 shows a schematic of the experimental two-column set-up. The distributed valve design is based on two-way valves, since they allow independent port switching and are quite versatile. Two-way valves allow the flow either to go through or not to go through.

A two-way valve is placed immediately downstream of the two outlet ports of each column, but preceding the two inlet ports, to control the flow rate of liquid from the column that is circulated to the other column. This valve is closed when the effluent from the upstream column is totally withdrawn as product

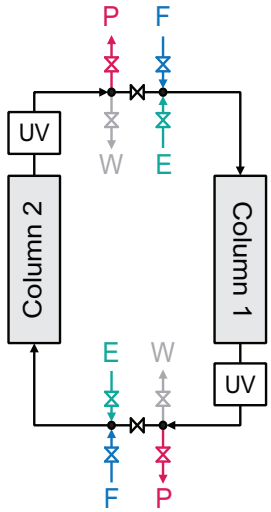

Figure 4.4: *Schematic of the preparative unit for the two-column, open-loop SEC purification step. Each column has five two-way valves associated to it; an UV detector is placed at the outlet of each column. E denotes the eluent inlet; F, the feed inlet; and P and W, the product and waste outlets, respectively*

or the fluid in the column needs to be temporarily frozen. Overall, the set-up employs 10 two-way valves to control the port switching. The two-way valves are model SFVO from Valco International (Schenkon, Switzerland) with pneumatic actuation. Each valve is automated by means of a single computer-controlled three-way solenoid: application of 50 psi opens the valve; venting the air allows the spring to return the valve to the closed position.

The two HPLC pumps—one for injecting feed and the other for injecting fresh mobile phase—are model K-501 from Knauer (Berlin, Germany) with 10 mL heads, and controlled via RS232 communication protocol. The experimental set-up is fully automated and driven by an in-house developed automation system using LabView software (National Instruments).

The UV absorbance of the effluent from each column was automatically monitored in real-time at 12 distinct wavelengths ranging from 230 nm to 300 nm using two USB4000 multiwavelength UV detectors (Ocean Optics, USA) with attenuator, sharing the same DH-2000-S-DUV light source (Micropack, Ostfildern, Germany) by means of a bifurcated optical fiber assembly.

4.2.7 SEC column breakthrough model

A simple equilibrium-dispersive adsorption column breakthrough model was adopted for computer-aided design of the SEC step. In this model the column efficiency is measured by the dimensionless plate height, $h_i = L/N_i$, where L is the column length and N_i is the number of theoretical plates for component i. The approximate additivity of the effects of axial dispersion, external mass transfer resistance, and diffusion for linear systems was demonstrated long ago by various authors (e.g., (Glueckauf, 1955; Glueckauf and Coates, 1947); also Haynes and Sarma (1973) using moments analysis). This means that in the modeling of chromatographic columns under inert or linear equilibrium conditions it is seldom worth modeling the band broadening using a more complex descriptor than an overall effective dispersion coefficient (or, alternatively, and overall effective rate coefficient) incorporating both effects of axial dispersion and the various mass transfer resistances (Ruthven, 1984).

The model can be written as

$$\epsilon_i \frac{\partial c_i}{\partial t} + \frac{Q}{V_\mathrm{c}} \left(\frac{\partial c_i}{\partial x} - \frac{h_i}{2} \frac{\partial^2 c_i}{\partial x^2} \right) = 0 \quad \forall x : 0 < x < 1, \tag{4.1}$$

where t is the time coordinate, $x = z/L$ is the dimensionless axial coordinate along the packed bed, L and V_c are the length and volume of the column, i is the solute index, c is the solute concentration in the mobile phase, and Q is the volumetric flow rate of mobile phase.

The symbol ϵ_i denotes the volumetric fraction of the SEC column that is accessible to component i (i.e., the overall porosity of the packed bed that is probed by component i); ϵ_i can be expressed as

$$\epsilon_i = \epsilon_\mathrm{o} + (1 - \epsilon_\mathrm{o}) H_i, \quad H_i = \epsilon_\mathrm{p} \int_{d_{\mathrm{m},i}}^{\infty} \psi(\sigma)\, d\sigma, \tag{4.2}$$

where $\psi(\cdot)$ is the pore size distribution of the size exclusion medium,[1] i.e., $\psi(\sigma)\, d\sigma$ is the fraction of the S4FF's porous volume with pore diameters between σ and $\sigma + d\sigma$, and $d_{\mathrm{m},i}$ is the size of the biomolecule (including any existing hydration layer).

[1] The function $\psi(\cdot)$ is a normalized distribution, $\int_0^\infty \psi(\sigma)\, d\sigma = 1$, and $\int_{d_{\mathrm{m},i}}^\infty \psi(\sigma)\, d\sigma$ can be regarded as the exclusion factor for a biomolecule of size $d_{\mathrm{m},i}$.

Equation 4.1 is subject to the usual boundary conditions:

$$c_i - \frac{h_i}{2}\frac{\partial c_i}{\partial x} = c_i^{\text{in}} \quad \text{for} \quad x = 0, \tag{4.3}$$

$$\frac{\partial c_i}{\partial x} = 0 \quad \text{for} \quad x = 1, \tag{4.4}$$

where $c_i^{\text{in}}(t)$ is the inlet concentration of component i; $c_i^{\text{out}}(t)$ shall denote the temporal concentration profile of component i in the outlet effluent of the column.

4.3 Design of the SEC step

Figure 4.5 shows the chromatograms for the elution of dilute pulse injections of the bioreaction bulk through each XK 26/20 column and through the two columns arranged in series. The solid, black lines plotted in Figs. 4.5A and 4.5B represent the experimental chromatograms obtained with each column separately, whereas the solid, black line in Fig. 4.5C is the chromatogram obtained with the serial arrangement of the two columns.

The rising fraction of the first peak in the chromatogram of Fig. 4.5C was collected separately and analyzed for its particle size distribution (PSD) and concentration in a Nanosight NS500 (Nanosight Ltd, UK); this peak is the one that elutes in the void volume of the columns. Figure 4.6 shows that the PSD profile is centered around 85–96 nm, which is the average size of an Ad5 particle, and drops sharply for smaller particle sizes, indicating that the fraction eluting in the void volume of the S4FF columns is practically free of impurities. The very mild tailing of the PSD over sizes larger than 96 nm indicates the absence of relevant amounts of aggregates. These results ensure that this first eluting peak consists essentially of purified Ad5 particles.

Unlike IEX or affinity chromatography, the solutes do not bind to the SEC medium, because of lack of reactivity and strong adsorptive interactions, so they elute through the SEC medium at a rate that depends on their molecular size and shape but not on the presence of the other solutes. Therefore, for the purposes of process design the complex multicomponent mixture in the clarified bioreaction bulk can be modeled as a simpler mixture of three key components: (1) the virus, which is the largest species and, hence, the fastest eluting component; (2) the group of impurities that elute nearest to the virus; and (3) the group of small impurities that elute at the slowest rate. The difference in the selectivity factor between the first two key components will essentially define the difficulty of the

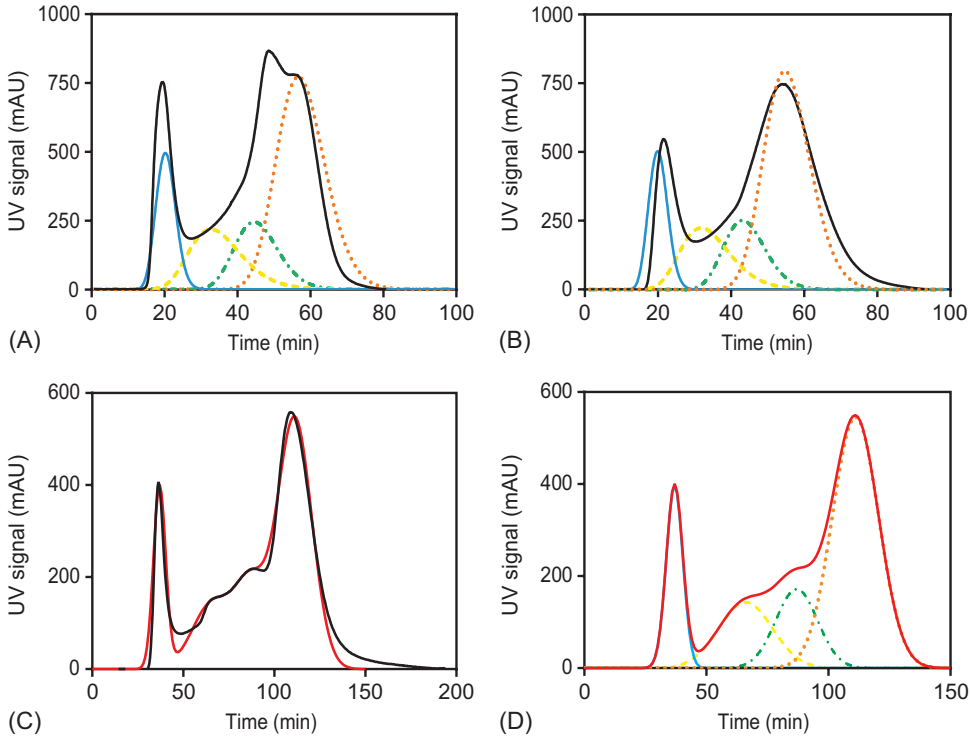

Figure 4.5: *Dilute pulse experiments of the clarified bioreaction bulk on the two XK 26/20 columns packed with S4FF medium. Plots A and B show the experimental chromatogram (black line, UV signal 230 nm) obtained with the individual columns, (column 1 and 2, respectively); the colored lines represent the deconvolution of the experimental chromatogram into the superimposition of fours noninteracting peaks. Plot C shows the experimental chromatogram (black line, UV signal 230 nm) obtained with the two columns placed in series and the best fit of the chromatogram to the superimposition of four noninteracting peaks (red line); the latter are represented individually in plot D (colored lines)*

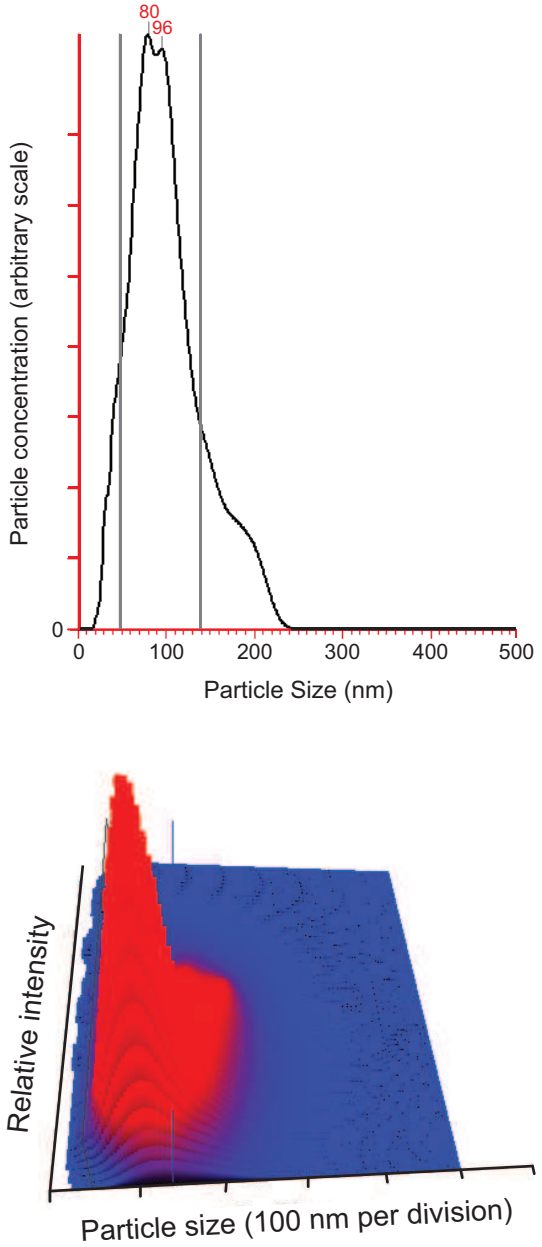

Figure 4.6: *Particle size distribution (PSD) and concentration of the rising fraction of the first elution peak shown in Fig. 4.5C; this peak is the one fitted by the solid blue line in Fig. 4.5D. The analysis was carried out in a Nanosight NS500 (NanoSight Ltd, UK). The PSD profile is centered around 85–96 nm, which is the average size of an Ad5 particle, and drops sharply at smaller particle sizes, indicating that the fraction eluting in the void volume of the S4FF columns is practically free of impurities. The very mild tailing of the PSD over sizes larger than 96 nm indicates the absence of relevant amounts of aggregates.*

Table 4.2: *Model parameters derived from analysis of pulse experiments performed on the two columns placed in series, $L = L_1 + L_2 = 21.2$ cm. i is the component index, c^{F} is the feed concentration, which is assumed to be proportional to the area under the UV absorbance peak (arbitrary units s.t. $\sum_i c_i^{\mathrm{F}} = 1$), ϵ is the accessible porosity, and N is the number of theoretical plates per column.*

i	1	2	3	4
c_i^{F}	0.140	0.165	0.154	0.541
ϵ_i	0.306	0.564	0.750	0.945
N_i	61	18	51	69

separation, whereas the difference in the selectivity factor between the first and last key components will define the cycle time. Since all the other molecules in the bioreaction bulk necessarily elute at intermediate rates between those of the second and third key components, they are withdrawn from the system in one of the waste fractions if the SEC process is well designed.

To design the SEC process it is necessary to measure the retention volume of each key component, from which the value of ϵ_i can be determined, and the extent of band broadening at the working flow rate to determine the value of h_i. We used PeakFit (Systat Software Inc., San Jose, CA) to quickly estimate the location, area, and broadening of the key chromatographic peaks for injections of the clarified bioreaction bulk in each column and in the two columns arranged in series. These data were then used as initial guess in a more accurate deconvolution procedure, which fits the superposition of multiple solutions of eq. 4.1 (one for each component) without neglecting the non-infinitesimal size of the injected sample.

The fitted chromatographic peaks for the three key components are shown in Fig. 4.5 as blue (virus), dashed yellow (large impurities), and dotted orange (small impurities) lines. Figure 4.5 also shows a fourth modeled component, plotted as a dash-dot green line, corresponding to the group of intermediate impurities that elute between the two groups of key impurities. This fourth component was not considered in the design of the SEC process, it was only used to get a better description of the simulated elution profiles for comparison with the experiments.

Table 4.2 lists the model parameters derived from the analysis of the pulse experiments performed on the two columns placed in series. The feed concentrations given in this table are normalized values, $\sum_i c_i^{\mathrm{F}} = 1$, and were determined assuming that the concentration is proportional to the area under the corresponding UV absorbance peak.

In a two-column SEC process the cycle is divided into two equal-length time intervals, which we shall henceforth refer to as switching intervals. To design the cycle it suffices to define the sequence of flow-line configurations for one of the switching intervals; the sequence for the other twin switching interval is similar, but the positions of the two columns are exchanged. In practice, it is easier to keep the columns fixed in space and to move the positions of the inlet and outlet lines by means of an automated arrangement of two- or three-way valves. Over a full cycle, each column undergoes the same sequence of steps but phased out in time by one switching interval.

The sequence for a switching interval is defined as a serial arrangement of flow-line configurations taken from the set shown in Fig. 4.3. To each flow-path configuration one has to assign (i) the positions of columns 1 and 2, (ii) the nature of each inlet (feed or eluent), and (iii) the nature of each outlet (product or waste). Although this picture may look too theoretical to the downstream process engineer, we advocate that this process-systems-engineering view of the downstream process, and of the SEC step in particular, is very helpful, as it clearly establishes the elementary steps that the columns should undergo and the number and type of design variables associated to each step.

In previous work (Silva et al., 2010; Araújo et al., 2010) we have demonstrated that a half-cycle consisting of steps *a*-*b*-*a* gives rise to a very efficient process for binary separation. This scheme supplies the feed mixture into the middle of the system where the composition of the circulating fluid is closest to that of the feedstock fluid, and recovers the purified product and waste fraction alternately at the downstream end of the unit, while desorbent is continuously supplied into the upstream end of the system. Moreover, we have shown that the injection of feed, step *b*, can be replaced by steps *c* or *d* without loss of performance and in some instances increased productivity (Rodrigues et al., 2008; Silva et al., 2012). These steps are mandatory when the duration of product collection is larger than the time taken to inject the feed (Silva et al., 2010), which is the case when there is large band broadening in the system as is the case in SEC.

Using these guidelines we developed the cycle shown in Fig. 4.7, whose half-cycle (or switching interval) is divided into the sequence of steps *a*-*d*-*a*-*c*:

Step 1. The upstream column is eluted while the effluent of the downstream column is diverted to the waste line.

Step 2. The upstream column is eluted but its effluent is diverted to the waste line instead of being directed to the downstream column. The downstream

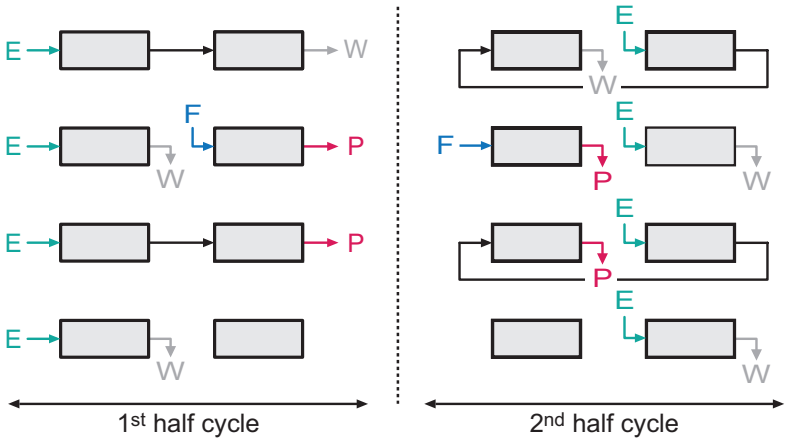

Figure 4.7: *schematic of the operating cycle for the two-column, open-loop SEC purification step; E denotes the eluent inlet; F, the feed inlet; and P and W, the product and waste outlets, respectively*

column is fed with the clarified bioreaction bulk while its effluent is collected as purified product.

Step 3. The system is operated as in step 1 but the effluent of the downstream column is collected as product.

Step 4.

The upstream column is eluted but its effluent is again diverted to the waste line instead of being directed to the downstream column. The downstream column is kept frozen, that is, the flow through that column is temporarily halted.

The feed and eluent flow rates, Q_{F} and Q_{E}, were both fixed at 3 mL/min because of the constraint imposed by the pressure drop through the SEC medium in steps 1 and 3 of the cycle.

After defining the step sequence, a rigorous model-based optimization approach was employed to determine the optimum duration of each step, τ_k, $k = 1, \ldots, 4$, for the fixed values of the process flow rates. The purpose of the nonlinear programming problem is to guarantee the fulfilment of product and process specifications, such as minimal purity and recovery, while optimizing process performance in terms of productivity.

Let

$$c_{i,j}(x,t) = f(c_{i,j}(x,0); \tau_1, \ldots, \tau_4) \quad \text{for} \quad 0 < t \leq \tau \tag{4.5}$$

represent the dynamic model for the first half ($0 < t \leq \tau$) of the cycle depicted in the schematic of Fig. 4.7 for given initial conditions $c_{i,1}(x,0)$ and $c_{i,2}(x,0)$ in columns 1 and 2, respectively; here, i is the index that runs over the set of solutes and j runs over the set of columns. For example, if we wanted to simulate the startup of the process when the two columns are initially clean, we would set

$$c_{i,1}(x,0) = 0, \quad c_{i,2}(x,0) = 0. \tag{4.6}$$

For process design, however, the initial transient behavior is of little interest but only the fully established steady, periodic state. Thus, we are interested in the solution of eq. 4.5 subject to the constraint

$$c_{i,1}(x,\tau) = c_{i,2}(x,0), \quad c_{i,2}(x,\tau) = c_{i,1}(x,0), \quad \tau = \sum_k \tau_k, \tag{4.7}$$

which simultaneously imposes the condition of simulated counter-current operation (the two columns exchange roles every switching interval) and time periodic behavior.

For the cycle depicted in Fig. 4.7 the amount of feed injected per switching interval, which is a direct measure of productivity, is given by

$$\overline{Q_{\mathrm{F}}} = (\tau_2/\tau) Q_{\mathrm{F}}, \tag{4.8}$$

and the purity and recovery of purified Ad5 under cyclic steady-state conditions, P_{Ad5} and R_{Ad5}, respectively, are

$$P_{\mathrm{Ad5}} = \frac{\displaystyle\int_{\tau_2} Q_{\mathrm{F}} c_{1,2}^{\mathrm{out}}\, dt + \int_{\tau_3} Q_{\mathrm{E}} c_{1,2}^{\mathrm{out}}\, dt}{\displaystyle\int_{\tau_2} Q_{\mathrm{F}} c_{\mathrm{tot},2}^{\mathrm{out}}\, dt + \int_{\tau_3} Q_{\mathrm{E}} c_{\mathrm{tot},2}^{\mathrm{out}}\, dt} = \frac{\displaystyle\int_{\tau_2+\tau_3} c_{1,2}^{\mathrm{out}}\, dt}{\displaystyle\int_{\tau_2+\tau_3} c_{\mathrm{tot},2}^{\mathrm{out}}\, dt}, \tag{4.9}$$

$$R_{\mathrm{Ad5}} = \frac{\displaystyle\int_{\tau_2} Q_{\mathrm{F}} c_{1,2}^{\mathrm{out}}\, dt + \int_{\tau_3} Q_{\mathrm{E}} c_{1,2}^{\mathrm{out}}\, dt}{Q_{\mathrm{F}} \tau_2 c_1^{\mathrm{F}}} = \frac{\displaystyle\int_{\tau_2+\tau_3} c_{1,2}^{\mathrm{out}}\, dt}{\tau_2 c_1^{\mathrm{F}}}, \tag{4.10}$$

where $c_{\mathrm{tot},j}^{\mathrm{out}} = \sum_i c_{i,j}^{\mathrm{out}}$ is the total concentration in the outlet stream of column j; the flow rates drop out of the expressions because they happen to be equal. If P_{Ad5} is high, say above 90%, the impurities in the collected product fraction will necessarily be the key components 2 and/or 3, the former because of its proximity to the product and the latter because of circulation around the system from the

Table 4.3: *Optimum duration of each step, τ_k ($k = 1, \ldots, 4$) of the cycle shown in Fig. 4.7 for the chromatographic parameters given in Table. 4.2; the values of τ_k are reported in minutes. The duration of the switching interval, or half-cycle, is $\tau =$ 17.76 min. The elution (Q_{E}) and feed flow (Q_{F}) rates are both fixed at 3 mL/min; $P_{\mathrm{Ad5,min}} = 0.98$, $R_{\mathrm{Ad5,min}} = 0.95$.*

Step index, k	τ_k	τ_k/τ
1	4.86	0.274
2	3.96	0.223
3	1.27	0.072
4	7.68	0.432

previous switching interval. This is why it is unnecessary to include more key impurities in the design procedure, although considering more components would, of course, make no harm but increase the computational overhead.

To determine the working values of the four τ_k's, the following optimization problem is solved:

$$\begin{aligned} \max_{\tau_1,\ldots,\tau_4} \quad & \overline{Q_{\mathrm{F}}} \\ \text{s.t.} \quad & \text{eq. 4.5 and eq. 5.8,} \\ & P_{\mathrm{Ad5}} \geq P_{\mathrm{Ad5,min}}, \\ & R_{\mathrm{Ad5}} \geq R_{\mathrm{Ad5,min}}. \end{aligned} \tag{4.11}$$

4.4 Results and Discussion

4.4.1 Simulation results

The solution of the design problem for the set of parameters listed in Table 4.2, column lengths $L_1 = L_2 = (10.8+10.4)/2 = 10.6$ cm, $P_{\mathrm{Ad5,min}} = 0.98$, $R_{\mathrm{Ad5,min}} = 0.95$, and $Q_{\mathrm{E}} = Q_{\mathrm{F}} = 3$ mL/min is given in Table 5.3.

One practical consideration in size exclusion chromatography is the volume of injected sample. For high-resolution fractionation, a sample volume from 0.5% to 4% of the total column volume (CV) is recommended, depending on the type of medium used; for most applications the sample volume should not exceed 2% to achieve maximum resolution. For group separations, however, volumes up to 30% of the total CV can be used (GE-Healthcare).

An advantage of the proposed two-column SMB-SEC process is the relaxation of the requirement of high resolution for achieving high purity. Therefore, the purification of the Ad5 bioreaction bulk using our two-column SEC system can

be classified as a group separation problem, for which sample volumes up to 30% of the total CV are admissible.

From Table 5.3 it is seen that the sample volume injected per switching interval is 11.8 cm^3, which is 20.9% of the total volume of one of the twin columns; this is the same as 2×11.84 cm^3 of feed injected per cycle, corresponding to 20.9% of the summed volumes of the two twin columns of SMB-SEC system. This is within the operating range recommend by the manufacturer of the gel filtration medium (GE-Healthcare).

For the optimized SEC process, Fig. 4.8 shows the simulated temporal concentration profiles at the outlet of the two columns for the first switching interval of the cycle under cyclic steady-state conditions. The temporal profiles for the second switching interval of the cycle are identical to those of the first but the two column indices are exchanged.

Fig. 5.9 provides more simulation results about the cyclic steady-state behavior of the process; it shows the simulated axial concentration profiles of the key components in the two columns at the start of each sub-step of the switching interval.

The simulation data plotted in Figs. 4.8 and 5.9 predict that the optimized SEC process can effectively purify the Ad5 bioreaction bulk to a high purity specification; as expected, the simulation profiles show that the group of impurities that most adversely affect the purity of the product fraction is the group of slowest eluting impurities—those whose profile is plotted as a dashed orange line.

Fresh feed is injected while the Ad5 product from the previous switching interval is being displaced from column 1 to column 2. A purified band will then slowly detach from the group of nearest eluting impurities. As soon as the product is confined into column 2, the impurities trapped in column 1 can be directed to the waste line and then the steps are repeated but with the two column positions exchanged. At the start of each cycle the concentration bands are nearly all confined to column 1, whereas column 2 is clean except for a small region at its downstream end that contains the trailing band of the group of more retained impurities. If required, at this instant of the cycle column 2 can be replaced by a clean one and subject to a cleaning-in-place (CIP) procedure to be readily available for use at a later cycle. This is a convenient way to implement a periodic CIP procedure in our process without changing the step sequence and durations.

An alternative CIP procedure, which could potentially decrease the process time, stems from the observation that, at the end of step 3, column 1 is loaded with impurities while the product is confined to column 2. Hence, this optional

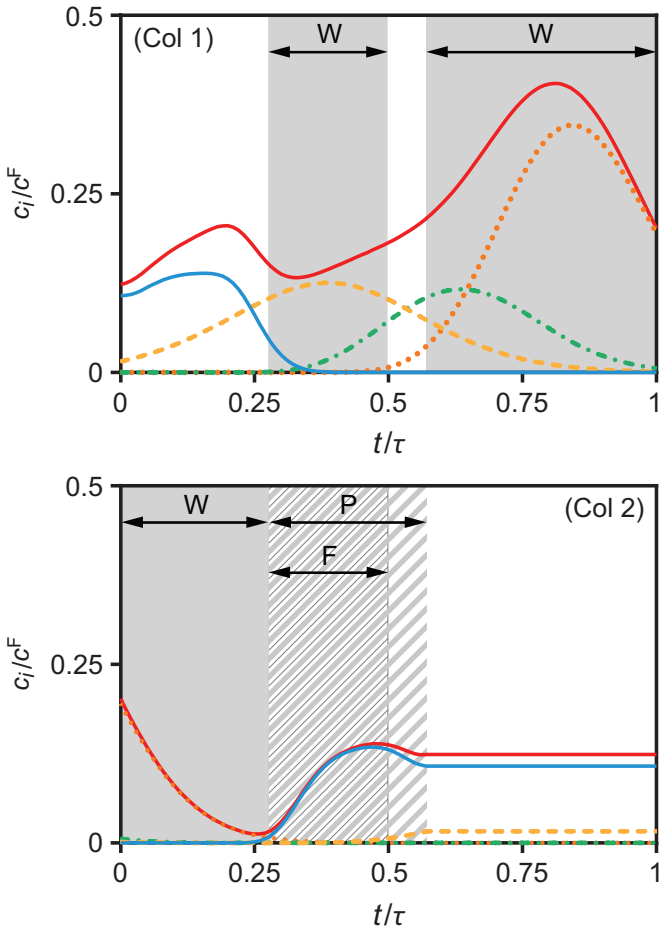

Figure 4.8: *Simulated temporal concentration profiles at the outlet of column 1 (top) and column 2 (bottom) for the first switching interval of the cycle under cyclic steady state conditions. The temporal profiles for the second switching interval of the cycle are identical to those of the first but the two column indexes are exchanged. The cycle parameters are given in Table 5.3. Color coding: solid blue line, virus; dashed yellow line, first group of eluting impurities; dash-dot green line, intermediate group of eluting impurities; dotted orange line, last group of eluting impurities; solid red line, total concentration.*

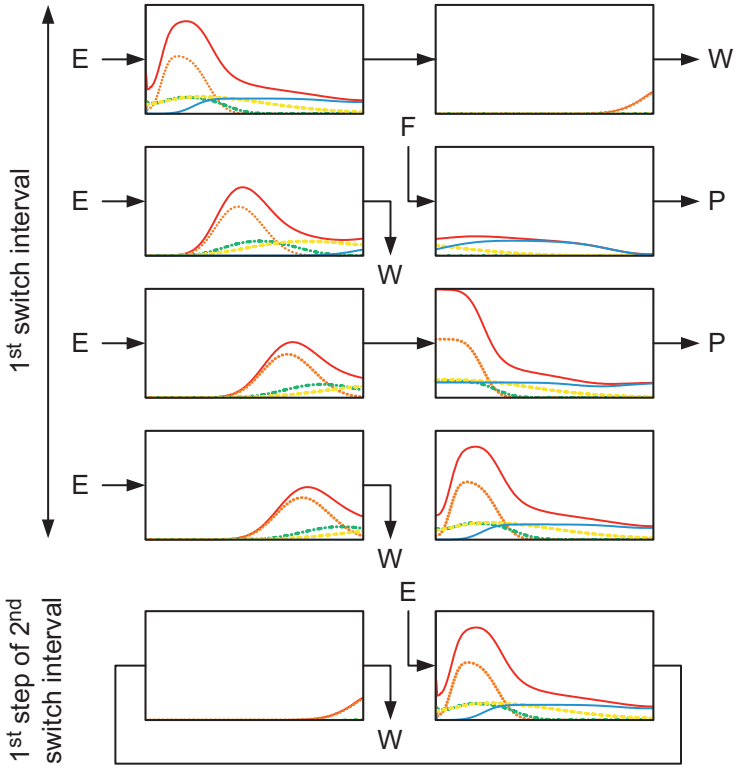

Figure 4.9: *Simulated axial concentration profiles at the start of each step of the first switching interval of the cycle under cyclic steady state conditions. For completeness, the concentration profiles at the end of the cycle, immediately after switching the ports to start the first step of the second switching interval of the cycle, are shown in the bottom. The y-axis in each column ranges from 0 to the total feed concentration. The cycle parameters are given in Table 5.3. Color coding: solid blue line, virus; dashed yellow line, first group of eluting impurities; dash-dot green line, intermediate group of eluting impurities; dotted orange line, last group of eluting impurities; solid red line, total concentration.*

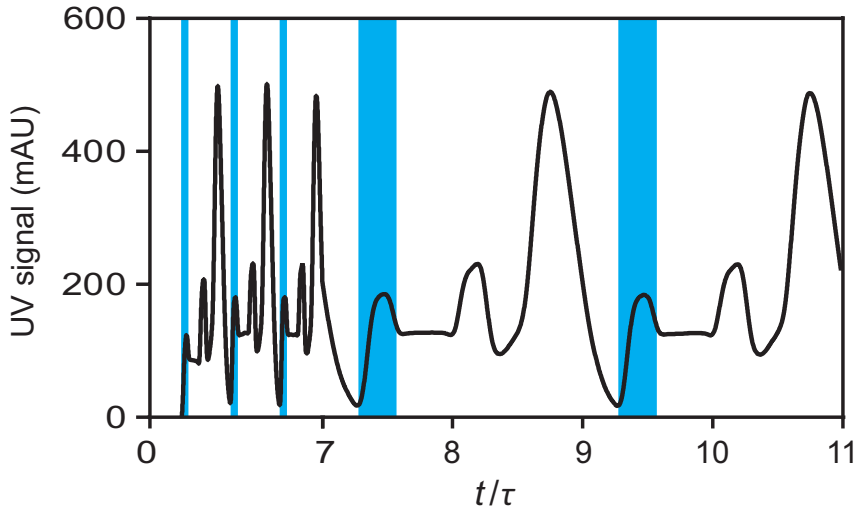

Figure 4.10: *Experimental UV signal (230 nm) measured at the outlet of column 1 over the first five cycles of operation. The blue strips show the time intervals for product collection from column 1. Note that the time scale for $t/\tau < 7$ has been compressed to improve the visualization of the UV signal for $t/\tau > 7$*

CIP procedure replaces column 1 by a clean one at the end of step 3 and moves directly to the beginning of the next half-cycle, thus bypassing step 4. However, since this CIP strategy shortens the duration of that particular half-cycle, it would have to be applied less frequently than the other CIP procedure.

4.4.2 Experimental validation

The optimized SEC process was implemented experimentally in the preparative prototype unit described in section 4.4. The unit was operated for five full cycles, which were more than enough to attain cyclic steady state conditions. Figure 4.10 shows the temporal profile of the UV signal measured at the outlet of column 1 over the duration of the experiment, which corroborates our observation about the fast attainment of the steady, periodic behavior, but also the excellent cycle-to-cycle reproducibility of the profile exhibited by the process.

Also noteworthy is the fairly good agreement between the periodic shape of the UV profile and the predicted total concentration profile plotted in Fig 4.8 as a solid red line, which is the information extracted from the simulation that is closest to being proportional to the UV signal. The similarity between these two profiles is a strong indication that the process is behaving as expected. Note that

to visually compare Fig. 4.8 and Fig. 4.10, the bottom graphic of Fig. 4.8 must be horizontally aligned at the right of the top graphic to generate the temporal profile for column 1 over a complete cycle.

The product fraction collected at each switching interval was analyzed separately to determine the Ad5, HCP, and DNA contents. These measurements are plotted in Fig. 4.11 as a function of the number of elapsed switching intervals. It is worth noting that a full cycle is completed every two switching intervals, and that even tics on the horizontal axis correspond to fractions collected from column 1 and odd tics to fractions collected from column 2. Given that the values plotted in Fig. 4.11 correspond to measurements of each product fraction collected into a perfectly mixed cup, the system's periodic behavior gives rise to steady values of those measurements upon attainment of the cyclic steady state.

The 4% difference between the two column heights does not visually manifest itself as an odd-even periodicity in the quality of the collected fractions, although one may argue the contrary about the DNA content.

A qualitative evaluation of the total protein profile in the product fractions collected during the fourth and fifth cycles of operation of the two-column SMB-SEC process was performed by SDS-PAGE (Fig. 4.12). For each lane 15 μg of protein were loaded. The proteins related to the adenovirus capside, namely hexon, penton, and core, are marked within the red boxes. Although the visual information provided by the SDS-PAGE analysis is only qualitative, it is seen that bands related to the adenovirus pattern in the purified product are more visible compare to the feed, where a smear is observed due to the presence of several indistinguishable contaminant proteins.

Using the data of Fig. 4.11 it is straightforward to compute the product recovery and impurity clearance. Table 4.4 summarizes the evaluated performance of the two-column SEC system. The virus recovery yield was determined by both RT-PCR and Nanosight quantification. The two-column process was also compared against the standard single-column batch process with the same amount of SEC medium. In the later case, the two columns were arranged in series to mimic the operation of a single column.

The optimization procedure for the batch SEC step is the same as that employed by Rodrigues et al. (2010) and Silva et al. (2010). In particular, the optimized cycle time is such that for every injection it minimizes the lag between the leading edge of the product fraction of Ad5 particles, which are the fastest migrating component, and the trailing band of the slowest migrating components of the previous injection. The performance metrics for the standard single-column

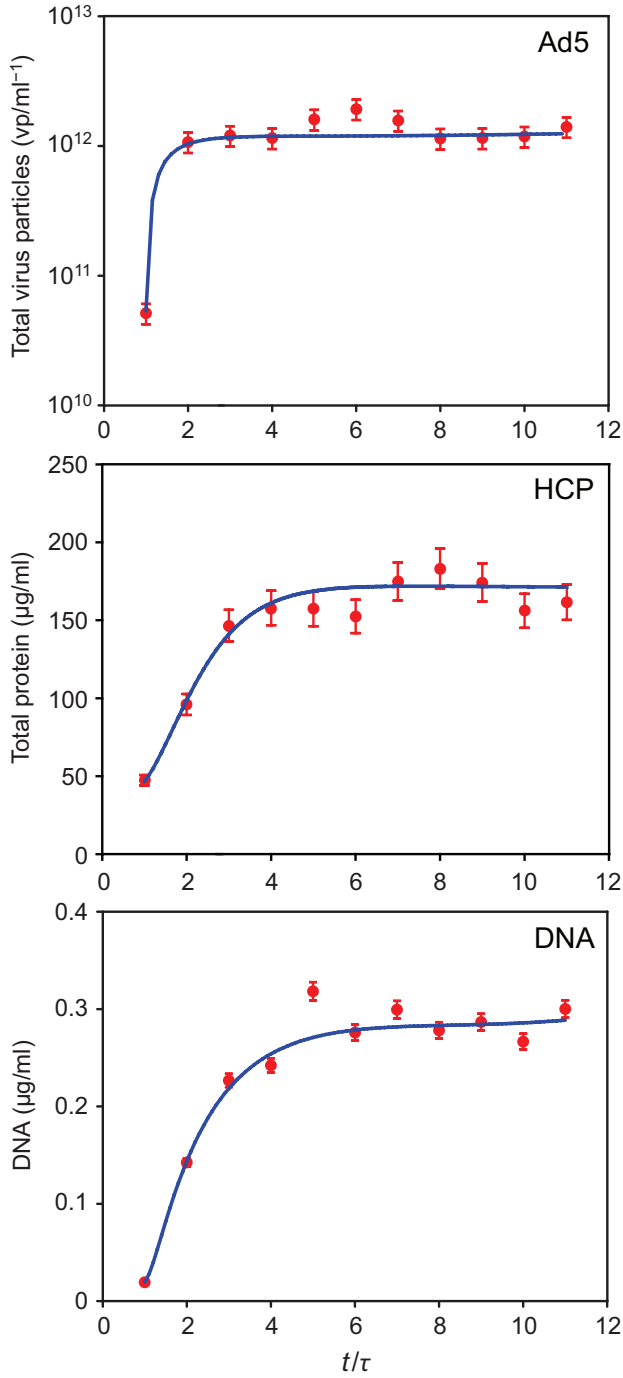

Figure 4.11: *Experimental concentrations of total virus particles, host cell protein (HCP), and DNA in the product fraction collected every switching interval during the first five cycles of operation.*

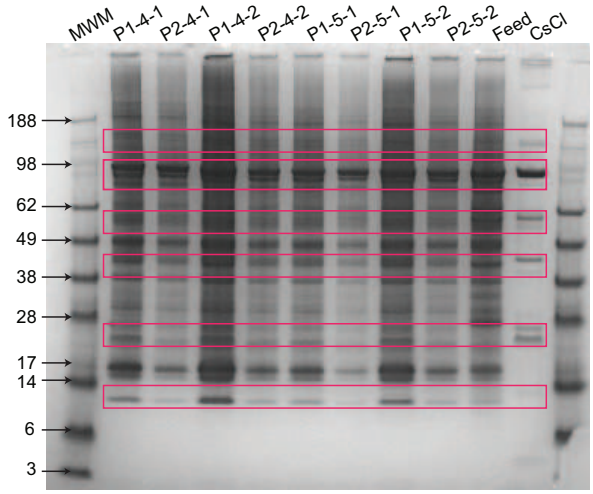

Figure 4.12: *SDS-PAGE protein profile analysis of the product fractions, P1 and P2, collected in cycles 4 and 5; P1 and P2 are the product fractions collected during the second and third steps of the switching interval, respectively (see Figs. 4.7 and 5.9). For each line 15 µg of protein were loaded. The protein related to the adenovirus capside, namely hexon, penton, and core, are marked by the red boxes. Labels: Pk-n-j, product fraction P_k collected from column j during cycle n; Feed, clarified bioreaction bulk; CsCl, CsCl-purified Ad5.*

Table 4.4: *Comparison of experimental performance between the two-column SEC system and a single-column SEC batch process for the same amount of stationary phase. The virus recovery yield was determined by RT-PCR and Nanosight quantification.*

Productivity (L/min)	Virus Yield (%)	DNA Clearance (%)	HCP Clearance (%)
Two-column, open-loop SCC-SEC			
0.67	86.3	90	89
Single-column batch SEC			
0.11	57.4	94	94

batch SEC process are listed in Table 4.4 alongside the results for the two-column process.

It worth pointing out that the purity level required by the authorities is usually expressed as amounts of DNA and HCP per dose, which implies that an application where the therapeutic dose is very high (e.g., gene therapy) can require several purification steps, whereas for VLP or mucose vaccine fewer purification steps can be sufficient to reach the desired purity level. For this reason, in the present work the process performance is always quantified in terms of percentage of clearance.

Table 4.4 shows that the two-column SEC process achieves about the same DNA and HCP clearances as the standard batch process. However, and most importantly, the virus yield is increased from 57% for the batch process to 86% for the two-column process, an improvement of 51%, because of internal recycling of the mixed fractions of contaminated Ad5 even though the process is operated strictly in an open-loop configuration. And last, but not least, the productivity is increase by 6-fold with the two-column process. This is a clear demonstration that with this increased productivity, size exclusion can go beyond the classical purposes of final polishing and buffer exchange in the downstream train of a biopurification.

The level of product dilution, as measured by the product-to-feed concentration ratio, $(c^{\mathrm{P}}/c^{\mathrm{F}})_{\mathrm{Ad5}}$, is given by the volume ratio of collected product and injected feed per cycle, adjusted for the product recovery yield, R_{Ad5}. This is valid for both the two-column SMB-SEC process and the standard batch SEC process. For example, for the former process the concentration ratio is given by $\tau_2 R_{\mathrm{Ad5}}/(\tau_2+\tau_3)$. The experimental value of $(c^{\mathrm{P}}/c^{\mathrm{F}})_{\mathrm{Ad5}}$ for the two-column SMB-SEC process is 1/1.5 and for the batch SEC process is 1/3, which is considerably smaller. Therefore, it is seen that the product fraction obtained with the two-column SMB-SEC process is significantly less diluted than the product fraction obtained with the standard batch SEC process.

Before concluding and summarizing the work, the problem of tackling process uncertainty, that is, of how to adjust the operating parameters to compensate for modeling uncertainty and process variability, is briefly discussed. When the model mismatch is significant, there is no other option than recalibration of the model and calculation of new operating parameters. But when the mismatch is small or moderate, there are two straightforward approaches to correct a purity that is out of specification. One option entails directing the outlet stream of column 2 to the waste line during a final fraction of step 3 of the switching interval (cf. Fig. 4.7),

but at the cost of reducing the product recovery, since it was shown in Fig. 5.9 that the last part of the collected product fraction is the more amenable to contamination. The other option, which sacrifices productivity instead of recovery, entails reducing the length of step 2—the feed step—and increasing by the same amount the duration of step 3. In any case, any measure to bring the purity to within specification has necessarily a cost in process performance with respect to the optimum conditions derived from the computer-aided process design.

4.5 Conclusions

This work reported on the design and experimental implementation of a simple, yet efficient, two-column, quasi-continuous, simulated moving-bed process for the separation of Ad5 by SEC. The process is strictly operated in an open-loop configuration to dispense the use of an internal recirculation pump; it uses two HPLC pumps only: one for injecting the clarified bioreaction bulk and another for injecting fresh eluent. At any instant of the operating cycle, the flow through a column is either temporarily stopped or completely directed to one of three destinations: the other column, the waste line, or the product line. This class of flow-path configurations is easily implemented with simple two-way valves and gives rise to very robust operating cycles.

Care was taken to experimentally monitor the process performance on a cycle-to-cycle basis. For example, clearance of impurities, namely DNA and HCP, and virus concentration, were experimentally assessed at each cycle. The experimental results show a virus recovery of 86%, and a clearance of 90% and 89% for DNA and HCP, respectively. These figures compare very favorably against single-column batch chromatography for the same volume of size-exclusion resin. The 6-fold productivity boost and 51% increase in Ad5 recovery, without compromising the impurity clearance, are strong arguments in favor of implementing the type of process presented here in a real production DSP train.

The adopted process-systems-engineering view of the downstream process, coupled with state-of-the-art process optimization and process automation, can pave the way to ready-to-process technologies where the complexity is hidden from the end user by easy-to-use interfaces.

Acknowledgments

The authors thank Duarte Lima Martins for the purified Ad5 material. Financial support from Sartorius Stedim Biotech and from the Portuguese Science Foundation (FCT-MCTES) (SFRH/BD/82032/2011, PTDC/EBB-BIO/101992/2008 and PTDC/EBB- BIO/119501/2010) is gratefully acknowledged. The authors do not have any conflicts of interest.

References

Araújo, J. M., Rodrigues, R. C., Eusébio, M. F., and Mota, J. P. (2010). Chiral separation by two-column, semi-continuous, open-loop simulated moving-bed chromatography. *J Chromatogr A*, *1217*, 5407–5419.

Aumann, L., and Morbidelli, M. (2007). A continuous multicolumn countercurrent solvent gradient purification (MCSGP) process. *Biotechnol Bioeng*, *98*, 1043–1055.

Barut, M., Podgornik, A., Brne, P., and Štrancar, A. (2005). Convective interaction media short monolithic columns: enabling chromatographic supports for the separation and purification of large biomolecules. *J Sep Sci*, *28*, 1876–1892.

Blanche, F., Cameron, B., Barbot, A., Ferrero, L., Guillemin, T., Guyot, S., Somarriba, S., and Bisch, D. (2000). An improved anion-exchange HPLC method for the detection and purification of adenoviral particles. *Gene Ther*, *7*, 1055–1062.

Burova, E., and Ioffe, E. (2005). Chromatographic purification of recombinant adenoviral and adeno-associated viral vectors: methods and implications. *Nat Rev Genet*, *12*, S5–S17.

Dormond, E., Chahal, P., Bernier, A., Tran, R., Perrier, M., and Kamen, A. (2010). An efficient process for the purification of helper-dependent adenoviral vector and removal of helper virus by iodixanol ultracentrifugation. *J Virol Methods*, *165*, 83–89.

E.G. Malawer, L. S. (2004). *Handbook Of Size Exclusion Chromatography And Related Techniques, 2nd ed,.* Marcel Dekker, New York, NY.

Eglon, M. N., Duffy, A. M., O'Brien, T., and Strappe, P. M. (2009). Purification of adenoviral vectors by combined anion exchange and gel filtration chromatography. *J Gene Med*, *11*, 978–989.

Francotte, E. R., and Richert, P. (1997). Applications of simulated moving-bed chromatography to the separation of the enantiomers of chiral drugs. *J Chromatogr A*, *769*, 101–107.

GE-Healthcare (). *Gel filtration: Principles and Methods, Uppsala, Sweden, 2010. Digital version available on-line at: http://www.gelifesciences.com/webapp/wcs/stores/servlet/catalog/pt/GELifeSciences/service-and-support/handbooks*. GE Healthcare.

Glueckauf, E. (1955). Theory of chromatography. part 10.formulæ for diffusion into spheres and their application to chromatography. *Trans Faraday Soc*, *51*, 1540–1551.

Glueckauf, E., and Coates, J. (1947). 241. theory of chromatography. part iv. the influence of incomplete equilibrium on the front boundary of chromatograms and on the effectiveness of separation. *J Chem Soc*, (pp. 1315–1321).

Godawat, R., Brower, K., Jain, S., Konstantinov, K., Riske, F., and Warikoo, V. (2012). Periodic counter-current chromatography - design and operational considerations for integrated and continuous purification of proteins. *Biotechnol J*, *7*, 1496–1508.

Goerke, A. R., To, B. C. S., Lee, A. L., Sagar, S. L., and Konz, J. O. (2005). Development of a novel adenovirus purification process utilizing selective precipitation of cellular DNA. *Biotechnol Bioeng*, *91*, 12–21.

Gomes, P. S., Minceva, M., and Rodrigues, A. E. (2006). Simulated moving bed technology: old and new. *Adsorption*, *12*, 375–392.

Haynes, H. W., and Sarma, P. N. (1973). A model for the application of gas chromatography to measurements of diffusion in bidisperse structured catalysts. *AIChE J*, *19*, 1043–1046.

Huyghe, B. G., Liu, X., Sutjipto, S., Sugarman, B. J., Horn, M. T., Shepard, H. M., Scandella, C. J., and Shabram, P. (1995). Purification of a type 5 recombinant adenovirus encoding human p53 by column chromatography. *Hum Gene Ther*, *6*, 1403–1416.

Kalbfuss, B., Flockerzi, D., Seidel-Morgenstern, A., and Reichl, U. (2008). Size-exclusion chromatography as a linear transfer system: Purification of human influenza virus as an example. *J Chromatogr B*, *873*, 102–112.

Kalbfuss, B., Wolff, M., Morenweiser, R., and Reichl, U. (2007). Purification of cell culture-derived human influenza a virus by size-exclusion and anion-exchange chromatography. *Biotechnol Bioeng*, *96*, 932–944.

Kamen, A., and Henry, O. (2004). Development and optimization of an adenovirus production process. *J Gene Med*, *6*, S184–S192.

Konz, J. O., Lee, A. L., Lewis, J. A., and Sagar, S. L. (2005a). Development of a purification process for adenovirus: controlling virus aggregation to improve the clearance of host cell DNA. *Biotechnol Prog*, *21*, 466–472.

Konz, J. O., Livingood, R. C., Bett, A. J., Goerke, A. R., Laska, M. E., and Sagar, S. L. (2005b). Serotype specificity of adenovirus purification using anion-exchange chromatography. *Hum Gene Ther*, *16*, 1346–1353.

Krättli, M., Müller-Späth, T., and Morbidelli, M. (2013). multifraction separation in countercurrent chromatography (mcsgp). *Biotechnol Bioeng*, *110*, 2436–2444.

Kröber, T., Wolff, M., Hundt, B., Seidel-Morgenstern, A., and Reichl, U. (2013). Continuous purification of influenza virus using simulated moving bed chromatography. *J Chromatogr A*, *1307*, 99–110.

Lee, D.-S., Kim, B.-M., and Seol, D.-W. (2009). Improved purification of recombinant adenoviral vector by metal affinity membrane chromatography. *Biochem Biophys Res Commun*, *378*, 640–644.

Peixoto, C., Ferreira, T., Carrondo, M., Cruz, P., and Alves, P. (2006). Purification of adenoviral vectors using expanded bed chromatography. *J Virol Methods*, *132*, 121–126.

Peixoto, C., Sousa, M. F. Q., Silva, A. C., Carrondo, M. J. T., and Alves, P. M. (2007). Downstream processing of triple layered rotavirus like particles. *J Biotechnol*, *127*, 452–461.

Rajendran, A., Paredes, G., and Mazzotti, M. (2009). Simulated moving bed chromatography for the separation of enantiomers. *J Chromatogr A*, *1216*, 709–738.

Riordan, W., Heilmann, S., Brorson, K., Seshadri, K., He, Y., and Etzel, M. (2009). Design of salt-tolerant membrane adsorbers for viral clearance. *Biotechnol Bioeng*, *103*, 920–929.

Rodrigues, R. C., Silva, R. J., and Mota, J. P. (2010). Streamlined, two-column, simulated countercurrent chromatography for binary separation. *J Chromatogr A*, *1217*, 3382–3391.

Rodrigues, R. C. R., Canhoto, T. J. S. B., Araújo, J. M. M., and Mota, J. P. B. (2008). Two-column simulated moving-bed process for binary separation. *J Chromatogr A*, *1180*, 42–52.

Rodrigues, T., Carvalho, A., Carmo, M., Carrondo, M. J. T., Alves, P. M., and Cruz, P. E. (2007). Scaleable purification process for gene therapy retroviral vectors. *J Gene Med*, *9*, 233–243.

Ruthven, D. (1984). *Principles of Adsorption and Adsorption Processes*. John Wiley & Sons.

Segura, M. M., Alba, R., Bosch, A., and Chillón, M. (2008). Advances in helper-dependent adenoviral vector research. *Curr Gene Ther*, *8*, 222–235.

Seidel-Morgenstern, A., Keßler, L. C., and Kaspereit, M. (2008). New Developments in Simulated Moving Bed Chromatography. *Chem Eng Technol*, *31*, 826–837.

Silva, R. J., Rodrigues, R. C., Osuna-Sanchez, H., Bailly, M., Valéry, E., and Mota, J. P. (2010). A new multicolumn, open-loop process for center-cut separation by solvent-gradient chromatography. *J Chromatogr A*, *1217*, 8257–8269.

Silva, R. J. S., Rodrigues, R. C. R., and Mota, J. P. B. (2012). Relay simulated moving bed chromatography: Concept and design criteria. *J Chromatogr A*, *1260*, 132–142.

Slepushkin, V., Chang, N., Cohen, R., Gan, Y., Jiang, B., Berlinger, D., Binder, G. et al. (2003). Large-scale purification of a lentiviral vector by size exclusion chromatography or mustang q ion exchange capsule. *Bioprocess J*, *2*, 89–95.

Tatsis, N., and Ertl, H. C. J. (2004). Adenoviruses as vaccine vectors. *Mol Ther*, *10*, 616–629.

Vicente, T., Faber, R., Alves, P. M., Carrondo, M. J. T., and Mota, J. P. B. (2011). Impact of ligand density on the optimization of ion-exchange membrane chromatography for viral vector purification. *Biotechnol Bioeng*, *108*, 1347–1359.

Warikoo, V., Godawat, R., Brower, K., Jain, S., Cummings, D., Simons, E., Johnson, T., Walther, J., Yu, M., Wright, B., McLarty, J., Karey, K. P., Hwang, C., Zhou, W., Riske, F., and Konstantinov, K. (2012). Integrated continuous production of recombinant therapeutic proteins. *Biotechnol Bioeng*, *109*, 3018–3029.

CHAPTER 5

Robust design of adenovirus purification by two-column, simulated countercurrent chromatography

---

Adapted from:

Nestola P, Silva RJS, Peixoto C, Alves PM, Carrondo MJT, Mota JPB. Robust design of adenovirus purification by two-column, simulated countercurrent, size-exclusion chromatography. *Journal of Biotechnology* Accepted.

Abstract

A simple, yet efficient, two-column simulated moving-bed (2CSMB) process for purifying adenovirus serotype 5 (Ad5) by size-exclusion chromatography (SEC) is presented and validated experimentally, and a general procedure for its robust design under parameter uncertainty is described. The pilot-scale run yielded a virus recovery of 86% and DNA and HCP clearances of 90% and 89%, respectively, without any fine tunning of the operating parameters. This performance compares very favorably against that of single-column batch chromatography for the same volume of size-exclusion resin. To improve the robustness of the 2CSMB-SEC process the best set of operating parameters is selected only among candidate solutions that are robust feasible, that is, remain feasible for all parameter perturbations within their uncertainty intervals. This robust approach to optimal design replaces the nominal problem by a worst case problem. Computational tractability is ensured by formulating the robust design problem with only the vertexes of the uncertainty region that have the worst effect on the product purity and recovery. The robust design is exemplified on the case where the column volume and interparticle porosity are subject to uncertainty. As expected, to increase the robustness of the 2CSMB-SEC process it is necessary to reduce its productivity and increase its solvent consumption. Nevertheless, the design solution given by the proposed robust approach is the least detrimental of all possible feasible candidate solutions.

Keywords: virus purification; size-exclusion chromatography; simulating moving bed; two-column chromatography; robust design.

5.1 Introduction

Viral vectors are playing an increasingly important role in the vaccine and gene therapy fields. Adenoviruses (Ads), in particular, are considered one of the most suitable platforms for production of viral vaccines and gene therapy vectors. They are medium-sized (90–100 nm), nonenveloped, icosahedral viruses composed of a nucleocapsid and linear, non-segmented double stranded DNA genome that is about 36 kb long. Their broad tissue tropism and large transgene packing capacity make them attractive candidates for innovative virotherapies (Eglon et al., 2009). Adenoviruses can be produced in a complementary cell line in both adherent and suspension culture systems, such as HEK-293 or PER-C6 cells, or A549 for oncolytic therapies (Segura et al., 2008; Kamen and Henry, 2004).

Liquid chromatography is currently the core technique for vector purification, and its use is often integrated vertically within the downstream processing (DSP) strategy, as it easily fits into the early capture stage as well as into the final purification phase. The use of high-performance liquid chromatography (HPLC) for large-scale adenoviral purification was first described by Huyghe et al. (1995), and several approaches have been applied since then, including ion-exchange (IEX), size-exclusion (SEC), hydrophobic interaction, and immobilized metal affinity chromatography (Blanche et al., 2000; Kalbfuss et al., 2008; Lee et al., 2009). Unlike traditional processes based on CsCl-gradient purification, HPLC offers a straightforward linear scale-up path, and procedures for purifying up to around 10^{14} input particles have been reported.

SEC and ultra/diafiltration (usually by tangential flow filtration) are two other widely used processes at the very latest stage for formulating the product (Dormond et al., 2010; Peixoto et al., 2007; Rodrigues et al., 2007). However, purification schemes where SEC is followed by IEX have also been reported in the literature; two prominent examples are the works of Kalbfuss et al. (2007) and Eglon et al. (2009) for influenza and adenovirus, respectively.

One process-based way to improve the performance of the DSP chromatographic steps is by changing to a (quasi-)continuous processing mode, which, in principle, yields higher throughput, lower buffer consumption, higher capacity utilization of the stationary phase and reduced column volume, hence increased productivity.

Studies concerning continuous or quasi-continuous downstream bioprocessing have targeted mostly proteins and monoclonal antibodies (mAb) (Aumann and Morbidelli, 2007; Silva et al., 2010; Godawat et al., 2012; Warikoo et al., 2012;

Krättli et al., 2013); this is primarily because the biopharmaceutical industry is currently dominated by these bioproducts. To date, the continuous purification of large biomolecules, such as viruses, has rarely been explored. A notable exception is the recent work of Kröber et al. (2013), who implemented a classical three-zone, open-loop simulated moving bed (SMB) for influenza virus purification. These authors have successfully increased the productivity by switching to simulated countercurrent operation.

Uncertainties in isotherm parameters, band broadening, pump stability and calibration, extra-column volumes, and packing reproducibility are inevitable in every multicolumn chromatographic process. This is particularly true in bioproduction-scale operation. Robust analysis of single-column batch biochromatography has been extensively studied by Nilsson's group at Lund University (Jakobsson et al., 2005, 2007; Degerman et al., 2008, 2009; Westerberg et al., 2012, 2013; Borg et al., 2013) and Gétaz et al. (2013). On the other hand, very few studies have addressed the problems of handling parameter uncertainty and robustness of operation of SMB processes (Mun et al., 2003; Mota et al., 2007) and none has studied configurations with few columns.

Robust design of DSP chromatography increased of importance since the US Food and Drug Administration's PAT initiative (FDA, 2004), followed by ICH guidelines (ICH, 2005, 2009, 2007), opened up the possibility for a risk-based approach to pharmaceutical production. Provided that sufficient process knowledge is available, the process can be run within a design space instead of at one fixed operating point. The design space is the space in which all possible process parameter values are represented, every degree parameter of the process being represented as an axis of a multidimensional space; the design space boundaries are selected so that the process, when operated under conditions within the design space, fulfills the quality specifications, i.e., the design space in the parameter space has a projection in the quality attribute space that is inside the specification ranges (Westerberg et al., 2012)

In the present work, a simple, yet efficient, two-column simulated moving-bed (2CSMB) process for purifying adenovirus serotype 5 (Ad5) by size-exclusion chromatography (SEC) is presented and validated experimentally. It is shown that the main drawbacks of SEC, namely low productivity and high product dilution, can be eliminated to a large extent by switching from single-column batch operation to two-column SMB-type operation.

In line with the framework proposed by FDA and ICH, a general procedure for robust design of the 2CSMB-SEC process under parameter uncertainty is

proposed wherein the best set of operating parameters is selected only among candidates that are robust feasible, that is, remain feasible for all parameter perturbations within their uncertainty intervals. This robust approach to optimal design replaces the nominal problem by a worst case problem (Grossmann and Sargent, 1978; Halemane and Grossmann, 1983; L.T. Biegler, 1997; Ben-Tal and Nemirovski, 2002). The proposed procedure was successfully employed to find the optimal robust values of the step durations when both the interparticle porosity and column volume are subject to two types of uncertainties.

The paper is organized as follows. After describing the 2CSMB-SEC process, the methodology and numerical tools for model-based optimal design of the operating conditions in the absence of parameter uncertainty are discussed. This discussion is followed by the experimental validation of the 2CSMB-SEC process, where the stability of its cyclic steady behavior and its good performance are demonstrated. Finally, the model-based nominal design procedure is generalized to the case of optimal design under parameter uncertainty. The proposed method is further enhanced to cope with the more general problem of robust design under probabilistic uncertainty.

5.2 Two-column, open-loop, simulated moving-bed, size-exclusion chromatography

In a two-column (2C) SMB process the cycle is divided in half into two intervals, or half cycles, which hereafter are referred to as switching intervals. To design the cycle it suffices to define the sequence of flow-line configurations for one of the switching intervals; the sequence for the other interval is similar, but the positions of the two columns are exchanged. In practice, it is easier to keep the columns fixed in space and to move the positions of the inlet and outlet lines by means of an automated arrangement of two- or three-way valves. Over a full cycle each column undergoes the same sequence of steps but phased out in time by one switching interval.

The 2CSMB-SEC scheme developed for Ad5 purification is shown in Fig. 5.1b (Nestola et al., 2014). It is an open-loop process that is physically realizable with simple two-way or three-way valves to control the flow paths in the system and requires a minimum number of pumps—one for injecting feed and another for injecting eluent. The half-cycle (or switching interval) is divided into the following sequence of steps:

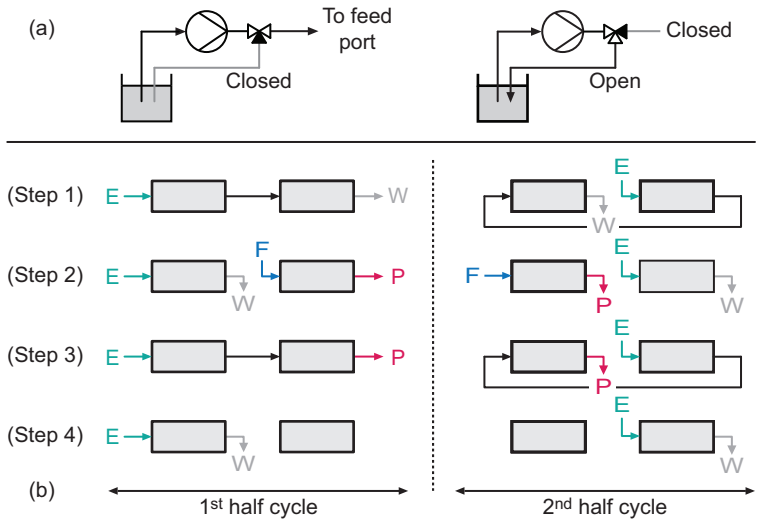

Figure 5.1: *(a) Schematic of the (b) Schematic of the 2CSMB-SEC operating cycle for Ad5 purification; E denotes the eluent inlet; F, the feed inlet; and P and W, the product and waste outlets, respectively*

Step 1. The upstream column is eluted while the effluent of the downstream column is diverted to the waste line.

Step 2. The upstream column is eluted but its effluent is diverted to the waste line instead of being directed to the downstream column. The downstream column is fed with the clarified bioreaction bulk while its effluent is collected as purified product.

Step 3. The system is operated as in step 1 but the effluent of the downstream column is collected as product.

Step 4. The upstream column is eluted but its effluent is again diverted to the waste line instead of being directed to the downstream column. The downstream column is kept frozen, that is, the flow through that column is temporarily halted.

This process is based on our group's previous work on the development of efficient multicolumn chromatographic processes for binary and center-cut separations (Silva et al., 2012; Rodrigues et al., 2008; Araújo et al., 2010; Rodrigues et al., 2010; R.J.S., 2013). The feed mixture is suppled into the middle of the system where the composition of the circulating fluid is closest to that of the feedstock fluid, and recovers the purified product and waste fraction alternately

at the downstream end of the unit, while desorbent is continuously supplied into the upstream end of the system. We have also shown that the feed step, in which the feed is usually admixed with the effluent from the upstream column, can be replaced by step 2 of Fig. 5.1 without loss of performance and in some instances increased productivity (Silva et al., 2012; R.J.S., 2013). Actually, it is advisable to use steps 2 and 3 of Fig. 5.1 when the duration of the product collection is larger than the time taken to inject the feed, which is the case when there is large band broadening in the system as is the case in SEC.

The 2CSMB-SEC process is quasi-continuous because the clarified bioreaction bulk is not continuously fed into the system but periodically injected as a series of rectangular pulses. The two HPLC pumps are operated under steady conditions at their prescribed flow rates to minimize disturbances in their operation. To interrupt the feed flow, the control software redirects it back to the feed tank by switching the three-way valve placed in front of the feed pump to the position shown in the left schematic of Fig. 5.1a. Since for all purposes the valve switching is instantaneous, the net effect is a very good approximation of the sharp edge of the step change in the flow rate. To redirect the feed flow to one of the column inlets, the three-way valve is switched to the position shown in the right schematic of Fig. 5.1a; the sharp edge of the step change in the flow rate is well reproduced again.

The selected size-exclusion medium employed in our process was Sepharose 4 Fast Flow (S4FF, GE Healthcare) supplied by the manufacturer with an average particle size of 90 μm. S4FF is suitable for Ad5 purification because it completely excludes the Ad5 particles from its porous matrix and, hence, they elute in the interparticle volume, whereas the impurities present in the clarified bioreaction bulk elute through the porous matrix at different rates. The S4FF medium and slurry packed into two XK 26/20 chromatographic columns (2.6 cm i.d., maximum bed height of 20 cm); the final, stabilized column lengths were 10.4 cm and 10.8 cm. No measures were taken to improve the balancing of the bed heights. Before each experiment the columns were sanitized with 1 M NaOH, washed with Milli Q water, and equilibrated with 5 bed volumes of running buffer (20 mM Tris, 150 mM NaCl, pH 8).

5.3 SEC column breakthrough model

A simple equilibrium, dispersed plug flow model is adopted for computer-aided design of the SEC step. In this model the column efficiency is measured by the

dimensionless plate height, $h_i = L/N_i$, where L is the column length and N_i is the number of theoretical plates for component i. The model can be written as

$$\frac{\partial c_i}{\partial t} + \frac{Q}{\epsilon_i V_\mathrm{c}} \left(\frac{\partial c_i}{\partial x} - \frac{h_i}{2} \frac{\partial^2 c_i}{\partial x^2} \right) = 0, \quad 0 < x < 1, \ t > 0, \tag{5.1}$$

where i is the solute index, t is the time coordinate, $x = z/L$ is the dimensionless axial coordinate along the packed bed, L and V_c are the length and volume of the column, c is the solute concentration in the mobile phase, and Q is the volumetric flow rate of mobile phase.

The symbol ϵ_i denotes the volumetric fraction of the SEC column that is accessible to component i (i.e., the overall porosity of the packed bed that is probed by component i); ϵ_i is given by

$$\epsilon_i = \epsilon_\mathrm{o} + (1 - \epsilon_\mathrm{o}) H_i, \quad H_i = \epsilon_\mathrm{p} \int_{d_{\mathrm{m},i}}^{\infty} \psi(\sigma)\, d\sigma. \tag{5.2}$$

where $\psi(\cdot)$ is the pore size distribution of the size exclusion medium, i.e., $\psi(\sigma)\, d\sigma$ is the fraction of the S4FF's porous volume with pore diameters between σ and $\sigma + d\sigma$, and $d_{\mathrm{m},i}$ is the size of the biomolecule.

Equation 5.1 is subject to the usual boundary conditions:

$$c_i - \frac{h_i}{2} \frac{\partial c_i}{\partial x} = c_i^\mathrm{in} \quad \text{for} \quad x = 0, \ t > 0, \tag{5.3}$$

$$\frac{\partial c_i}{\partial x} = 0 \quad \text{for} \quad x = 1, \ t > 0, \tag{5.4}$$

where $c_i^\mathrm{in}(t)$ is the inlet concentration of component i. Hereafter, $c_i^\mathrm{out}(t) \equiv c_i(t)|_{x=1}$ denotes the temporal concentration profile of component i in the outlet effluent of the column.

5.4 Model-based optimal process design

Unlike IEX or affinity chromatography, the components of the bioreaction bulk do not bind to the SEC medium, because of lack of reactivity and strong adsorptive interactions, so they elute through the SEC medium at a rate that depends on their molecular size and shape but not on the presence of the other solutes. Therefore, for the purposes of process design the complex multicomponent mixture in the clarified bioreaction bulk can be modeled as a simpler mixture of three key components: (1) the virus, which is the largest species and, hence, the fastest

Table 5.1: *Model parameters derived from the analysis of pulse experiments performed with the two XK 26/20 columns placed in series, $L = L_1 + L_2 = 21.2$ cm. i is the component index, c^{F} is the feed concentration, which is assumed to be proportional to the area under the UV absorbance peak (arbitrary units s.t. $\sum_i c_i^{\mathrm{F}} = 1$), ϵ is the accessible porosity, and N is the number of theoretical plates per column.*

i	1	2	3	4
c_i^{F}	0.140	0.165	0.541	0.154
ϵ_i	0.306	0.564	0.945	0.750
N_i	61	18	69	51

eluting component; (2) the group of impurities that elute nearest to the virus; and (3) the group of small impurities that elute at the slowest rate. All the other components in the bioreaction bulk necessarily elute at intermediate rates between those of the second and third key components; if the SEC process is properly designed, these components will be withdrawn from the system in one of the waste fractions.

To design the SEC process it is necessary to measure the retention volume of each key component, from which the value of ϵ_i can be determined, and the extent of band broadening at the working flow rate to determine the value of h_i. These parameters were determined from the position, area, and broadening of the key chromatographic peaks of the samples of clarified bioreaction bulk injected into the two columns arranged in series.

Table 5.1 lists the model parameters derived from the analysis of the pulse experiments performed with the two columns arranged in series. The feed concentrations given in this table are normalized values, $\sum_i c_i^{\mathrm{F}} = 1$, and were determined assuming that the concentration is proportional to the area under the corresponding UV absorbance peak. Table 5.1 includes a fourth component (component 4) corresponding to the group of intermediate impurities that elute between the two groups of key impurities. This fourth component was not considered in the design of the SEC process, but only to obtain a better description of the simulated elution profiles for comparison with the experiments.

The optimal durations of the cycle steps, τ_k ($k = 1, \ldots, 4$), were determined using a rigorous model-based design procedure. The feed and eluent flow rates, Q_{F} and Q_{E}, were both fixed at 3 mL/min because of the constraint imposed by the pressure drop through the SEC medium in steps 1 and 3 of the cycle, but they could have easily been included in the set of decision variables. The purpose of

Table 5.2: *Flow rates and boundary conditions for the first half ($0 < t \leq \tau$) of the 2CSMB-SEC cycle (cf. Fig. 5.1). The boundary condition $c_{i,2}^{\text{in}} = c_{i,2}|_{x=0}$ for column 2 during step 4 is equivalent to $(\partial c_{i,2}/\partial x)_{x=0} = 0$.*

Step	Column 1		Column 2	
	Q	c_i^{in}	Q	c_i^{in}
1	Q_{E}	0	Q_{E}	$c_{i,1}^{\text{out}}$
2	Q_{E}	0	Q_{F}	c_i^{F}
3	Q_{E}	0	Q_{E}	$c_{i,1}^{\text{out}}$
4	Q_{E}	0	0	$c_i\|_{x=0}$

the optimization procedure is to guarantee the fulfillment of product and process specifications, namely minimal product purity and recovery, while maximizing the productivity of the 2CSMB-SEC process.

Let

$$c_{i,j}(x,t) = g(c_{i,j}(x,0); \tau_1, \ldots, \tau_4), \quad 0 < t \leq \tau, \tag{5.5}$$

represent the desired solution for the set of decision variables parameters $\{\tau_1, \ldots, \tau_4\}$ and initial conditions $c_{i,j}(x,0)$; here, i is the index that runs over the set of solutes and j the index that runs over the set of columns. For example, to simulate the startup of the process when the two columns are initially clean, the initial conditions would be

$$c_{i,j}(x,0) = 0. \tag{5.6}$$

The dynamic response of the 2CSMB-SEC process for the first-half of the cycle ($0 < t \leq \tau$) is given by the solution of 6 instances (2 columns $\times$ 3 key components) of the equilibrium, dispersed plug flow model (eq. 5.1), subject to the boundary conditions given by eqs. 5.3 and 5.4, together with the coupling conditions listed in Table 5.2 For process design, however, only the fully established steady, periodic state, also known as cyclic steady state (CSS), is of interest. The CSS for a two-column SMB process is the solution $c_{i,j}(x,t)$ that satisfies

For process design, however, only the fully established steady, periodic state, also known as cyclic steady state (CSS), is of interest. The CSS for a two-column SMB process is the solution $c_{i,j}(x,t)$ that satisfies

$$c_{i,1}(x,\tau) = c_{i,2}(x,0), \quad c_{i,2}(x,\tau) = c_{i,1}(x,0), \quad \tau = \sum_k \tau_k. \tag{5.7}$$

This constraint imposes the conditions of simulated counter-current operation (the two columns exchange roles at the end of every switching interval) and time periodic behavior. Let $c_{i,j}(x,t) = g^{\text{css}}(\tau_1,\ldots,\tau_4)$ represent the CSS solution for the first half of the cycle; the solution for the second half of the cycle is simply

$$c_{i,1}(x,t) = c_{i,2}(x,t-\tau), \quad c_{i,2}(x,t) = c_{i,1}(x,t-\tau), \quad \tau < t \leq 2\tau. \tag{5.8}$$

For the 2CSMB-SEC cycle shown in Fig. 5.1 the amount of feed injected per switching interval, which is a direct measure of productivity, is given by

$$\overline{Q_{\text{F}}} = (\tau_2/\tau)Q_{\text{F}}, \tag{5.9}$$

and the purity and yield of purified Ad5 are, respectively,

$$P_{\text{Ad5}} = \frac{\displaystyle\int_{\tau_2} Q_{\text{F}} c_{1,2}^{\text{out}}\,dt + \int_{\tau_3} Q_{\text{E}} c_{1,2}^{\text{out}}\,dt}{\displaystyle\int_{\tau_2} Q_{\text{F}} c_{\text{tot},2}^{\text{out}}\,dt + \int_{\tau_3} Q_{\text{E}} c_{\text{tot},2}^{\text{out}}\,dt} = \frac{\displaystyle\int_{\tau_2+\tau_3} c_{1,2}^{\text{out}}\,dt}{\displaystyle\int_{\tau_2+\tau_3} c_{\text{tot},2}^{\text{out}}\,dt}, \tag{5.10}$$

$$R_{\text{Ad5}} = \frac{\displaystyle\int_{\tau_2} Q_{\text{F}} c_{1,2}^{\text{out}}\,dt + \int_{\tau_3} Q_{\text{E}} c_{1,2}^{\text{out}}\,dt}{Q_{\text{F}}\tau_2 c_1^{\text{F}}} = \frac{\displaystyle\int_{\tau_2+\tau_3} c_{1,2}^{\text{out}}\,dt}{\tau_2 c_1^{\text{F}}}, \tag{5.11}$$

where $c_{\text{tot},j}^{\text{out}} = \sum_i c_{i,j}^{\text{out}}$ is the total concentration in the outlet effluent of column j; the flow rates drop out of the expressions because they happened to be equal in the experimental run.

If P_{Ad5} is high, say above 90%, the impurities in the collected product fraction are necessarily the key component 2, because of its proximity to the Ad5 product, and/or key component 3 from the previous switching interval because of its circulation around the system. Given that the components elute through the SEC medium at rates that depend on their molecular sizes and shapes but not on the presence of other solutes, in the design procedure it is unnecessary to consider more key components than the product and the two above-mentioned key impurities.

$$\begin{aligned} \max_{\tau_1,\ldots,\tau_4} \quad & \overline{Q_{\text{F}}} \\ \text{s.t.} \quad & c_{i,j}(x,t) = g^{\text{css}}(\tau_1,\ldots,\tau_4), \\ & P_{\text{Ad5}} \geq P_{\text{Ad5,min}}, \quad R_{\text{Ad5}} \geq R_{\text{Ad5,min}}. \end{aligned} \tag{5.12}$$

This problem was formulated numerically in AMPL (R. Fourer, 2003) (http://ampl.com) using a full discretization approach (Mota and Araújo, 2005; Araújo et al., 2006). The column length was discretized using third-order orthogonal collocation on 50 finite elements and the time domain (half cycle) was discretized using third-order Radau collocation on 15 finite elements per sub-step of the switching interval. The resulting nonlinear programming problem was solved using Ipopt (Wächter and Biegler, 2006), version 3.11.2 (https://projects.coin-or.org/Ipopt), coupled to the Watson Sparse Matrix Package (WSMP) (Gupta, 2000), version 13.6.10 (http://www.research.ibm.com/projects/wsmp). Ipopt implements a primal-dual interior-point method and uses line searches based on filter methods; it directly exploits first and second derivative (Hessians) information provided by AMPL via automatic differentiation.

5.5 Experimental validation

The optimal step durations for the set of parameters listed in Table 5.1, column lengths $L_1 = L_2 = (10.8 + 10.4)/2 = 10.6$ cm, $P_{\mathrm{Ad5,min}} = 0.95$, $R_{\mathrm{Ad5,min}} = 0.95$, and $Q_{\mathrm{E}} = Q_{\mathrm{F}} = 3$ mL/min are given in Table 5.3 in the column labeled 'Nominal'.

Figure 5.2 shows a surface plot of the simulated concentrations of the four key components in the fluid phase as a function of time (vertical axis) and axial distance in each column (horizontal axis) for a full cycle of the optimized 2CSMB-SEC process under CSS conditions.

At the start of the cycle the concentration bands are nearly all confined to column 1, whereas column 2 is practically clean. Fresh feed is injected while the Ad5 product from the previous switching interval is displaced from column 1 to column 2. A purified band will then slowly detach from the group of nearest eluting impurities. As soon as the product is confined into column 2, the impurities trapped in column 1 can be directed to the waste line and then the steps are repeated but with the two column positions exchanged. Notice that the trailing edge of the slowest impurity (key component 3) is displaced from the upstream end to the downstream end of a column over the duration of a switching interval (half-cycle). As expected, the intermediate group of impurities is always confined between the key components (impurities) 2 and 3.

The surface plot embeds all the information about the movement of the concentration fronts inside the two columns: slicing the surface plot horizontally generates a snapshot of the axial concentration profiles at a given instant of the cycle; slicing the plot vertically gives the time history over the cycle of the

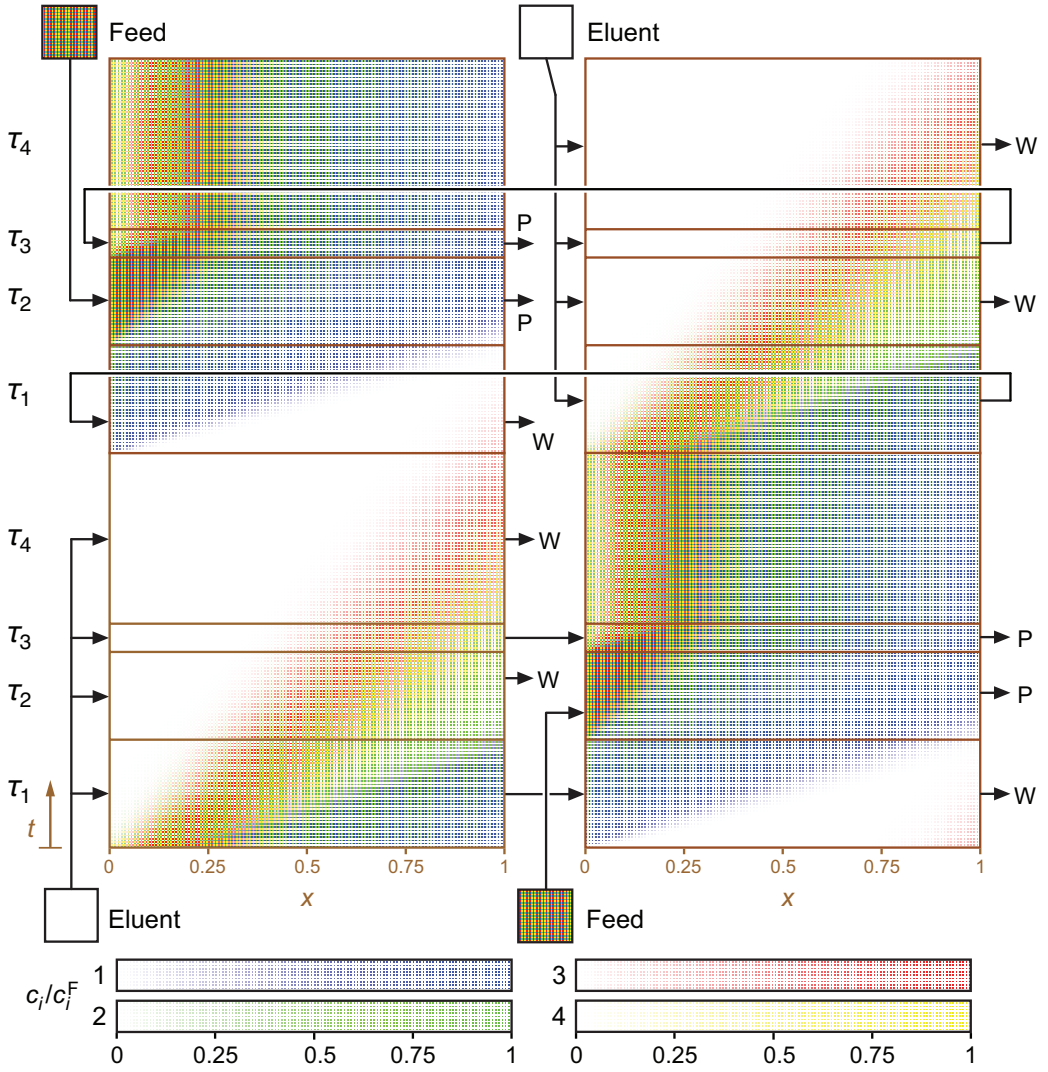

Figure 5.2: *Surface plot of the simulated concentrations of the four key components in the fluid phase as a function of time (vertical axis) and axial position in each column (horizontal axis) for a full cycle of the optimized 2CSMB-SEC process under CSS conditions.*

Table 5.3: *Optimal step durations, τ_k ($k = 1, \ldots, 4$), of the 2CSMB-SEC cycle for the chromatographic parameters given in Table. 5.1; the τ_k are reported in minutes. The elution (Q_{E}) and feed (Q_{F}) flow rates are both fixed at 3 mL/min; $P_{\mathrm{Ad5,min}} = 0.95$, $R_{\mathrm{Ad5,min}} = 0.95$. $\overline{Q_{\mathrm{F}}}$ is the average feed flow rate (mL/min), which is a direct measure of productivity; $Q_{\mathrm{E}}/\overline{Q_{\mathrm{F}}}$ is a measure of solvent consumption. Robust 1: robust solution for the case in which ϵ_{o}' and V_{c}' are uncorrelated, uniformly distributed, random variables in the interval $[-2.5\%, +2.5\%]$. Robust 2: robust solution with 95% success rate for the case in which ϵ_{o}' and V_{c}' are uncorrelated, normally distributed, random variables with zero mean and standard deviations $\sigma_\epsilon/\delta\epsilon_{\mathrm{o}} = \sigma_V/\delta V_{\mathrm{c}} = 1.96$.*

	Nominal		Robust 1		Robust 2	
Step index, k	τ_k	τ_k/τ	τ_k	τ_k/τ	τ_k	τ_k/τ
1	4.868	0.273	4.965	0.291	4.938	0.289
2	3.958	0.222	3.161	0.185	3.371	0.197
3	1.275	0.072	1.629	0.095	1.522	0.089
4	7.704	0.433	7.305	0.428	7.273	0.425
$\tau = \sum_k \tau_k$	17.81	1	17.06	1	17.10	1
$\overline{Q_{\mathrm{F}}}$	0.667		0.556		0.591	
$Q_{\mathrm{E}}/\overline{Q_{\mathrm{F}}}$	4.50		5.40		5.07	

concentration profiles at a fixed position in the column. For example, to get the temporal concentration profiles in the outlet effluent of, say, column 1, it suffices to march in time over the surface plot along the right edge of column 1 ($x = 1$); the obtained profiles are plotted in Fig. 5.3a.

The optimized 2CSMB-SEC process was implemented experimentally in a preparative prototype unit (Nestola et al., 2014). The unit was operated for five full cycles, which were more than enough to attain cyclic steady state conditions. Figure 5.3b shows the temporal profile of the UV signal measured at the outlet of column 1 over the duration of the experiment, which shows a fast attainment of the steady, periodic behavior, and also an excellent cycle-to-cycle reproducibility of the profile exhibited by the process. There is also fairly good agreement between the periodic shape of the UV profile and the predicted total concentration profile ($\sum_i c_i$) plotted in Fig 5.3a as a solid brown line, which is the information extracted from the simulation that is closest to being proportional to the UV signal. The similarity between these two profiles is a strong indication that the process behaved as expected.

The product fraction collected at each switching interval was analyzed sepa-

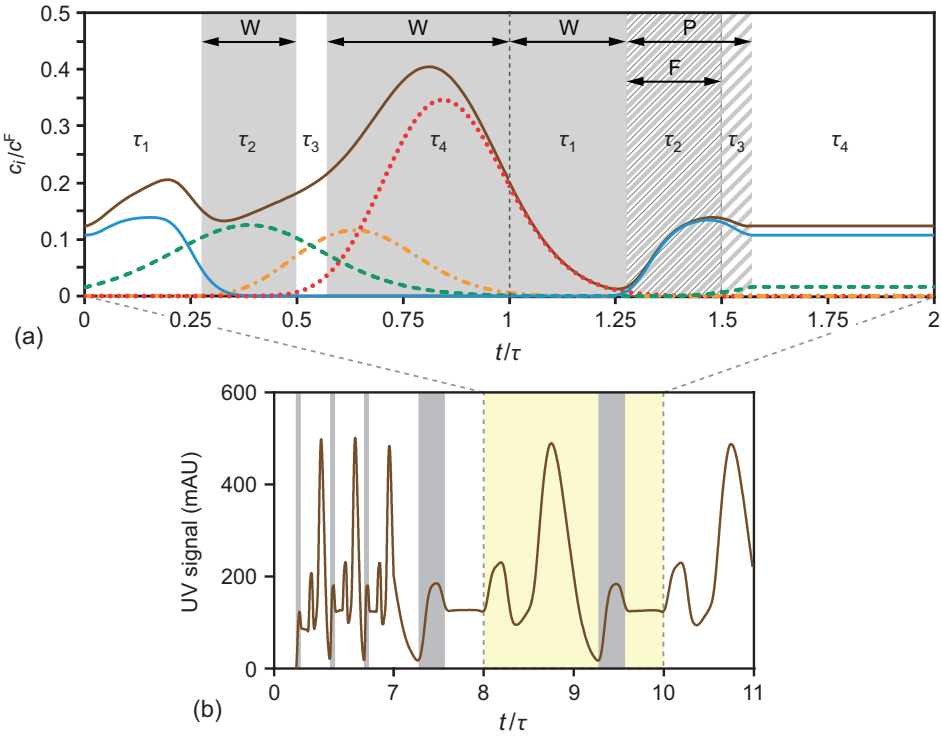

Figure 5.3: *Temporal concentration profiles in the outlet effluent of column 1. (a) Simulated profiles for a full cycle under cyclic steady state conditions; color coding: blue solid line, Ad5 product; green dashed line, group of fastest eluting impurities; dark yellow dash-dotted line, group of intermediate eluting impurities; red dotted line, group of slowest eluting impurities; brown solid line, total concentration. (b) Experimental UV signal (239 nm) measured over the first five cycles of operation; the gray strips show the time intervals for product collection from column 1; the time scale for $t/\tau < 7$ is compressed to improve the visualization of the UV signal for $t/\tau > 7$.*

rately to determine the Ad5, HCP, and DNA contents. The virus recovery yield was determined by both RT-PCR and Nanosight quantification. The following data summarize the evaluated performance of the 2CSMB-SEC process: productivity, 0.67 L/min; virus yield, 86.3%; DNA clearance, 90%; HCP clearance, 89%. It worth pointing out that the purity level required by the authorities is usually expressed as amounts of DNA and HCP per dose, which implies that an application where the therapeutic dose is very high (e.g., gene therapy) can require several purification steps, whereas for VLP or mucose vaccine fewer purification steps can be sufficient to reach the desired purity level. For this reason, in the present work the process performance is quantified in terms of clearance percentage. The performance of the 2CSMB-SEC process compares very favorably against that of the standard single-column batch SEC process with the same amount of stationary phase (Nestola et al., 2014) (productivity, 0.11 L/min, 6 times lower; virus yield, 57.4%, 34% lower; DNA clearance, 94%; HCP clearance, 94%).

5.6 Optimal robust design under parameter uncertainty

The ability of a process to handle normal process variations and parameter uncertainty is known as process robustness and it can be achieved by making the allowed range of variations in process parameters small and/or the process operating point insensitive to variations or uncertainties (Degerman et al., 2008). The procedure described below is a method to enlarge the design space in an optimal way, so that the process, when operated under conditions within the design space, fulfills the quality specifications with the least impact on productivity and solvent consumption.

It is assumed that the major process uncertainty is due to variability of the packing procedure, which influences the interparticle porosity, ϵ_o, and column volume, V_c. It is further assumed in a first instance that although these two parameters are unknown, their uncertainties are bounded by known maximum deviations, $\delta\epsilon_o$ and δV_c, from their nominal (or average) values, $\bar{\epsilon_o}$ and $\bar{V_c}$. Thus, ϵ_o and V_c can be split as follows:

$$\epsilon_o = \bar{\epsilon_o} + \epsilon'_o, \quad \epsilon'_o \in [-\delta\epsilon_o, +\delta\epsilon_o], \tag{5.13}$$

$$V_c = \bar{V_c} + V'_c, \quad V'_c \in [-\delta V_c, +\delta V_c]. \tag{5.14}$$

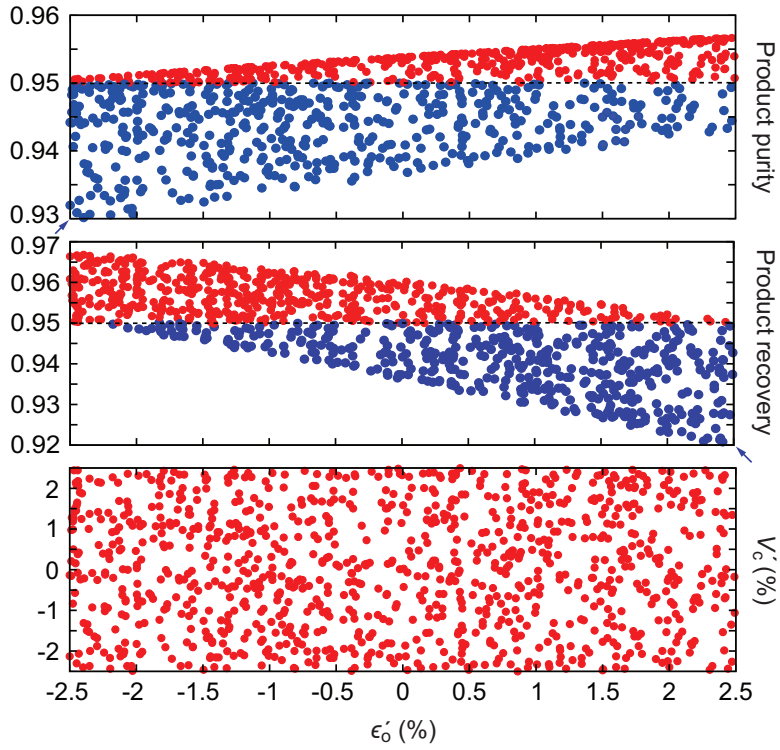

Figure 5.4: *Product purity (top) and recovery (center) for 1000 random values of* ϵ_o' *and* V_c' *(bottom) uniformly distributed in the* $[-2.5\%, +2.5\%]$ *interval for the optimal nominal values of the step durations. The blue symbols below the horizontal dashed line in each of the two top graphs represent the perturbations that do not satisfy the corresponding product quality constraint, whereas those above it meet the target. The arrows identify the points on the* (ϵ_o', V_c') *plane where the purity and recovery attain their lowest values*

where ϵ_o' and V_c' are the deviations from the nominal values, which as a first approximation are assumed to be uncorrelated, uniformly distributed random variables in the intervals given above.

The parameters ϵ_o and V_c influence the process dynamics through the products $V_i \equiv \epsilon_i V_c$ in eq. 5.1, which take a different value for each key component in the system; using eqs. 5.13 and 5.14, the V_i's can be rewritten as

$$V_i = [\bar{\epsilon_o} + \epsilon_o' + (1 - \bar{\epsilon_o} - \epsilon_o')H_i](\bar{V_c} + V_c'). \tag{5.15}$$

Figure 5.4 shows the result of randomly perturbing the values of ϵ_o and V_c over a $\pm 2.5\%$-uncertainty interval around $\bar{\epsilon_o}$ and $\bar{V_c}$ for the design values of the

step durations given in Table 5.3. As expected, when the 2CSMB-SEC process is operated with the nominal design values of the step durations, many perturbations fail to satisfy the purity or recovery constraints, or both. Figure 5.4 also shows that the lowest purity is obtained for $(\epsilon'_{\rm o}, V'_{\rm c}) = (-\delta\epsilon_{\rm o}, -\delta V_{\rm c})$ whereas the lowest recovery is obtained for $(\epsilon'_{\rm o}, V'_{\rm c}) = (+\delta\epsilon_{\rm o}, +\delta V_{\rm c})$. Moreover, it is clear that if a set of τ_k's satisfies the purity and recovery constraints for the two worst cases, it will satisfy the two constraints for all perturbations of $\epsilon_{\rm o}$ and $V_{\rm c}$ within the specified uncertainty intervals, i.e.,

$$\left.\begin{array}{c} P^{-}_{\rm Ad5} \geq P_{\rm Ad5,min} \\ \text{and} \\ R^{+}_{\rm Ad5} \geq R_{\rm Ad5,min} \end{array}\right\} \Rightarrow \left\{\begin{array}{c} P_{\rm Ad5}(\epsilon'_{\rm o}, V'_{\rm c}) \geq P_{\rm Ad5,min} \\ \text{and} \\ R_{\rm Ad5}(\epsilon'_{\rm o}, V'_{\rm c}) \geq R_{\rm Ad5,min} \end{array}\right. \quad \forall \begin{bmatrix} \epsilon'_{\rm o} \\ V'_{\rm c} \end{bmatrix} \in \begin{bmatrix} -\delta\epsilon_{\rm o}, +\delta\epsilon_{\rm o} \\ -\delta V_{\rm c}, +\delta V_{\rm c} \end{bmatrix}. \tag{5.16}$$

Here, $P^{-}_{\rm Ad5}$ and $R^{+}_{\rm Ad5}$ are shorthand notations for $P_{\rm Ad5}(-\delta\epsilon_{\rm o}, -\delta V_{\rm c})$ and $R_{\rm Ad5}(+\delta\epsilon_{\rm o}, +\delta V_{\rm c})$, respectively, and it is assumed that $\epsilon'_{\rm o}$ and $V'_{\rm c}$ are indeed perturbations, $|\epsilon'_{\rm o}| \ll \epsilon_{\rm o}$ and $|V'_{\rm c}| \ll V_{\rm c}$, and not significant changes of the nominal values. The reason why the worst cases occur at vertexes of the boundary of the uncertainty region is the monotonic dependence of the V_i's on $\epsilon_{\rm o}$ and $V_{\rm c}$:

$$\frac{\partial V_i}{\partial \epsilon_{\rm o}} = (1 - H_i)V_{\rm c} > 0 \quad \text{and} \quad \frac{\partial V_i}{\partial V_{\rm c}} = [\epsilon_{\rm o} + (1 - \epsilon_{\rm o})H_i]V_{\rm c} > 0 \quad \forall i. \tag{5.17}$$

Equation 5.16 is the basis for the robust design procedure, which can be formulated as the following nonlinear programming problem:

$$\begin{aligned} \max_{\tau_1,\ldots,\tau_4} \quad & \overline{Q_{\rm F}} \\ \text{s.t.} \quad & c^{-}_{i,j}(x,t) = g^{\rm css}(\bar{\epsilon_{\rm o}} - \delta\epsilon_{\rm o}, \bar{V_{\rm c}} - \delta V_{\rm c}; \tau_1, \ldots, \tau_4), \\ & P^{-}_{\rm Ad5} \geq P_{\rm Ad5,min}, \quad R^{-}_{\rm Ad5} \geq R_{\rm Ad5,min}. \\ & c^{+}_{i,j}(x,t) = g^{\rm css}(\bar{\epsilon_{\rm o}} + \delta\epsilon_{\rm o}, \bar{V_{\rm c}} + \delta V_{\rm c}; \tau_1, \ldots, \tau_4), \\ & P^{+}_{\rm Ad5} \geq P_{\rm Ad5,min}, \quad R^{+}_{\rm Ad5} \geq R_{\rm Ad5,min}. \end{aligned} \tag{5.18}$$

Note that whereas the nominal design procedure requires the optimization of a single instance of the CSS model of the 2CSMB-SEC unit, the robust design procedure requires the simultaneous optimization of two instances of the CSS model of the 2CSMB-SEC unit with the same step durations but different values of $\epsilon_{\rm o}$ and $V_{\rm c}$. There is thus an increase in complexity while moving from the nominal problem to its robust counterpart, because the latter works simultaneously with

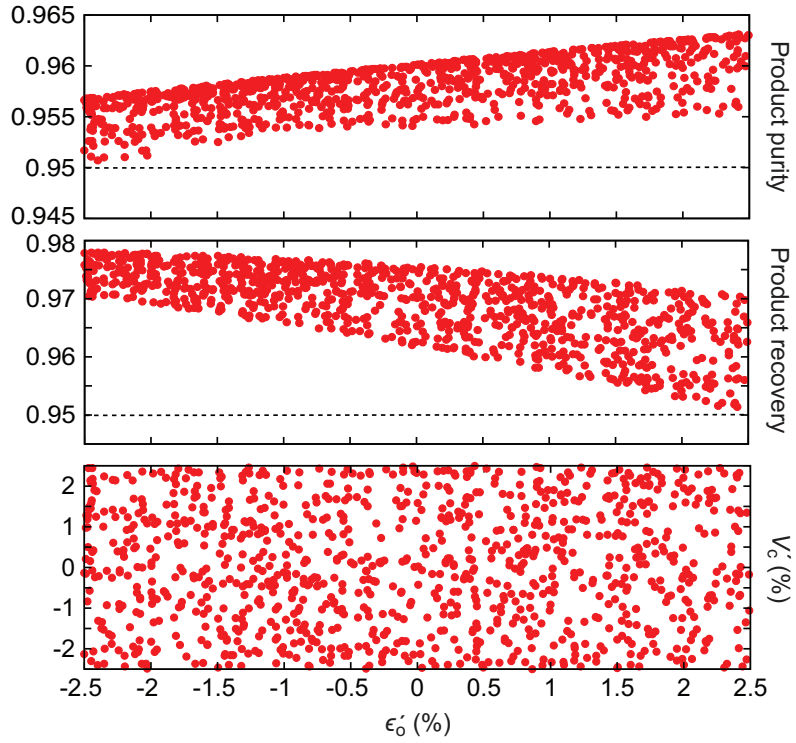

Figure 5.5: *Product purity (top) and recovery (center) for 1000 random values of* ϵ_o' *and* V_c' *(bottom) uniformly distributed in the* $[-2.5\%, +2.5\%]$ *interval for the optimal robust values of the step durations. In the two top graphs all symbols are above the horizontal dashed lines and thus satisfy both product quality constraints.*

more than one instance of the chromatographic model. However, the robust problem remains computationally tractable if the right solution approach and optimization solver are employed. It is also worth noting that in the above equation the two worst cases are forced to satisfy both quality constraints and not just the critical one as implied by eq. 5.16; this increases the robustness of the numerical procedure without introducing any computational overhead.

The solution of the robust design problem for $\delta\epsilon_o = \delta V_c = 2.5\%$ are the optimal step durations given in Table 5.3 in the column labeled 'Robust 1'. Figure 5.5 shows the result of randomly perturbing the values of ϵ_o and V_c over a $\pm 2.5\%$-uncertainty interval around $\bar{\epsilon_o}$ and $\bar{V_c}$ for the robust values of the step durations. It is seen that when the 2CSMB-SEC process is operated with the robust values of the step durations, all perturbations of ϵ_o and V_c satisfy the purity and recovery constraints. The robust solution is thus fully immunized against variability in

the values of ϵ_o and V_c, as long as they stay confined to the specified confidence intervals.

The bottom rows of Table 5.3 show that, as expected, robust operation is achieved at the expense of reducing the feed throughput and increasing the solvent consumption. This is further detailed in Fig. 5.6, which shows the influence of the size of the ϵ_o and V_c uncertainty intervals on the productivity and solvent consumption of the 2CSMB-SEC process. It is seen that the isolines of constant productivity and those of constant solvent consumtion are straight lines on the $\delta\epsilon_o \times \delta V_c$ plane. Moreover, the ratio of $\overline{Q_F}$ to its nominal value drops to 0.83, a 16.6% reduction, when the uncertainty intervals of ϵ_o and V_c increase to $\pm 2.5\%$, and that of $Q_E/\overline{Q_F}$ goes up to 1.2, a 20% increase.

This loss in separation performance, 16.6% reduction in $\overline{Q_F}$ and 20.0% increase in $Q_E/\overline{Q_F}$, is larger than what might be anticipated for an uncertainty interval of only $\pm 2.5\%$. This shows that the optimal step durations for nominal operation are not robust at all, and that the process must be operated rather conservatively to withstand even slight uncertainties in the packing quality of the columns. Nevertheless, it is worth pointing out that the robust set of step durations provided by our approach is optimal, since it is the one that yields the best performance for the specified uncertainties.

Figure 5.7 shows how the sizes of the ϵ_o and V_c uncertainty intervals influence the durations of the cycle steps. Changes in $\delta\epsilon_o$ have only a slightly impact on the step durations and nearly none on those of steps 1 and 4: for $\delta\epsilon_o = \pm 2.5\%$, the size of step 2 is reduced by 7.2%, i.e., less feed is injected into the system per cycle, and the size of step 3 is increased by 11.1% to compensate for the reduction of step 2 and thus maintain the same amount of collected product. Changes in δV_c have a larger effect on the step durations but still nearly none on step 1; for $\delta V_c = \pm 2.5\%$, the size of step 2 is reduced by 12.2% and that of step 3 is increased by 14.8%; moreover, the size of step 4 is slightly decreased (-5.2%). Overall, δV_c has a larger effect on the cycle time than $\delta\epsilon_o$.

5.6.1 Optimal process design under probabilistic uncertainty

A more realistic and less stringent way of tackling the problem of parameter uncertainty is to work with probability distributions instead of well defined uncertainty intervals. We thus assume that ϵ_o and V_c are uncorrelated, normally distributed, random variables with means $\bar{\epsilon_o}$ and $\bar{V_c}$ and standard deviations σ_ϵ and σ_V; this is the same as assuming that ϵ'_o and V'_c have zero means and standard

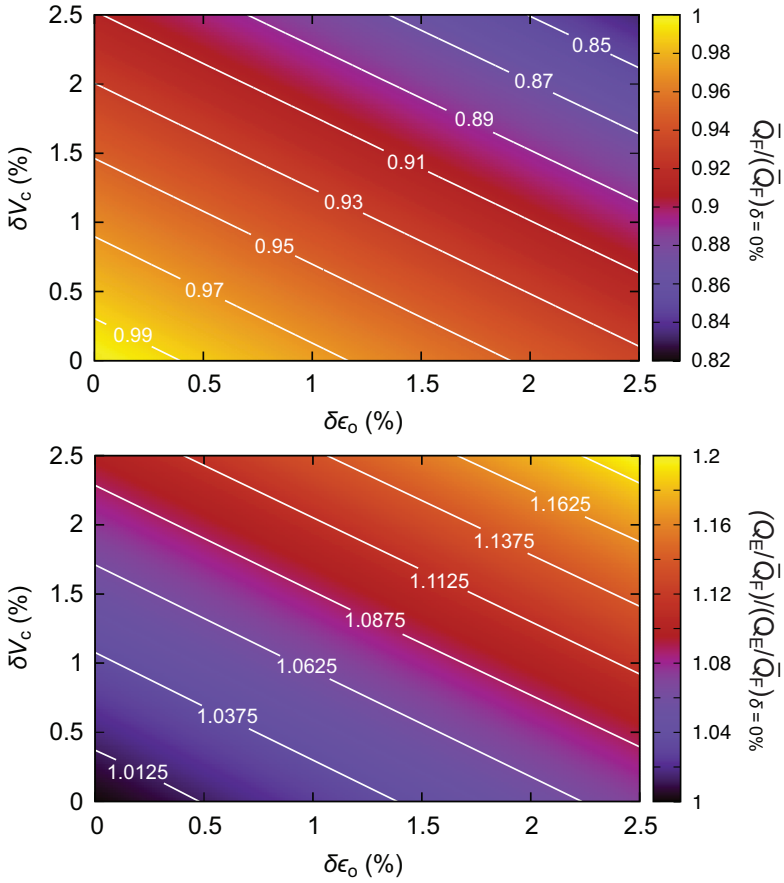

Figure 5.6: *Surface plots of relative productivity,* $\overline{Q_{\mathrm{F}}}/(\overline{Q_{\mathrm{F}}})_{\delta=0\%}$*, and relative solvent consumption,* $(Q_{\mathrm{E}}/\overline{Q_{\mathrm{F}}})/(Q_{\mathrm{E}}/\overline{Q_{\mathrm{F}}})_{\delta=0\%}$*, as a function of the size of the* ϵ_{o} *and* V_{c} *uncertainty intervals; both plotted variables are scaled by the their values for* $\delta = 0\%$*. The lines represent paths of constant productivity or solvent consumption on the* $\delta\epsilon_{\mathrm{o}} \times \delta V_{\mathrm{c}}$ *plane.*

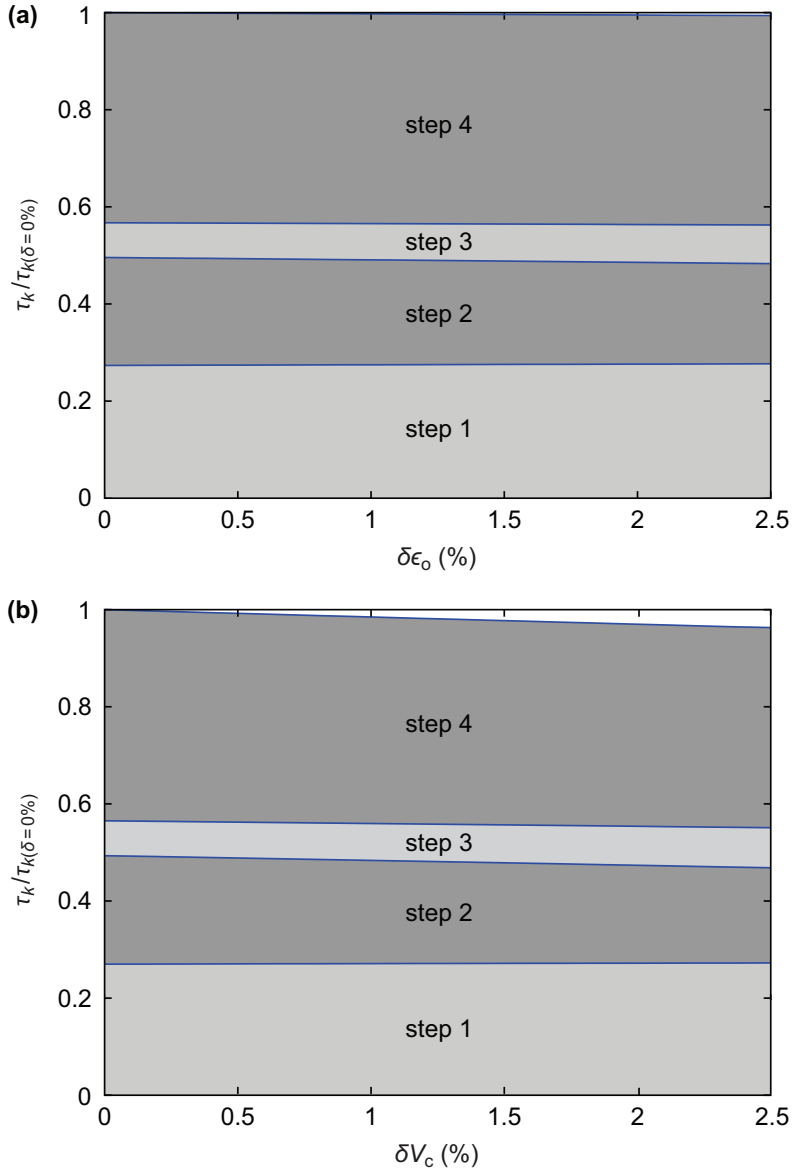

Figure 5.7: *Step durations of the 2CSMB-SEC cycle as a function of the sizes of the (a) ϵ_o and (b) V_c uncertainty intervals. The that is not varied along the horizontal axis of each plot is kept fixed at 0%.*

deviations σ_ϵ and σ_V.

To generate results that can be more or less compared to those obtained by the previous approach, we first determine the values of σ_ϵ and σ_V for which the 95% confidence intervals of $\epsilon'_{\rm o}$ and $V'_{\rm c}$ are $[-\delta\epsilon_{\rm o}, +\delta\epsilon_{\rm o}]$ and $[-\delta V_{\rm c}, +\delta V_{\rm c}]$, respectively. The values sought are

$$\sigma_\epsilon/\delta\epsilon_{\rm o} = \sigma_V/\delta V_{\rm c} = \Phi(1 - 0.95/2) = 1.9600, \tag{5.19}$$

where $\Phi(x)$ is the cumulative distribution function (CDF) of the standard normal distribution.

The problem now is to determine the optimal values of the step durations that maximize the productivity of the 2CSMB-SEC process while satisfying both the purity and recovery specifications with a given probability of success, say 95%, i.e., such that on average at most only 5 out of 100 attempts to pack the two columns at the nominal values of $\epsilon_{\rm o}$ and $V_{\rm c}$ make the 2CSMB-SEC process violate one or both product specifications.

At first glance this robust design problem appears to be much more difficult to solve than the previous approach, but in fact it is not. It suffices to find the two worst cases of process performance that lie on the boundary that delimits the set of all $(\epsilon_{\rm o}, V_{\rm c})$ pairs that have a probability of occurring of at least 95%. One of the cases is the one that yields the worst product purity whereas the other case is the one that yields the worst product recovery. These two cases are then plugged into eq. 5.16 to solve an optimization problem similar to that employed in the previous robust design procedure.

A way to determine the two worst conditions that lie on the 95%-probability boundary is described next. Suppose that many normally distributed, random values of $\epsilon'_{\rm o}$ and $V'_{\rm c}$ with zero mean and standard deviations σ_ϵ and σ_V are generated. Let N be the number of randomly generated $(\epsilon'_{\rm o}, V'_{\rm c})$ pairs. Now, 5% of those pairs are randomly discarded to generate a 95%-confidence set. For each of the remaining pairs, say the nth one, the value of parameter V_i for each key component, say $V_i^{(n)}$, is calculated. Then, the two worst cases are given by the smallest and largest values of the $V_i^{(n)}$: the former, $V_{i,\min}$, is an estimate of V_i for the conditions that yield the worst product purity, whereas the latter, $V_{i,\max}$, is an estimate of V_i for the conditions that yield the worst product purity.

An alternative and more efficient procedure is to sort the array of $V_i^{(n)}$ values in ascending order without discarding any $(\epsilon'_{\rm o}, V'_{\rm c})$ pairs. Then, $V_i^{(0.025N)}$ is an estimate of $V_{i,\min}$ because it is the largest value of the 2.5% smallest V_i's and

Table 5.4: *Minimal and maximal values of the parameters V_i for $\delta\epsilon_o = \delta V_c = 2.5\%$ (worst case interval) and those for which the 95%-confidence intervals of ϵ'_o and V'_c are $[-2.5\%, +2.5\%]$; $\overline{V}_i$ denotes the nominal value.*

	1	2	3
$\overline{V}_i$	17.55	32.36	55.31
	Worst case interval		
$V_{i,\min}$	16.68	31.28	53.91
$V_{i,\max}$	18.43	33.45	56.72
	95%-confidence interval		
$V_{i,\min}$	16.93	31.50	53.93
$V_{i,\max}$	18.17	33.21	56.69

$V_i^{(0.975N)}$ is an estimate of $V_{i,\max}$ because it is the smallest value of the 2.5% largest V_i's. Both procedures yield improved estimates of $V_{i,\min}$ and $V_{i,\max}$ by increasing the number of points, N.

The second procedure was coded in a small python script, which took less than a second to run for $N = 10^4$. The obtained values of $V_{i,\min}$ and $V_{i,\max}$ are listed and compared in Table 5.4 to the nominal values, $\overline{V}_i$, and to the values for the two worst cases of the previous robust design procedure, $(\epsilon'_o, V'_c) = (-2.5\%, -2.5\%)$ and $(\epsilon'_o, V'_c) = (+2.5\%, +2.5\%)$.

From the array of $V_i^{(n)}$ values it is also straightforward to derive the corresponding probability density functions. They are plotted in Fig. 5.8 for the three key components; the shaded areas bounded by $V_{i,\min}$ and $V_{i,\max}$ represent the 95%-confidence intervals.

It is clear that if a set of τ_k's satisfies the purity and recovery constraints for the case in which $V_i = V_{i,\min}$ and for the case in which $V_i = V_{i,\max}$, it will satisfy the two constraints for any normally distributed values of ϵ_o and V_c with a probability of success of at least 95%. If the nonlinear programming problem defined by eq. 5.18 is solved with $c^-_{i,j}(x,t) = g^{\text{css}}(V_{i,\min}; \tau_1, \ldots, \tau_4)$ and $c^+_{i,j}(x,t) = g^{\text{css}}(V_{i,\max}; \tau_1, \ldots, \tau_4)$, the optimal set of τ_k's will satisfy the two constraints for any normally distributed values of ϵ_o and V_c with a probability of success of exactly 95% while maximizing the feed throughput.

Figure 5.9 shows the result of randomly perturbing 1000 times the values of ϵ_o and V_c according to the normal distributions (bottom graph); the top two graphs

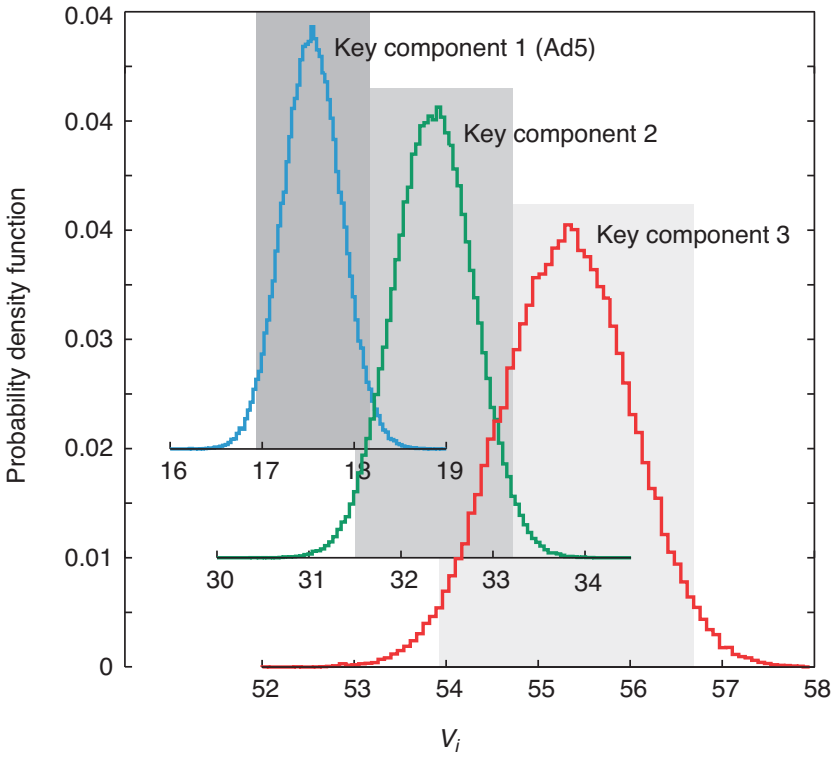

Figure 5.8: *Probability distribution function of* $V_i = [\epsilon_o + (1 - \epsilon_o)H_i]V_c$ *for each of the three key components when* ϵ_o *and* V_c *are uncorrelated, normally distributed, random variables with means* $\bar{\epsilon_o}$ *and* $\bar{V_c}$ *and standard variations* $\sigma_\epsilon = 1.96\delta\epsilon_o$ *and* $\sigma_V = 1.96\delta V_c$*, where* $\delta\epsilon_o$ *is 2.5% of* $\bar{\epsilon_o}$ *and* δV_c *is 2.5% of* $\bar{V_c}$*. The shaded areas represent the 95%-confidence intervals.*

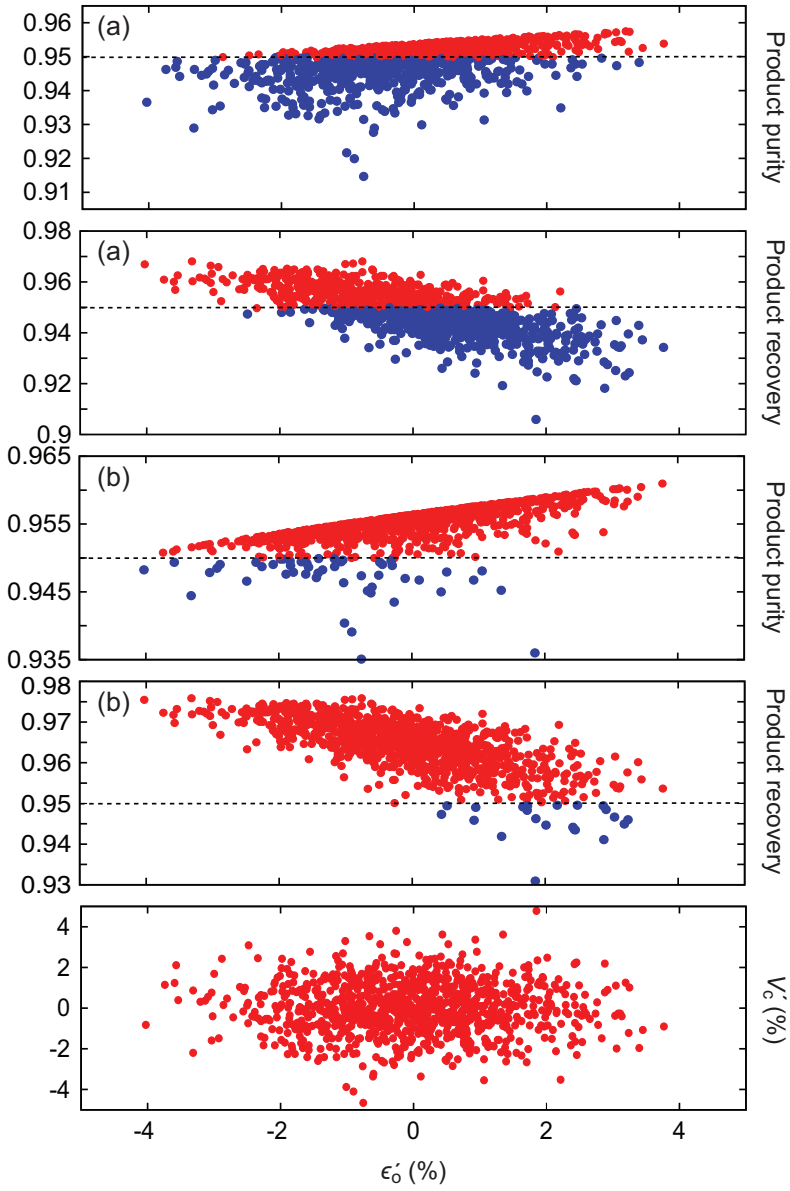

Figure 5.9: *Product purity and recovery for 1000 normally distributed random values of* ϵ_o *and* V_c *with means* $\bar{\epsilon_o}$ *and* $\bar{V_c}$ *and standard variations* $\sigma_\epsilon = 1.96\delta\epsilon_o$ *and* $\sigma_V = 1.96\delta V_c$*, where* $\delta\epsilon_o$ *is 2.5% of* $\bar{\epsilon_o}$ *and* δV_c *is 2.5% of* $\bar{V_c}$*. Results obtained for the (a) nominal and (b) robust design values of the step durations.*

show the purity and recovery values obtained for the nominal design values of the step durations, whereas the other two graphs were obtained for the robust design values of the step durations. As expected, when the 2CSMB-SEC process is operated with the nominal design values of the step durations, many perturbations fail to satisfy the purity or recovery constraints, or both. However, when the unit is operated with the robust values of the step durations, most of the perturbations of ϵ_o and V_c satisfy the purity and recovery constraints; in fact, only 5% of the perturbations fail to satisfy both quality constraints, which is exactly what was intended.

5.7 Conclusions

A general procedure for robust design of the 2CSMB-SEC process under parameter uncertainty was proposed under the framework of rigorous optimization theory. The optimal values of the operating variables are chosen only among candidates that are robust feasible, that is, that remain feasible for all possible variations of the uncertain parameters within their uncertainty intervals. Computational tractability is ensured by formulating the robust optimization problem with only the vertexes of the uncertainty domain that most adversely affect the product purity and recovery. In practice the nominal design problem is replaced by a worst-case design problem. The procedure was successfully employed to find the optimal robust values of the step durations when both the interparticle porosity and column volume are subject to two types of uncertainties. In one case ϵ_o and V_c are uncorrelated, uniformly distributed random variables, whereas in the other case ϵ_o and V_c are normally distributed random variables. Moreover, in the second case the 2CSMB-SEC operating conditions were optimized to yield a given probability of success of satisfying both product quality specifications, say 95%, so that on average at least 95 out of 100 attempts to pack the two columns yield purified batches in which the product is within the specifications—this is achieved while maximizing the feed throughput.

Acknowledgments

Financial support from Sartorius Stedim Biotech and from the Portuguese Science Foundation (FCT-MCTES) (SFRH/BD/82032/2011 and PTDC/EBB-BIO/119501/2010) is gratefully acknowledged. The authors do not have any conflicts of interest.

References

Araújo, J. M., Rodrigues, R. C., Eusébio, M. F., and Mota, J. P. (2010). Chiral separation by two-column, semi-continuous, open-loop simulated moving-bed chromatography. *J Chromatogr A*, *1217*, 5407–5419.

Araújo, J. M., Rodrigues, R. C., and Mota, J. P. (2006). Use of single-column models for efficient computation of the periodic state of a simulated moving-bed process. *Ind Eng Chem Res*, *45*, 5314–5325.

Aumann, L., and Morbidelli, M. (2007). A continuous multicolumn countercurrent solvent gradient purification (MCSGP) process. *Biotechnol Bioeng*, *98*, 1043–1055.

Ben-Tal, A., and Nemirovski, A. (2002). Robust optimization–methodology and applications. *Math Program*, *92*, 453–480.

Blanche, F., Cameron, B., Barbot, A., Ferrero, L., Guillemin, T., Guyot, S., Somarriba, S., and Bisch, D. (2000). An improved anion-exchange HPLC method for the detection and purification of adenoviral particles. *Gene Ther*, *7*, 1055–1062.

Borg, N., Westerberg, K., Andersson, N., von Lieres, E., and Nilsson, B. (2013). Effects of uncertainties in experimental conditions on the estimation of adsorption model parameters in preparative chromatography. *Comput Chem Eng*, *55*, 148–157.

Degerman, M., Jakobsson, N., and Nilsson, B. (2008). Designing robust preparative purification processes with high performance. *Chem Eng Technol*, *31*, 875–882.

Degerman, M., Westerberg, K., and Nilsson, B. (2009). A model-based approach to determine the design space of preparative chromatography. *Chem Eng Sci*, *32*, 1195–1202.

Dormond, E., Chahal, P., Bernier, A., Tran, R., Perrier, M., and Kamen, A. (2010). An efficient process for the purification of helper-dependent adenoviral vector and removal of helper virus by iodixanol ultracentrifugation. *J Virol Methods*, *165*, 83–89.

Eglon, M. N., Duffy, A. M., O'Brien, T., and Strappe, P. M. (2009). Purification of adenoviral vectors by combined anion exchange and gel filtration chromatography. *J Gene Med*, *11*, 978–989.

FDA (2004). *Guidance for Industry PAT – A Framework for Innovative Pharmaceutical Manufacturing and Quality Insurance,*. Technical Report US Departmenet of Health and Human Services, Rockville, MA,.

Gétaz, D., Butté, A., and Morbidelli, M. (2013). Model-based design space determination of peptide chromatographic purification processes. *J Chromatogr A*, *1284*, 80–87.

Godawat, R., Brower, K., Jain, S., Konstantinov, K., Riske, F., and Warikoo, V. (2012). Periodic counter-current chromatography - design and operational considerations for integrated and continuous purification of proteins. *Biotechnol J*, *7*, 1496–1508.

Grossmann, I., and Sargent, R. (1978). Optimum design of chemical plants with uncertain parameters. *AIChE J*, *24*, 1021–1028.

Gupta, A. (2000). *WSMP: Watson Sparse Matrix Package*. Technical Report IBM Research Report RC.

Halemane, K. P., and Grossmann, I. E. (1983). Optimal process design under uncertainty. *AIChE J*, *29*, 425–433.

Huyghe, B. G., Liu, X., Sutjipto, S., Sugarman, B. J., Horn, M. T., Shepard, H. M., Scandella, C. J., and Shabram, P. (1995). Purification of a type 5 recombinant adenovirus encoding human p53 by column chromatography. *Hum Gene Ther*, *6*, 1403–1416.

ICH (2005). *ICH Harmonized Tripartite Guideline: Quality Risk Management Q9,*. Technical Report International Conference on Harmonisation of Technical Requirements for Registration of Pharmaceuticals for Human Use (ICH), Geneva.

ICH (2007). *Draft Consensus Guideline: Pharmaceutical Development Annex to Q8, ..* Technical Report International Conference on Harmonisation of Technical Requirements for Registration of Pharmaceuticals for Human Use (ICH), Geneva.

ICH (2009). *ICH Harmonized Tripartite Guideline: Pharmaceutical Development Q8, Rev. 2,*. Technical Report International Conference on Harmonisation of Technical Requirements for Registration of Pharmaceuticals for Human Use (ICH), Geneva, 2009.

Jakobsson, N., Degerman, M., and Nilsson, B. (2005). Optimisation and robustness analysis of a hydrophobic interaction chromatography step. *J Chromatogr A*, *1099*, 157–166.

Jakobsson, N., Degerman, M., Stenborg, E., and Nilsson, B. (2007). Model based robustness analysis of an ion-exchange chromatography step. *J Chromatogr A*, *1138*, 109–119.

Kalbfuss, B., Flockerzi, D., Seidel-Morgenstern, A., and Reichl, U. (2008). Size-exclusion chromatography as a linear transfer system: Purification of human influenza virus as an example. *J Chromatogr B*, *873*, 102–112.

Kalbfuss, B., Wolff, M., Morenweiser, R., and Reichl, U. (2007). Purification of cell culture-derived human influenza a virus by size-exclusion and anion-exchange chromatography. *Biotechnol Bioeng*, *96*, 932–944.

Kamen, A., and Henry, O. (2004). Development and optimization of an adenovirus production process. *J Gene Med*, *6*, S184–S192.

Krättli, M., Müller-Späth, T., and Morbidelli, M. (2013). multifraction separation in countercurrent chromatography (mcsgp). *Biotechnol Bioeng*, *110*, 2436–2444.

Kröber, T., Wolff, M., Hundt, B., Seidel-Morgenstern, A., and Reichl, U. (2013). Continuous purification of influenza virus using simulated moving bed chromatography. *J Chromatogr A*, *1307*, 99–110.

Lee, D.-S., Kim, B.-M., and Seol, D.-W. (2009). Improved purification of recombinant adenoviral vector by metal affinity membrane chromatography. *Biochem Biophys Res Commun*, *378*, 640–644.

L.T. Biegler, A. W., I.E. Grossmann (1997). *Systematic Methods of Chemical Process Design. Chap. 21*. NJ: Prentice Hall.

Mota, J. P., and Araújo, J. M. (2005). Single-column simulated-moving-bed process with recycle lag. *AIChE J*, *51*, 1641–1653.

Mota, J. P., Araújo, J. M., Rodrigues, R. et al. (2007). Optimal design of simulated moving-bed processes under flow rate uncertainty. *AIChE J*, *53*, 2630–2642.

Mun, S., Xie, Y., and Wang, N.-H. L. (2003). Robust pinched-wave design of a size-exclusion simulated moving-bed process for insulin purification. *Ind Eng Chem Res*, *42*, 3129–3143.

Nestola, P., Silva, R. J., Peixoto, C., Alves, P. M., Carrondo, M. J., and Mota, J. P. (2014). Adenovirus purification by two-column, size-exclusion, simulated countercurrent chromatography. *J Chromatogr A*, *1347*, 111–121.

Peixoto, C., Sousa, M. F. Q., Silva, A. C., Carrondo, M. J. T., and Alves, P. M. (2007). Downstream processing of triple layered rotavirus like particles. *J Biotechnol*, *127*, 452–461.

R. Fourer, B. K., D.M. Gay (2003). *AMPL: A Modeling Language for Mathematical Programming*. Brooks/Cole Publishing Co.

R.J.S., S. (2013). *Compact Simulated Countercurrent Chromatography for Downstream Processing of (bio)Pharmaceuticals,*. Ph.D. thesis Universidade Nova de Lisboa.

Rodrigues, R. C., Silva, R. J., and Mota, J. P. (2010). Streamlined, two-column, simulated countercurrent chromatography for binary separation. *J Chromatogr A*, *1217*, 3382–3391.

Rodrigues, R. C. R., Canhoto, T. J. S. B., Araújo, J. M. M., and Mota, J. P. B. (2008). Two-column simulated moving-bed process for binary separation. *J Chromatogr A*, *1180*, 42–52.

Rodrigues, T., Carvalho, A., Carmo, M., Carrondo, M. J. T., Alves, P. M., and Cruz, P. E. (2007). Scaleable purification process for gene therapy retroviral vectors. *J Gene Med*, *9*, 233–243.

Segura, M. M., Alba, R., Bosch, A., and Chillón, M. (2008). Advances in helper-dependent adenoviral vector research. *Curr Gene Ther*, *8*, 222–235.

Silva, R. J., Rodrigues, R. C., Osuna-Sanchez, H., Bailly, M., Valéry, E., and Mota, J. P. (2010). A new multicolumn, open-loop process for center-cut separation by solvent-gradient chromatography. *J Chromatogr A*, *1217*, 8257–8269.

Silva, R. J. S., Rodrigues, R. C. R., and Mota, J. P. B. (2012). Relay simulated moving bed chromatography: Concept and design criteria. *J Chromatogr A*, *1260*, 132–142.

Wächter, A., and Biegler, L. T. (2006). On the implementation of an interior-point filter line-search algorithm for large-scale nonlinear programming. *Math Program*, *106*, 25–57.

Warikoo, V., Godawat, R., Brower, K., Jain, S., Cummings, D., Simons, E., Johnson, T., Walther, J., Yu, M., Wright, B., McLarty, J., Karey, K. P., Hwang, C., Zhou, W., Riske, F., and Konstantinov, K. (2012). Integrated continuous production of recombinant therapeutic proteins. *Biotechnol Bioeng*, *109*, 3018–3029.

Westerberg, K., Borg, N., Andersson, N., and Nilsson, B. (2012). Supporting design and control of a reversed-phase chromatography step by mechanistic modeling. *Chem Eng Technol*, *35*, 169–175.

Westerberg, K., Broberg-Hansen, E., Sejergaard, L., and Nilsson, B. (2013). Model-based risk analysis of coupled process steps. *Biotechnol. Bioeng.*, *110*, 2462–2470.

CHAPTER 6

Rational development of flowthrough purification strategies for viruses and VLP

Adapted from: **Nestola P**, Peixoto C, Villain L, Alves PM, Carrondo MJT, Mota JPB. Rational development of flowthrough purification strategies for viruses and VLP *In preparation.*

Abstract

Purification of complex biopharmaceuticals, such as recombinant proteins, antibodies or vaccines, is gaining increasing importance in order to fulfill the requirements for a reliable production process with high purity and yield, and, also importantly, cost efficiency. The downstream train of biopharmaceuticals has been extensively developed in the past years by combining different chromatography steps, namely ion-exchange and size-exclusion chromatography (and less frequently affinity chromatography), intermingled with concentration and ultra/diafiltration steps. Currently,purification of viruses and VLP by using IEX is typically operated in positive (bind-elute) mode: most of the impurities are collected in the flow-through pool, while the virus particles and some of the impurities are retained in the matrix. Nevertheless, recently new bead based resin has been developed by for intermediate and polishing in flow-through mode. In the present work a rational design of a flowthrough process was implemented by employing SPR as scale down tool to evaluate the ligands of two recently launched chromatography matrices: STIC membrane and Capto Core. The full process development showed that the DNA clearance achieved is roughly 4 logs reduction. Also, adenovirus recovery is boosted, especially in the first chromatographic unit operation (STIC membranes) where summing up the virus in FT and the virus eluted the recovery is close to 100%. As for HCP reduction is 5 logs, however while most of the DNA clearance is achieved in the STIC membrane, the HCP reduction is mainly achieved by using the Capto Core 700. Overall the flowthrough process designed is suitable for a platform concept and was implemented for adenovirus and retro-VLP purification with minimal amount of optimization required.

Keywords:flow-through purification, Surface plasmon resonance, ligand screening, adenovirus, virus-like-particle.

6.1 Introduction

Viral vectors are playing an increasingly important role in the vaccine and gene therapy fields. Adenoviruses (Ads), in particular, are considered one of the most suitable platforms for production of viral vaccines and gene therapy vectors; they are medium-sized (90–100 nm), nonenveloped, icosahedral viruses composed of a nucleocapsid and linear, non-segmented double stranded (ds) DNA genome that is about 36 kb long. Their broad tissue tropism and large transgene packing capacity make them attractive candidates for innovative virotherapies (Eglon et al., 2009). Adenoviruses can be produced in a complementary cell line in both adherent and suspension culture systems, such as HEK-293 or PER-C6 cells, or A549 for oncolytic therapies (Segura et al., 2008; Kamen and Henry, 2004). Recently the development of virus-like particle (VLP) for vaccine applications is gaining attention (Kushnir et al., 2012; Roldão et al., 2010). VLPs are non-infective and non-replicating, since they are essentially devoid of infectious genetic material. VLPs display antigenic epitopes in the correct conformation and in a highly repetitive manner, leading to cross-linking of B cell immunoglobulin receptors and B cell activation. The lack of DNA makes this biopharmaceutical safer compared to Adenovirus. Currently, both adenovirus and VLP are very important platforms fo vaccine development in several applications (Lua et al., 2013; Tatsis and Ertl, 2004) .

Purification of complex biopharmaceuticals, such as recombinant proteins, antibodies or vaccines, is gaining increasing importance in order to fulfill the requirements for a reliable production process with high purity and yield, and, also importantly, cost efficiency (Wang et al., 2009). The downstream train of biopharmaceuticals has been extensively developed in the past years by combining different chromatography steps, namely ion-exchange and size-exclusion chromatography (and less frequently affinity chromatography), intermingled with concentration and ultra/diafiltration steps (Eglon et al., 2009; Konz et al., 2005a,b; Burova and Ioffe, 2005; Peixoto et al., 2006; Goerke et al., 2005). Chromatography is a well-established purification tool of recombinant adenovirus used for vaccine and gene therapy. Indeed, ion exchange (IEX) is the most used technique for purication of complex biopharmaceuticals. However, packed-bed chromatography suffers from a number of disadvantages: the pressure drop across the bed is usually high and may increase during operation due to media deformation or blockage; pore diffusion is slow and often leads to degradation of the protein product; also, the scale up of packed beds is difficult. In addition, packed beds display a

low dynamic binding capacity for virus particles at common process-scale linear velocities of 150–450 cm/h, because binding is restricted to the surface of resin particles.

Convective chromatography media, such as membranes and monoliths, offer substantial improvements in capacity, recovery, and reduction of process time (Hahn et al., 2007). To date, monoliths have generally offered higher capacity and higher resolution (Gerster et al., 2013; Whitfield et al., 2009), but membranes have proven less prone to clogging, and their relatively low cost has made it practical to discard them after a single use rather than invest additional resources developing and validating regeneration and sanitization procedures.

Currently,purification of viruses and VLP by using IEX is typically operated in positive (bind-elute) mode: most of the impurities are collected in the flow-through pool, while the virus particles and some of the impurities are retained in the matrix. Due to the differences in charge of the different components, it is possible to use this process with high resolution elution gradients, separating the adsorbed materials into fractionated cuts, even though they are closely related. Nevertheless, recently new bead based resin has been developed by for intermediate and polishing in flow-through mode. Iyer et al. (2011) proposed the increased of the beads mean diameter maximizing the binding capacity for the impurities and reducing the surface available for virus binding. GE healthcare recently launched Capto Core 700, a resin composed by an activated core functionalized with octylamine ligand, and an inactivated ligand shell excluding larger molecules entering the core thus collecting them in the flow-through. Each core of the beads present a multimodal biding allowing to operate at various range of pH and NaCl concentrations.

Negative mode purification, with membrane chromatography is used almost exclusively in mAb industry (Zhou and Tressel, 2006; Knudsen et al., 2001; Boi, 2007). Anionic exchange membranes are utilized to bind impurities such as viruses, host cell proteins, and DNA, while allowing the mAb to flow through. Usually the feed pH is greater than 7.0 and the ionic strength is low, as high ionic strength can disrupt the electrostatic interactions and reduce the removal of contaminants. However, new chromatography membranes are being developed mainly to overcome to drawabacks of the Q ligand where the binding is compromised to high salt concentrations. Therefore new ligands based on primary amine have been investigated. STIC® chromatography membrane (Sartorius Stedim Biotech) and CromaSorb (Merck Millipore) are two examples commercially available products based on primary amine ligands. Nevertheless a limited number of works are

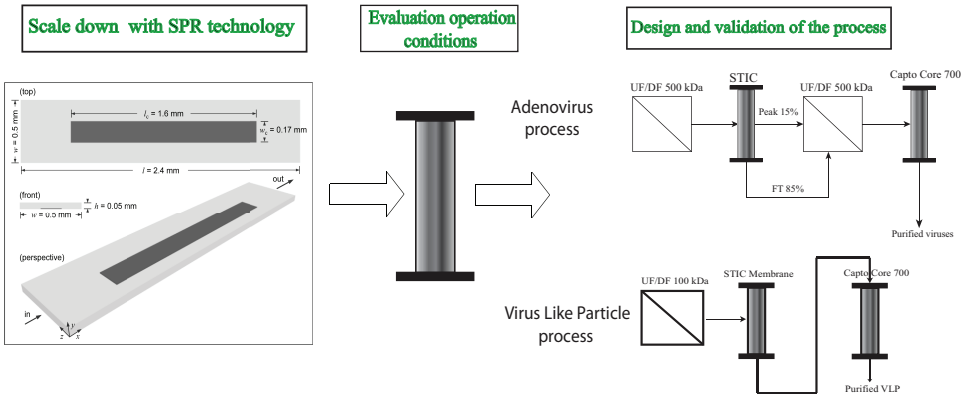

Figure 6.1: *Design strategy employed in the optimization of a platform flowthrough process. PAA and Octylamine were evaluated in respect their ability to bind DNA by using SPR technique. The results were confirmed and the operation conditions were evaluated by using STIC membrane and Capto Core 700 beads. With the constrains indentified, the FT process was designed and experimental validated by using adenovirus and retro VLP.*

present in the literature investigating the performances of these novel chromatographic membranes (Woo et al., 2011; Kang et al., 2012). Yet, no attempts are reported using membrane chromatography in flow-through mode for virus purification. Also it is known that multivalent ions (e.g phosphate, citrate) strongly bind onto polyallylamin (HOLMES-FARLEY et al., 1999), therefore one goal of this study is to evaluate how far such buffers can modulate the binding of both contaminants and target virus on the membrane, thus achieving high selectivity in FT mode.

In the present work a rational design of a flowthrough process was implemented as shown in figure 6.1. SPR was employed to evaluated the ligands of the STIC membrane and Capto Core.

Surface Plasmon Resonance (SPR) is a powerful technique to measure biomolecular interactions in real-time in a label free environment(Majka and Speck, 2007; Jason-Moller et al., 2006). While one of the interactants is immobilized to the sensor surface, the other are free in solution and passed over the surface. Association and dissociation is measured in arbitrary units and displayed in a graph called the sensorgram. As described by Vicente et al (Vicente et al., 2010) SPR techniques can be used for downstream bioprocess development as scale down tool of chromatography column. Although some physical characteristics of the purification bed cannot be mimic by SPR chip some early screening, for instance, immobilization chemistries, buffer properties and washing procedure might be

rapidly evaluated by using a small sample volumes (Thillaivinayagalingam et al., 2010). The design space predicted by SPR experiments were then confirmed by using a small scale device for the STIC membrane and packed column for Captocore resin under various buffer type and concentration.Virus recovery yield, DNA and Host cell protein clearance were assessed. Furthermore, dinamic binding capacity for DNA under various NaCl concentrations were determined for both system. Lastly, the data from the batch experiments were used in order to design a platform flowthrough process for adenovirus and retro-VLP.

6.2 Material and Methods

6.2.1 Cell line and medium

For adenovirus production two hundred and ninety-three (293) cells purchased from ATCC (ATCC-CRL-1573) were adapted to suspension and grown in a commercial serum-free medium, Ex-Cell 293 (SAFC Biosciences, USA), supplemented with 4 mM of glutamine (Invitrogen, UK), in a humidified atmosphere of 8% CO_2 in air at 37°C using shake flasks (Corning, USA). The cells were routinely propagated twice a week using an inoculum of 0.5×10^6 cells/mL. Cell concentration and viability were determined by counting cells on a Fuchs-Rosenthal haemocytometer (Brand, Germany) using the trypan blue (Invitrogen, UK) dye exclusion method.

For retro-VLP production 293 Ceb25 cells were cultured in Dulbeccos modied Eagle medium (Gibco, Life Technologies, Paisley, UK) supplemented with 10% (v/v) fetal bovine serum (FBS) (Gibco), maintained at 37°C in a humied atmosphere containing 7% CO_2. Cells were amplified to twenty 175 cm^2 flasks with a split ratio dilution of 1:5.

6.2.2 Virus production

We used a replication-defective adenovirus derived from serotype 5 adenovirus (Ad5) expressing GFP protein. The viruses were produced in a 2 L bioreactor with 1 L working volume (Sartorius-Stedim Biotech, Germany). The agitation rate was set at 70 rpm and the dissolved oxygen was controlled at 50% air saturation by gas mixing and stirred cascade control with an airflow of 0.01 L/min; the pH was controlled at 7.2 by aeration with a gaseous CO_2 mixture and 1 M $NaHCO_3$; all infections were done at a cell concentration (CCI) of 10^6 cells/mL using a multiplicity of infection (MOI) of 5; the adenoviruses were harvested at 48 hpi

(hours post-infection). The amount of infections particples (IP) in the bulk (before clarification) was in the range 10^9–10^{10} IP/mL.

VLP are constitutively expressed and contrarily with the adenovirus no lytic infection is required. After 3 days with cells 80% confluent, 10 hyperflasks were inoculated with a dilution split ratio of 1:5 (2 T175 flasks, 20 mL of cell suspension + 540 mL DMEM per Hyperflask). DMEM without phenol red (Gibco, Life Technologies, Paisley, UK), supplemented with 10% (v/v) FBS and 4 mM L-glutamine (Gibco) was used as culture media. When the cells reached 90% confluence a media exchange was performed with DMEM without phenol red (Gibco, Life Technologies, Paisley, UK) and FBS. The T-flasks were harvested 3 days later. Since the production of retro-VLP is not trivial at all, sucrose cushion was performed and TEM analysis carried out to ensure the presence of VLP (Figure 6.2). The production titer was 5x10^9 VLP particle/ml.

6.2.3 Transmission Electron microscopy (TEM)- Negative staining

The sample suspensions have been shaken gently, approx. 10 μL drops retrieved and placed on clean parafilm sheets. Formvar- and carbon-coated positively glow-discharge treated grids were incubated on the top of the suspension droplets for 10 minutes and subsequently blotted dry with a filter paper. After this, each sample was negative stained with 2% aqueous phosphotungstic acid (pH 7.2) for 1 minute using the droplet technique and air-dried for at least 30 minutes. The samples were examined in a LEO912AB electron microscope (Zeiss, Oberkochen/Germany) operating at 100 kV, equipped with a side-mounted CCD-camera capable to record images with 2kx2k pixels. The documentation and calibrated measurements of the observed structures were done with the iTEM-software, Ver. 5.2 (Olympus Soft Imaging Solutions GmbH, Muenster/Germany).

6.2.4 Clarification and concentration

Upon harvesting, the adenovirus bioreaction bulk was supplemented with 0.1% Triton X100 (Sigma Aldrich,USA) and incubated for 2 hours at 37°C with 50 U/ml of Benzonase (Merck Millipore, Germany) to digest the DNA and to release the adenoviral vectors from the intracellular material by cell lysis.

Subsequently, the bulk was microfiltrated using a Sartopore 2 membrane capsule (Sartorius Stedim Biotech, Germany) comprising a 0.8 μm prefilter and a 0.45 μm filter, and concentrated up to 10 times and diafiltered up to 5 times with

(A)

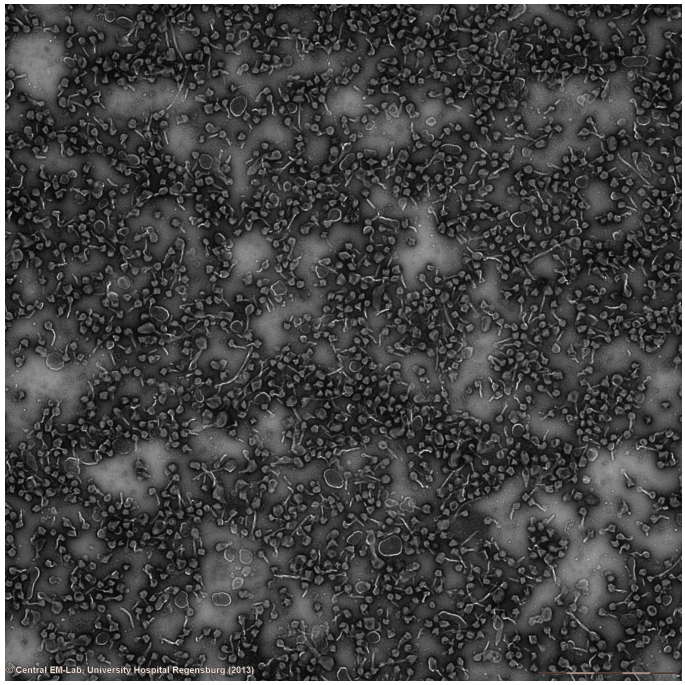

(B)

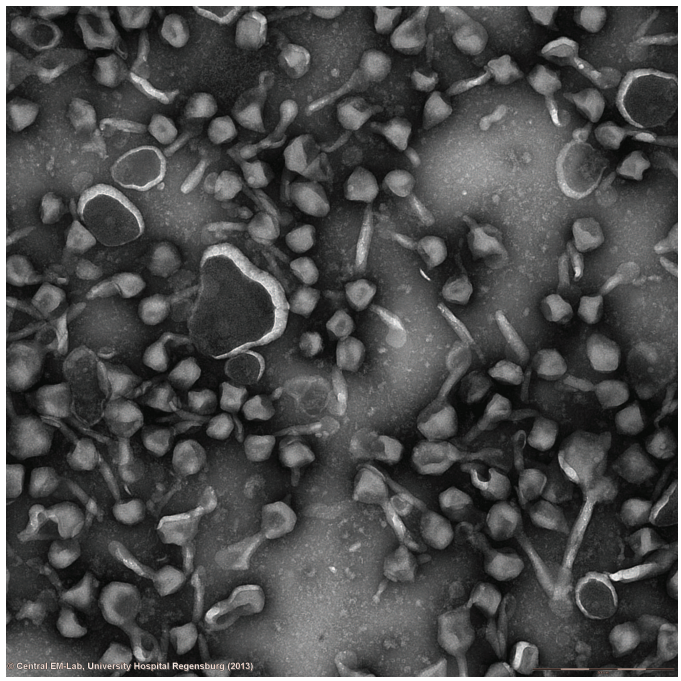

Figure 6.2: *TEM analysis of retro-VLPs at two different magnifications 5µm (Figure A) and 500 nm (Figure B.) An omogeneuous population of VLP can be observed with irregular shapes originated by the budding process.*

20 mM Tris saline buffer (Tris Buffered Saline, Sigma Aldrich, USA) at pH 8 on a Sartorius Stedim Biotech cassette prototype with cut-off of 500 kDa selected after an accurate evaluation and published by Nestola P (2014) Before use, the capsules were thoroughly washed with one capsule volume of Milli Q water and two capsule volumes of buffer.

VLP bulk contrarily of the adenovirus bulk was not treated with Triton X100 as the release of VLP occurs by budding. The bulk was microfiltrated with a 0.45μm Stericup filter (Merck Millipore, Germany). Ultrafiltration and diafiltration were performed with Viva flow 100kDa (Sartorius Stedim Biotech). Both adenovirus and VLP bulks, were stored in aliquots at $-80°$C until further use.

6.2.5 Chromatography

One XK 16/20 chromatographic columns (i.d. of 1.6 cm, maximum bed height of 20 cm) were slurry packed with Capto Core 700 (Ge) resin according to the manufacturer's specifications. The excess ethanol supplied with Capto Core 700 (CC700) was decanted and replaced with working buffer (20 mM Tris, 150 mM NaCl, pH 8) before packing into the column. The column was initially filled with 70% slurry of CC700 and allowed to settle by gravity overnight. Flow rate was increased step wise up to packing velocity of 300 cm/h. The final bed volume resulting of the packing was 7mL. After each experiments the column was thoroughly regenerate with 1M NaOH.

Membrane volume for the STIC ® device (VivaPure) was of 0.023 mL allowing fast processing time, and cost efficiency screening at various conditions. The device was connected to an Akta 10 system. Loading was performed at a constant linear velocity of 212 cm/h. Linear gradient of 20 CV was applied for eluting the product. Elution buffer was either Phosphate 1M or Citrate 1M. This high concentration of elution buffers were chosen in order to completely strip the membrane assessing the percentage of virus recovered. Membrane devices were not regenerated at the end of chromatography run, therefore a new membrane was used for each experiments. Fraction were collected every 0.5 mL and stored at $-80°$C until further analysis.

DNA dynamic binding capacity was evaluated by using DNA salmon sperm (Invitrogen) at the concentration of 0.05 mg/mL. In order to be similar to the process conditions, DNA was treated with 50 U/ml of Denerase (Sartorius Stedim Biotech).

6.2.6 Analytics

The protocol for the quantification of total viral particles was a two-step procedure: DNA extraction according to the instructions on the "High Pure Viral Nucleic Acid Kit" (Roche) manual and real-time PCR. The number of viral DNA copies was determined by real-time PCR and LightCycler system (Roche Diagnostics) using a Fast Start DNA master SYBR Green I kit to track a specific Ad5 sequence (Roche Diagnostics). Internal plasmid of $4.15 \times 10^9/2\mu l$ was chosen as reference standard. The total particle concentrations were confirmed using Nanosight NS500 (NanoSight Ltd, UK), and the size distribution was determined. The average of the two measurements was the value chosen for assessing the virus recovery yield.

The amount of host cell proteins (HCP) was determined using a commercial available ELISA kit for HEK293 cell line (Cygnus Technologies, Inc.). The sample was diluted in PBS and the assay was performed according to the manufacture protocol, the 96 well plate was read by an absorbance microplate reader at 450/650 nm (SpectraMax 340). DNA was quantified by QuanT-iT Picogreen kit (Invitrogen). After 5 minutes of incubation, the fluorescence was measured by Luminometery (Turner BioSystems). Purified DNA was used as standard.

6.2.7 Hg Instruction Porosimetry (MIP)

MIP experiments were performed on a Micromeritics AutoPore IV instruments which operate in the range of 0.2 to 60000 psia, with incremental pressure increase of 0.05 psia. The PSD was determined using a surface tension of 480 dynes/cm. The contact angle was experimental determined to be 140 degrees.

6.2.8 Sensor Chip

Biacore gold sensor chips (CM5) was purchased from Biacore/GE Healthcare,Sweden. Polyallyalime (PAA) with a size of 17kDa and Octylamine (99%) purity grade solution were purchased from SigmaAldrich, Germany. Both compounds were functionalized on two different sensor chips acting respectively anionic exchanger and multimodal ligands. Freshly prepared solutions of 0.4 M 1-ethyl-3-(3-dimethylaminopropyl)carbodiimide hydrochloride (EDC) and 1.0 M N-hydroxysuccinimide (NHS) (amine coupling kit from Biacore/GE Healthcare) in water were mixed 1:1 and injected in a pulse of 200μL at 20 μL/min to activate the terminal carboxyl group for amide bond formation. 1.0 M PAA or 0.05M octylamine in MES running buffer was added in serial 100μL pulses at 20μ L/min until the SPR signal stabilized. It

should be noted that the lower concentration of octylamine compared to the PAA is merely due to its lower water solubility, this required higher number of pulses for signal stabilization.

6.2.9 SPR protocol

The SPR experiments were performed on a Biacore 2000 system at 25°C. UltraPure Salmon Sperm DNA was purchased from Invitrogen. All buffers were prepared sterile and degassed prior to use in the equipment.

The experiments were performed at constant flow rate of running buffer and sample injection of 100μ L/min. Each run consisted of the following sequence of steps repeated over three or four cycles: (i) equilibration of the flow cell with running buffer at a prescribed NaCl concentration (c0); (ii) injection of 100 μL of DNA solution at given concentration (c0,cB); (iii) desorption and equilibration with running buffer (again, at c0). Before starting a new run, the flow cell was subjected to an aggressive desorption step using 100 μL of 1M NaCl in 10 mM Tris buffer at pH 8 (c0,ref), and then cleaned/sanitized with 100 μL of 0.1 M NaOH for complete regeneration of the surface. The experiments were conduct of each sensor chip, with the two respectively ligand.

Sensor chips have been shown to be fully resistant to pulses of NaOH (or HCl) up to 1 M. The baseline stability was controlled throughout the course of each experiment. All sensorgrams were duplicated by repeating each run once for confirmation of their reproducibility and surface regeneration.

In order to quantitatively analize SPR data one must first understand the underlying probing mechanism of the biacore machine—the refractive index of the medium within the sensing evanescent field depth.

The refractive index, η_0, of an aqueous salt solution (0) with concentration c_0 is

$$\eta_0 = \tilde{\eta}_{\mathrm{w}} + (\tilde{\eta}_0 - \tilde{\eta}_{\mathrm{w}}) v_0 c_0, \tag{6.1}$$

where c_0 (M) is the salt concentration, v_0 is the molar volume of the salt ions (M^{-1}), $\tilde{\eta}_0$ is their refractive index, and $\tilde{\eta}_{\mathrm{w}}$ is the refractive index of water.

The above equation is strictly valid if the salt solution is made as follows: (i) weight the required amount m_0m of dry salt and then add it to the flask; (ii) slowly fill the flask with water while stirring up to a volume V; the mass concentration of the salt solution is then $\rho_0 = m_0/V$ and the concentration is $c_0 = \rho_0/M_0$, where M_0 is the molecular weight of the salt.

But there's another way a making the salt solution: (i) fill the flask with

water up to a volume V; then add the mass m of salt. In this case, the mass concentration is $\rho_0' = m_0/(V + (m_0/M_0)v_0)$, where v_0 is the molar volume of the salt; the corresponding molar concentration will be $c_0' = rho_0'/M_0$. But suppose that we still measure the concentration as c_0. In this case, the refractive index will be

$$\eta_0' = \tilde{\eta}_\mathrm{w} + (\tilde{\eta}_0 - \tilde{\eta}_\mathrm{w})v_0 c_0, \tag{6.2}$$

Similarly, the refractive index, η_B, of the aqueous salt solution with a given dissolved solute (B) (this can take the form of any analyte, e.g., a protein), can be expressed as

$$\eta_\mathrm{B} = \eta_0 + (\tilde{\eta}_\mathrm{B} - \eta_0)v_\mathrm{B} c_\mathrm{B}, \tag{6.3}$$

where c_B (M), v_B (M^{-1}) and $\tilde{\eta}_\mathrm{B}$ are the solute concentration, specific volume, and refractive index, respectively.

The Biacore signal, $R(\eta)$, expressed, e.g., in resonance units (RU), is a function of the refractive index, η, in the flow cell; if η does not vary greatly (i.e., the shift $\Delta\eta$ is not very large), then the corresponding change in the Biacore signal, ΔR, will be proportional to the change in η, that is, $\Delta R \approx m\Delta\eta$ (Jung et al., 1998). It is also known that η is not probed uniformly throughout the depth of the flow cell height; it is probed proportionally to the intensity of light at each point.

Thus, the effective refractive index, η_eff, measured by the Biacore system is the average of η over the depth of the evanescent electromagnetic field (Jung et al., 1998):

$$\eta_\mathrm{eff} = \frac{1}{d_\mathrm{p}} \int_0^\infty \eta(z)\, e^{-z/d_\mathrm{p}}\, dz, \tag{6.4}$$

where d_p is the effective penetration depth; for the Biacore 2000 machine, $d_\mathrm{p} \approx$ 150 nm.

Let us first consider the case of an uniform adsorbent film, of thickness d_s, attached to the metal sensor surface, under conditions where there is no adsorption from the fluid solution flowing over its surface (e.g., when the salt concentration is large enough to prevent it).

The refractive index, η_s, of the adsorbent film is constant unless there are external perturbations, such as temperature changes in the flow cell, which is not the case in the present work. Assuming that η_s is constant, Eq. 6.4 can be

rewritten as follows:

$$\begin{aligned}\eta_{\text{eff}} &= \frac{\eta_{\text{s}}}{d_{\text{p}}}\int_0^{d_{\text{s}}} e^{-z/d_{\text{p}}}\,dz + \frac{1}{d_{\text{p}}}\int_{d_{\text{s}}}^{\infty}\eta(z)\,e^{-z/d_{\text{p}}}\,dz \\ &= \eta_{\text{s}}(1-e^{-d_{\text{s}}/d_{\text{p}}}) \;+ \frac{1}{d_{\text{p}}}\int_{d_{\text{s}}}^{\infty}\eta(z)\,e^{-z/d_{\text{p}}}\,dz \\ &= \eta_{\text{s}}(1-\phi_{\text{s}}) \qquad\quad + \eta'_{\text{eff}}, \end{aligned} \tag{6.5}$$

where $\phi_{\text{s}} = \exp(-d_{\text{s}}/d_{\text{p}})$. In the absence of adsorption, $\eta(z) = \eta$ for $z > d_{\text{s}}$, where η is the refractive index of the bulk solution, hence $\eta'_{\text{eff}} = \eta\phi_{\text{s}}$. Therefore, under nonadsorbing conditions, η_{eff} is given by

$$\eta_{\text{eff}} = \eta_{\text{s}} + \phi_{\text{s}}(\eta - \eta_{\text{s}}). \tag{6.6}$$

When the salt solution has no dissolved solute ($c_0 > 0, c_{\text{B}} = 0$), the effective refractive index, η_0^{eff}, is given by Eq. (6.6) with η replaced by η_0 defined in Eq. (6.1), that is,

$$\eta_0^{\text{eff}} = \eta_{\text{s}} + \phi_{\text{s}}[\tilde{\eta}_{\text{w}} + (\tilde{\eta}_0 - \tilde{\eta}_{\text{w}})v_0c_0 - \eta_{\text{s}}] \tag{6.7}$$

If the baseline (or reference) signal is established for a salt solution with concentration $c_{0,\text{ref}}$, then the change in the effective refractive index when the salt concentration is altered to c_0 is

$$(\eta_0 - \eta_{0,\text{ref}})_{\text{eff}} = \phi_{\text{s}}(\tilde{\eta}_0 - \tilde{\eta}_{\text{w}})v_0(c_0 - c_{0,\text{ref}}). \tag{6.8}$$

The corresponding signal shift in the Biacore system is

$$\Delta R = m(\eta_0 - \eta_{0,\text{ref}})_{\text{eff}} = m_0(c_0 - c_{0,\text{ref}}), \tag{6.9}$$

where $m_0 = m\phi_{\text{s}}(\tilde{\eta}_0 - \tilde{\eta}_{\text{w}})v_0$ is the slope of the linear fitting (with intercept set to zero) of ΔR vs $(c_0 - c_{0,\text{ref}})$.

When solute is added to the reference salt solution ($c_0 = c_{0,\text{ref}}, c_{\text{B}} > 0$) and flown over the sensing surface under nonadsorbing conditions, the effective refractive index is given by

$$(\eta_{\text{B,ref}})_{\text{eff}} = \eta_{\text{s}} + \phi_{\text{s}}(\eta_{\text{B,ref}} - \eta_{\text{s}}), \tag{6.10}$$

where $\eta_{\text{B,ref}}$ is defined by Eq. (6.3) with $\eta_0 = \eta_{0,\text{ref}}$. The corresponding change in

the effective refractive index is

$$(\eta_{\mathrm{B,ref}} - \eta_{0,\mathrm{ref}})_{\mathrm{eff}} = \phi_{\mathrm{s}}(\tilde{\eta}_{\mathrm{B}} - \eta_{0,\mathrm{ref}})v_{\mathrm{B}}c_{\mathrm{B}} \qquad = \phi_{\mathrm{s}}[(\tilde{\eta}_{\mathrm{B}} - \tilde{\eta}_{\mathrm{w}}) - (\tilde{\eta}_0 - \tilde{\eta}_{\mathrm{w}})v_0 c_{0,\mathrm{ref}}]v_{\mathrm{B}}c_{\mathrm{B}},$$

and the corresponding shift of the Biacore signal given by

$$\Delta R = m(\eta_{\mathrm{B,ref}} - \eta_{0,\mathrm{ref}})_{\mathrm{eff}} = (m_{\mathrm{B}} - m_0 v_{\mathrm{B}} c_{0,\mathrm{ref}})c_{\mathrm{B}}, \tag{6.11}$$

where $m_{\mathrm{B}} = m\phi_{\mathrm{s}}(\tilde{\eta}_{\mathrm{B}} - \tilde{\eta}_{\mathrm{w}})v_{\mathrm{B}}$; note that $(m_{\mathrm{B}} - m_0 v_{\mathrm{B}} c_{0,\mathrm{ref}})$ will be slope of the linear fitting (with intercept set to zero) of ΔR vs c_{B}.

Once m_0 and m_{B} are known, we can predict the shift in the Biacore signal due to the change in the effective refractive index, $(\eta_{\mathrm{B}} - \eta_{0,\mathrm{ref}})_{\mathrm{eff}}$, for an aqueous buffer with salt concentration c_0 and solute concentration c_{B} (assuming that the baseline was defined for the buffer salt solution with concentration $c_{0,\mathrm{ref}}$); the expression is

$$\Delta R = (m_{\mathrm{B}} - m_0 c_0 v_{\mathrm{B}})c_{\mathrm{B}} + m_0(c_0 - c_{0,\mathrm{ref}}). \tag{6.12}$$

Let us now consider the more complicated case where there is solute adsorption onto the sensor surface film. The problem is illustrated in Fig. 4.4. The aqueous buffer solution in the bulk has salt concentration c_0 and solute concentration c_{B}; the thickness of the adsorbed layer is d_{m} and its inter-solute volume is filled with buffer solution assumed to contain the same salt concentration as that of the bulk. In Fig. 6.3, d_{m} is assumed to be equal to the diameter of the adsorbed solute molecules, in accordance with the formation of a single adsorbed monolayer, though this is not a restriction imposed in our formulation.

The effective refractive index, $\eta_{\mathrm{m}}^{\mathrm{eff}}$, probed by the Biacore machine is

$$\eta_{\mathrm{m,eff}} = \frac{\eta_{\mathrm{s}}}{d_{\mathrm{p}}} \int_0^{d_{\mathrm{s}}} e^{-z/d_{\mathrm{p}}}\, dz + \frac{\eta_{\mathrm{m}}}{d_{\mathrm{p}}} \int_{d_{\mathrm{s}}}^{d_{\mathrm{s}}+d_{\mathrm{m}}} e^{-z/d_{\mathrm{p}}}\, dz \frac{\eta_{\mathrm{B}}}{d_{\mathrm{p}}} \int_{d_{\mathrm{s}}+d_{\mathrm{m}}}^{\infty} e^{-z/d_{\mathrm{p}}}\, dz, \tag{6.13}$$

which gives

$$\eta_{\mathrm{m,eff}} = \eta_{\mathrm{s}} + \phi_{\mathrm{s}}(\eta_{\mathrm{m}} - \eta_{\mathrm{s}}) + \phi_{\mathrm{s}}\phi_{\mathrm{m}}(\eta_{\mathrm{B}} - \eta_{\mathrm{m}}), \tag{6.14}$$

where $\phi_{\mathrm{m}} = \exp(-d_{\mathrm{m}}/d_{\mathrm{p}})$. In these equations, η_{m} and η_{B} are the refractive indices of the adsorbed monolayer (c_{m}) and of the bulk solution (c_0, c_{B}), respectively.

Considering the adsorption model of Fig. 4.4, and assuming that the analyte molecule, when adsorbed, does not change its refractive index and specific (or

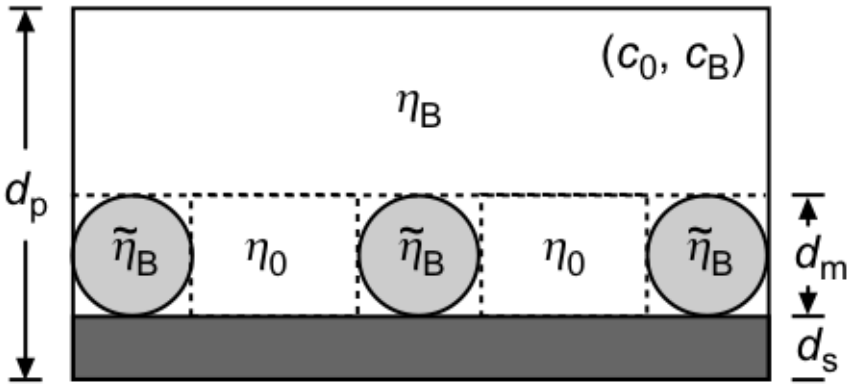

Figure 6.3: *Schematic of protein monolayer adsorbed onto a surface of thickness d_s in the Biacore sensor chip flow cell. The bulk aqueous solution has salt concentration c_0, protein concentration c_B, and refractive index η_B; the refractive index of the isolated (dry) protein is $\tilde{\eta}_B$; salt solution with concentration c_0 and refractive index η_0 is assumed to fill the gaps between adsorbed proteins; the thickness of the adsorbed monolayer, d_m, is roughly equal to the diameter of the proteins*

molar) volume, then the refractive index of the adsorbed monolayer is

$$\eta_m = \eta_0 + (\tilde{\eta}_B - \eta_0) v_B c_m, \tag{6.15}$$

where c_m (M) is the protein concentration in the volume occupied by the adsorbed monolayer; c_m can be converted into a surface concentration, q (g/dm^2), through the simple formula $q = d_m c_m$. If the baseline has a refractive index $(\eta_{0,ref})_{eff}$ (obtained with a salt solution of concentration $c_{0,ref}$), then the change in the effective refractive index probed by the Biacore machine will be

$$(\eta_m - \eta_{0,ref})_{eff} = \phi_s(\eta_m - \eta_{0,ref}) + \phi_s\phi_m(\eta_B - \eta_m). \tag{6.16}$$

Expanding the two right-hand-side differences gives

$$(\eta_m - \eta_{0,ref})_{eff} = \phi_s(\tilde{\eta}_B - \eta_0) v_B [c_m + \phi_m(c_B - c_m)] + \phi_s(\eta_0 - \eta_{0,ref}). \tag{6.17}$$

The corresponding shift of the Biacore signal is

$$\Delta R = (m_B - m_0 c_0 v_B)[c_m + \phi_m(c_B - c_m)] + m_0(c_0 - c_{0,ref}). \tag{6.18}$$

Solving for c_{m} gives

$$c_{\mathrm{m}} = \frac{\Delta R - m_0(c_0 - c_{0,\mathrm{ref}})}{(1-\phi_{\mathrm{m}})(m_{\mathrm{B}} - m_0 c_0 v_{\mathrm{B}})} - \frac{\phi_{\mathrm{m}}}{1-\phi_{\mathrm{m}}}\, c_{\mathrm{B}}. \tag{6.19}$$

Equations (6.18) and (6.19) are the most general ones since they encompass all the cases discussed above. For example, setting $\phi_{\mathrm{m}} = 1$ (i.e., $d_{\mathrm{m}} = 0$) eliminates the adsorbed monolayer; setting $c_{\mathrm{m}} = c_{\mathrm{B}}$ sets the solute concentration in the adsorbed phase equal to that in the bulk solution and the two phases become optically indistinguishable. In both cases, Eq. (6.18) correctly reduces to Eq. (6.12).

Equation (6.11) shows that m_{B} can be determined from the slope b of the linear fitting (with intercept equal to zero) of ΔR against c_{B}, as $m_{\mathrm{B}} = b + m_0 v_{\mathrm{B}} c_{0,\mathrm{ref}}$. These calibration experiments, however, must be carried out under conditions where the solute does not adsorb; this may be difficult to achieve in practice. When there is only mild solute adsorption, the adsorbed phase will quickly reach saturation conditions, that is, c_{m} will quickly attain a constant value. Equation (6.18) shows that, in this case, a plot of ΔR against c_{B} will still exhibit a linear relationship for sufficiently large values of c_{B} (i.e., those values of c_{B} for which $c_{\mathrm{m}} \approx \mathrm{const}$), but with slope equal to $\phi_{\mathrm{m}}(m_{\mathrm{B}} - m_0 v_{\mathrm{B}} c_{0,\mathrm{ref}})$ and intercept equal to $(1-\phi_{\mathrm{m}})(m_{\mathrm{B}} - m_0 v_{\mathrm{B}} c_{0,\mathrm{ref}})c_{\mathrm{m}}$.

A typical SPR experiment, whose schematic is depicted in Fig. 4.2, consists of a bind-and-elute run. In the following it is assumed that there are no mass-transfer resistances because the system is operated at a sufficiently high flow rate ($\sim 100\mu$L/min or higher).

Initially, the SPR cell is equilibrated with aqueous salt solute with concentration c_0; this establishes the baseline of the Biacore signal. The binding step consists of injecting the SPR cell with the aqueous salt solution with the dissolved solute (B) at concentration c_{B}.

This step corresponds to the curve $\Delta R_{\mathrm{a}}(t)$ in Fig.6.4 If the injection is large enough, the SPR signal will attain an horizontal plateau whose value is $\overline{\Delta R}_{\mathrm{a}}$. The plateau is the visual proof that the equilibrium between the solute in the bulk solution and in the adsorbed monolayer is really established—this plateau corresponds to one point in the adsorption isotherm.

If we can convert the signal $\overline{\Delta R}_{\mathrm{a}}$ into the concentration $\overline{c_{\mathrm{m}}}$ of the solute in the adsorbed monolayer, then we have the equilibrium point $(c_0, c_{\mathrm{B}}, \overline{c_{\mathrm{m}}})$: this means that $\overline{c_{\mathrm{m}}}$ is the solute concentration in the adsorbed monolayer that is in equilibrium with an aqueous solution with salt concentration c_0 and solute

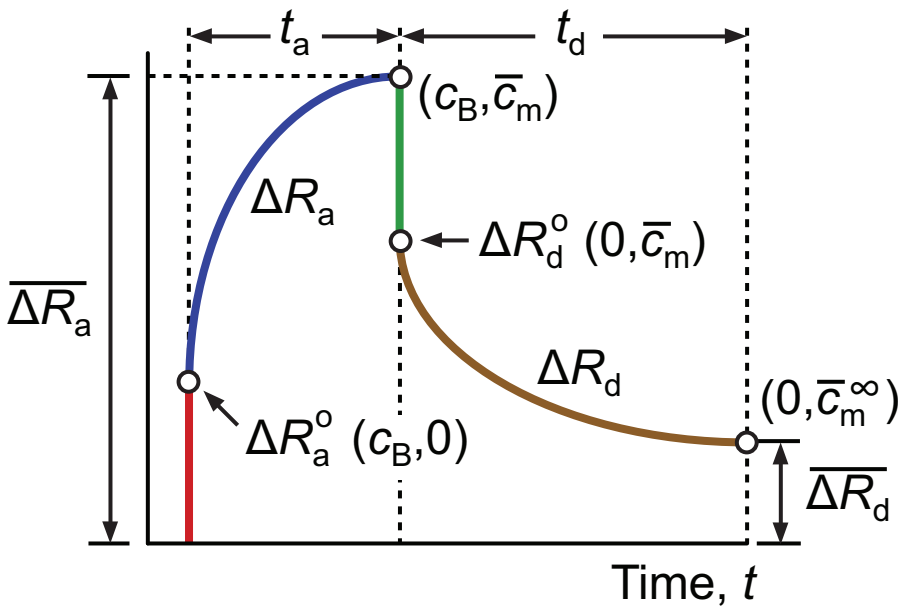

Figure 6.4: *Typical bind-and-elute SPR experiment in the absence of mass-transfer resistances.*

concentration c_B; we express this as $\overline{c_m} = c_m^*(c_0, c_B)$ and denote this function as the adsorption isotherm.

After the binding step, we flush the SPR cell with aqueous salt solution with concentration c_0. If there are no mass-transfer resistances, there will be an abrupt drop in the SPR signal from $\overline{\Delta R}_a$ to ΔR_d^o. This happens because the bulk solution in the SPR cell (c_0, c_B) is quickly replaced by the salt solution $(c_0, 0)$ while the adsorbed phase concentration is kept at the equilibrium value $\overline{c_m}$.

Applying 6.18 to the adsorption equilibrium plateau and to the point where the SPR signal is ΔR_d^o gives, respectively,

$$\overline{\Delta R}_a = (m_B - m_0 c_0 v_B)[\overline{c_m} + \phi_m(c_B - \overline{c_m})] \tag{6.20}$$

$$\Delta R_d^o = (m_B - m_0 c_0 v_B)[\overline{c_m} + \phi_m(0 - \overline{c_m})]. \tag{6.21}$$

Therefore,

$$\overline{\Delta R}_a - \Delta R_d^o = (m_B - m_0 c_0 v_B)\phi_m c_B. \tag{6.22}$$

This equation is important: it states that if we do a series of bind-and-elute experiments with the same salt concentration but different solute concentrations

Table 6.1: *Characteristics of the Capto™ Core 700*

Matrix	High flow agarose
Size cut-off outer layer	$M_r \approx 700\ 000$
pKa of protonated octhylamine	10.65
Functional group in the core	$CH_3CH_2CH_2CH_2CH_2CH_2CH_2CH_2NH$-
Total ionic capacity/ml medium	40 to 85 μmol (Cl^-)
Particle size $(d_{50v})^2$	90μm
Maximum operational flow velocity	500 cm/h in columns with 20 cm bed height at < 2 bar
Binding capacity/ml of medium	$\approx$ 13mg ovalbumin

and plot $\overline{\Delta R}_a - \Delta R_d^o$ against c_B, then we should get a straight line with intercept equal to zero and slope equal to $(m_B - m_0 c_0 v_B)\phi_m$.

The Biacore can be precalibrated for the salt effect through a couple of simple experiments with different salt concentrations c_0, where each run consists of equilibrating the cell with water and then injecting the salt solution; the SPR signal for each experiment should be given by

$$\Delta R = m_0 c_0, \tag{6.23}$$

and thus yield a straight line with intercept equal to zero and slope equal to m_0 when plotted against c_0.

6.3 Results and Discussion

6.3.1 Principle of flowthrough purification

In designing a flowthrough process the combination of membrane and bead technology was employed. In particular Sartobind-STIC and Capto Core were chosen. The first is characterized of having a cellulose backbone where is directly attached a primary amine ligand, polyallylamine (Table 6.1). This ligand was proposed for the first time by Kim and Kuga (2002), as a potential new class of anion exchanger for proteins separation. The membrane present a pore size distribution of 2.5μm 4.5. This was elucidated by employing two techniques for porous material characterization: mercury porosimetry and gas liquid displasment porometry.

Mercury porosimetry depicted a broad pore size distribution (PSD) with pore size between between 4 and 7 μm corresponding to the mesopore range (Rouquerol

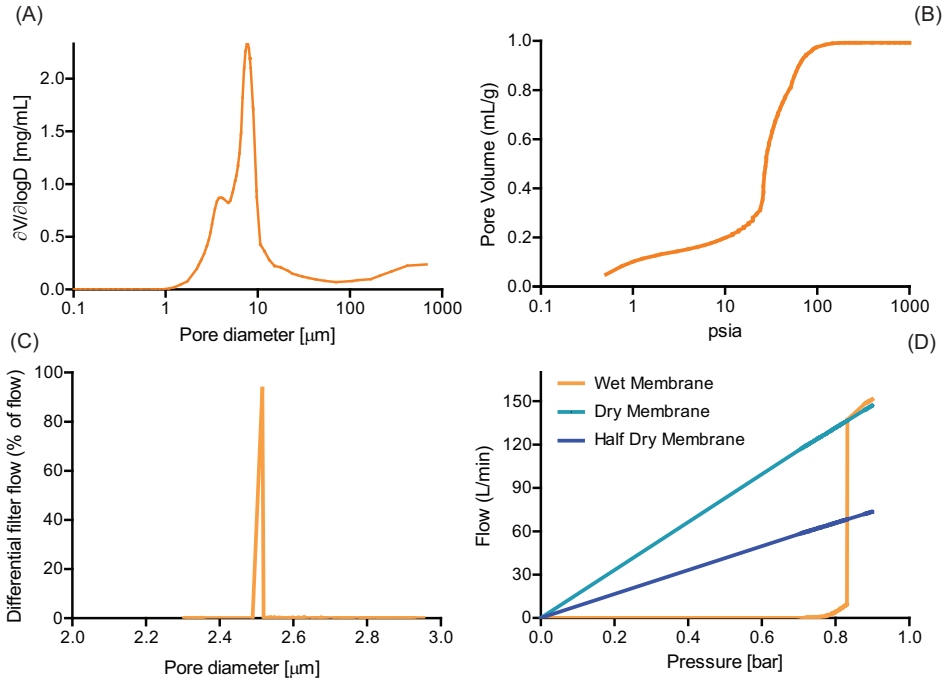

Figure 6.5: *Figures A and B display a pore size distribution of the STIC membrane measured by mercury porosimetry in a dry state conditions. The pore size distribution is cantered in the mesopore region with pore size between of 4–7 µm. Figures C and D show the pore size distribution obtained by capillary flow porometry under wet state conditions. Pore size distributions results nicely centred at 2.5 µm.*

et al., 1994). However, it should be pointed out that the analysis was performed under dry conditions and the pore size distribution may change when hydrating the membrane with buffer or water due to a swelling effect. Therefore to assess the real pore size under operating conditions capillary flow porometry was employed. This method is based on the measurement of the pressure necessary to blow gas through a liquid-filled porous membrane. As the pressure of gas increases to a point, the applied pressure overcomes surface tension of liquid in the pore and pushes liquid out of the pore. Figure 6.5 C, shows that when the membrane is hydrated a narrow pore size distribution of 2.5μm is observed.

The experimentes were conducted by using a minimized column with a volume of 0.023 mL in order to identify the operational conditions suitable for a flowthrough purification yielding higher virus recovery.

Capto core 700 is a beads based resin recently introduced in the market by GE Healthcare for virus purification in negative mode (Fernandes et al., 2013). The

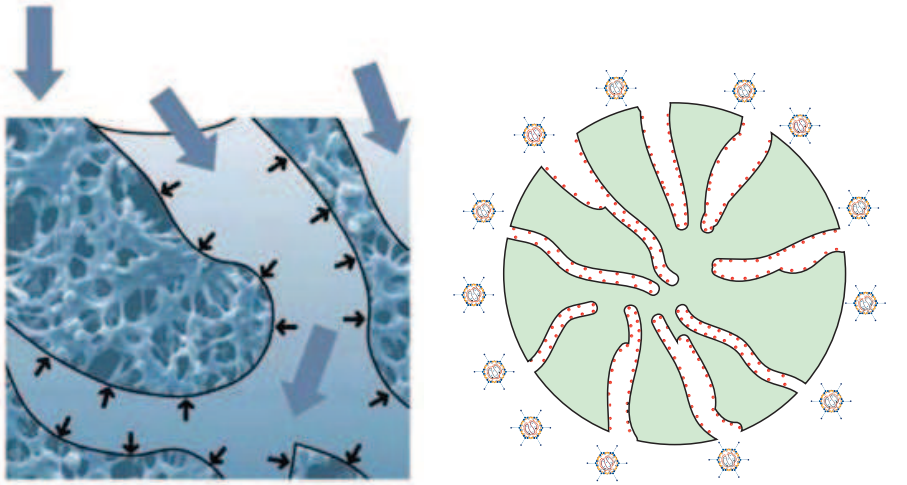

(A) (B)

Figure 6.6: *Schematic representation of the chromatographic membrane (STIC) on figure A. Large arrows indicate the prevalence of convective flow while small arrows indicate film diffusion. Figure B shows the structure of Capto Core 700 beads, Adenoviruses cannot access into the inner core of the beads and are therefore collected in the flowthrough (FT). The exclusion limit is around 700 kDa.*

ligand employed is multimodal ligand able to bind impurities under a wide range of pHs or NaCl concentrations (Table 6.1). The structure is illustrated in Fig. 6.6 and the cut off declared by the manufactured is 700kDa, thus adenoviruses that have a molecular weight of 1.5^8 Da are excluded for the pore size. Unfortunately mercury porosimetry to better elucidate the porosimetry is not applicable for wet resins. The pore structures are determined by the distance between the polymer chains and crosslinks which vary with the crosslink level of the polymer, the polarity of the solvent and the operating conditions.

6.3.2 Down scale model: SPR technology

The results of PAA and Octylamine are presented. In order to identify the best possible scheme for a flowthrough process the two ligands, PAA and Octylamine, respectively functional groups of STIC®and Capto™Core 700 were investigated. Being DNA one of the most important impurities to separated from the target product its binding to the two ligand was studied. The scale down was performed in a sensor chip (CM5) where the dextran layer is roughly 100 nm thicker, thus increasing the surface available for binding. Figure 6.7 illustrated the total binding of DNA $(cm)$for both PAA and octylamine.

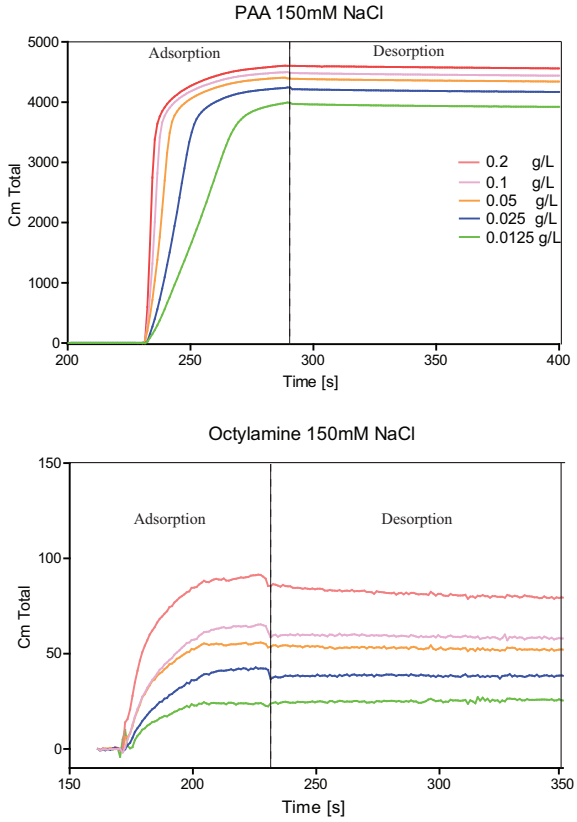

Figure 6.7: *Adsorbate concentration c_m for DNA under 150mM NaCl for PAA and octylamine respectively. The total amount of DNA adsorbed for PAA is 40-fold higher then the one observed for octylamine. For both ligands the desorption is negligible indicating a irreversible DNA binding.*

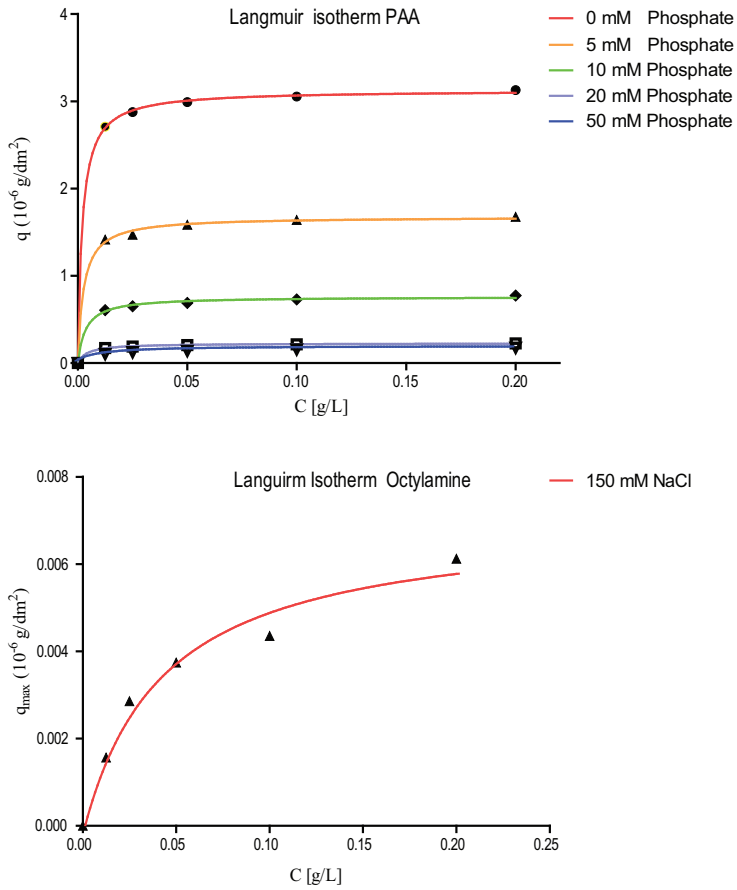

Figure 6.8: *Langmuir isotherm of PAA under different Na_2HPO_4 concentrations ranging from 5 to 50mM(upper figure).Fitting shows a Langmuir dependency with an R^2 of 0.99 for all the phosphate concentrations evaluated. The effect of the Na_2HPO_4 on the binding behavior shows a exponential decay.*

The results illustrated that the binding is 40-fold higher for PAA compared octylamine, this was also confirmed by the isotherm in figure 6.8. The desorption of the DNA as shown in figure 6.7 indicates the irreversible adsorption mechanisms.

From the process point of view this will imply that Octylamine ligand cannot be implemented at earlier stage of the process where the concentrations of DNA is often greater.

Figure 6.8 depicted the binding isotherm which follow a classic Langmuir behavior obtained by fitting the following :

$$q = \frac{q_m bc}{1 + bc} = \frac{Hc}{1 + bc} \tag{6.24}$$

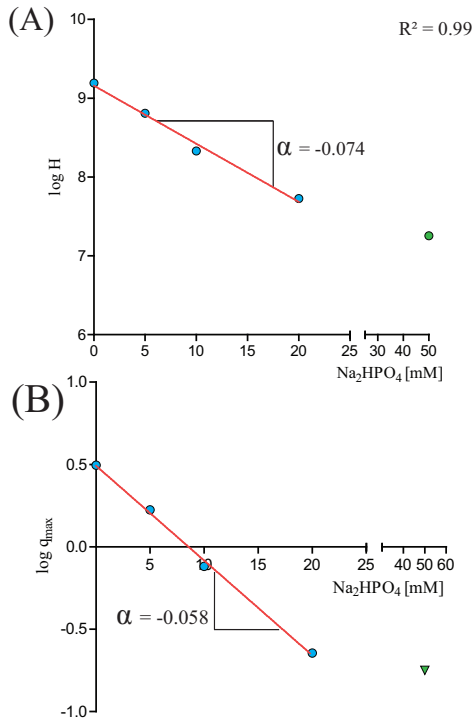

Figure 6.9: *Figure A and B illustrated the dependency of the Henry constant (H) and $q_{max}(10^{-6}g/dm^2)$ as function of the Na_2HPO_4 concentrations respectively. The fitting show an exponential decrease up to 20mM Na_2HPO_4. Both Henry constant q_{max} show a fairly good agreement. Above 50mM Na_2HPO_4 the adsorption is strongly comprised and aspecific interactions dominate the binding*

Henry constant (H) and q_{max} are therefore given by :

$$H = q_{max}b \qquad q_{max} = \frac{H}{b} \tag{6.25}$$

Figure 6.9 displayed a strong dependency with the Na_2HPO_4 up to 20mM. Both Henry constant and q_{max} present,as expected, a negative slope with an excellent R^2 fitting of 0.99. Above 50mM a linear correlation is no visible, mainly because the adsorption is strongly compromised and aspecific binding might take place.

Should be here mentioned that the aspecific binding is not due to the ligand but most likely to the CM5 support, in particular the dextran layer.

In the light of these results PAA showed to be the ideal ligand to be used as in first step of the chromatography train. Therefore a better characterization was conducted under several Na_2HPO_4 and NaCl concentration to identify the critical

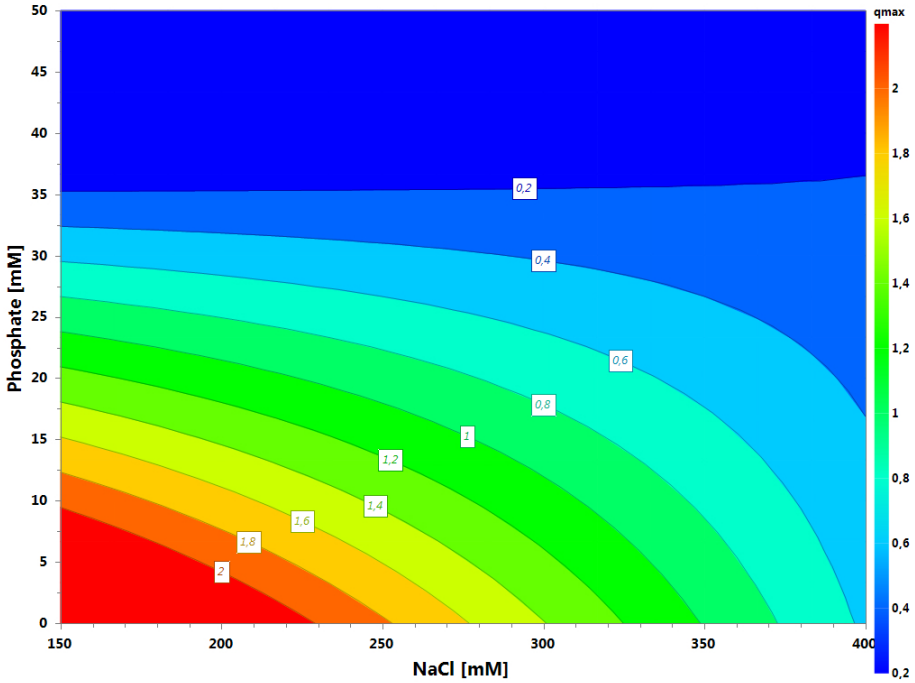

Figure 6.10: *Prediction of the q_{max} binding behavior for the salmon sperm DNA under several concentration of NaCl and Na_2HPO_4. As the isotherm suggested above 20mM the binding is compromised. However high salt concentration of NaCl up to 400mM do not affect the binding is strong manner.*

operational value and evaluated them in the latter scale up (Fig. 6.10).

In regard to the NaCl the PAA ligand exhibit a salt tolerant profile, the binding is in fact maintained up to 300mM NaCl. The results obtained were used to set condition at which STIC membrane should be evaluated by using a real feedstock. Capto Core, was less extensively evaluated. Indeed,although the adsorption onto octylamine for DNA is lower compared to PAA, being a multimodal ligand it is able to maintain the binding at wider range of salt concentrations and pHs.

6.3.3 Virus recovery

The SPR experiments indicated that phosphate buffer ranking between 5 to 50 mM is a strong modulator of the impurities binding. In order to assure the highest trade off between contaminant clearance and virus recovery concentrations ranging between 6.25mM and 50mM of both phosphate and citrate buffer were evaluated. HEPES 50mM and Tris 20mM were included since they are two widely

used buffers in virus purification. Figure 6.11 shows the percentage of the virus in flowthrough and in the elution. Interestingly in all the conditions evaluated viruses binding to the membrane was lower than 25%,thus yielding in flow-through mode recovery higher than 75%. The membrane ligand can explain the reasons of the limited virus adsorption. The ligands located on the larger pore size are then mostly occupied by contaminants mainly DNA due to the high affinity of this biomolecule to PAA, as previously shown in the SPR experiments. The only exception was observed by using Tris, indeed, virus in flow-though were below 10 %, nevertheless virus desorption did not occur even at 1M phosphate, indicating the presence irreversible binding. HEPES buffer showed a similar behavior to the multivalent anions , this may be due to the presence in the chemical structure of a sulfonic acid group.

The mass balance for the virus , with the exception of the Tris buffer, was easily closed reaching 100% recovery by summing up the flow-though and the eluted peak. In the Captocore the mechanism for which the virus do not bind is mainly size exclusion like. Therefore no investigation on the modulator of the binding was required. HEPES 50mM with 150 mM NaCl was chosen to assess the recovery. The NaCl of 150mM was used in order to reduce possible aspecific interaction with the beads matrix. The bulk employed was the same used for STIC experiments. Recovery yield is shown to be of 80.10 % (Table 6.3) slightly lower compared to the STIC , probably due to some non-specific binding or virus entrapment that occur in the outer shell of the beads. Therefore, unlikely to what observed with STIC® membrane mass balance could not be closed.

6.3.4 Impurities clearance

For proper assessing the feasibility of a flow-though purification process, the removal impurities should be properly evaluated. Furthermore, this will indicate if the prediction of the design space illustrate in 6.10 are consistent the knowledge generate on the sensor chip can be translate to membrane chromatography system. Table 6.2 reports the clearance for DNA and total proteins. The results suggested that polyallylamine (PAA) ligand has higher affinity to phosphate groups, in particular above 10mM phosphate the DNA clearance dropped to nearly 20%. This is in line with what observed in Figure 6.8 suggested by the isotherm determination.

However, the high affinity to the phosphate results in higher removal of DNA, when the concentration of Na_2HPO_4 is reduced, since the phosphate groups are

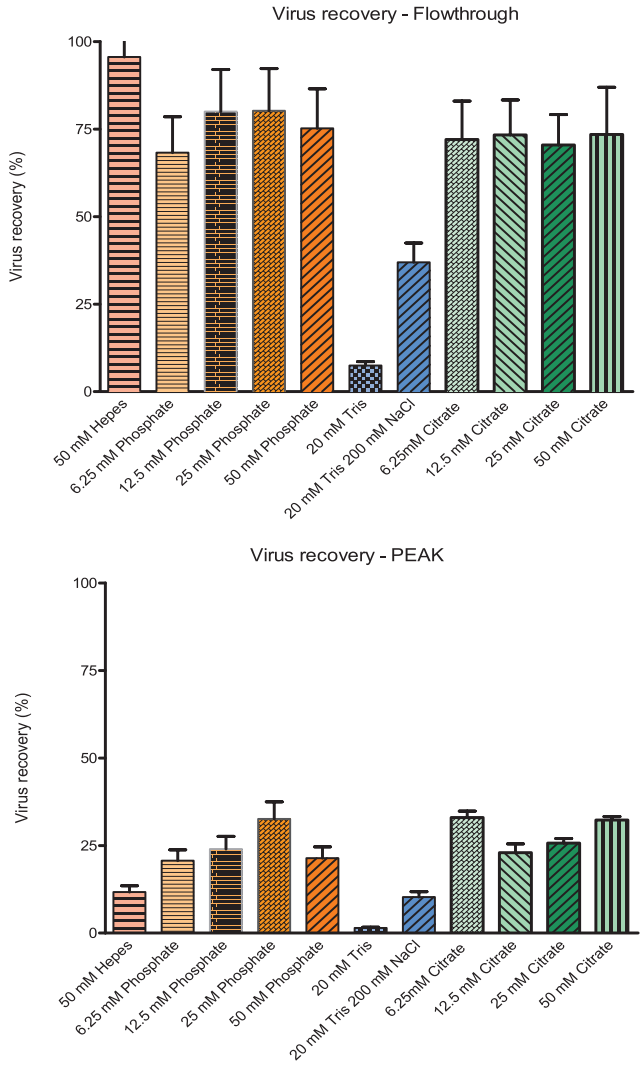

Figure 6.11: *The recovery both in flowthrough (top plot) and after elution (bottom plot). Orange color depicted the phosphate buffer, while in green is citrate buffer. Tris and HEPES buffers are depicted in blue and pink respectively. Virus quantification was performed by RT-PCR and Nanosight NS500.*

Table 6.2: *DNA and total protein clearance in the flow-through under several concentrations of multivalent anions with the use of STIC® membrane. Buffer can be rated in regard to their clearance as: HEPES > Citrate > Tris > Phosphate*

Buffers	DNA clearance [%]	Total protein clearance [%]
50 mM HEPES	93.28	69.61
6.25 mM Phosphate	85.52	61.73
12.5 mM Phosphate	58.71	71.43
25 mM Phosphate	58.61	78.23
50 mM Phosphate	55.41	65.72
20 mM Tris	65.00	85.62
20 mM Tris 200 mM NaCl	79.77	27.38
6.25 mM Citrate	78.74	65.73
12.5 mM Citrate	78.73	70.35
25 mM Citrate	78.16	68.43
50 mM Citrate	74.14	67.30

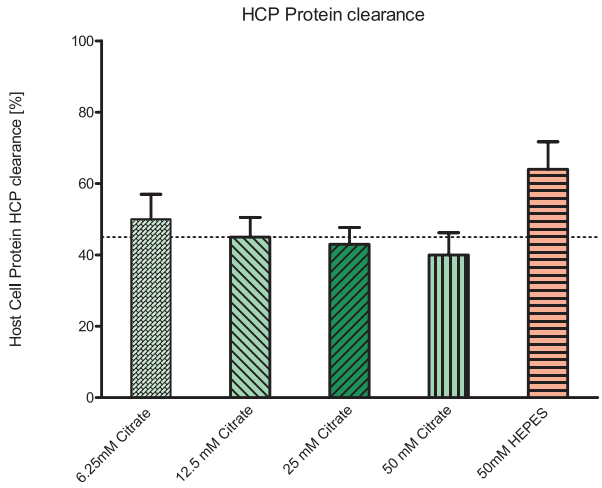

Figure 6.12: *Host cell protein clearance for the flowthrough of STIC® membrane. Increasing in citrate concentration leads to reduced HCP clearance. HEPES yields the highest clearance.*

Table 6.3: *DNA and host cell protein clearance in the flow-through for Capto Core.*

Virus Recovery Yield [%]	DNA Clearance [%]	HCP Clearance [%]
75.23	80.10	89.75

known to surround the DNA double helix. The best trade-off between DNA and total protein clearance is given by HEPES 50mM with 100mM NaCl and citrate buffer, with a clerance of 93.28 % and 78.74% respectively. No significance differences are observed among the citrate concentrations evaluated.

Further analysis were carried out in order to assess the level of HCPs present in the flow-through. Figure 6.12 displayed HCPs clearance, measured by ELISA (see Materials and Methods). These results are complementary to the total protein clearance, giving a more accurate determination of the amount of proteins that do not belong to growth media, or viruses.

The HCPs clearance was similar among the citrate concentrations whereas HEPES buffer showed a superior performance yielding a clearance of 64 %. Overall HEPES results to be the most appropriate buffer, with a virus recovery yield higher than 90 % coupled with a satisfactory purity level. Capto™ Core 700 yields a 80.10%, DNA clearance, respectively. HCPs removal compare favorably to membrane chromatography with a 25% increased of clearance, most likely due to the different nature of the ligand (Table6.3).

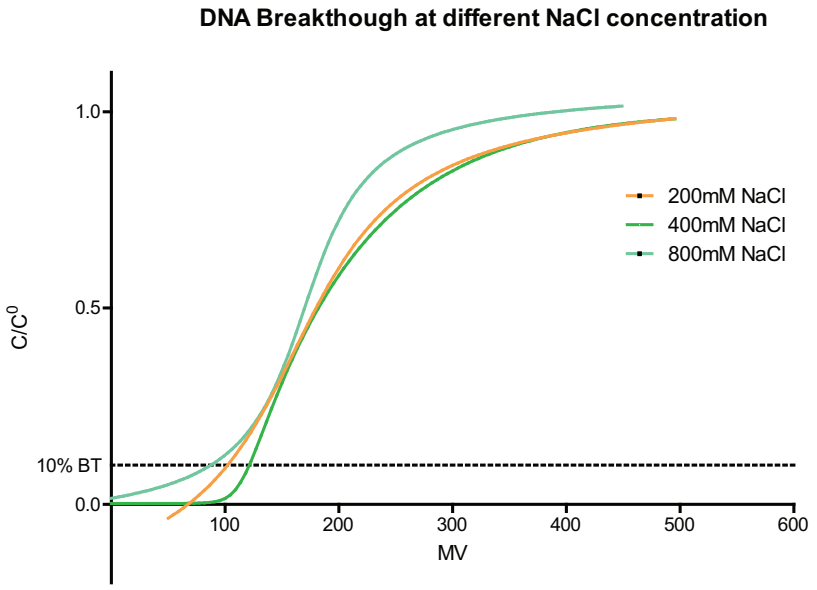

Figure 6.13: *Salmon sperm DNA breakthrough at different NaCl concentrations. As predicted by the SPR experiments the binding is salt tolerant and a slightly decrease is observed at 800mM.*

Since HCPs are an heterogeneous pool of proteins with various size and charge and isoeletric points, having a ligand that can adsorb impurities through ion exchange and hydrophobic mechanism, might improve the clearance of a wide range of proteins (Kallberg et al., 2012; Pezzini et al., 2011; Joucla et al., 2013).

In regards to the DNA removal, the results are comparable to STIC®. However dynamic binding capacity and binding isotherm using salmon sperm DNA, showed a $DBC_{10\%}$ of 0.84 mg/ml which is 6-fold lower compared to the 5.43 mg/ml of the STIC® membrane. Such lower $DBC_{10\%}$ was not expected and the hypothesis reason could be that double helix DNA is rather big molecules and could not access the inner core of beads, therefore salmon sperm DNA was treated with Denerase (an equivalent of the well known Benzonaze). However the results showed a similar $DBC_{10\%}$ (data not shown).

In the ligth of this result Capto™ Core 700 may be not be suitable for being employed in the early steps of a downstream train, where high DNA concentrations are usually observed. Breakthrough curves under various NaCl illustrated a salt tolerant behavior for both systems.

PAA can still bind DNA until 800mM NaCl with an only slightly reduction in the DBC (Fig. 6.13).

Table 6.4: *Residual DNA and protein that coeluted with the virus fraction. STIC® membrane*

Buffers Loading concentration [mM]	DNA [%]	Total protein [%]	Conductivity [mS/cm]
50 mM HEPES	1.20	1.26	24.30
6.25 mM Phosphate	0.00	8.18	33.47
12.5 mM Phosphate	0.0	4.48	33.10
25 mM Phosphate	1.42	0.0	32.87
50 mM Phosphate	8.70	0.0	31.50
20 mM Tris	4.32	1.89	35.25
20 mM Tris 200 mM NaCl	9.59	60.77	30.70
6.25 mM Citrate	12.64	22.75	24.50
12.5 mM Citrate	12.65	21.59	24.31
25 mM Citrate	10.92	19.69	23.78
50 mM Citrate	13.22	20.75	23.55

However this data might be seem contradictory compared to the biacore data prediction counterplot, where a reduction of the binding is observed above 400mM of NaCl. Nevertheless, in a chromatographic system, the ligand salt tolerant behaviour can be enhanced by increasing the ligand density. The overall trends which are intrinsic in the ligand remains, although their values may raise with the increase of ligand density. In regard to the DNA elution also on the membrane a irreversible adsorption was observed, again indicating a good prediction of the SPR experiments.

The analysis of the virus peak fraction shows a remarkable clearance of both DNA and total proteins. Table 6.4 shows that the DNA eluted is below the detection limit of the assay when the concentration of phosphate is low. Yet, the conductivities at which virus desorption occurs are close to 25 mS/cm, thus 250mM phosphate buffer.

On the other hand, by using citrate buffer 1M as elution buffer viruses can desorb at similar conductivity around 24 mS/cm, however impurities clearance are reduced by 10 %.

6.3.5 Flowthrough process

Analyzing the data showed previously it becomes clear that by only using STIC® membrane or Capto ™ Core 700 alone would not satisfy purity constrains, in terms of both DNA and HCP. However, implementing these two flowthrough technologies in series as shown in Figure 6.14 lead to a platform flowthrough process that could serve for the purification of other large biopharmaceuticals, such as VLPs. The results from the Biacore and the proof of concept with a small scale device, identify the following constrains in the whole process optimization. Firstly,(i) Capto Core 700 should be placed at later stage of the process, (ii) binding of STIC membranes can be compromised by high concentration of phosphate, (iii) negative mode results in dilution of the product therefore UF/DF unit operations should then integrated in the whole process. Taking into account these constrains the process showed in Figure 6.14 top plot was developed. The first UF/DF is mainly present to remove trace of phosphate buffer and condioniting the bulk with HEPES buffer. Afterwards another UF/DF is employed in order to combined the two fractions (FT and peak) and to remove remains DNA. This will help also the purification performance of the Capto core.

The full process development showed that the DNA clearance achieved is roughly 4 logs reduction. Also, virus recovery is boosted, especially in the first chromatographic unit operation (STIC membranes) where summing up the virus in FT and the virus eluted the recovery is close to 100%. As for HCP reduction is 5 logs, however while most of the DNA clearance is achieved in the STIC® membrane, the HCP reduction is mainly achieved by using the Capto ™ Core 700.

Overall by combining the two flow through technologies it is possible to design a process that has higher productivity, more robustness, and easily scalable. Scale up was performed by simply calculate the DBC%10 for DNA for the STIC membrane with a full breakthrough experiments. The concentration of the bulk was kept constant. This kind of approach in negative mode, it is more suitable for a platform concept. Due to the high degree of uncertainty associated with the clinical studies process development at early stage aims to produce material for phase 1 and phase 2 clinical trials using standardized process conditions and procedure. The use of platform process allow the acceleration of the process development activities as already shown for mAbs application (Tugcu et al., 2008). The similarity amongs different viruses or serotype make the platform concept feasible although the process is not fully optimized for every complex

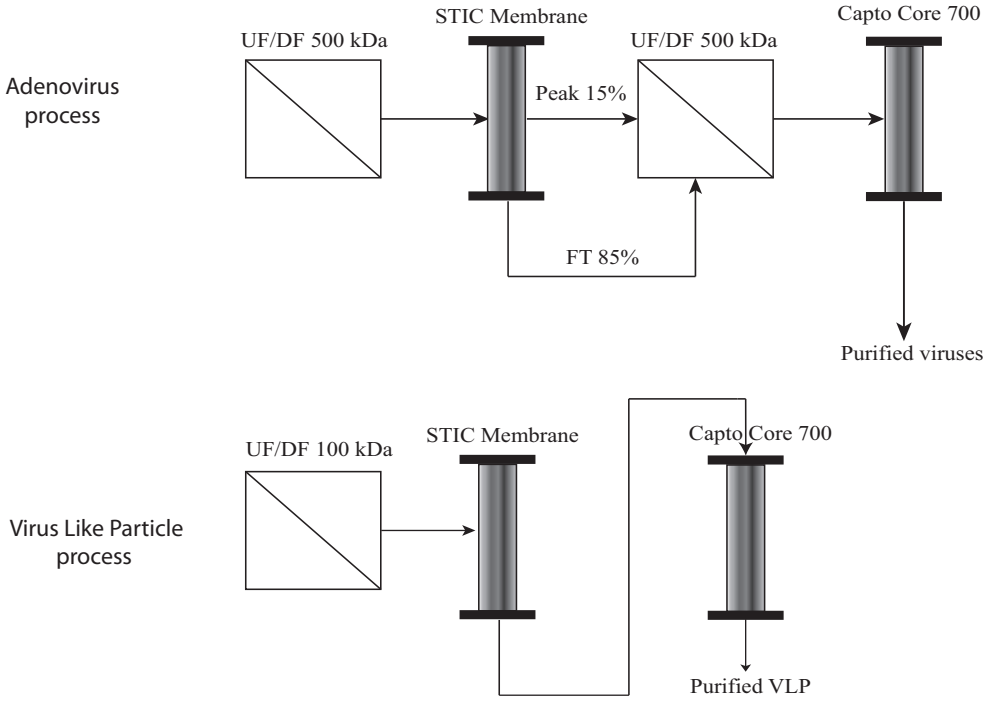

Figure 6.14: *Flowthrough purification scheme for adenovirus (top plot) and VLP (bottom plot). The bulk after clarification is concentrated 10 times and 5 times diafiltrated with a prototytpe 500kDa cassette. The feed is then loaded into the Sartobind STIC® membrane; flowtrough and peak contanining 85% and 15 % of the virus respectively are collected and concentrate/diafiltrate by a factor of three. Capto™ Core 700 is then loaded and the purified virus collected in the flowthrough.For the VLP flow scheme a Vivaflow 100 kDa cassette was used for concentration and diafiltration.The STIC membrane and the Capto Core were connected in series.*

biopharmaceuticals.

In fact, by changing virus serotype or different VLPs in a classic bind and elute process often results in changes in the elution behavior, thus the process should be always fine tuned. In contrast in a flowthrough process, such as the one described here, the elution behavior is constant cause no adsorption of the target product occurs. Scale up is easier to perform since DBC of the impurities is the factor that has to be taken into account keep linear velocity or resident time constant. Selectivity during gradient elution and peak tailing are not an issue anymore.

In order to prove that the negative mode can be suitable for preliminary purification of other large biopharmaceutical, the scheme used for adenovirus was sligthly changed and employed for VLP purification. In contrast with the adenovirus bulk, VLP feedstock have the following characteristic: (i) the production occurs via budding therefore no lysis is required resulting in a cleaner bulk,(ii) the presence of less contaminant namely DNA and host cell protein, on one hand release the constrain for purity on the other required the use of a modulator such as phosphate buffer in the STIC membrane (iii) VLPs are shear stress sensitive (Negrete et al., 2014; Chalmers, 1996), therefore the use of UF/DF should be limited. Taking into account these constrains the FT process for adenovirus was modified by connecting in series STIC membrane and Capto core. Only one UF/DF was unit operation was implemented at the beginning of the chromatography train, with the aim of concentration and to condition the bulk with a PBS containing 50mM phosphate. Also, being enveloped VLPs relatively complex structures consisting of the host cell membrane (an envelope) with integrated target antigens displayed on the outer surface results in high instability. Factors such as vortexing stirring, skaking and pumping were observed by Li shi et al, from Merck and Co to induce significant VLP aggregation and protein concentration(Shi et al., 2005). To reduce this phenomena a small amount of non-ionic surfactant polisorbate 80 at the concentration of 0.01 (v/v)% was used during the entire downstream train. Overall the stabilizing effect exhibits in two mechanisms: solubilization and replacement. The solubilization mechanism requires the formation of a complex between between the protein and the surfactant. The replacement mechanism requires the competition of surfactants with proteins for the adsorption surfaces.

The results showed a recovery yield in the UF/DF of 50% and 45 % recovery yield in the chromatography train. Although these results may not appear outstanding if compared with adenovirus, in the field of enveloped VLP are

considered in line with other purification strategies (Segura et al., 2006; McNally, 2014). The labile nature of retro VLP and their instability makes their purification very challenging.

In regard to the purity, the two column in series achieved a log reduction for DNA and HCP of 2.0 and 3.5 respectively. The UF/DF unit operation adds a further 1 log reduction for both impurities. Since the bulk is obtained by budding and cell lysis is not required, this results in having a lower initial amount of impurities which improve the purification performance of the downstream train.

6.4 Conclusions

The work presented showed a rational development of a flowthrough process first by understanding the behaviour of DNA (major contaminant) binding onto the two ligands and afterwards scaling up and confirming the design space. The flowthrough process designed is suitable for a platform concept and was implemented for adenovirus and retro-VLP purification with minimal amount of optimization required.

Acknowledgments

The authors thank Rute Casto and Ana Sofia Coroadinha for providing the retro-VLP bulk. Financial support from Sartorius Stedim Biotech and from the Portuguese Science Foundation (FCT-MCTES) (SFRH/BD/82032/2011 and EXPL/BBB-EBB/0790/2012) is gratefully acknowledged. The authors do not have any conflicts of interest.

References

Boi, C. (2007). Membrane adsorbers as purification tools for monoclonal antibody purification. *Journal of Chromatography B*, *848*, 19–27.

Burova, E., and Ioffe, E. (2005). Chromatographic purification of recombinant adenoviral and adeno-associated viral vectors: methods and implications. *Gene Ther.*, *12*, S5–S17.

Chalmers, J. (1996). Shear sensitivity of insect cells. *Cytotechnology*, *20*, 163–171.

Eglon, M. N., Duffy, A. M., O'Brien, T., and Strappe, P. M. (2009). Purification of adenoviral vectors by combined anion exchange and gel filtration chromatography. *J.Gene Med.*, *11*, 978–989.

Fernandes, P., Peixoto, C., Santiago, V., Kremer, E., Coroadinha, A., and Alves, P. (2013). Bioprocess development for canine adenovirus type 2 vectors. *Gene therapy*, *20*, 353–360.

Gerster, P., Kopecky, E.-M., Hammerschmidt, N., Klausberger, M., Krammer, F., Grabherr, R., Mersich, C., Urbas, L., Kramberger, P., Paril, T. et al. (2013). Purification of infective baculoviruses by monoliths. *J. Chromatogr. A*, *1290*, 36–45.

Goerke, A. R., To, B. C. S., Lee, A. L., Sagar, S. L., and Konz, J. O. (2005). Development of a novel adenovirus purification process utilizing selective precipitation of cellular dna. *Biotechnol. Bioeng.*, *91*, 12–21.

Hahn, R., Tscheliessnig, A., Bauerhansl, P., and Jungbauer, A. (2007). Dispersion effects in preparative polymethacrylate monoliths operated in radial-flow columns. *J. Biochem. Biophys. Methods*, *70*, 87–94.

HOLMES-FARLEY, S. R., Mandeville, W. H., Ward, J., and Miller, K. (1999). Design and characterization of sevelamer hydrochloride: a novel phosphate-binding pharmaceutical. *J. Macromol. Sci., Pure Appl. Chem.*, *36*, 1085–1091.

Iyer, G., Ramaswamy, S., Asher, D., Mehta, U., Leahy, A., Chung, F., and Cheng, K.-S. (2011). Reduced surface area chromatography for flow-through purification of viruses and virus like particles. *Journal of Chromatography A*, *1218*, 3973–3981.

Jason-Moller, L., Murphy, M., and Bruno, J. (2006). Overview of biacore systems and their applications. *Curr Protoc Protein Sci*, *Chapter 19*, Unit 19 13. Journal Article Review United States.

Joucla, G., Le Sénéchal, C., Bégorre, M., Garbay, B., Santarelli, X., and Cabanne, C. (2013). Cation exchange versus multimodal cation exchange resins for antibody capture from cho supernatants: Identification of contaminating host cell proteins by mass spectrometry. *J. Chromatogr. B*, *942*, 126–133.

Kallberg, K., Johansson, H.-O., and Bulow, L. (2012). Multimodal chromatography: An efficient tool in downstream processing of proteins. *Biotechnol. J.*, *7*, 1485–1495.

Kamen, A., and Henry, O. (2004). Development and optimization of an adenovirus production process. *J.Gene Med.*, *6*, S184–S192.

Kang, Y. K., Ng, S., Lee, J., Adaelu, J., Qi, B., Persaud, K., Ludwig, D., and Balderes, P. (2012). Development of an alternative monoclonal antibody polishing step. *BioPharm International*, *25*, 34–46.

Kim, U.-J., and Kuga, S. (2002). Ion-exchange separation of proteins by polyallylamine-grafted cellulose gel. *Journal of Chromatography A*, *955*, 191–196.

Knudsen, H. L., Fahrner, R. L., Xu, Y., Norling, L. A., and Blank, G. S. (2001). Membrane ion-exchange chromatography for process-scale antibody purification. *J. Chromatogr. A*, *907*, 145–154.

Konz, J. O., Lee, A. L., Lewis, J. A., and Sagar, S. L. (2005a). Development of a purification process for adenovirus: controlling virus aggregation to improve the clearance of host cell dna. *Biotechnol. Prog.*, *21*, 466–472.

Konz, J. O., Livingood, R. C., Bett, A. J., Goerke, A. R., Laska, M. E., and Sagar, S. L. (2005b). Serotype specificity of adenovirus purification using anion-exchange chromatography. *Hum. Gene Ther.*, *16*, 1346–1353.

Kushnir, N., Streatfield, S. J., and Yusibov, V. (2012). Virus-like particles as a highly efficient vaccine platform: diversity of targets and production systems and advances in clinical development. *Vaccine*, *31*, 58–83.

Lua, L. H., Connors, N. K., Sainsbury, F., Chuan, Y. P., Wibowo, N., and Middelberg, A. P. (2013). Bioengineering virus-like particles as vaccines. *Biotechnol Bioeng*, *111*, 425–440.

Majka, J., and Speck, C. (2007). Analysis of protein-dna interactions using surface plasmon resonance. *Adv Biochem Eng Biotechnol*, *104*, 13–36. Journal Article Review Germany.

McNally, D. F. P. L. N. S., D.J. Darling (2014). Optimized concentration and purification of retrovirus using membrane chromatography. *J. Chromatogr. A*, *http://dx.doi.org/doi:10.1016/j.chroma.2014.03.023*, Accepted Manuscript.

Negrete, A., Pai, A., and Shiloach, J. (2014). Use of hollow fiber tangential flow filtration for the recovery and concentration of hiv virus-like particles produced in insect cells. *J. Virol. Methods*, *195*, 240–246.

Nestola P, P. C. S. R. S. T. A. P. M. J. C. M., Martins DL (2014). Evaluation of novel large cut-off ultrafiltration membranes for adenovirus serotype 5 (ad5) concentration. *PLOS ONE*, *Accepted*.

Peixoto, C., Ferreira, T. B., Carrondo, M. J. T., Cruz, P. E., and Alves, P. M. (2006). Purification of adenoviral vectors using expanded bed chromatography. *J. Virol. Methods*, *132*, 121–126.

Pezzini, J., Joucla, G., Gantier, R., Toueille, M., Lomenech, A.-M., Le Sénéchal, C., Garbay, B., Santarelli, X., and Cabanne, C. (2011). Antibody capture by mixed-mode chromatography: A comprehensive study from determination of optimal purification conditions to identification of contaminating host cell proteins. *J. Chromatogr. A*, *1218*, 8197–8208.

Roldão, A., Mellado, M. C. M., Castilho, L. R., Carrondo, M. J., and Alves, P. M. (2010). Virus-like particles in vaccine development. *Expert review of vaccines*, *9*, 1149–1176.

Rouquerol, J., Avnir, D., Fairbridge, C., Everett, D., Haynes, J., Pernicone, N., Ramsay, J., Sing, K., Unger, K. et al. (1994). Recommendations for the characterization of porous solids (technical report). *Pure and Applied Chemistry*, *66*, 1739–1758.

Segura, M. d. l. M., Garnier, A., and Kamen, A. (2006). Purification and characterization of retrovirus vector particles by rate zonal ultracentrifugation. *Journal of virological methods*, *133*, 82–91.

Segura, M. M., Alba, R., Bosch, A., and Chillon, M. (2008). Advances in helper-dependent adenoviral vector research. *Curr. Gene Ther.*, *8*, 222–235.

Shi, L., Sanyal, G., Ni, A., Luo, Z., Doshna, S., Wang, B., Graham, T. L., Wang, N., and Volkin, D. B. (2005). Stabilization of human papillomavirus virus-like particles by non-ionic surfactants. *J. Pharm. Sci.*, *94*, 1538–1551.

Tatsis, N., and Ertl, H. C. (2004). Adenoviruses as vaccine vectors. *Molecular Therapy*, *10*, 616–629.

Thillaivinayagalingam, P., Gommeaux, J., McLoughlin, M., Collins, D., and Newcombe, A. R. (2010). Biopharmaceutical production: Applications of surface plasmon resonance biosensors. *Journal of Chromatography B*, *878*, 149–153.

Tugcu, N., Roush, D. J., and Göklen, K. E. (2008). Maximizing productivity of chromatography steps for purification of monoclonal antibodies. *Biotechnology and bioengineering*, *99*, 599–613.

Vicente, T., Mota, J. P., Peixoto, C., Alves, P. M., and Carrondo, M. J. (2010). Modeling protein binding and elution over a chromatographic surface probed by surface plasmon resonance. *J Chromatogr A*, *1217*, 2032–41.

Wang, J., Faber, R., and Ulbricht, M. (2009). Influence of pore structure and architecture of photo-grafted functional layers on separation performance of cellulose-based macroporous membrane adsorbers. *J. Chromatogr. A*, *1216*, 6490–6501.

Whitfield, R. J., Battom, S. E., Barut, M., Gilham, D. E., and Ball, P. D. (2009). Rapid high-performance liquid chromatographic analysis of adenovirus type 5 particles with a prototype anion-exchange analytical monolith column. *J. Chromatogr. A*, *1216*, 2725–2729.

Woo, M., Khan, N. Z., Royce, J., Mehta, U., Gagnon, B., Ramaswamy, S., Soice, N., Morelli, M., and Cheng, K. S. (2011). A novel primary amine-based anion exchange membrane adsorber. *J Chromatogr A*, *1218*, 5386–92.

Zhou, J. X., and Tressel, T. (2006). Basic concepts in q membrane chromatography for large-scale antibody production. *Biotechnology Progress*, *22*, 341–349.

Part IV

Outlook

CHAPTER 7

Discussion

7.1 Discussion

The increasing interest in virotherapies, either gene therapy or viral vaccines, is propelling the development of novel and more efficient bioprocesses. In particular, advances in upstream processing (USP) have substantially increased bioreactor yields and the bioprocess bottlenecks are now mainly in the downstream processing (DSP) . To overcome these bottlenecks technological advances have taken place to develop straightforward purification processes aimed to deliver a final product fulfilling the critical quality attributes required by the authorities. Nevertheless, the implementation of an integrated downstream purification process for virus-like-particles or viral vectors is not yet mature; indeed, it is still difficult to achieve a high-purity grade while keeping host cell protein (HCP) and deoxyribonucleic acid (DNA) within the specifications set by regulatory bodies.

The work presented in this thesis aimed to develop and/or test new processes for adenoviruses purification. This virus is considered to be one of the most suitable platforms for producing viral vaccines and gene therapy vectors. It can be produced using complementary cell lines in both adherent and suspension culture systems, such as HEK–293 or PER-C6 cells, CAP or A549 for oncolytic adenoviruses (Segura et al., 2008).

Chapter 1 offers an extended revision of the state-of-the-art by analyzing prominent case studies and underlying the current limitations and challenges.

Part II, comprising chapters 2 and 3, focuses on the understanding and performance improvement of some DSP unit operations, such as ultrafiltration and anion exchange chromatography. We have successfully selected and implemented a novel class of large cut-off ultrafiltration membranes that achieve 100% of infective virus recovery after 10-fold concentration. In addition, we have extended the fundamental knowledge regarding the impact of ligand density and membrane structure providing new insights into the development of next generation membrane chromatography.

The third part of the thesis is essentially focused on developing continuous processes based on the simulating moving bed (SMB) technology. The result is a remarkable increase in the productivity for the purification of adenovirus by size-exclusion chromatography. Finally, in the last chapter a flowthrough purification strategy was implemented by combining the salt tolerant membrane chromatography (STIC) and the scavenger bead technology (CaptoCore). With this new approach, we were able to design a versatile, effective, and robust flowthrough process for adenovirus and VLP purification.

7.1.1 Improved ultrafiltration processes

Ultrafiltration has been widely used for both concentration and buffer exchange (diafiltration, DF), and is present in almost every virus DSP described in the literature (Segura et al., 2013; Bandeira et al., 2012; Kamen and Henry, 2004; Rodrigues et al., 2007; Segura et al., 2012; Wickramasinghe et al., 2005; Kalbfuss et al., 2007; Subramanian et al., 2008) and disclosed patents (Luitjens and van Herk, 2012; Konz et al., 2008; Weggeman and van Corven, 2005). The membranes used in virus UF have MWCOs in the range of 100–750 kDa allowing for high virus recoveries (70–85%). Despite the effort in developing robust DSPs and platforms, most of the research in the field of virus purification has been focused on the chromatographic steps. The results discussed in Chapter 2 provide an important contribution to ultrafiltration processes for viral processing. We designed a novel large cut-off ultrafiltration membrane (∼500kDa) based on highly cross-linked regenerated cellulose. The membrane exhibits a remarkable virus particle recovery yield, and higher productivity when compared to a hollow fiber (HF) (∼750kDa) device. Most notably, this is the first study to investigate adenovirus concentration by ultrafiltration cassette. Futhermore, our findings complement the previous studies based on VLP and influenza (Negrete et al., 2014; Wickramasinghe et al., 2005) where only PES membranes were evaluated. In addition, unlike the other reported studies, important process ultrafiltration parameters, such as fouling behavior and flux recovery before and after cleaning in place (CIP), were also assessed.

7.1.2 Understanding anion-exchange membrane chromatography

Convective chromatography media, such as membranes and monoliths, offer substantial improvements in capacity, recovery, and reduction of process time (Hahn et al., 2007). Membrane adsorbers are used in the biopharmaceutical industry almost exclusively in flowthrough mode for mAb purification (Boi, 2007; Knudsen et al., 2001; Zhou and Tressel, 2006). More recently, membrane adsorption chromatography has been applied to the purification of viral vectors using a bind-and-elute mode, yielding good overall recovery rates (Lee et al., 2009; Peixoto et al., 2006, 2008). However, two major challenges still remain: on one hand, adequate removal of impurities (DNA and HCP) that are closely related to the viral product, and on the other hand low binding capacity for highly concentrated feeds. The design of new matrices with appropriate ligand density

and degree of grafting is key to further improve the bind-and-elute purification mode for viruses.

In Chapter 3 we complement the results obtained by Vicente et al. (2011) for baculovirus (an enveloped virus) with adenovirus (a non-enveloped virus). In addition we further extend our study by comparing two different membrane platforms (direct-grafted vs hydrogel-grafted) which led to the following outcomes:

- Hydrogel-grafted membranes yield higher virus recoveries than the directly-grafted membranes.
- Moving toward hydrogel-grafted membranes with ligand densities lower than 2.4 μmol/cm^2 led to virus recoveries higher than 70%, in line with the findings of Vicente et al. (2011). A decreased ligand density and increased ionic strength to a value of 150-200 mM NaCl are suitable conditions for hydrogel-grafted membranes.
- The directly-grafted membranes show low binding for the virus and give rise to significant percentages of viruses in the flow-through, up to 60-70%. Increasing the ligand density and lowering the ionic strength to a maximum of 25 mM NaCl is more suitable for directly-grafted membranes.
- An attempt is made to elucidate the shapes of the breakthrough curves by matching the frontal analysis experiments to a simple equilibrium-dispersive adsorption breakthrough model.
- Overall, when designing new chromatographic membrane for virus purification, ligand density is not the only factor to consider, as the membrane structure also plays an important role.

Finally, future work should investigate the effect of larger ligand density values (>4.5 μmol/cm^2) for improving the performance of the direct-grafted membrane platform. This platform holds promise for replacing the current hydrogel-grafted technology.

7.1.3 Moving towards continuous chromatography

From chapter 4 we step into the design of a semi-continuous process based on SMB technology. The results demonstrate the feasibility of a compact and efficient, simulated countercurrent multi-column chromatographic process for adenovirus purification. The process is strictly operated in an open-loop configuration to

dispense the use of an internal recirculation pump; it needs two HPLC pumps only: one for injecting the clarified bioreaction bulk and another for injecting fresh eluent. At any instant of the operating cycle the flow through a column is either temporarily stopped or completely directed to one of three destinations: the other column, the waste line, or the product line. This class of flow-path configurations is easily implemented with simple two-way valves and gives rise to very robust operating cycles. The experimental results show:

- a virus recovery of 86%, and a clearance of 90% and 89% for DNA and HCP, respectively. These figures compare very favorably against single-column batch chromatography for the same volume of size-exclusion resin.
- 6-fold productivity boost and 51% increase in Ad5 recovery, without compromising the impurity clearance. These are strong arguments in favor of implementing the type of process presented here in a real production DSP train.

The designed 2-column process is further studied by assessing its robustness by selecting the best set of operating parameters. These operating parameters are robust feasible and remain feasible for all parameter perturbations within their uncertainty intervals. Our procedure successfully identifies the optimal robust values of the step durations when both the interparticle porosity (ϵ_o)and column volume (V_c) are subject to two types of uncertainty scenarios. In one case ϵ_o and V_c are uncorrelated, uniformly distributed random variables, whereas in the other case ϵ_o and V_c are uncorrelated, normally distributed random variables.

Overall the work presented in chapter 4 and chapter 5 together with the study of Kröber et al. (2013) constitute the state-of-the-art for continuous or quasi-continuous chromatography for viral vaccines or vectors.

Continuous processing of complex biopharmaceuticals, such as viruses or VLPs, is still in its infancy and much more work should be done in the coming years. The work of Nestola et al. (2014a) and Kröber et al. (2013) were both based on isocratic elution by size exclusion chromatography (SEC); therefore future studies should investigate a multicolumn process using an IEX matrix. IEX continuous processes are not trivial because the development of a model able to predict the binding and elution behavior is required. When steric mass action (SMA) model is applied to describe the IEX mechanism of large biopharmaceuticals, it is somewhat difficult to determine the characteristic charge, as shown by Yamamoto et al. (2007) who studied the retention behavior of oligo-DNA onto an anionic exchange monolith. Indeed, for a characteristic charge larger than ca. 50 it can be

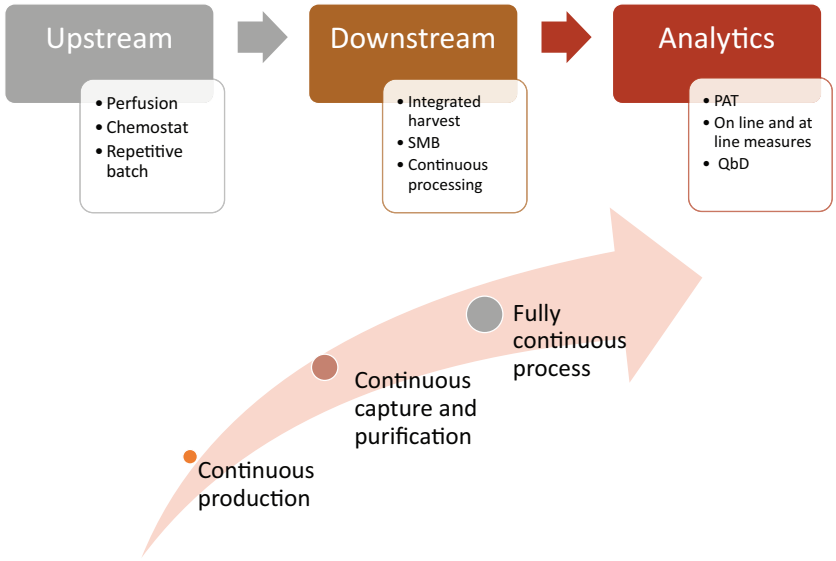

Figure 7.1: *Ideal flow for a fully integrated continuous processing. A close link between upstream and downstream is required to switch from batch to continuous production. The role of analytical tools is critical because it is essential to develop on-line or at-line measurements to monitor a continuous processes.*

quite challenging to determine this parameter experimentally. However, even more trickier is to use the SMA model in model-based process design and optimization due to the difficulties of numerically solving the differential material balance of an IEX adsorber for large values of the characteristic charge. Therefore, efforts should be made to develop a robust model that can be suitable for designing a continuous or semi-continuous IEX process.

Overall, chromatography is only a part of the global process including upstream and downstream, and there are really beneficial improvements when a large part of the process is switched to continuous operation. Figure 7.1 illustrates an ideal continuous integrated strategy where upstream and downstream are closely linked. The development of analytical tools for on-line and at-line measurements becomes critical for continuous processing. Nonetheless, the work presented in this thesis is an important starting point for further studies.

7.1.4 From bind elute to flow-through process

In the last chapter of this thesis we continue our journey through the development of new processes by focusing on a flowtrough strategy. Most of the applications

described in the literature for virus purification are based on positive mode, where the target product binds to the matrix. Nevertheless, negative modes are being developed and an interesting review by Lee et al. (2014) details several applications.

One apparent limitation of negative mode is due to the difficulty of efficiently removing the impurities as compared to positive-mode chromatography; thus so far, negative mode has only been implemented as a polishing step. In the process proposed in chapter 6 we combined together two recently launched matrices, Capto Core 700 from GE healthcare and a salt tolerant chromatographic membrane (STIC®) from Sartorius Stedim Biotech. The process is integrated with the large cut-off ultrafiltration membrane selected in chapter 2. In addition, the ligands immobilized on the two matrices were thoroughly studied using SPR technology providing useful insights for identifying optimal operating conditions, namely ionic strength, buffer type and phosphate concentrations. Overall, by combining the two flowthrough technologies it was possible to design a process with higher productivity, more robust, and easily scalable. The scale up was performed by simply calculating the DBC%10 for DNA for the STIC membrane from breakthrough experiments.

The negative mode strategy described herein is more suitable for a platform concept; due to the high degree of uncertainty associated with the clinical studies process development at early stage aims to produce material for phase 1 and phase 2 clinical trials using standardized process conditions and procedures. The use of platform processes allows the acceleration of the early process development activities as already shown for the mAb applications. The similarity amongst different viruses or serotypes make the platform concept feasible although the process need to be optimized for each complex biopharmaceutical.

Although much work is still required to promote negative-mode chromatography as a purification platform, its potential should not be underestimated, especially for viral vaccines where different serotypes or strains may influence the binding and elution behavior, leading to routine optimization for every new viral vaccine candidate in the pipeline.

7.2 Final remarks and future perspectives

This thesis successfully contributes to the design of new processes by studying, integrating, and validating novel matrices and materials. The overall strategy used is shown in Fig. 7.2. A more efficient and robust process can only be

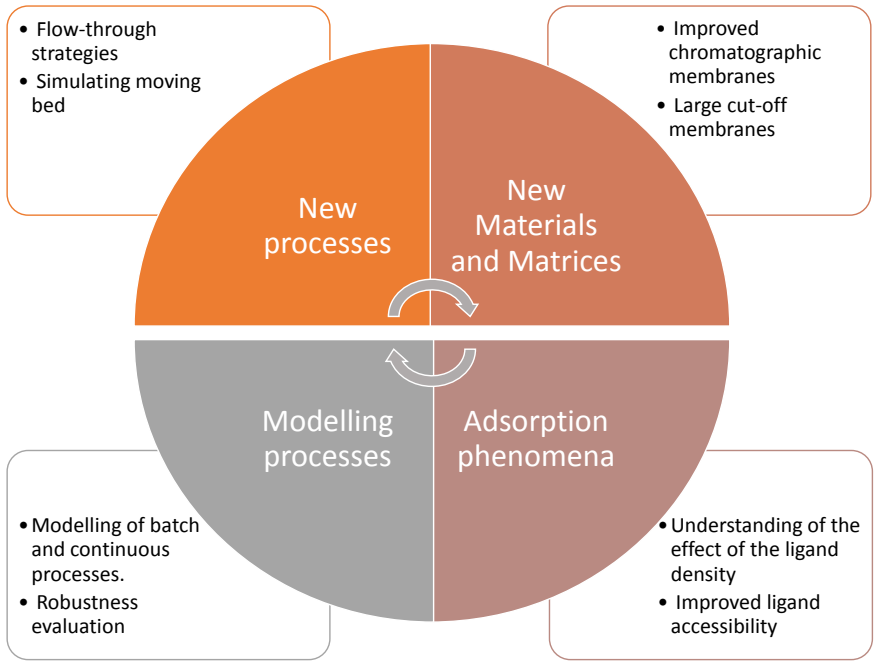

Figure 7.2: *Strategies for delivering new downstream processes applied in this thesis. The combination of both new materials and processes is crucial, and the two aspects need to be strongly connected for a proper process design.*

achieved by the integration of new materials within new process designs. A strong interconnection of these two aspects is therefore required to generate either new materials from existing processes or new processes from new materials.

Current advances in material science, such as new chromatographic supports based on nanofibers (Hardick et al., 2012) and the novel 3D printing for monolith development (Fee et al., 2014), have the potential to revolutionize the current processes. At the same time, better understanding of ligand density and structure can lead to new stationary phases optimized for virus purification, where binding site competition between viral particles and process related contaminants can be sterically promoted; these new matrices should have high dynamic binding capacity for virus particles and little or none for the contaminants (DNA and HCP) (Villain et al. Oral presentation, Recovery Conference, 27-31 July 2014). This thesis contributes to a greater extent to developing this concept further.

On the other hand, mixed-mode and biomimetic chromatography ligands are foreseen to increase the performance of chromatographic unit operations (Li

et al., 2014). The future of virus-ligand library screening can be as promising as ProMetic currently is for other protein/Ab products. Materials science is also developing stimuli-responsive polymers (known as smart polymers) with unique properties that can be precisely modulated by a number of factors, such as light, temperature, pH, electric or magnetic fields, etc. (Bajpai et al., 2011). These new polymers might be employed in aqueous two phase separation (ATPS) for better modulating two-phase partitioning (González-González and Rito-Palomares, 2013), or even employed as mobile phase in chromatographic separations. Nevertheless, toxicity and biocompatibility require proper assessment.

The implementation of HTPS technologies is slowly being established in academic settings to improve process design (Nfor et al., 2012; Osberghaus et al., 2012; Nestola et al., 2014b). Companies such as Tecan or Beckman Coulter—industrial leaders in automation and robotic platforms—are already developing full customizable solutions for big pharma, SMEs, or small academic groups. HTPS tools will increase the understanding of the design space coupled with a more mechanistic analysis of the physico-chemical properties of virus particles. HTPS technologies are relevant not merely for the optimization of downstream processing but also for investigating the appropriate formulation to use. For example, Freeslate is providing a configurable, robotic laboratory automation system for formulation and stability tests. So far, formulation has often been regarded as the last step of the process, mainly related to the filling and finishing processes. However, for labile viruses such as enveloped viruses, formulation becomes critical earlier as it allows to stabilize the virus particles along the downstream processing train, giving rise to a more robust downstream process.

The vaccine industry will most likely follow the same trend as the mAb industry by designing new purification trains with a reduced number of unit operations. Moreover, the implementation of numerical and scaled down tools for process optimization will facilitate the identification of proper design spaces for both single unit operations and integrated processes. Complex stochastic approaches, such as the Giddings and Eyring models, or Monte Carlo models, can elucidate in more detail the elution profile of heterogeneous viral bulks.

Furthermore, efforts to develop platform technologies, which can be used for several virus serotypes, will be given the highest priority to allow the acceleration of the process development.

New drag-and-drop production platforms could be developed by better understanding and modelling the different production steps. Although technology platforms for vaccine manufacturing are indeed diverse, the diversity is seen

mostly in the fermentation/cell culture and DSP purification. Qualified utilities, equipment preparation areas, and buffer and media preparation areas are not significantly different across technology platforms. With appropriate segregation and control, it is possible to design multi-product facilities that can be used for more than one product. This type of modular approach would improve asset usage and minimize the impact of failure of one product. A modular design approach requires an understanding of the pipeline of products in development and the company's long-term vision of the manufacturing site. Nevertheless, platform concepts have the disadvantage and the risk of limiting somewhat the innovation of the process by focusing all the resources to the already developed platform (Wen et al., 2014).

Above all, the biopharmaceutical and, in particular, the vaccine industry should embrace new changes and technologies as supported by the QbD initiative from FDA/EMA, and the recent industry motto "If it ain't broken don't fix it" should be overcome (Gottschalk et al., 2013). Process innovation will certainly be key for delivering affordable viral vaccines and vectors. Indeed quoting Peter F. Drucker *"If you want something new, you have to stop doing something old"*.

References

Bajpai, A., Bajpai, J., Saini, R., and Gupta, R. (2011). Responsive polymers in biology and technology. *Polymer Rev*, *51*, 53–97.

Bandeira, V. S., Peixoto, C., Rodrigues, A. F., Cruz, P., Alves, P., Coroadinha, A. S., and Carrondo, M. (2012). Downstream Processing of Lentiviral Vectors: releasing bottlenecks. *Hum Gene Ther Methods*, *23*, 255–263.

Boi, C. (2007). Membrane adsorbers as purification tools for monoclonal antibody purification. *J Chromatogr B*, *848*, 19–27.

Fee, C., Nawada, S., and Dimartino, S. (2014). 3d printed porous media columns with fine control of column packing morphology. *J Chromatogr A*, *1333*, 18–24.

González-González, M., and Rito-Palomares, M. (2013). Aqueous two-phase systems strategies to establish novel bioprocesses for stem cells recovery. *Crit Rev Biotech*, *0738-8551*, 1–10.

Gottschalk, U., Brorson, K., and Shukla, A. A. (2013). Innovation in biomanufacturing: the only way forward. *Pharm Bioproces*, *1*, 141–157.

Hahn, R., Tscheliessnig, A., Bauerhansl, P., and Jungbauer, A. (2007). Dispersion effects in preparative polymethacrylate monoliths operated in radial-flow columns. *J Biochem Biophys Methods*, *70*, 87–94.

Hardick, O., Dods, S., Stevens, B., and Bracewell, D. G. (2012). Nanofiber adsorbents for high productivity downstream processing. *Biotechnol Bioeng*, *110*, 1119–1128.

Kalbfuss, B., Genzel, Y., Wolff, M., Zimmermann, A., Morenweiser, R., and Reichl, U. (2007). Harvesting and concentration of human influenza A virus produced in serum-free mammalian cell culture for the production of vaccines. *Biotechnol Bioeng*, *97*, 73–85.

Kamen, A., and Henry, O. (2004). Development and optimization of an adenovirus production process. *J Gene Med*, *6*, S184–S192.

Knudsen, H. L., Fahrner, R. L., Xu, Y., Norling, L. A., and Blank, G. S. (2001). Membrane ion-exchange chromatography for process-scale antibody purification. *J Chromatogr A*, *907*, 145–154.

Konz, J. O., Lee, A. L., To, B. C. S., and Goerke, A. R. (2008). Methods of adenovirus purification. *US Patent 0118970 A1*, .

Kröber, T., Wolff, M., Hundt, B., Seidel-Morgenstern, A., and Reichl, U. (2013). Continuous purification of influenza virus using simulated moving bed chromatography. *J Chromatogr A*, *1307*, 99–110.

Lee, D.-S., Kim, B.-M., and Seol, D.-W. (2009). Improved purification of recombinant adenoviral vector by metal affinity membrane chromatography. *Biochem Biophys Res Commun*, *378*, 640–644.

Lee, M. F. X., Chan, E. S., and Tey, B. T. (2014). Negative chromatography: Progress, applications and future perspectives. *Process Biochem*, *49*, 1005–1011.

Li, Y., Liu, X., Dong, X., Zhang, L., and Sun, Y. (2014). Biomimetic design of affinity peptide ligand for capsomere of virus-like particle. *Langmuir*, *30*, 8500–8508.

Luitjens, A., and van Herk, H. (2012). Method for the production of Ad26 adenoviral vectors. *US Patent 0315696 A1*, .

Negrete, A., Pai, A., and Shiloach, J. (2014). Use of hollow fiber tangential flow filtration for the recovery and concentration of hiv virus-like particles produced in insect cells. *J Virol Methods*, *195*, 240–246.

Nestola, P., Silva, R. J., Peixoto, C., Alves, P. M., Carrondo, M. J., and Mota, J. P. (2014a). Adenovirus purification by two-column, size-exclusion, simulated countercurrent chromatography. *J Chromatogr A*, *1347*, 111–121.

Nestola, P., Villain, L., Peixoto, C., Martins, D. L., Alves, P. M., Carrondo, M. J., and Mota, J. P. (2014b). Impact of grafting on the design of new membrane adsorbers for adenovirus purification. *J Biotechnol*, *181*, 1–11.

Nfor, B. K., Ripić, J., van der Padt, A., Jacobs, M., and Ottens, M. (2012). Model-based high-throughput process development for chromatographic whey proteins separation. *Biotechnol J*, *7*, 1221–1232.

Osberghaus, A., Drechsel, K., Hansen, S., Hepbildikler, S., Nath, S., Haindl, M., Von Lieres, E., and Hubbuch, J. (2012). Model-integrated process development demonstrated on the optimization of a robotic cation exchange step. *Chem Eng Sci*, *76*, 129–139.

Peixoto, C., Ferreira, T., Carrondo, M., Cruz, P., and Alves, P. (2006). Purification of adenoviral vectors using expanded bed chromatography. *J Virol Methods*, *132*, 121–126.

Peixoto, C., Ferreira, T. B., Sousa, M. F. Q., Carrondo, M. J. T., and Alves, P. M. (2008). Towards purification of adenoviral vectors based on membrane technology. *Biotechnol Prog*, *24*, 1290–1296.

Rodrigues, T., Carvalho, A., Carmo, M., Carrondo, M. J. T., Alves, P. M., and Cruz, P. E. (2007). Scaleable purification process for gene therapy retroviral vectors. *J Gene Med*, *9*, 233–243.

Segura, M. M., Alba, R., Bosch, A., and Chillón, M. (2008). Advances in helper-dependent adenoviral vector research. *Curr Gene Ther*, *8*, 222–235.

Segura, M. M., Mangion, M., Gaillet, B., and Garnier, A. (2013). New developments in lentiviral vector design, production and purification. *Expert Opin Biol Ther*, *13*, 987–1011.

Segura, M. M., Puig, M., Monfar, M., and Chillón, M. (2012). Chromatography Purification of Canine Adenoviral Vectors. *Hum Gene Ther Methods*, *23*, 182–197.

Subramanian, S., Altaras, G. M., Chen, J., Hughes, B. S., Zhou, W., and Altaras, N. E. (2008). Pilot-Scale Adenovirus Seed Production through Concurrent Virus Release and Concentration by Hollow Fiber Filtration. *Biotechnol Prog*, *21*, 851–859.

Vicente, T., Faber, R., Alves, P. M., Carrondo, M. J. T., and Mota, J. P. B. (2011). Impact of ligand density on the optimization of ion-exchange membrane chromatography for viral vector purification. *Biotechnol Bioeng*, *108*, 1347–1359.

Weggeman, M., and van Corven, E. J. J. M. (2005). Virus purification methods. *European Patent 1780269 B1*, .

Wen, E. P., Ellis, R., and Pujar, N. S. (2014). *Vaccine Development and Manufacturing*. John Wiley & Sons.

Wickramasinghe, S. R., Kalbfuß, B., Zimmermann, A., Thom, V., and Reichl, U. (2005). Tangential flow microfiltration and ultrafiltration for human influenza A virus concentration and purification. *Biotechnol Bioeng*, *92*, 199–208.

Yamamoto, S., Nakamura, M., Tarmann, C., and Jungbauer, A. (2007). Retention studies of dna on anion-exchange monolith chromatography binding site and elution behavior. *J Chromatogr A*, *1144*, 155–60.

Zhou, J. X., and Tressel, T. (2006). Basic concepts in q membrane chromatography for large-scale antibody production. *Biotechnol Prog*, *22*, 341–349.